

# **COMPUTER AIDED DESIGN OF NOVEL NOSCAPHINOLIDS AND THEIR EXPERIMENTAL EVALUATION AS TUBULIN BINDING ANTI-CANCER DRUGS**

**BY**

**SENEHA SANTOSHI**  
**Enrollment No. 106501**

**A THESIS SUBMITTED IN FULFILLMENT OF THE REQUIREMENTS FOR  
THE DEGREE OF DOCTOR OF PHILOSOPHY  
IN  
BIOINFORMATICS**



**DEPARTMENT OF BIOTECHNOLOGY & BIOINFORMATICS  
JAYPEE UNIVERSITY OF INFORMATION TECHNOLOGY  
WAKNAGHAT, SOLAN-173234, HP, INDIA  
AUGUST 2014**

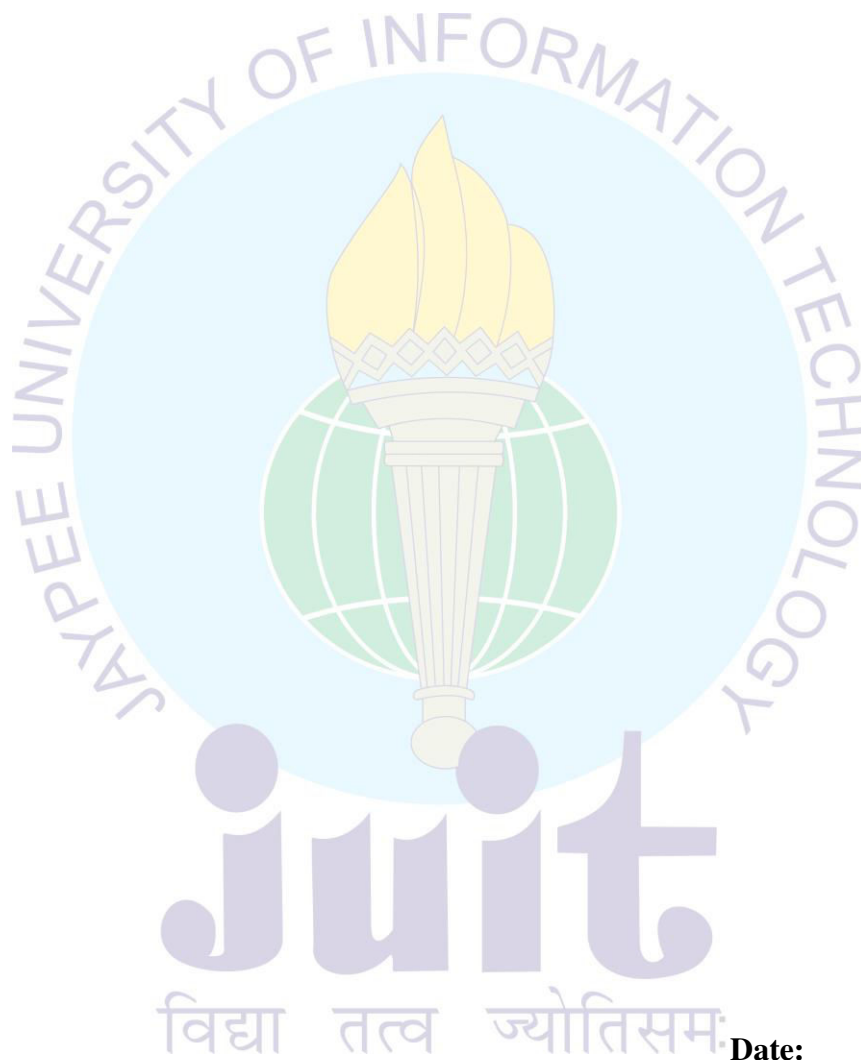
Copyright  
@  
JAYPEE UNIVERSITY OF INFORMATION TECHNOLOGY,  
WAKNAGHAT  
August, 2014  
ALL RIGHTS RESERVED

*In fond memory of*  
*Daddy (Late Sh. P. N. Santoshi)*

## DECLARATION

I certify that:

- a. The work contained in this thesis is original and has been done by me under the guidance of my supervisor.
- b. The work has not been submitted to any other organisation for any degree or diploma.
- c. Wherever, I have used materials (data, analysis, figures or text), I have given due credit by citing them in the text of the thesis.



**Seneha Santoshi**

(Enrollment No. 106501)

Department of Biotechnology and Bioinformatics

Jaypee University of Information Technology, Wagnaghat, India

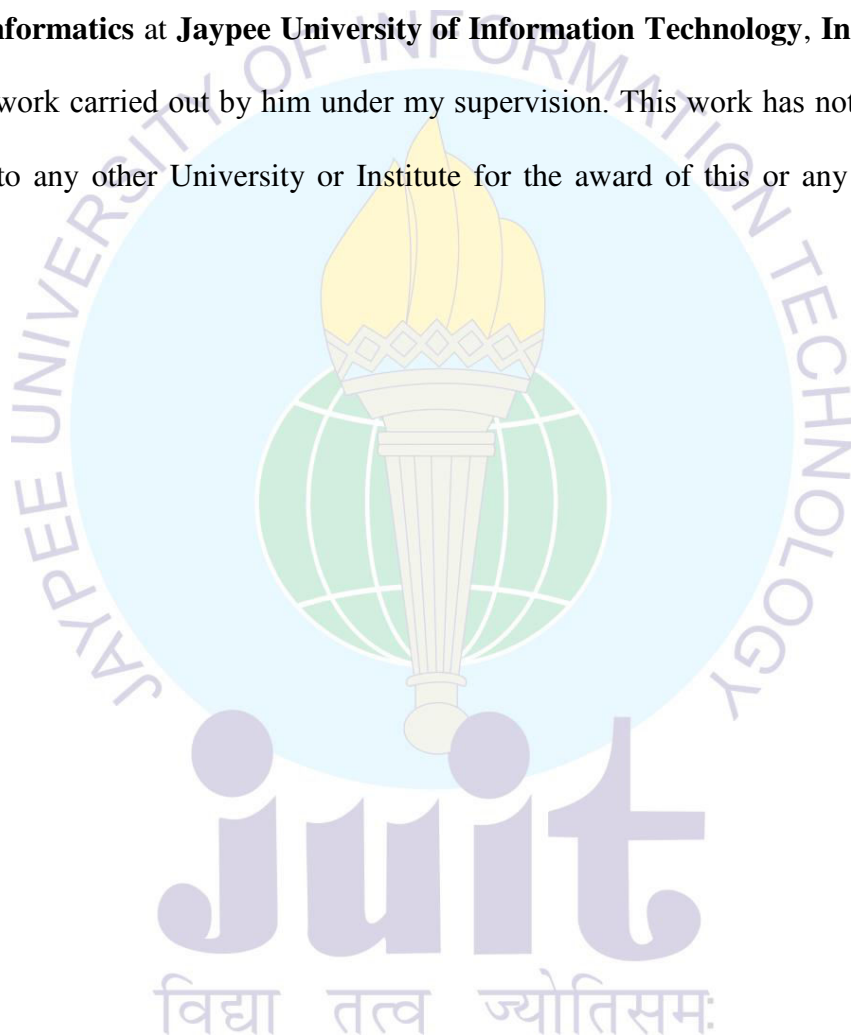
Email: seneha.santoshi@gmail.com

**Date:**



## CERTIFICATE

This is to certify that the thesis entitled, “**Computer aided design of novel noscapinoids and their experimental evaluation as tubulin binding anti-cancer drugs**” which is being submitted by **Seneha Santoshi (Enroll. No. - 106501)** in fulfillment for the award of degree of **Doctor of Philosophy in Bioinformatics** at **Jaypee University of Information Technology, India** is the record of candidate’s own work carried out by him under my supervision. This work has not been submitted partially or wholly to any other University or Institute for the award of this or any other degree or diploma.



**Dr. Pradeep Kumar Naik**  
Associate Professor,  
**Email:** pknaik1973@gmail.com

**Date:**

## ACKNOWLEDGMENT

Firstly, I would like to thank **Prof. (Dr.) Y. Medury**, (Ex COO Jaypee Education System) **Prof. (Dr.) S. K. KAK** Vice Chancellor, JUIT; **Brig. (Retd.) Balbir Singh**, Director JUIT; **Prof. (Dr.) T.S. Lamba**, Dean (Academic & Research) and **Prof. (Dr.) R.S. Chauhan**, Dean (Biotechnology) and **HoD (Biotechnology & Bioinformatics)** for entrusting and providing me the opportunity to pursue my research work at Jaypee University of Information Technology, Wagnaghat, India.

From the depth of my heart, I would like to thank my guide and mentor **Dr. Pradeep Kumar Naik**, Associate Professor (Bioinformatics) for his constant encouragement & guidance in pursuing my research. He has been more than a guide to me by being there every time and leading me through all these years. His positive attitude and zest for quality research always encouraged me and brought the best out of me. I deem it a privilege to be doing my Ph.D research under him, who has endeared himself to his students.

I am grateful to DIHAR - DRDO Chandigarh, as a part of this research work was carried out there. I would like to thank **Dr. Sunil K. Hota** Scientist 'D' Head Experimental Biology Division DIHAR, DRDO Chandigarh, **Mr. Saroj K. Das**, **Mr. Surya** and **Ms. Manya Sharma** for guiding and helping me out in the animal studies. I would also like to thank **Dr. B. N. Datta** (Medicos centre Chandigarh) for helping me in carrying out the histo-pathological and blood biochemical analysis.

I am highly thankful to **Dr. Srinivas Kantevari** (Organic Chemistry, CSIR-Indian Institute of Chemical Technology, Hyderabad) for helping me out in the experimental evaluations.

A big thanks to **Prof. (Dr.) Harish C. Joshi** for his valuable guidance and his team at Emory University for their constant inputs and help provided during the tenure of my research.

I can never forget my fellow researcher and friend **Ms. Charu Suri** who has helped me with the simulation studies and numerous other ways throughout this journey.

Also, I would like to thank all my friends especially Vatsala, Kanika, Bharti, Tamanna, Gazala and Nadish for they have played a very important role by being there so as to make me sail through all the twists and turns of this journey.

It was the blessing and love of my Grandmother (**Mrs. Lalita Rani**) and my parents (**Mr. Chaman Ji Santoshi and Mrs. Bitu Santoshi**), which have constantly been with me so as to make my life and career successful. Apart from my parents my brothers Bobby Bhaiya, Rinku Bhaiya, Minu Bhaiya, Goldy and Shradha bhabhi have been my angels. It was only because of their support, constant encouragement, prayers and blessings that I could overcome all frustrations and failures.

Also, I would like to thank all the **faculty members** especially **Dr. Simran Tandon, Dr Harvinder Singh, Dr. Dipankar Sengupta** and **Dr. Hemant Sood** for constantly encouraging and guiding me in my research endeavours. I am thankful to support staff especially **Mrs. Somlata Sharma** and **students** of Jaypee University of Information Technology, for their helping attitude and moral support. I will always cherish the years spent in the Department of Biotechnology & Bioinformatics, Jaypee University of Information Technology.

I would like to express my heartfelt gratitude to all those who have contributed directly or indirectly towards obtaining my doctorate degree and apologize if have missed out anyone.

**(Seneha Santoshi)**

## TABLE OF CONTENTS

<b>DECLARATION</b>	<b>IV</b>
<b>CERTIFICATE</b>	<b>V</b>
<b>ACKNOWLEDGMENT</b>	<b>VI-VII</b>
<b>LIST OF FIGURES</b>	<b>X-XII</b>
<b>LIST OF TABLES</b>	<b>XIII -XIV</b>
<b>ABSTRACT OF THE DISSERTATION</b>	<b>XV-XVIII</b>
<b>CHAPTER 1: INTRODUCTION</b>	<b>1 – 36</b>
1.1 INTRODUCTION.....	3-8
1.2 MICROTUBULE SYSTEM AS POTENTIAL TARGET FOR ANTICANCER DRUGS.....	7-16
1.3 NOSCAPINE AND ITS ANALOGS: A NEW CLASS OF MICROTUBULE BINDING DRUGS.....	17-27
1.4 ORGANIZATION OF THE THESIS WORK.....	27-28
REFERENCES.....	29-36
<b>CHAPTER 2: RATIONAL DESIGN OF NOVEL NOSCAPINOIDS USING LIGAND BASED (QSAR) APPROACH, THEIR THEORETICAL EVALUATION, SYNTHESIS AND BIOLOGICAL EVALUATION.</b>	<b>37 - 66</b>
ABSTRACT.....	39
2.1 INTRODUCTION.....	40
2.2 MATERIALS & METHODS.....	40-50
2.3 RESULTS & DISCUSSIONS.....	50-63
2.4 CONCLUSION.....	63-64
REFERENCES.....	65-66
<b>CHAPTER 3: MOLECULAR INSIGHT OF ISOTYPES SPECIFIC <math>\beta</math>-TUBULIN INTERACTION OF TUBULIN HETERODIMER WITH NOSCAPINOIDS.</b>	<b>67-124</b>
ABSTRACT.....	69
3.1 INTRODUCTION.....	70-72
3.2 MATERIALS & METHODS.....	72-78
3.3 RESULTS & DISCUSSIONS.....	78-116

3.4 CONCLUSION.....	116-117
REFERENCES.....	118-124

## **CHAPTER 4: RATIONAL DESIGN OF BIARYL PHARMACOPHORE SUBSTITUTED NOSCAPINE DERIVATIVES AS POTENT TUBULIN BINDING ANTICANCER AGENTS. 125-166**

ABSTRACT.....	127
4.1 INTRODUCTION.....	128-129
4.2 MATERIALS & METHODS.....	130-141
4.3 RESULTS & DISCUSSIONS.....	141-160
4.4 CONCLUSION.....	161
REFERENCES.....	162-166

## **CONCLUSION AND FUTURE DIRECTION 167-172**

## **APPENDIX 173-198**

## **LIST OF PUBLICATIONS 199-201**

## LIST OF FIGURES

- Figure 1.1** Continental distribution of cancer cases. Visual depiction of the estimates projected by the American Cancer society in 2007.
- Figure 1.2** Year wise total cancer prevalence in India [ICMR, 2006; ICMR, 2009].
- Figure 1.3** The most common cancers found in India in comparison to USA.
- Figure 1.4** Proportions of various mechanisms/drugs currently in-use in anti-cancer therapy.
- Figure 1.5** Molecular structure of tubulin hetero-dimer consisting of  $\alpha$ - and  $\beta$ -tubulin.
- Figure 1.6** Microtubules having 13 linear protofilaments forming the wall of the hollow tube and these protofilaments in turn result from a head-to-tail assembly of tubulin dimmers.
- Figure 1.7** Microtubule dynamics and the measured dynamic parameters.
- Figure 1.8** The structure of various tubulin interacting agents sharing structural similarity with the promising tubulin binding agent Noscapine (from opium poppy).
- Figure 1.9** Noscapine as tubulin binding agent. Titration of fluorescence spectra of tubulin and Scatchard plot.
- Figure 1.10** Figure showing that noscapine increases the average time cellular microtubules remain inactive (pause duration).
- Figure 1.11** Halogenated derivatives of noscapine.
- Figure 1.12** Aryl-derivatives of noscapine.
- Figure 1.13** Design strategy for new  $\alpha$ -noscapine analogues.
- Figure 1.14** The overview of structure based drug design cycle.
- Figure 1.15** The schematic representation of various steps of QSAR model building and prediction.
- Figure 2.1** View of noscapine with the atom-labelling scheme.
- Figure 2.2** Two-dimensional NOESY spectrum of noscapine.
- Figure 2.3** Two most probable noscapine conformations in solution derived from the NOESY spectroscopy followed by NAMFIS analysis.
- Figure 2.4** Elucidation of dynamic structure of noscapine.
- Figure 2.5** Schematic representations of different steriomolecular parameters used in the study.
- Figure 2.6** Relationship between predicted and experimental biological activities of training set compounds as per the final QSAR equation.
- Figure 2.7** Relationship between predicted and experimental biological activities of test set compounds as per the final QSAR equation.
- Figure 2.8** Synthesis of 9-azido-noscapine and reduced 9-azido-noscapine.
- Figure 3.1** Multiple sequence alignment of the stretches of amino acids located in or near the 12 Å of the binding site of noscapinoids in  $\alpha$ -tubulin in the tubulin heterodimer.

<b>Figure 3.2</b>	Snapshots of pdb file 1SA0 showing errors in numbering in $\beta$ chain.
<b>Figure 3.3</b>	Representation of gaps (missing residues) in the crystal structure (1SA0) of tubulin dimer showing the gaps in the structure.
<b>Figure 3.4</b>	Screen shot of missing residues in $\alpha$ (A) and $\beta$ (B) chain shown in the pdb file (1SA0).
<b>Figure 3.5</b>	Chemical structure of noscapine and its derivatives used in the study.
<b>Figure 3.6</b>	Multiple sequence alignment of $\beta_I$ - $\beta_{VIII}$ isotypes showing mismatches at certain places.
<b>Figure 3.7</b>	Modeled tubulin dimer along with ligand colchicine, GTP and GDP with gaps filled.
<b>Figure 3.8</b>	Figure showing the superimposition of the 1SA0 template and the modeled tubulin dimer.
<b>Figure 3.9</b>	Typical snapshots of pdb file showing C $\alpha$ coordinates of the filled gap in $\alpha$ (A) chain and $\beta$ (B).
<b>Figure 3.10</b>	Pairwise alignment between sequences of modeled structure of chain A and chain B and template 1SA0 chains A & B along with secondary structure alignment.
<b>Figure 3.11</b>	Structure validation diagrams based on Programs Errat, Verify 3D and Procheck (Ramachandran plot).
<b>Figure 3.12</b>	Time series of the root-mean-square deviations (RMSD) for the C $\alpha$ carbon atoms of template ( $\alpha\beta$ ) and all the 8 tubulin isotypes ( $\alpha\beta_I$ to $\alpha\beta_{VIII}$ ) during 10 ns of MD simulation starting from the initial structure.
<b>Figure 3.13</b>	Superimposition of $\alpha\beta$ -tubulin isotypes ( $\alpha\beta_I$ to $\alpha\beta_{VIII}$ ) with the template structure (1SA0).
<b>Figure 3.14(a-h)</b>	All-vs-all structure superimposition and comparison of the $\alpha\beta$ -tubulin isotypes.
<b>Figure 3.15</b>	Superimposition of the noscapinoid binding site of the template structure (1SA0) and all the 8 isotypes of tubulin ( $\alpha\beta_I$ - $\beta_{VIII}$ ).
<b>Figure 3.16(a-h)</b>	All-vs-all superimposition and comparison of the noscapinoid binding site of the amino acids within 12 Å diameter of noscapinoid binding site of the different $\alpha\beta$ -tubulin isotypes.
<b>Figure 3.17</b>	The hydrogen bonding pattern of amino-noscapine with respect to all the $\alpha\beta$ -tubulin isotypes.
<b>Figure 3.18</b>	Differences in the electrostatic and van der Waals energy contribution of residues within the 12 Å diameter of noscapinoid binding site of docked amino-noscapine with respect to $\beta_I$ - $\beta_{VIII}$ -tubulin isotypes.
<b>Figure 3.19</b>	Typical snapshot of binding mode of amino-noscapine with tubulin obtained after MD simulation.
<b>Figure 3.20</b>	The root-mean square deviations (RMSD) of C $\alpha$ carbon atoms of tubulin during 10 ns of MD simulation of the docking complexes of $\alpha\beta_{III}$ with amino-noscapine, bromo-noscapine and noscapine.

<b>Figure 3.21</b>	Root mean square fluctuation (RMSF) of residues around the ligand binding site of $\alpha\beta_{III}$ (13-393) complexed with amino-noscapine, bromo-noscapine and noscapine.
<b>Figure 3.22</b>	Per residue binding free energy ( $\delta G_{\text{bind}}$ ) contribution of $\alpha\beta_{III}$ for the binding of noscapine, bromo noscapine and amino-noscapine.
<b>Figure 3.23</b>	Energy decomposition of the key residues (contributing $\delta G_{\text{bind}} < -1.0$ kcal/mol) in $\alpha\beta_{III}$ that are involved in the binding of noscapine, bromo noscapine and amino-noscapine.
<b>Figure 4.1</b>	Natural and synthetic analogues that are acting as microtubule targeting agents.
<b>Figure 4.2</b>	Molecular structure of newly designed noscapinoids, <b>5a-5f</b> in this study.
<b>Figure 4.3</b>	Molecular structure of previously reported noscapinoids used in the training set.
<b>Figure 4.4</b>	Optimized Suzuki coupling reaction conditions for synthesis of noscapine derivatives <b>5a-f</b> .
<b>Figure 4.5</b>	Design strategy for new biaryl type $\alpha$ -noscapine congeners
<b>Figure 4.6</b>	The root-mean square deviations (RMSD) of C $\alpha$ carbon atoms of tubulin during 10 ns of MD simulation of tubulin–ligand complexes with respect to initial structures as a function of time.
<b>Figure 4.7</b>	Root mean square fluctuation (RMSF) of the residues of tubulin within 20 Å diameter (includes 13-393 residues) of the docked ligands in the bound form and in the unbound form of tubulin heterodimer.
<b>Figure 4.8</b>	The newly designed noscapinoids <b>5a-5f</b> shown to be well accommodated in the noscapinoid binding site at the interface between $\alpha$ - and $\beta$ - tubulin.
<b>Figure 4.9</b>	Typical snapshot of the binding mode of noscapinoids <b>5a-5f</b> with tubulin.
<b>Figure 4.10</b>	Total binding energy ( $\delta G_{\text{bind}}$ ) contribution on per residue basis in tubulin-drug complexes.
<b>Figure 4.11</b>	Decomposition of the binding energy on per residue basis of the key residues in tubulin-drug complexes.
<b>Figure 4.12</b>	A view of <b>5b</b> , (crystal structure) showing the atom-labelling scheme.
<b>Figure 4.13</b>	The tubulin fluorescence emission intensity is quenched by noscapinoids <b>5a</b> , <b>5c</b> , <b>5d</b> and <b>5e</b> in a concentration dependent manner
<b>Figure 4.14</b>	Panels showing morphological evaluation of nuclei stained with DAPI in the absence and presence of the analogues (25 $\mu$ M each).
<b>Figure 4.15</b>	Noscapine analogs inhibit cell cycle progression at mitosis followed by the appearance of a characteristic hypodiploid (sub-G1) DNA peak, indicative of apoptosis.
<b>Figure 4.16</b>	Panels represent H&E staining of paraffin-embedded 5 micron-thick sections of the liver, kidney, spleen, lung, heart, duodenum and brain at magnifications 200x and 400x.
<b>Figure 4.17</b>	Panel showing blood biochemical parameters between control and treated groups



## LIST OF TABLES

<b>Table 1.1</b>	Drugs currently used for cancer treatment.
<b>Table 1.2</b>	Inhibitors of tubulin polymerization in clinical development.
<b>Table 1.3</b>	Promoters of tubulin polymerization in clinical development.
<b>Table 2.1</b>	Chemical structures of noscapine and its congeners used in the study.
<b>Table 2.2</b>	Crystal data and structure refinement for noscapine.
<b>Table 2.3</b>	Experimental and theoretical values of the isoquinoline and isobenzofuranone ring parameters (bond lengths in Å, bond angles and torsional angles in degrees).
<b>Table 2.4</b>	Atomic coordinates ( $\times 10^4$ ) and equivalent isotropic displacement parameters ( $\text{\AA}^2 \times 10^3$ ) for noscapine.
<b>Table 2.5</b>	Anisotropic displacement parameters ( $\text{\AA}^2 \times 10^3$ ) for noscapine.
<b>Table 2.6</b>	The results of multiple linear regression (MLR) analysis with different type of descriptors.
<b>Table 2.7</b>	Predicted anti-tumor activity of the training set compounds.
<b>Table 2.8</b>	Predicted anti-tumor activity of the test set compounds.
<b>Table 2.9</b>	Predicted biological activity ( $\text{pIC}_{50}$ ) obtained from the QSAR models and experimental biological activity for the designed set of noscapinoids.
<b>Table 3.1</b>	Tissue distribution of $\beta$ -tubulin isotypes in normal cells.
<b>Table 3.2</b>	Mismatches in amino acids comprising the noscapinoid binding site among different $\beta$ isotypes in comparison to the template (1SA0).
<b>Table 3.3</b>	All-vs-all structure comparison of the $\alpha\beta$ -tubulin isotypes.
<b>Table 3.4</b>	Physico-chemical properties of the noscapinoid bind site of different $\alpha\beta$ -tubulin isotypes as calculated from SiteMap.
<b>Table 3.5</b>	All-vs-all comparison of the amino acids within 12 Å diameter of noscapinoid binding site of the different $\alpha\beta$ -tubulin isotypes.
<b>Table 3.6</b>	Docking results (Glide XP) of noscapinoids with different $\alpha\beta$ -tubulin isotypes.
<b>Table 3.7</b>	Binding free energy and its components (kcal/mol) for the receptor, $\alpha\beta_{\text{III}}$ heterodimer and noscapine derivatives.
<b>Table 3.8</b>	Hydrogen bonding (H-bond) patterns between the residues of $\alpha\beta_{\text{III}}$ with amino-noscapine, bromo-noscapine and noscapine.
<b>Table 4.1</b>	Grouping of the experimental animals as acute, sub-acute and vehicle (control) treatment and the dosage and duration of dosage.
<b>Table 4.2</b>	Molecular docking results (Glide XP) as well as calculated energies based on LIE-SGB model of training set noscapine derivatives.

<b>Table 4.3</b>	Molecular docking results (Glide XP) as well as calculated energies based on LIE-SGB model of newly designed noscapinoids ( <b>5a-5f</b> ).
<b>Table 4.4</b>	Change in binding free energy and its components (kcal/mol) for the noscapine derivatives <b>5a-5f</b> binding with tubulin.
<b>Table 4.5</b>	IC <sub>50</sub> values of noscapine derivatives <b>5a-5f</b> for various cancer cell types.
<b>Table 4.6</b>	Effect of noscapine derivatives on cell cycle progression of MCF-7 cells treated with 25 $\mu$ M solution for the indicated time.

## ABSTRACT OF THE DISSERTATION

Microtubules are major cytoskeletal structures responsible for maintaining genetic stability during cell division. The dynamics of these polymers are absolutely crucial for this function that can be described as their growth rate at the plus ends, catastrophic shortening, frequency of transition between the two phases, pause between the two phases, their release from the microtubule organizing center and treadmilling. Interference with microtubules dynamics often leads to programmed cell death and thus microtubule-binding drugs such as paclitaxel, docetaxel and the vinca alkaloids are currently used to treat various malignancies in the clinic. However, these chemotherapy drugs are confounded by complications with serious toxicity (particularly, peripheral neuropathies, gastrointestinal toxicity, myelosuppression and immunosuppression) owing to their non-selective action and extreme overpolymerizing effects (by taxanes) or depolymerizing effects (by vincas) on microtubules. Thus, there is an urgent need to explore novel tubulin-binding agents that are significantly effective and comparatively less toxic compared to currently-available drugs for the treatment of human cancers. Systematic screening of new compounds based on structural similarity of known drugs (such as colchicine, podophyllotoxin, etc.) that interfere with microtubules has led to the discovery of noscapine, an opium alkaloid, that binds stoichiometrically to tubulin, alters its conformation upon binding and arrests mammalian cells in mitosis. It was demonstrated that unlike many other microtubule inhibitors, noscapine does not significantly promote or inhibit microtubule polymer mass even at high concentrations. Instead, it alters the steady-state dynamics of microtubule assembly, primarily by increasing the amount of time that the microtubules spend in an attenuated (pause) state when neither microtubule growth nor shortening is detectable. As a result of this and compromised checkpoints, cancer cells selectively get killed by noscapinoids, while unaffected the normal cells. In addition, noscapine has some other advantageous properties as lead molecule: (1) retains activity against paclitaxel-resistant cell line (1A9/PTX10, 1A9/PTX22) and epothilone-resistant cell line (1A9/A8); (2) has a favourable pharmacokinetics (clearance in 6-10 hours); (3) is a poor substrate for drug-pumps (polyglycoproteins and MDR-related proteins) that comprise a major cause of drug resistance; (4) it does not show immunological and neurological toxicities and (5) inhibits tumorigenesis *in vivo* albeit at high concentrations (~ 300 mg/kg body weight). Although noscapine is cytotoxic in a variety of different cancer cell lines (NCI 60 cell lines panel), the IC<sub>50</sub> values remain in the high micromolar ranges (~21.1 to 100  $\mu$ M). For further enhancing its activity, research is being focused on rational drug design and synthesis of a new generation of noscapine derivatives (we called as noscapinoids) for better therapeutic outcome.

Availability of structure activity data of many derivatives of noscapine could lead to development of a reasonable prediction model and thus guide in rational design of more potent derivatives of noscapine. Furthermore, chemical synthesis and experimental evaluations of newly designed potent noscapinoids could indicate their great potential as chemotherapeutic agents for the treatment of human cancers to treat various malignancies in the clinic. This inspired me to use both the ligand based and structure based computer aided drug design approaches to design novel derivatives of noscapine. In the ligand based computer aided molecular design approach I have developed a QSAR model for predicting the anti-cancer activity of noscapinoids as well as to design new derivatives of noscapine. To develop QSAR model a data set of 32 previously reported noscapinoids was used. Anti-cancer activity (measured as IC<sub>50</sub> value) of these compounds was experimentally determined using human acute lymphoblastic leukemia cells (CEM) which vary from 1.2 to 56.0  $\mu$ M. To develop the QSAR model, the biologically active conformations of the compounds were obtained by performing geometrical optimization using semi-empirical quantum chemical calculations at 3-21G\* level. These conformations were screened out in reference to the experimentally obtained structure with NMR Analysis of Molecular Flexibility in Solution--NAMFIS, and crystal structure of noscapine. Genetic function approximation algorithm of variable selection was used to generate the QSAR model. The robustness of the QSAR model ( $R^2 = 0.942$ ) was analyzed by the values of the internal cross-validated regression coefficient ( $R^2_{\text{LOO}} = 0.815$ ) for the training set and determination coefficient ( $R^2_{\text{test}} = 0.817$ ) for the test set. The appearance of the electronic descriptors such as electronegativity, electrophilicity and softness (calculated from HOMO and LUMO energies) in the QSAR model demonstrates that these descriptors significantly influence the anti-tumor activity of noscapinoids. They favor columbic interaction between ligands and receptor. Therefore, the developed QSAR model guided us to substitute a functional group such as “azido” ( $\text{N}^- = \text{N}^+ = \text{N}^-$ ), satisfying the above descriptors in the scaffold structure of noscapine pertaining to better anti-tumor activity. I have designed two new derivatives of noscapine, 9-azido-noscapine and reduced-9-azido-noscapine and these compounds were predicted to have better activity, than the lead compound, by the QSAR model. Validation was achieved by synthesis and experimental determination of pIC<sub>50</sub> for both the compounds (5.585  $\mu$ M) which turned out to be very close to predicted pIC<sub>50</sub> (5.731 and 5.710  $\mu$ M). Thus it was established that the model has a high predictive power for the further design of better noscapinoids as well as would perform as a good rapid screening tool to uncover new and more potent anti-tumor drugs based on noscapine derivatizations.

In my attempt of analyzing molecular interaction of noscapinoids with tubulin heterodimer with a special focus on isotypes of  $\beta$ -tubulin, I have used the structure based approach. Tubulin molecule is composed of  $\alpha$ - and  $\beta$ -tubulin, which exist as various isotypes whose distribution and drug-binding properties are significantly different. Although noscapinoids are found to bind at the interface of two dimers, their interaction is more biased towards  $\beta$ -tubulin. To achieve this, a set of already known noscapine derivatives was used to study the molecular interactions. The structures of tubulin heterodimers comprising different isotypes of  $\beta$ -tubulin are not available. Therefore molecular structures of tubulin dimers composed of  $\alpha$ - and different  $\beta$ -tubulin isotypes were modelled based on the crystal structure of tubulin. The modelled structures of the tubulin isotypes were analyzed to reveal differences in the conformation and the environment of the noscapinoid binding site, which could affect the binding of noscapinoids with different isotypes. The binding affinity of a known set of noscapinoids with each type of tubulin was evaluated using molecular docking. It was found that the binding score of a specific noscapinoid with each type of tubulin isotype is different. Specifically, amino-noscapine has the highest binding score of -6.432, -7.179, -7.416 and -7.417 kcal/mol with  $\alpha\beta_I$ ,  $\alpha\beta_{II}$ ,  $\alpha\beta_{III}$  and  $\alpha\beta_{IV}$  isotypes, respectively. Similarly compound **10** (a noscapine derivative) showed a higher binding affinity of -6.792 kcal/mol with  $\alpha\beta_V$ , whereas compound **8** (a noscapine derivative) has highest binding affinity of -7.182, -7.136 and -7.236 kcal/mol, respectively with  $\alpha\beta_{VI}$ ,  $\alpha\beta_{VII}$  and  $\alpha\beta_{VIII}$  isotypes. In particular the specific interaction of  $\alpha\beta_{III}$ - tubulin isotype (overexpression of  $\alpha\beta_{III}$  has been associated with resistance to a wide range of chemotherapeutic drugs for several human malignancies) with noscapine, amino-noscapine (the most potent derivative) and bromo noscapine (the clinical derivative) was investigated using MD simulation, MMGBSA and MMPBSA approaches. All the three ligands showed better binding affinity with  $\alpha\beta_{III}$  in the pattern of amino-noscapine (-34.70 and -46.23 kcal/mol), bromo-noscapine (-32.05 and -38.09 kcal/mol) and noscapine (-28.02 and -38.86 kcal/mol) based on both MM-PBSA and MM-GBSA calculations. All the three ligands (noscapine, bromo-noscapine and amino-noscapine) were well accommodated into the binding site of  $\alpha\beta_{III}$ -tubulin isotype, at the interface between  $\alpha$ - and  $\beta$ - tubulin, however, their binding interactions with the amino acids inside the binding cavity were distinct as the binding site residues of  $\alpha\beta_{III}$ -tubulin isotype contributed differently towards binding. But it was observed that some of the amino acids, Ser 239, Leu253, Ile 368, consistently contributed to the binding energy for all the three ligands, indicating their importance in interaction with the ligands targeted towards  $\alpha\beta_{III}$ -tubulin isotype. The information gained in this study about the isotype specificity of a noscapinoid could pave a way for more efficient design of novel noscapinoid, which could be specifically targeted towards cancer cells.

In pursuit of developing novel noscapinoid with improved anti-cancer activity, I have used structure based drug design approach. I have strategically designed a series of noscapine derivatives by substituting biaryl pharmacophore (a major structural constituent of many of the microtubule-targeting natural anticancer compounds) onto the scaffold structure of noscapine. Molecular interaction of these derivatives with  $\alpha\beta$ -tubulin heterodimer was investigated by molecular docking, molecular dynamics simulation, and binding free energy calculation. The predictive binding affinity indicates that the newly designed noscapinoids bind to tubulin with a greater affinity. The predictive binding free energy ( $\Delta G_{\text{bind,pred}}$ ) of these derivatives (ranging from -5.568 to -5.970 kcal/mol) based on linear interaction energy (LIE) method with a surface generalized Born (SGB) continuum solvation model showed improved binding affinity with tubulin compared to the lead compound, natural  $\alpha$ -noscapine (-5.505 kcal/mol). Guided by the computational findings, these new biaryl type  $\alpha$ -noscapine congeners were synthesized from 9-bromonoscapine using optimized Suzuki reaction conditions for further experimental evaluation. The derivatives showed improved inhibition of the proliferation of human breast cancer cells (MCF-7), human cervical cancer cells (HeLa) and human lung adenocarcinoma cells (A549) compared to natural noscapine. The cell cycle analysis in MCF-7 further revealed that these compounds alter the cell cycle profile and cause mitotic arrest at G2/M phase more strongly than noscapine. Tubulin binding assay revealed higher binding affinity to tubulin, as suggested by dissociation constant ( $K_d$ ) of  $126 \pm 5.0 \mu\text{M}$  for **5a**,  $107 \pm 5.0 \mu\text{M}$  for **5c**,  $70 \pm 4.0 \mu\text{M}$  for **5d**, and  $68 \pm 6.0 \mu\text{M}$  for **5e** compared to noscapine ( $K_d$  of  $152 \pm 1.0 \mu\text{M}$ ). In fact, the experimentally determined value of  $\Delta G_{\text{bind,expt}}$  (calculated from the  $K_d$  value) are consistent with the predicted value of  $\Delta G_{\text{bind,pred}}$  calculated based on LIE-SGB. Based on these results, one of the derivatives (**5e**) of this series was used for further toxicological evaluation. Treatment of mice with a daily dose of 25 mg/kg and a single dose of 50 mg/kg indicate that the compound does not induce detectable pathological abnormalities in normal tissues. Also there was no significant difference in hematological parameters between the treated and untreated groups. Hence the newly designed noscapinoid, **5e** is an orally bioavailable, safe and effective anticancer agent with a potential for the treatment of cancer and might be a candidate for clinical evaluation.

# **CHAPTER – 1**

## **INTRODUCTION**

## Chapter 1



## 1.1 INTRODUCTION

Cancer is one of the leading causes of death. It is a class of diseases in which a group of cells display uncontrolled growth, invasive intrusion, destruction of adjacent tissues, and metastasis to other locations in the body via lymph and/or blood. Cancer may affect people at all ages, even foetuses, but the risk for most varieties increases with age throughout the world (Figure 1.1). While a cure for cancer is still a dream, considerable advances have been made in curbing the suffering and the progression of this devastating disease, which has taken the centre stage in the arena of healthcare professionals.

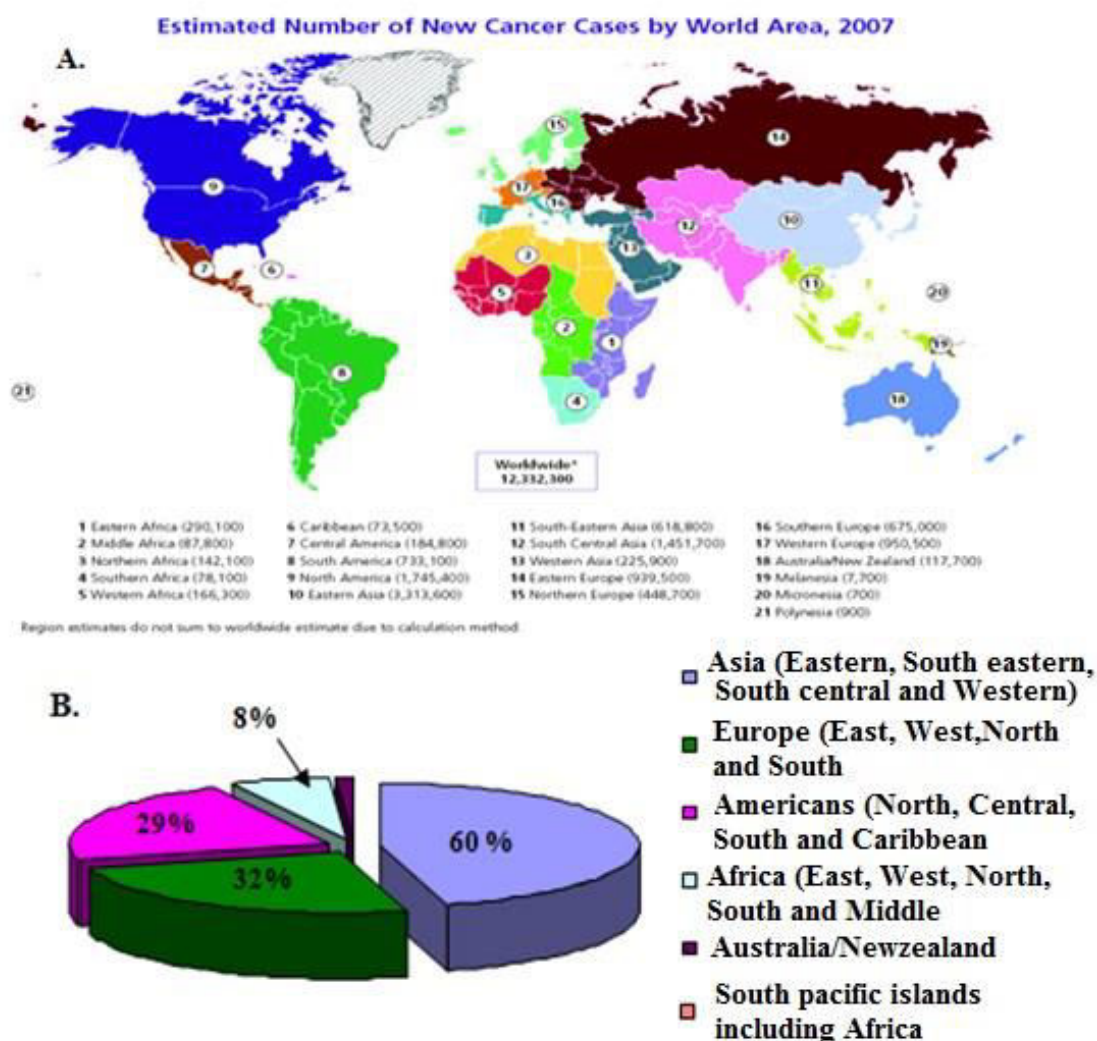


Figure 1.1. Continental distribution of cancer cases. (A). Visual depiction of the estimates projected by the American Cancer society in 2007. (B). Compilation of data from panel A. This compilation clearly notes Asia as the leader with 5.6 million notes only around 764 thousand cases. Interestingly, Australia, New Zealand taken together projected only around 117 thousand cases. This figure, presents the stark realization that cancer cannot be viewed as a disease of wealthy, and it should be a united global effort to find curative/palliative measures.

According to the latest report released in December 2013 by International Agency for Research on Cancer (IARC), the specialized cancer agency of the World Health Organization, global burden of cancer rises to 14.1 million new cases and 8.2 million deaths in 2012. The report provides information on existence of 28 types of cancers in 184 countries worldwide. The most common cancers diagnosed worldwide were those of lung (1.8 million, 13.0% of the total), breast (1.7 million, 11.95 of the total) and colorectum (1.4 million, 9.7%). The most common causes of cancer deaths were cancers of the lung (1.6 million, 19.4% of the total), liver (0.8 million, 9.1%), and stomach (0.7 million, 8.8%). This is the second most common disease after cardiovascular disorders for maximum deaths in the world. In the context of India, cancer is the second most common disease responsible for maximum mortality with about 0.3 million deaths per year. According to the cancer data compiled from 2004 to 2010 by ICMR (Figure 1.2), the number of male, female and the total cancer patients in 2004 were 390809, 428545 and 819354 respectively. The number of male and female cancer patients increased continuously up to 2009, with 454842, 507990 and 962832 cases for male, female and total cancer patients, respectively. Similarly, 462408 male cancer patients and 517378 female cancer patients were recorded, with a total number of 979786 patients in 2010. Thus, it is clear from the figure that the number of cancer cases has increased gradually with time. All types of cancers have been reported in Indian population including the cancers of skin, lungs, breast, rectum, stomach, oral, pharyngeal, prostate, liver, cervix, esophagus, bladder, blood etc. Among these lung, oesophagus, stomach and oral cancers are most common in men, where as in women, cervix and breast cancers are most common in India in comparison to USA Figure 1.3.

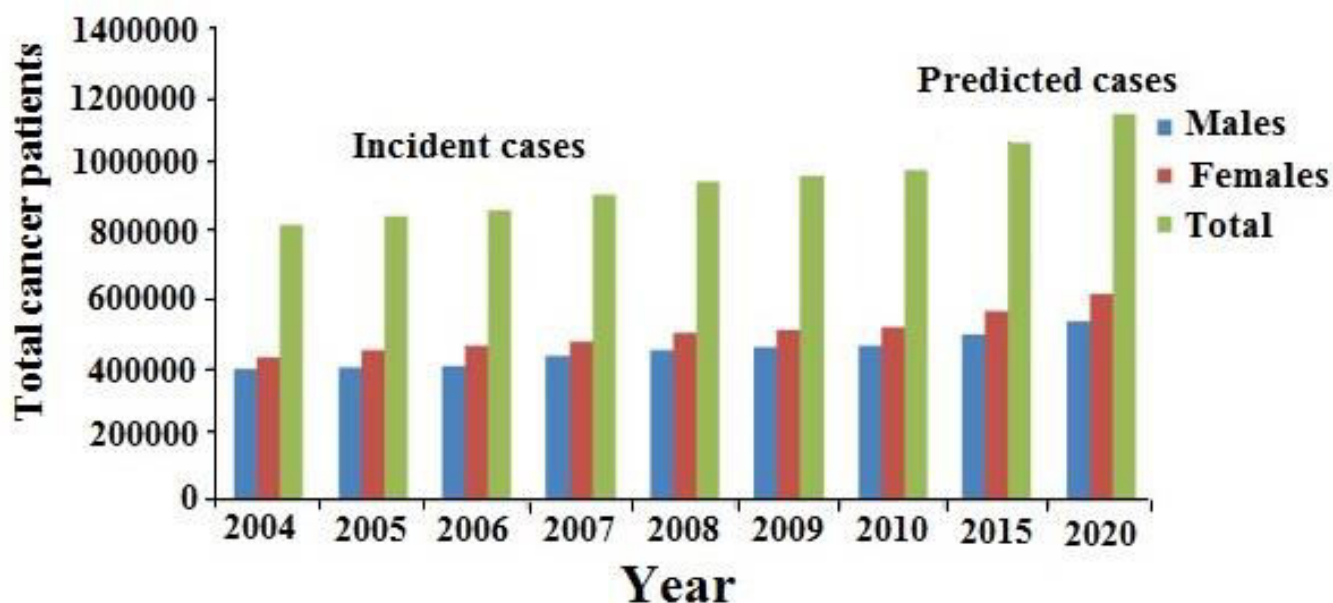


Figure 1.2. Year wise total cancer prevalence in India [ICMR, 2006; ICMR, 2009].

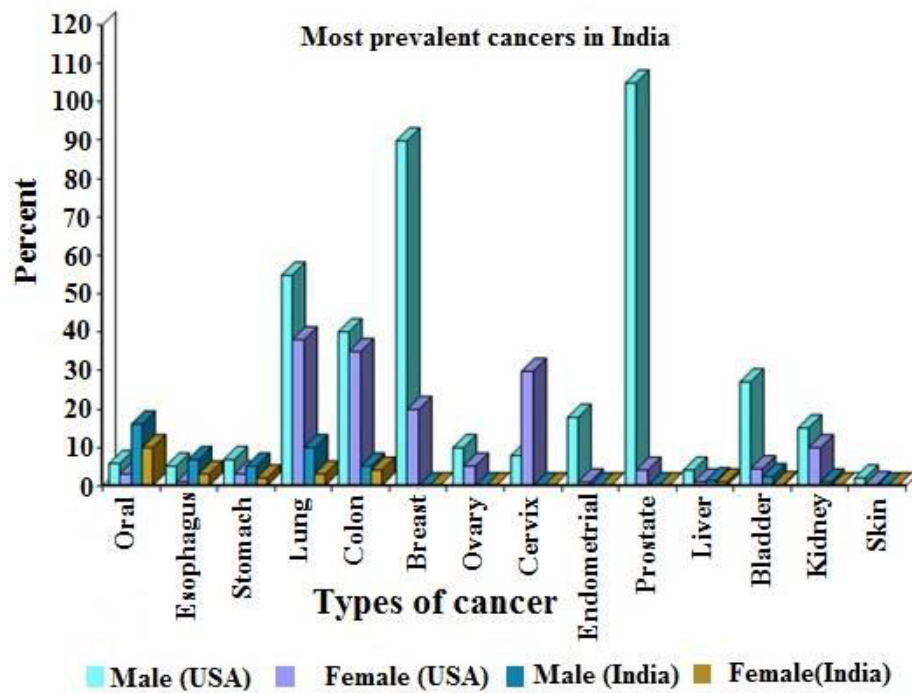


Figure 1.3. The most common cancers found in India in comparison to USA. Source - Cancer Scenario in India with Future Perspectives, Cancer Therapy Vol 8, 56-70, 2011.

### 1.1.1 Cancer treatments

Due to vast work in the field of cancer, we have gained remarkable new knowledge about the exact steps necessary for cancer cells to grow, divide, and spread. This has opened the door for new and better ways to stop or reverse these steps. Besides the conventional major targets such as DNA integrity/metabolism, several more specific new targets have continually been emerging. The relative contributions to date, of various targets of cancer therapeutic regimens are depicted graphically in Figure 1.4.

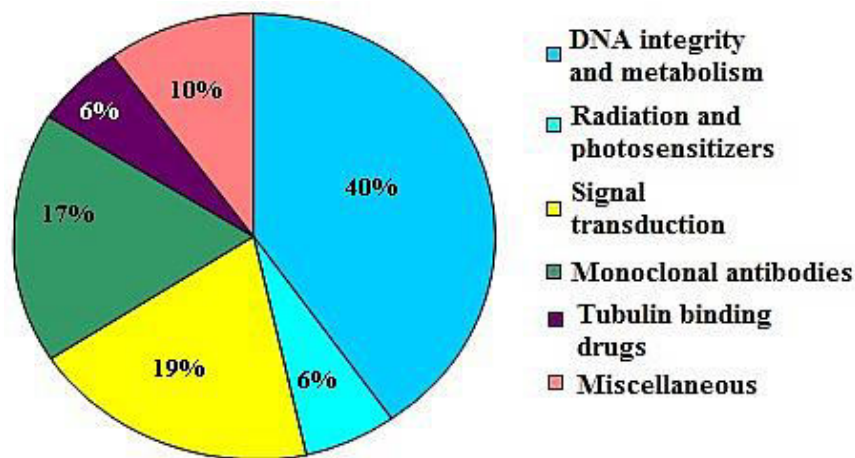


Figure 1.4. Proportions of various mechanisms/drugs currently in-use in anti-cancer therapy.(compiled using table 1.1)

## Chapter 1

Chemotherapy is the general term for any treatment involving the use of chemical agents to stop cancer cells from multiplying. These chemical agents can work by any of the mechanisms such as interfering with DNA metabolism, cell division or signal transduction. Because of the systemic administration and generalized bioavailability, these treatment regimens can eliminate cancer cells at sites great distances from the original cancer. Chemotherapy remains a widely used means of treatment, prevention of reoccurrence and palliative care for a variety of cancer types. Therefore, not surprisingly over half of the patients diagnosed with cancer, receive chemotherapy. Conventionally, these types of agents were identified from the libraries of naturally derived compounds or of chemically synthesized compounds by evaluating their cytotoxicities to identify the promising lead compounds. The technical advances in the robotics, very sensitive yet simple assay systems, and state of the art development in combinatorial chemistry have now become a mainstay of this line of research. In addition, further advances in chirally biased chemical synthetic techniques and the advances in the separation of chiral compounds have now opened up novel vistas in this area. Basically, the drugs that are simply identified by cytotoxicity towards cancer cells do not particularly target the cancer cells exclusively but can equally be cytotoxic to normally dividing cells of the healthy tissues. Although highly cytotoxic, some of these drugs still remain most effective against complex solid tumors such as ovarian and breast as well as some hematological cancers [1-4].(Table 1.1)

Table 1.1. Drugs currently used for cancer treatment. [1-4]

Mode of inhibition	Drugs and their targets
<b>DNA integrity and metabolism</b>	<b>Folic acid metabolism:</b> Dihydrofolate reductase inhibitor (Aminopterin, Methotrexate, Pemetrexed); Thymidylate synthase inhibitor (Raltitrexed, Pemetrexed).
	<b>Purine metabolism:</b> Adenosine deaminase inhibitor (Pentostatin); Halogenated/ribonucleotide reductase inhibitors (Cladribine, Clofarabine, Fludarabine); Thiopurine (Thioguanine, Mercaptopurine).
	<b>Pyrimidine metabolism:</b> Thymidylate synthase inhibitor (Fluorouracil, Capecitabine, Tegafur, Carmofur, Floxuridine); DNA polymerase inhibitor (Cytarabine); Ribonucleotide reductase inhibitor (Gemcitabine); Hypomethylating agent (Azacitidine, Decitabine).
	<b>Deoxyribonucleotides metabolism:</b> Ribonucleotide reductase inhibitor (Hydroxyurea).
	<b>Topoisomerase I inhibitor:</b> Camptotheca (Camptothecin, Topotecan, Irinotecan, Rubitecan, Belotecan).
	<b>Topoisomerase II inhibitor:</b> Podophyllum (Etoposide, Teniposide).
	<b>TopoisomeraseII+ intercalation:</b> Anthracyclines (Aclarubicin, Daunorubicin, Doxorubicin, Epirubicin, Idarubicin, Amrubicin, Pirarubicin, Valrubicin, Zorubicin); Anthracenediones (Mitoxantrone, Pixantrone).

	<p><b>Crosslinkers:</b> <i>Nitrogen mustards:</i> Mechlorethamine; Cyclophosphamide (Ifosfamide, Trofosfamide); Chlorambucil (Melphalan, Prednimustine); Bendamustine; Uramustine; Estramustine.</p> <p><b>Nitrosoureas:</b> Carmustine; Lomustine (Semustine); Fotemustine; Nimustine; Ranimustine; Streptozocin.</p> <p><b>Alkyl sulfonates:</b> Busulfan (Mannosulfan, Treosulfan).</p> <p><b>Aziridines:</b> Carboquone; ThioTEPA; Triaziquone; Triethylenemelamine; Platinum (Carboplatin, Cisplatin, Nedaplatin, Oxaliplatin, Triplatin tetranitrate, Satraplatin); Hydrazines (Procarbazine); Triazines (Dacarbazine, Temozolomide); Altretamine; Mitobronitol; Streptomyces (Actinomycin, Bleomycin, Mitomycin, Plicamycin).</p>
<b>Radiation and photosensitizers</b>	<p><b>Radiation therapy:</b> High-energy radiation from x-rays, gamma rays, neutrons, protons, and other sources.</p> <p><b>Photosensitizers:</b> Aminolevulinic acid/Methyl aminolevulinate; Efaproxiral; Porphyrin derivatives (Porfimer sodium, Talaporfin, Temoporfin, Verteporfin).</p>
<b>Signal Transduction</b>	<p><b>Receptor tyrosine kinase inhibitors:</b> <i>ErbB:</i> HER1/EGFR (Erlotinib, Gefitinib, Lapatinib, Vandetanib, Neratinib); HER2/neu (Lapatinib, Neratinib)</p> <p><b>RTK class III:</b> C-kit (Axitinib, Sunitinib, Sorafenib); FLT3 (Lestaurtinib); PDGFR (Axitinib, Sunitinib, Sorafenib); VEGFR (Vandetanib, Semaxanib, Cediranib, Axitinib, Sunitinib, Sorafenib).</p> <p><b>Non receptor tyrosine kinase inhibitors:</b> bcr-abl (Imatinib, Nilotinib, Dasatinib), Src (Bosutinib), Janus kinase 2 (Lestaurtinib).</p> <p><b>Enzyme inhibitors:</b> Farnesyl transferase FI (Tipifarnib); CDK inhibitors (Alvociclib, Seliciclib); proteasome inhibitor PrI (Bortezomib); PDE II inhibitor PhI (Anagrelide); Imp dehydrogenase inhibitor IMPDI (Tiazofurine); Lipoxigenase inhibitor LI (Masoprocol).</p> <p><b>Receptor antagonists/hormones:</b> Endothelial receptor antagonist ERA (Atrasentan); retinoid X receptor (Bexarotene); sex steroid (Testolactone).</p>
<b>Monoclonal antibodies</b>	<p><b>Receptor tyrosine kinase:</b> <i>ErbB:</i> HER1/EGFR (Cetuximab, Panitumumab); HER2/neu (Trastuzumab).</p> <p><b>Solid tumors:</b> EpCAM (Catumaxomab, Edrecolomab); VEGF-A (Bevacizumab).</p> <p><b>Leukemia/lymphoma.</b></p> <p><b>Lymphoid:</b> CD20 (Rituximab, Tositumomab, Ibritumomab).</p> <p><b>Myeloid:</b> CD52 (Alemtuzumab).</p> <p><b>Lymphoid+Myeloid:</b> CD33 (Gemtuzumab).</p> <p><b>Others:</b> Afutuzumab, Alemtuzumab, Bevacizumab/Ranibizumab, Bivatuzumab mertansine, Cantuzumab mertansine, Citatuzumab bogatox, Dacetuzumab, Etaracizumab, Farletuzumab, Gemtuzumab ozogamicin, Inotuzumab ozogamicin, Labetuzumab, Lintuzumab, , Milatuzumab, Nimotuzumab, Oportuzumab monatox, Pertuzumab, Sibrotuzumab, Sontuzumab, Tacatuzumab tetraxetan, Tigatuzumab.</p>

<b>Tubulin binding drugs</b>	<b><i>Inhibit microtubule assembly:</i></b> Vinca alkaloids (Vinblastine, Vincristine, Vinflunine, Vindesine, Vinorelbine) <b><i>Promote microtubule assembly:</i></b> Taxanes (Paclitaxel, Docetaxel, Larotaxel, Ortataxel, Tesetaxel); Epothilones (Ixabepilone)
<b>Miscellaneous</b>	Amsacrine; Trabectedin; Retinoids (Alitretinoin, Tretinoin); Arsenic trioxide; Asparagine depleter (Asparaginase/Pegaspargase); Celecoxib; Demecolcine; Elesclomol; Elsamitrucin; Etoglucid; Lonidamine; Lucanthone; Mitoguazone; Mitotane; Oblimersen; Temsirolimus; Vorinostat

## 1.2 MICROTUBULE SYSTEM AS POTENTIAL TARGET FOR ANTICANCER DRUGS

### 1.2.1 Microtubule structure and dynamics

Microtubules (MTs) are ubiquitous tubular structures that are key component of cytoskeletal structure. They are crucial for the formation and maintenance of the mitotic spindle that, in turn, is responsible for separation of duplicated chromosomes during cell division [5-7]. MTs are dynamic hollow rods approximately 25 nm in diameter and polymers of  $\alpha$ - and  $\beta$ -tubulin dimers that undergo continual assembly and disassembly within the cell. The three dimensional structure of the tubulin heterodimer was obtained by electron crystallography studies (Figure 1.5). Each monomer is asymmetric with approximate dimensions of  $46 \times 40 \times 65$  Å (width, height and depth, respectively) and consists of a core of two sheets surrounded by helices [8]. Functionally, each subunit of tubulin is divided into three domains: the amino terminal domain containing the nucleotide binding region, an intermediate domain and the carboxyl terminal domain that regulate the interaction of drugs such as vinblastine and colchicine [9-11]. Individual MTs comprise 13 linear protofilaments forming the wall of the hollow tube [12-15] and these protofilaments in turn result from a head-to-tail assembly of tubulin dimers (Figure 1.6). Owing to the head-to-tail contact of the  $\alpha$  subunit of one tubulin dimer to the  $\beta$  subunit of the next, one end of the protofilament has  $\alpha$  subunit exposed while the other end is capped by the  $\beta$  subunit [6]. These ends are designated (–) and (+) respectively (Figure 1.6). While the bulk reaction mixture appears to be in chemical equilibrium, individual polymers can continually be in transition between growing and shortening phases, a property aptly named as dynamic instability (Figure 1.7) [16,17]. The transition from a growth phase to a rapid shortening phase is called a “catastrophe” and the transition from a shortening phase to a growth or a pause state is called a “rescue” (Figure 1.6 and 1.7). These two phases are often interrupted by a pause or an attenuated state [16-21]. This results in the continual and rapid turnover of most MTs, which have half-lives of only several minutes within a cell [22-26]. This rapid turnover of MTs is particularly critical for the remodeling of the cytoskeleton that occurs during mitosis.



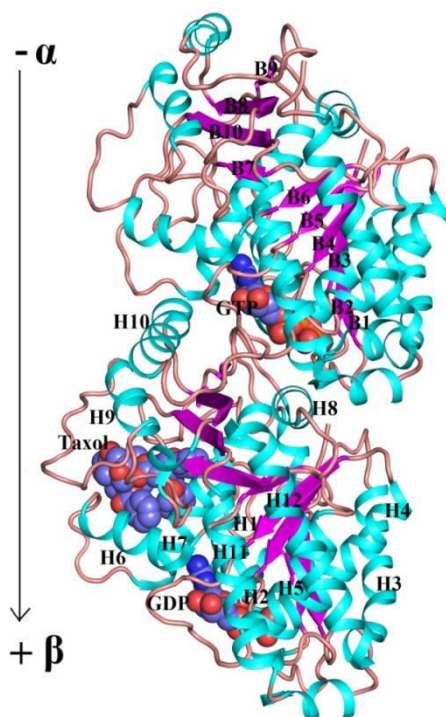


Figure 1.5. Molecular structure of tubulin hetero-dimer consisting of  $\alpha$ - and  $\beta$ -tubulin. Ribbon diagram showing the  $\alpha$ - and  $\beta$ -monomers of tubulin from X-ray crystallographic data at a resolution of 3.7 Å viewed from inside of the microtubules. The tubulin consisted of alpha helix, beta strands and loops. The GTP (non-hydrolyzable) is shown to bind to the  $\alpha$ -monomer whereas GDP (formed from the hydrolysis of GTP, hydrolyzable site of GTP) and Taxol are bound to  $\beta$ -monomer. The arrow indicates the growth of the protofilaments during microtubule formation. [8]

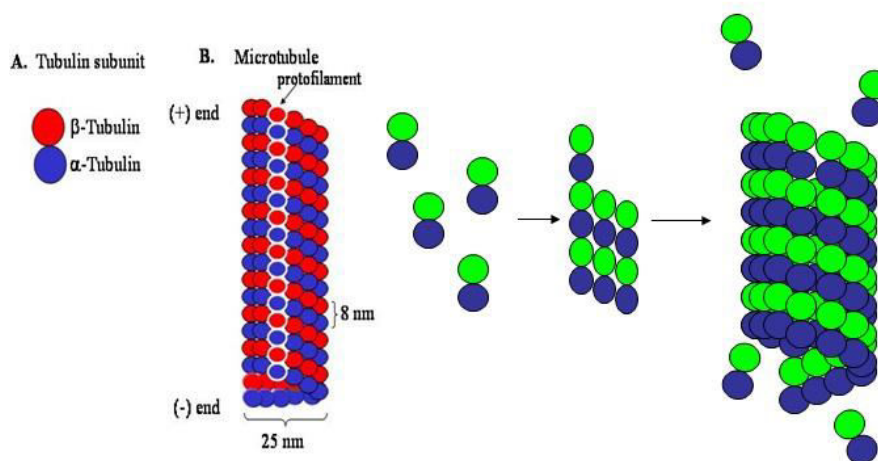
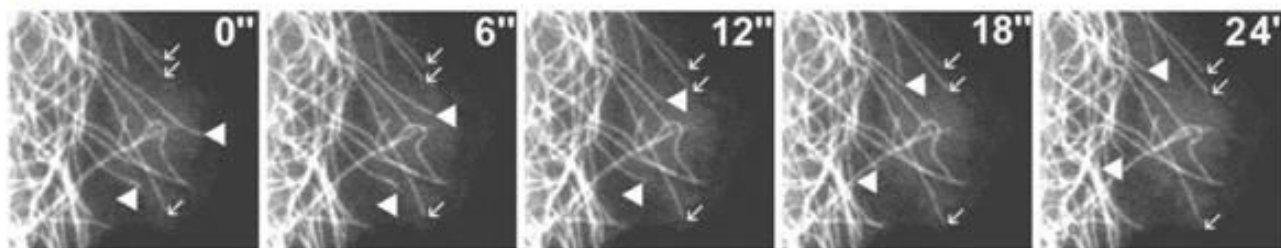
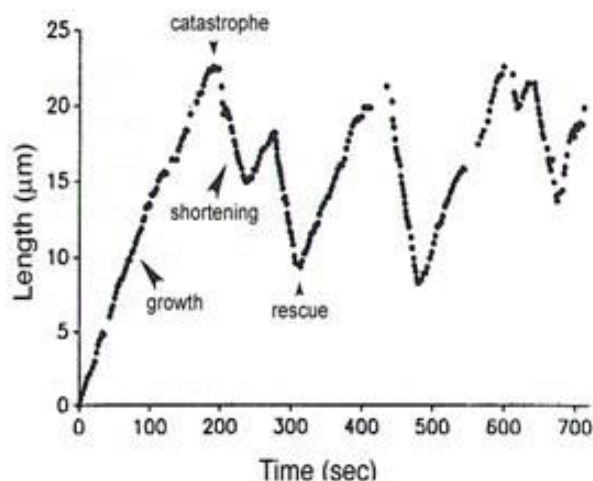


Figure 1.6. Microtubules having 13 linear protofilaments forming the wall of the hollow tube and these protofilaments in turn result from a head-to-tail assembly of tubulin dimers. The head-to-tail contact of the  $\alpha$  subunit of one tubulin dimer to the  $\beta$  subunit of the next, one end of the protofilament has  $\alpha$  subunit exposed while the other end is capped by the  $\beta$  subunit. These ends are designated (-) and (+) respectively.

(A)



(B)



(C)

Dynamic parameters	74 MTs (n=20)
<b>Growth</b>	
Rate (mm/min)	$9.15 \pm 2.72$
Distance (mm)	$1.88 \pm 0.44$
Duration (sec)	$14.33 \pm 1.22$
<b>Shrink</b>	
Rate (mm/min)	$12.04 \pm 3.63$
Distance (mm)	$1.99 \pm 0.56$
Duration (sec)	$13.11 \pm 1.45$
Average pause duration	$8.16 \pm 2.42$
<b>Percentage time per phase</b>	
Growth/ Shrink/ Pause	41.8/36.3/21.8
Rescue frequency (sec <sup>-1</sup> )	$0.077 \pm 0.015$
Catastrophe frequency (sec <sup>-1</sup> )	$0.086 \pm 0.023$
Dynamicity (mm/min)	$6.61 \pm 2.36$

Figure 1.7. Microtubule dynamics and the measured dynamic parameters. (A) A gallery of video frames, 6 seconds apart, showing the plus ends of several microtubules. (B) One representative microtubule plus end behavior is shown. As time goes in seconds the microtubule plus end is growing and growing and all of a sudden the microtubule can revert into a phase of shortening and the shortening can be rescued by another growth phase. So it is continuously growing and shortening as you can see hardly any pausing between both the phases. (C) The measured dynamic parameters of microtubules [26].

### 1.2.2 Microtubule - targeting agents

Microtubule binding drugs can be broadly classified in two groups. The first class comprises drugs that inhibit tubulin polymerization and hence promote MT disassembly. Vinca alkaloids, colchicine, estramustine, and combretastatin are some important drugs of this class. The other class comprises drugs that promote tubulin polymerization and cause MT over assembly. Taxanes, laulimalides, and discodermolides are representatives of this class.

Besides recent advances in the binding interactions of paclitaxel, docitaxel, laulimalides and colchicine, the precise nature of binding site interactions of anti-MT dugs remain a subject of intense research. The tertiary structure of  $\alpha\beta$  tubulin heterodimer was reported in 1998 by Downing and co-workers at a resolution of  $3.7\text{\AA}$  using electron crystallography [8]. Several direct and indirect binding site elucidation techniques have identified three key binding sites on tubulin: (1)



the Colchicine site [28]; (2) the Vinca alkaloid site [29]; and (3) the Taxane binding site on the polymerized MT [30]. These compounds predominantly arrest the cell cycle at prometaphase of mitosis. They affect MT dynamics to different extents, altering the growth rate and duration, shortening rate and duration, the frequency of transitions between the growth and the shortening phases, and the duration of a pause state when neither the growth nor shortening is detectable. Some of these tubulin binding drugs are described below.

### 1.2.2.1 Agents that inhibit polymerization of tubulins

**Drugs binding at Vinca alkaloid-binding sites:** Vinca alkaloids are a subset of drugs that are derived from the periwinkle plant, *Catharanthus roseus* (also *Vinca rosea*, *Lochnera rosea*, and *Ammocallis rosea*). This is the founder class of MT-depolymerizing agents used as effective anti-cancer drug. Some of the primary vinca alkaloids are vinflunine, vinorelbine, vincristine and vindesine and are used in treatment of lymphomas such as Hodgkin's and non-Hodgkin's lymphoma. These drugs bind  $\beta$ -tubulin, block MT polymerization and arrest mitosis at prometaphase [10, 31-33] and finally lead to death in many cancer cells [33]. Another group of recently characterized compounds, the cryptophycins, might bind at the vinca site and effectively kill dividing cells at very low concentrations than other chemotherapeutic agents [34].

**Drugs binding at colchicine-binding sites:** Colchicine is a toxic natural product and secondary metabolite, originally extracted from plant *Colchicum autumnale*, also known as the "Meadow saffron". Colchicine inhibits MT polymerization by binding to  $\alpha\beta$ -tubulin at a site different from vinca-alkaloid binding site. Some drugs such as Indanocene, estrogen metabolite 2-methoxyestradiol (2-ME) and the oxadiazoline derivative A204197, 2-aryolindoles, bind tubulin at colchicine binding site and disrupts mitotic spindle arresting the cells in mitosis [35-37]. Current status of development of newer anti-cancer drugs that inhibit polymerization of tubulin is shown in Table 1.2.

Table 1.2. Inhibitors of tubulin polymerization in clinical development.

Drug	Highest Phase	Indication	Drug type
2-Methoxyestradiol	Phase-I	Cancer	Endogenous metabolite
ABT 751	Phase-II	Breast cancer, Colorectal cancer, Non-small cell lung cancer, Renal cancer	Sulphonamide
ALB 109564(a)	Phase-I	Solid tumors	Semi-synthetic derivative of Madagascar periwinkle flower extract

## Chapter 1

AVE 8062	Phase-III	Cancer, Sarcoma (Second-line therapy), Solid tumors	Combretastatin A4 analogue
Batabulin	Phase-III	Breast cancer, Colorectal cancer, Glioma, Liver cancer, Non-small cell lung cancer	Synthetic pentafluorophenylsulfonamide
Carbendazim	Phase-I	Cancer, HIV infections	Broad-spectrum benzimidazole fungicide
Cevipabulin	Phase-I	Solid tumors	Tubulin polymerization inhibitors
CYT 997	Phase-II	Glioblastoma, Multiple myeloma, Solid tumors,	Pyridimine amine
Dolastatin analogue	Phase-I	Solid tumors	Synthetic peptide
E 7974	Phase-I	Solid tumors	Synthetic hemiasterlin analogue
EC 0225	Phase-I	Cancer	Folate linked to vinka alkaloid and mitomycin C
EC 145	Phase-II	Cancer	Folate linked to vinka alkaloid
Eribulin	Phase-III	Cancer	Synthetic helichondrin B analogue
Indibulin	Phase-I/II	Cancer	Synthetic small molecule: indolyl-3-glyoxylic acid
LP 261	Phase-I	Solid tumors	Colchicine derivative
MKC 1	Phase-II	Cancer	Small molecule inhibitor
MPC 6827	Phase-II	Cancer	Quinazoline derivative
Noscapine	Phase-I/II	Chronic lymphocytic leukaemia, Multiple myeloma, Non-Hodgkin's lymphoma	Benzyloquinoline alkaloid
NPI 2358	Phase-II	Lymphoma, Non-small cell lung cancer, Solid tumors	Synthetic analog of NPI-2350 helimide, a natural product isolated from <i>Aspergillus</i> sp.
NSC 631570	Launched	Cancer, Influenza virus infections	Semi-synthetic compound of thiophosphoric acid and the alkaloid chelidonine
SAR 3419	Phase-I	Non-Hodgkin's lymphoma	Immunoconjugate of anti-CD19 mab conjugated to the cytotoxic agent maytansinoid DM4
SDZ LAV 694	Preclinical	Hodgkin's disease, Non-Hodgkin's lymphoma, Solid tumors	Quinazoline
SGN 35	Phase-II	Cancer	Anti-CD30 antibody attached to a potent, synthetic drug monomethyl auristatin E (MMAE)
Soblidotin	Phase-I	Solid tumors	Dolastatin-10 derivative

Taltobulin	Phase-I	Cancer	Hemiasterlin derivative
Tasidotin	Preclinical	Cancer	Dolastatin-15 analogue
Vincristine liposomal	Phase-II	Cancer	Vinca alkaloid with liposomal delivery system
Vinflunine	Preregistration	Cancer	Vinca alkaloid
Vinorelbine	Launched	Cancer	Vinca alkaloid
Vinorelbine emulsion	Phase-I	Cancer	Vinca alkaloid
Vinorelbine liposomal - Hana Biosciences	Phase-I	Cancer	Vinca alkaloid with liposomal delivery system
ZEN 012	Phase-I	Lymphoma, Solid tumors	Small molecule inhibitor (binds to colchicine binding domain)

### 1.2.2.2 Agents that promote polymerization of tubulin

**Drugs binding at taxane binding site:** Paclitaxel (Taxol) is the founding member of the taxane family of drugs and was originally isolated from the stem bark of *Taxus brevifolia*, the western Pacific yew tree and was found to bind and stabilize MTs [38, 39]. We now have a much better understanding of this family of compounds; paclitaxel and docetaxel (Texotere), both of which bind  $\beta$ -tubulin, surprisingly, from within the lumen of the MT [40-43] stabilizing inter protofilament lattice 3 and blocking disassembly. In addition to increased stability of the existing MTs, taxanes nucleate new assembly of additional polymers. As a consequence, the dramatic reorganization of bipolar spindle arrays is not achieved and cells arrest in prometaphase prior to apoptosis [19]. These taxane family members are active in a range of solid tumor malignancies such as breast cancer, NSCLC, ovarian cancer, gastro oesophageal cancer, germ cell tumors as well as the cancer of the head and neck [40,44,45]. Incidentally, perturbations caused by taxanes and many other anti-MT drugs also perturb the cellular homeostasis and are reported to affect genes encoding inflammatory mediators such as tumor necrosis factor alpha, interleukins and enzymes such as nitric-oxide synthase and cyclooxygenase-2 [46-49].

Epothilones are some newer drugs in this class. They are macrolide antibiotics and represent a novel class of anti-MT agent. Like taxanes, epothilone A and B also bind to  $\alpha\beta$ -tubulin in the same pocket and exert their stabilizing influence in the same manner as taxanes [50]. The success of the taxanes, epothilones, and other MT-interacting anti-cancer agents has inspired the discovery of new MT-interacting drugs [51, 52]. For example, the chemotherapeutic agents, discodermolide and dicoumarol are potent drugs that act synergistically with paclitaxel, creating an enhanced effect [53, 54]. Additionally, the natural compounds laulimalide and peloruside-A share the open-ring structure

of the epothilones and stabilize MTs and arrest cells in mitosis [55, 56]. The current development status of this class of anti-cancer drugs that promote MT assembly is shown in Table 1.3.

Table 1.3. Promoters of tubulin polymerization in clinical development.

<b>Drug</b>	<b>Highest Phase</b>	<b>Indication</b>	<b>Drug type</b>
AI 850	Phase-I	Solid tumors	Paclitaxel, in a novel polyoxyethylated castor oil-free hydrophobic microparticle delivery system
ANG 1005	Phase-I	Brain cancer (Metastatic disease), Glioma	Taxane derivative
ARC 100 (TPI-287)	Phase-II	Cancer, Pancreatic cancer, Prostate cancer (Hormone refractory)	3rd generation Taxane to overcome drug resistance
BMS 188797	Phase-I	Cancer	Taxane
BMS 275183	Phase-II	Non-small cell lung cancer, Prostate cancer, Solid tumors	Taxane
BMS 310705	Phase-I	Cancer	Epothilone analog
BMS 753493	Phase-I/II	Solid tumors	Folate receptor targeted epothilone
Cabazitaxel	Phase-III	Breast cancer, Prostate cancer (Hormone refractory )	Taxane
Docetaxel	Launched	Cancer	Taxane
Docetaxel emulsion	Phase-I	Breast cancer	Taxane
DTS 301	Phase-II	Glioblastoma, Oesophageal cancer, Pancreatic cancer	Paclitaxel delivered in copolymer gel ReGel.
EndoTAG 1	Phase-II	Cancer	Positively charged lipid complex to transport paclitaxel
Ixabepilone	Launched	Cancer	Epothilone
KOS 1584	Phase-II	Non-small cell lung cancer, Solid tumors	Epothilone
Larotaxel	Phase-III	Cancer	Taxane
Liposome encapsulated docetaxel	Phase-I	Solid tumors	Taxane
Liposome encapsulated paclitaxel	Phase-II	Breast cancer	New formulation of Paclitaxel
Milataxel	Phase-II	Cancer	Taxane analog
NK 105	Phase-I	Solid tumors	Paclitaxel-incorporating polymeric micellar nanoparticle (85 nm in size)

OAS PAC 100	Phase-III	Ovarian cancer (Combination therapy: In combination with carboplatin)	Paclitaxel micellar
Ortataxel	Phase-II	Non-Hodgkin's lymphoma, Renal cancer, Solid tumors	Taxane
Paclitaxel - Bristol- Myers Squibb	Launched	Cancer	Paclitaxel
Paclitaxel - Yew Tree Pharmaceuticals	Launched	Breast cancer, Ovarian cancer	Taxane
Paclitaxel – Angiotech	Launched	Inflammation and cancer	Taxane
Paclitaxel-Aphios	Preclinical	Cancer	Taxane
Paclitaxel –Hanmi	Phase-I	Cancer	Taxane
Paclitaxel – SuperGen	Preclinical	Solid tumors	Taxane
Paclitaxel liposomal – Aphios	Preclinical	Cancer	Taxane
Paclitaxel nanoparticle - Dabur Pharma	Launched	Cancer	Taxane
Paclitaxel nanoparticles - BioAlliance Pharma	Preclinical	Solid tumors	Taxane
Paclitaxel poliglumex	Preregistration	Cancer	Taxane
Paclitaxel polymer implant	Preclinical	Solid tumors	Taxane
Albumin-bound paclitaxel	Launched	Cancer	Taxane
Patupilone	Phase-III	Cancer	Epothilone B
Pegylated docetaxel	Phase-I	Solid tumors	Taxane
Sagopilone	Phase-II	Cancer	Epothilone
Simotaxel	Phase-I	Solid tumors	Taxane
Tesetaxel	Phase-II	Cancer	Taxane
TL 310	Phase-I	Cancer	Taxane analog

### 1.2.3 Challenges with current microtubule binding drugs and therapeutics

Among the currently available systemic cancer treatment strategies, chemotherapy is by far the largest subset of treatment options. Despite the initial impressive response by MT binding drugs such as taxanes and vinca alkaloids, their potential is somewhat restricted by the development of multi drug resistance [57], toxicity, hypersensitivity and limited bioavailability [58]. Therefore there is a continual need to develop novel drugs that are efficacious, well-tolerated, non-toxic, orally available, can overcome resistance to other chemotherapeutics and display better

pharmacologic profiles. Some of the major concerns associated with currently used MT binding drugs are discussed as follows.

### **1.2.3.1 Solubility**

Most anti-cancer drugs have limitations in clinical administration due to their poor solubility and other physicochemical and pharmaceutical properties. Almost all major anticancer drugs are hydrophobic. They require the use of adjuvants and intravenous mode of administration that often cause serious side effects. Moreover, intravenous injections and slow infusions are unavoidably associated with considerable fluctuations of drug concentration in the blood and therefore, the drugs can only be administered over a limited dosage and time period. As discussed earlier, paclitaxel (Taxol®) is one of the best antineoplastic drugs and has excellent therapeutic efficacy for a wide spectrum of cancers, especially for ovarian and breast cancers. Due to its poor solubility, however, an adjuvant called Cremophor EL has to be used in its current clinical administration, which causes serious side effects including hypersensitivity reaction, nephrotoxicity, neurotoxicity and cardiotoxicity, some of which are life-threatening [59].

### **1.2.3.2 Bioavailability**

Quality of life issues, patient compliance, treatment advantages and pharmaco-economics are major arguments in favour of oral administration of drugs in patients. Oral applicability is also crucial for anti-cancer agents which should be applied chronically to become effective. Unfortunately, the great majority of currently available cytostatics cannot be administered orally, because of low and highly variable oral bioavailability [60-62]. Until recently, investigators focused on absorption enhancers such as salicylates, methylxantines and surfactants, which can slightly damage the intestinal surface and improve the oral bioavailability of drugs. Typical examples are the clinically important taxanes, paclitaxel and docetaxel [63, 64].

Two major mechanisms can explain the variable oral pharmacokinetics. These are (1) high affinity for drug-transporters, such as P-glycoprotein (P-gp) that is expressed in the intestinal epithelium and directed towards the gut lumen and (2) high extraction of the drug by extensive metabolism in the gut wall and/or liver, during first-pass, i.e., prior to entering the systemic circulation [65]. The combined activity of drug-transporters and metabolic enzymes of the cytochrome P450 system (CYP) explains the low and variable bioavailability of a range of shared substrate drugs. Lack of information about the involvement of these parameters during the early process of anti-cancer drug development often results in unpredictable exposure and consequences [61]. This makes the development process of novel drugs slow, inefficient, patient-unfriendly and extremely costly, emphasizing a need for more rational approaches based on preclinical concepts.

### 1.2.3.3 Resistance

One of the major problems associated with tubulin binding drugs is development of drug resistance. Vinca alkaloids and taxanes bind to different sites on the tubulin dimer and within the MT, exerting varying effects on MT dynamics and block cells in mitosis at the prometaphase transition and induce cell death [66,67]. However, these anticancer drugs select for resistant cells to thrive while killing only drug-sensitive cells. This limits the long term use of these drugs [67-69]. There are potentially three basic mechanisms by which cancer cells acquire resistance. First, the multi-drug resistance (MDR) protein might be amplified to enhance efflux of the drug, thus preventing the accumulation of drugs within cells [70-72]. Second, mutations might also develop in the genes encoding  $\alpha$ - and  $\beta$ - tubulin subunits and thus prevent binding of drugs [73]. Third, both  $\alpha$ - and  $\beta$ - tubulins are expressed as multiple isotypes in varying ratios in different mammalian tissues [74-78] and there have been suggestions that differential expression of diverse tubulin isotypes might ameliorate drug binding efficiencies [79-81]. Because of this diversity, and the changes in the relative concentrations of various tubulin isotypes, resistance to MT-binding drugs might arise [82-84].

### 1.2.3.4 Toxicity

Alluding to an earlier section, toxicity is another major challenge for existing MT binding drugs. In clinics, use of vinca alkaloids and taxanes is limited by the toxicities such as peripheral sensory neuropathies, gastrointestinal toxicity, myelosuppression, immunosuppression and alopecia [58, 85].

Considering all these aspects and drawbacks of currently available tubulin binding anticancer drugs there is a constant need to search for new drugs. Many research labs and pharmaceuticals are constantly working in this area and developing newer drugs as promising anticancer therapeutics and cancer management options.

## 1.3 NOSCAPINE AND ITS ANALOGS: A NEW CLASS OF MICROTUBULE BINDING DRUGS

Noscapine (413.43Da) a benzyloquinoline alkaloid was originally discovered by French pharmacist and Professor Pierre-Jean Robiquet in 1817 [86] from opium plant (*Papaver somniferum*). For decades it has been used medicinally as an antitussive (cough-suppressant) drug in humans [87]. In 1958, cell culture studies performed for the United States National Cancer Institute found noscapine to possess significant cytotoxic properties [88]. This was similar to findings that had also been reported in 1954 [89]. Perhaps due to the fact that it was no longer

patentable, no further studies were carried out to determine its effect on treating cancer. Noscaphine's anticancer effect was rediscovered in 1998 [27]. This was achieved by a structurally based rationale to screen a small library of naturally derived compounds that shared certain structural similarities with toxic MT depolymerizing drugs such as colchicine, podophyllotoxin, MTC [2-methoxy-5-(2,3,4-trimethoxyphenyl)-2,4,6-cycloheptatrien-1-one] and TKB [2,3,4-trimethoxy-4'-acetyl-1,1'-biphenyl] (Figure 1.8).

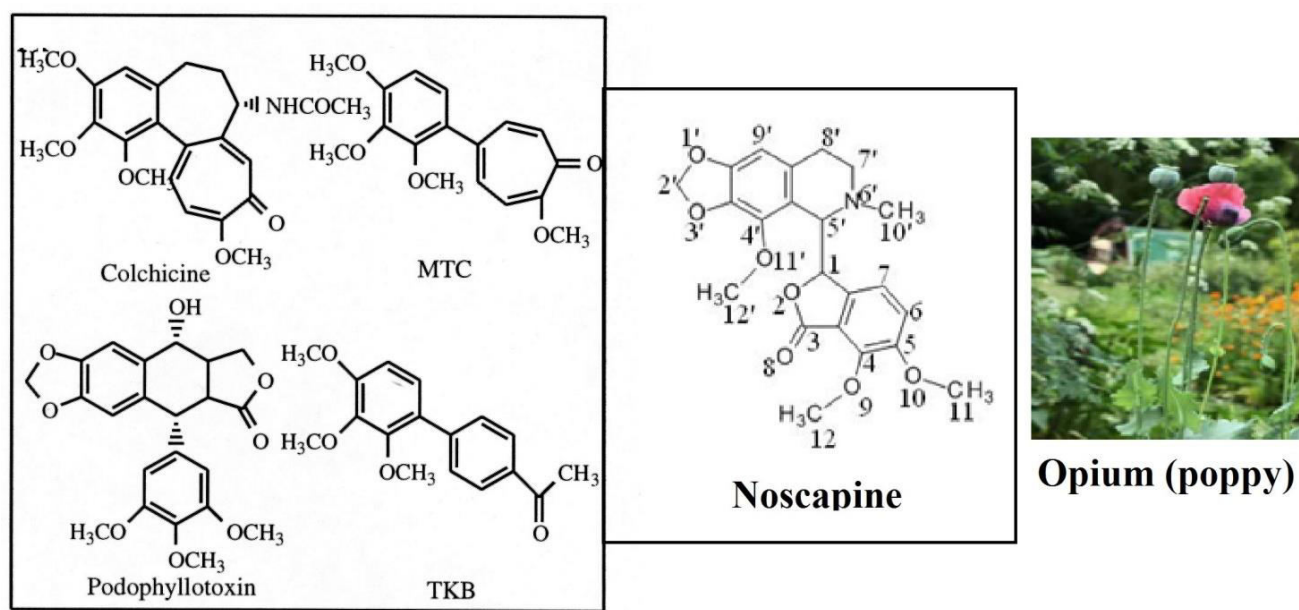


Figure 1.8. The structure of various tubulin interacting agents sharing structural similarity with the promising tubulin binding agent Noscaphine (from opium poppy).

It was found out that many of these compounds contain a hydrophobic trimethoxyphenyl group, a variety of other hydrophobic domains such as lactone, tropolone or other aromatic rings, and a small hydrophilic group such as OH and NH<sub>2</sub>. Based on these features, among the library of naturally derived compounds, noscaphine was screened out to be a tubulin binding agent. On further analysis it was found that noscaphine binds stoichiometrically to tubulin (one noscaphine molecule per  $\alpha\beta$ -tubulin dimer), alters tubulin conformation, and arrests mammalian cells at mitosis (Figure 1.9). But unlike vinca alkaloids and taxanes, it does not cause over-polymerization, depolymerization, or any changes in the overall organization of interphase MT arrays. It arrests mitosis at prometaphase due to its subtle effect on the kinetic parameters of dynamic instability of MTs and causes apoptosis in a variety of cancer cell types [27]. The subtle effect in the MT dynamics is a prolonged attenuated 'pause' state in which growth or shortening of MTs is not detectable (Figure 1.10).



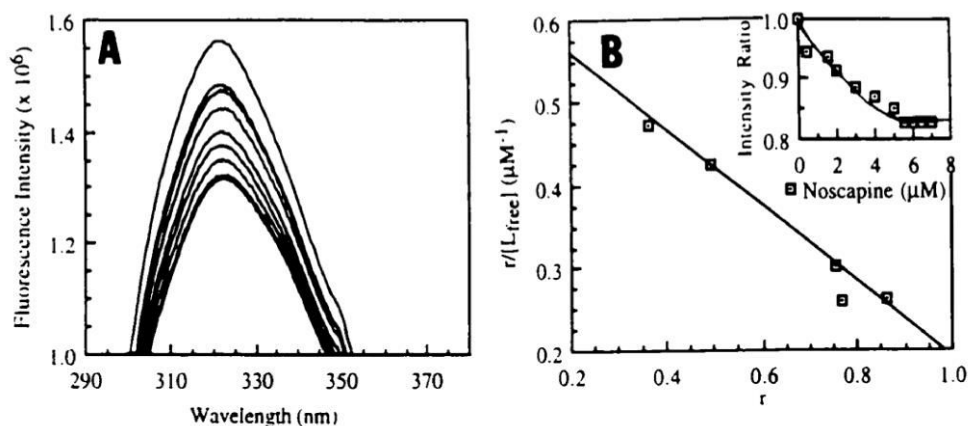
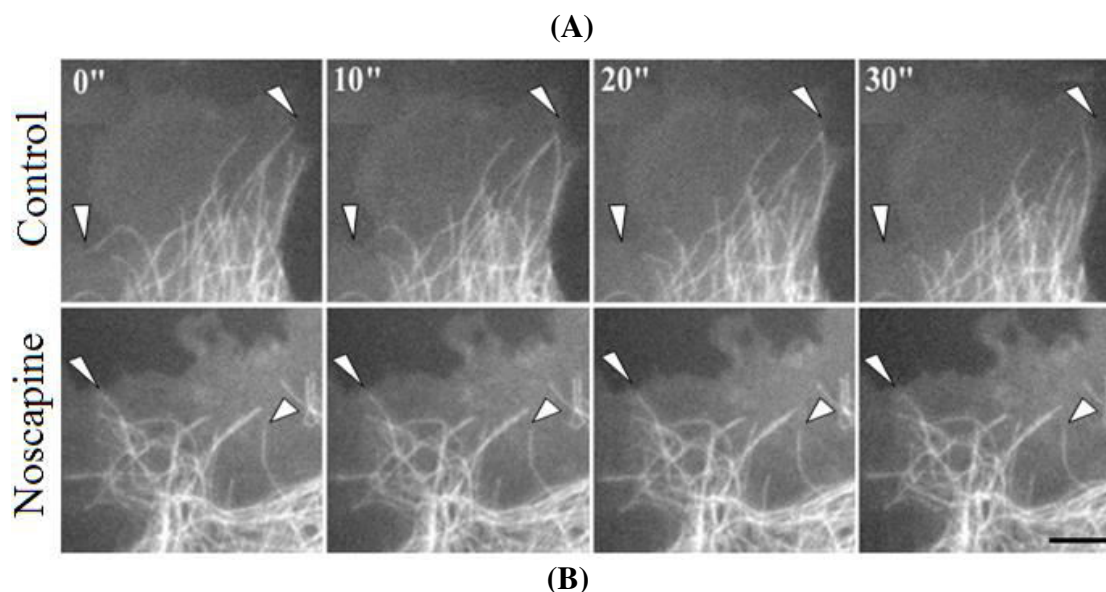


Figure 1.9. Noscaphine as tubulin binding agent. (A) Titration of fluorescence spectra of tubulin at different concentration of noscaphine. (B) Scatchard plot showing an apparent dissociation constant ( $K_d$ ) of  $144 \pm 1.0 \mu\text{M}$ . [27]

Figure 1.10(A) shows a gallery of video frames, 10s apart, of the plus ends of several microtubules in control and noscaphine-treated cells. As expected in control cells, microtubules alternated between phases of growth, shortening, and pause, as determined by noting the position of the plus ends over time (in seconds). Control cells show different positions of microtubule plus ends in a 30s time period. In contrast, noscaphine markedly suppressed microtubule dynamics in cells as indicated by unaltered position of their plus ends (Figure 1.10(A), arrowheads). Results from a detailed analysis of microtubule growth, microtubule shortening, the frequencies of catastrophe and rescue, and the average duration of pause are shown in Figure 1.10(B). The most significant change that noscaphine induced was an increased pause duration from 54% (at 25  $\mu\text{M}$  noscaphine) to 244% (at 250  $\mu\text{M}$  noscaphine) and the rate of microtubule shortening decreased by 20% (at 25  $\mu\text{M}$  noscaphine) and 22% (at 250  $\mu\text{M}$  noscaphine). Perhaps the best measure of overall dynamics is dynamicity, which represents the summed gain and loss (exchange) of tubulin subunits at microtubule ends. Noscaphine significantly reduced microtubule dynamicity by 44% (at 25  $\mu\text{M}$  noscaphine) and by 90% (at 250  $\mu\text{M}$  noscaphine). It conclude that noscaphine induces a prolonged attenuated 'pause' state in which growth or shortening of MTs is not detectable (Figure 1.10). By delaying the onset of the sister chromatid separation, noscaphine induces apoptosis in many cancer cell lines, including those resistant to paclitaxel [160, 161]. It has subsequently been found that several divergent pathways converge in bringing about apoptosis in cancer cells treated with noscaphine and its derivatives. These pathways include induction of stress activated jun N-terminal kinase, mitochondrial depolarization, down regulation of cell survival cascades and up regulation of pro-apoptotic signals and finally all converging into activation of caspase 3/7 [160].



Dynamic Parameters	Control	Noscapine	
		25 $\mu$ M	250 $\mu$ M
Growth	37 MTs n=96	45 MTs n=89	44 MTs n=14
Rate ( $\mu$ m/min)	9.89 $\pm$ 0.78	9.29 $\pm$ 1.05	6.34 $\pm$ 0.72
Distance (mm)	1.16 $\pm$ 0.09	0.97 $\pm$ 0.10	0.75 $\pm$ 0.03*
Duration (sec)	9.62 $\pm$ 0.95	8.30 $\pm$ 1.44	8.04 $\pm$ 0.74
Shrink	n=78	n=79	n=19
Rate ( $\mu$ m/min)	11.39 $\pm$ 0.81	9.06 $\pm$ 0.76*	8.89 $\pm$ 1.19*
Distance (mm)	1.60 $\pm$ 0.30	1.04 $\pm$ 0.09	1.26 $\pm$ 0.36
Duration (sec)	8.75 $\pm$ 1.26	8.06 $\pm$ 0.58	9.62 $\pm$ 2.13
Average Pause Duration (sec)	n=109 22.54 $\pm$ 2.18	n=132 34.66 $\pm$ 3.27*	n=68 77.60 $\pm$ 5.68*
% Time per Phase Growth/Shrink/Pause	22.7/16.8/60.5	12.3/10.8/76.9	2.0/3.3/94.7
Rescue Frequency (sec <sup>-1</sup> )	0.147 $\pm$ 0.02	0.128 $\pm$ 0.01	0.138 $\pm$ 0.03
Catastrophe Frequency (sec <sup>-1</sup> )	0.029 $\pm$ 0.004	0.028 $\pm$ 0.004	0.007 $\pm$ 0.001*
Dynamicity ( $\mu$ m/min)	102.70 $\pm$ 12.94	57.50 $\pm$ 7.72*	10.40 $\pm$ 2.83*

Figure 1.10. Noscapine increases the average time cellular microtubules remain inactive (pause duration). (A), a gallery of video frames, 10s apart, showing the plus ends of several microtubules in a control cell and a noscapine-treated cell. As expected in control cells, microtubules alternated between phases of growth and shortening; thus, the position of their plus ends changed significantly over 30s (fixed pixel locations are marked with arrowheads). In contrast, noscapine markedly suppressed microtubule dynamics in cells, as indicated by the unaltered position of their plus ends (bar  $\pm$  0.5  $\mu$ m). Quantitative parameters of microtubule dynamics are listed in (B). Values are the mean  $\pm$  SE. Dynamicity represents the sum of changes in length (growth or shrinkage) over the life time of a microtubule. \*,  $P \leq 0.01$ . [27]

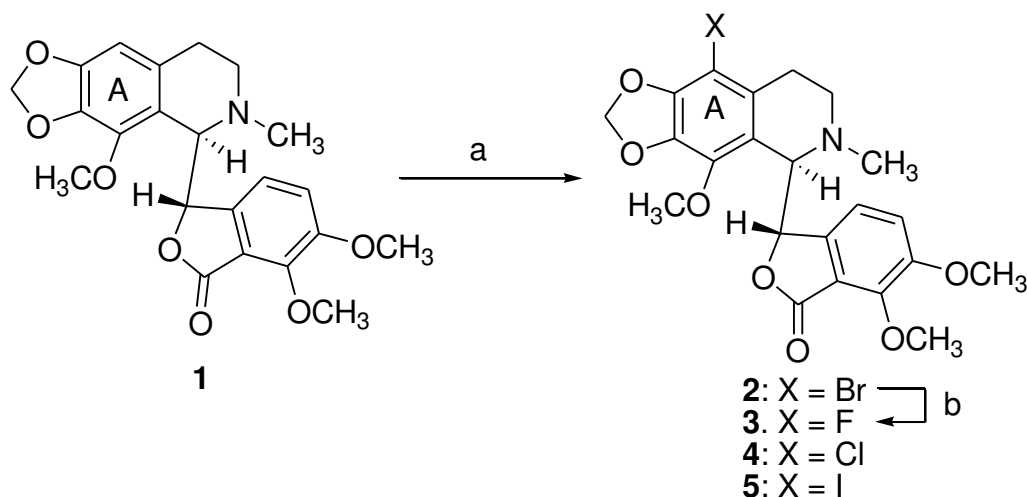
As compared to other MT binding drugs such as taxanes and vinca alkaloids, noscapine offers several advantages in cancer treatment: (a) noscapine arrests a variety of mammalian cells

including drug-resistant variants in mitosis and targets them for apoptosis [90-92]; (b) it is a poor substrate for drug-pumps (polyglycoproteins and MDR-related proteins) that comprise a major cause of drug resistance [91]; (c) it inhibits progression of murine melanoma, lymphoma, glioblastoma, and human breast tumors implanted in nude mice with no detectable toxicity to the rapidly dividing cells and post mitotic cells such as neurons [91-95]; (d) it does not inhibit primary humoral and cellular responses in mice [95]; (e) it does not show immunological and neurological toxicities; (f) can be orally administered bypassing parenteral injections and intravenous infusions that can be complicated by anaphylactic responses and infection at the injection site causing pain, thrombosis of blood vessels, or embolisms as in the case for current clinically available anti-MT drugs [91-95]; (g) It shows a mean bioavailability of ~30-32% across a dose range of 10 mg/kg-300 mg/kg in mice [96]; (h) It has a favourable pharmacokinetics (clearance in 6-10 hours) [96]. However, noscapine possess low cytotoxicity activity to cancer cells of different tissue origin. The  $IC_{50}$  values remain in the high micromolar ranges (~21.1 to 100  $\mu$ M) [27]. To enhance its activity further, efforts have been focused on rational drug design and synthesis of new generation of noscapine derivatives for the better therapeutic outcome.

### 1.3.1 Noscapinoids: the synthetic analogues of noscapine

To enhance the cytotoxicity activity of noscapine, a battery of analogues were designed and chemically synthesized previously (collectively called as noscapinoids) as included in Figure 1.11. and 1.12 [97-102]. Some of these derivatives (mostly the halogen derivatives, Figure 1.11.) have much better therapeutic indices and improved pharmacological profiles. The effectiveness of noscapine was improved by synthesizing many potent noscapine derivatives with increasing tubulin binding affinity by decreasing the dissociation constant ( $K_d$ ) between tubulin-drug complex from 144  $\mu$ M to 86  $\mu$ M by nitro-noscapine, 80  $\mu$ M by F-noscapine, 54  $\mu$ M by Br-noscapine, 40  $\mu$ M by Cl-noscapine and 22  $\mu$ M by I-noscapine [97-102].

In further continuation of developing new derivatives of noscapine, our laboratory have recently designed and systematically synthesized a series of 11 derivatives (we called as third generation) (Figure 1.13) [103]. All these derivatives were rationally designed by functionalization of 'N' in isoquinoline unit of natural  $\alpha$ -noscapine. These derivatives were exhibited substantial cytotoxicity activity towards cancer cells of different tissues of origin. These compounds perturbed DNA synthesis, delayed the cell cycle progression at G2M phase, and induced apoptotic cell death in cancer cells.

**Scheme 1.** Semi-synthetic derivatives of noscapine<sup>a</sup>

<sup>a</sup>Reagents and reaction conditions. a) compound **2**. Br<sub>2</sub>-H<sub>2</sub>O, 48% HBr, 82%; compound **4**. SO<sub>2</sub>Cl<sub>2</sub>, CHCl<sub>3</sub>, 90%; compound **5**. Pyr-ICl, CH<sub>3</sub>CN, 71%; b) F<sub>2</sub>, Amberlyst-A, THF, 74%.

Figure 1.11. Halogenated derivatives of noscapine. All these derivatives showed improved cytotoxicity activity of noscapine.

It is noteworthy that noscapinoids cause no histopathological, hematological, immunological and neuronal toxicity at concentrations as high as 300 mg/kg. Many of these noscapine derivatives have been shown previously to inhibit cellular proliferation of a wide variety of cancer cells (panel of NCI 60 cancer cell lines) including many drug-resistant variants while evading normal cells. In addition they effectively regress human tumor xenografts (lymphomas, breast, prostate and melanomas) implanted in preclinical mice models to a fair degree. However, a complete elimination of the disease was not achieved even on increasing dosages as high as 600 mg/kg. Therefore, there is a need to design a new generation of noscapine derivatives for better therapeutic outcome.

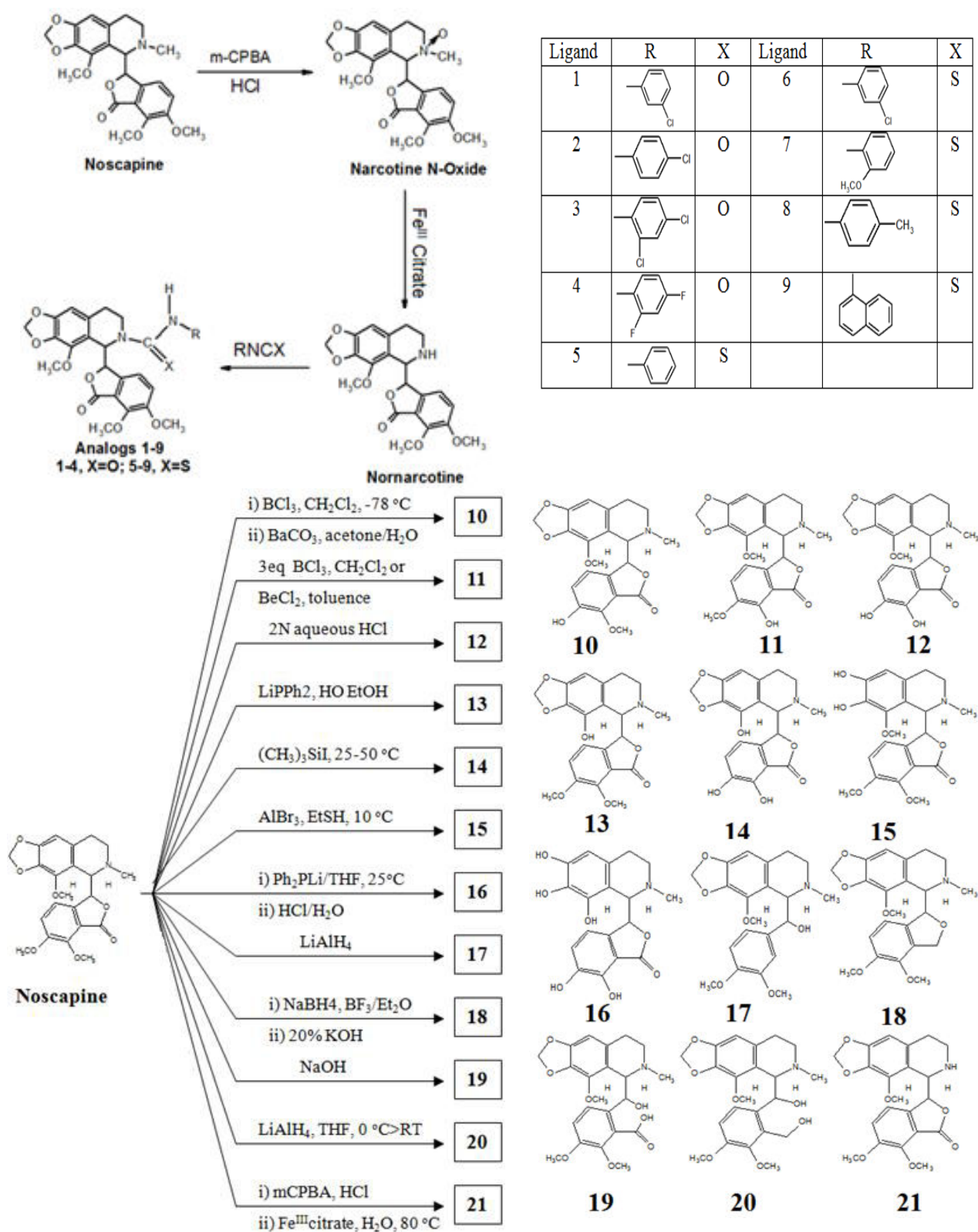
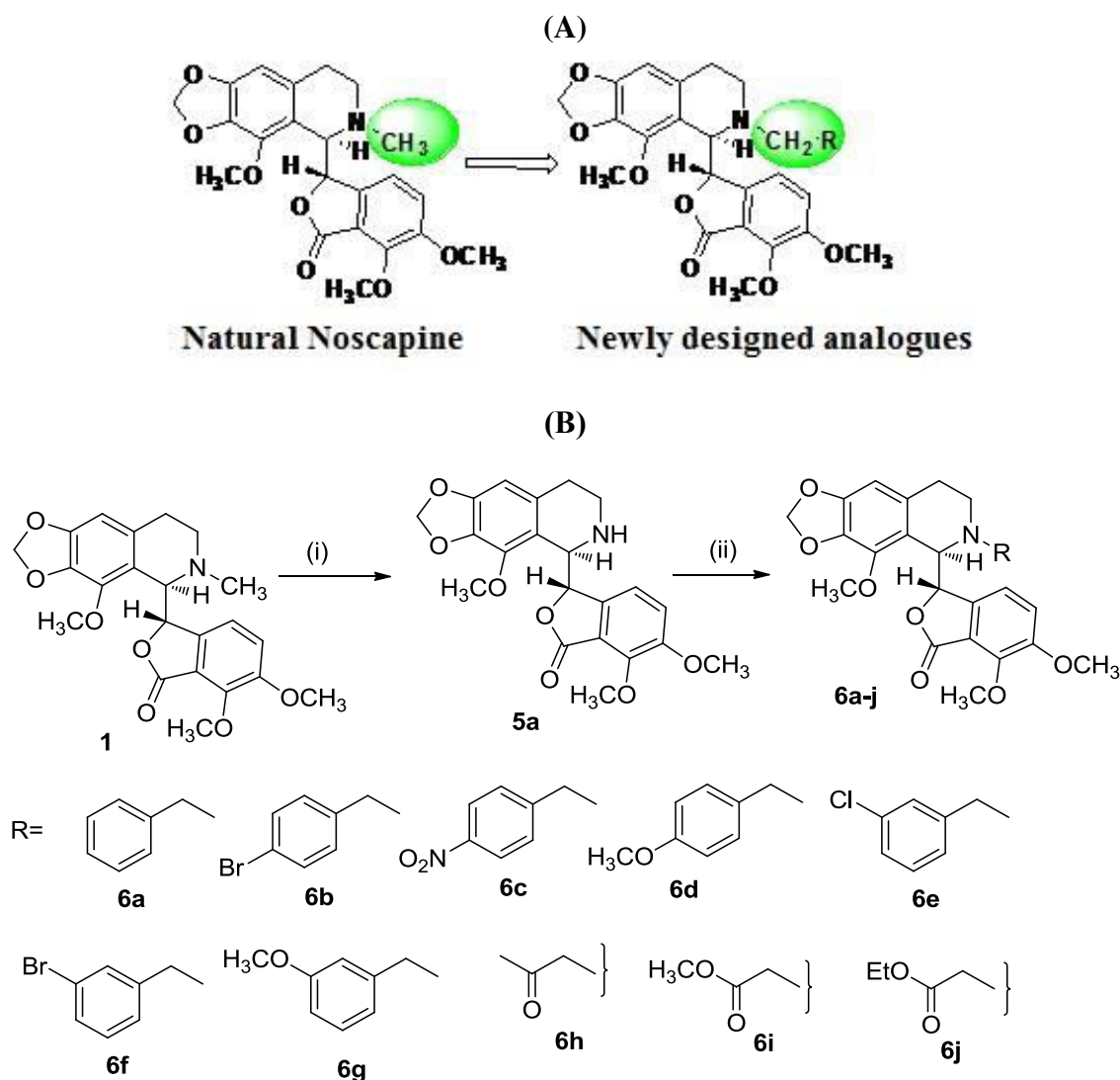


Figure 1.12. Aryl-derivatives of nospapine. These derivatives were synthesized by functionalization (by deleting or substitution) of various functional groups as mentioned in the nospapine scaffold. All these derivatives showed very little or no improvement in cytotoxicity activity of nospapine.



Reaction conditions: (i) a: *m*CPBA, DCM; b: 2N HCl; c: FeSO<sub>4</sub>·7H<sub>2</sub>O; (ii) R-Br, KI, K<sub>2</sub>CO<sub>3</sub>, Acetone.

Figure 1.13. (A) Design strategy for new  $\alpha$ -noscapine analogues (basic skeleton and stereochemistry is same as in the natural  $\alpha$ -noscapine). (B) Synthesis of nornoscapine **5a** and noscapine derivatives **6a-j** from noscapine (**1**) as starting material.

### 1.3.2 Computer-aided design of potent and novel noscapine analogues

Drug discovery and development is a time-consuming and expensive process. On average, it takes 10–15 years and US \$500–800 million to introduce a drug into the market [104,105]. This is why computer-assisted drug design (CADD) approaches have been widely used in the pharmaceutical industry to improve the efficiency of the drug discovery and development pipeline [106,107]. CADD helps scientists focus on the most promising compounds so that they can minimize the synthetic and biological testing efforts. To identify and design small molecules as clinically effective therapeutics, various computational methods have been evaluated as promising



strategies, depending on the purpose and systems of interest. In practice, the choice of CADD approaches to be employed is usually determined by the availability of the experimentally determined 3D structures of target proteins. If the target structures are known, structure-based approaches can be used such as molecular docking, which employs the target 3D structures to design novel active compounds with improved potency. The proposed ligands after chemical synthesis and experimental evaluation become successful drug candidate (Figure 1.14). As more structures are becoming available, the structure based drug designing techniques are state-of-the-art tools to discover potent and novel molecules.

The application of structure design of promising molecules

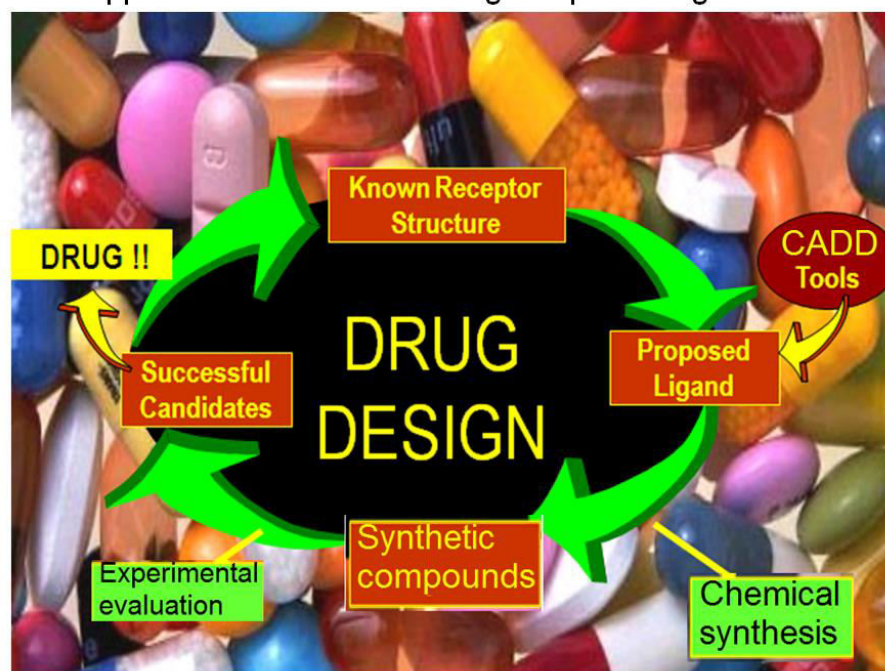


Figure 1.14. The overview of structure based drug design cycle.

Furthermore, if protein structures are unknown, various methods of ligand-based drug design can be employed, such as Quantitative Structure Activity Relationship (QSAR) and pharmacophore analysis. QSAR is a mathematical relationship between a biological activity of a molecular system and its geometric and chemical characteristics. It attempts to find consistent relationship between the biological activity and molecular properties from a given dataset, so that these ‘rules’ can be used to evaluate the activity of newly design compounds. The details of the QSAR model building and prediction is demonstrated in Figure 1.15.

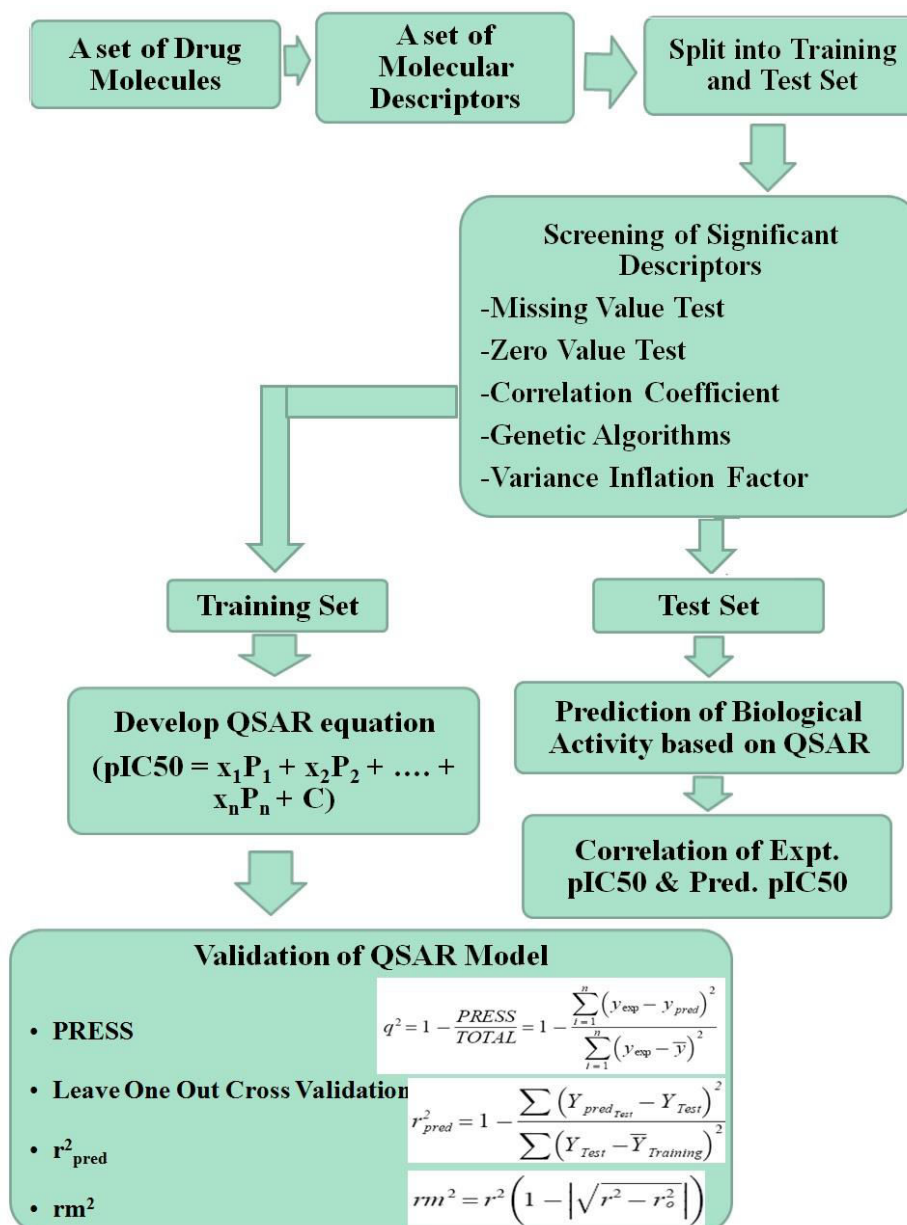


Figure 1.15. The schematic representation of various steps of QSAR model building and prediction.

Availability of structure activity data of many derivatives of noscapine leads to the development of a reasonable theoretical prediction model that guides in a rational design of more potent derivatives of noscapine. Theoretical calculations, in particular the molecular docking method seems to be a primary tool for gaining such understanding. The docking algorithms provide good-quality binding pose for a compound that fits into the binding cavity of target receptor and evaluates its binding affinity using scoring function. However, the scoring functions used by docking algorithms are very simple. They generally do not include shape complementarity parameters between binding cavity and the ligand as well as the solvation effect in calculating the electrostatic interactions energy between protein and ligand. Thus, using of molecular docking only



in designing or screening of ligands may be problematic and can result in a decrease of accuracy. To overcome the problem in molecular docking, more precise but time consuming computational methodologies are necessary to rescore the docking results. This inspired me to use molecular mechanics in combination with implicit continuum solvation based scoring functions such as linear interaction energy method (LIE) with a surface generalized Born (SGB) continuum solvation model, generalized Born solvation area (GBSA), etc in calculating the binding affinity between protein and ligands.

## 1.4 ORGANIZATION OF THE THESIS WORK

In this dissertation work I have developed various theoretical prediction models that were used in designing more potent noscapinoids followed by chemical synthesis and experimental evaluation as potent anticancer drugs. In the second chapter, I have developed a QSAR model based on a list of noscapinoids reported previously. This has been achieved by testing all these derivatives for their anti-tumor activity in identical condition using human acute lymphoblastic leukemia cells (CEM). To develop the QSAR model, the biological active conformations of the compounds were obtained by performing geometrical optimization using semi-empirical quantum chemical calculations at 3-21G\* level. These conformations were screened out in reference to the experimentally obtained structure with NMR Analysis of Molecular Flexibility in Solution--NAMFIS, and crystal structures of noscapine. Genetic function approximation algorithm of variable selection was used to generate the QSAR model. The QSAR model suggested electronic descriptors such as electronegativity and electrophilicity favor columbic interaction between ligands and receptor. Therefore, the developed QSAR model guided me to substitute a functional group such as “azido” ( $\text{N}^-=\text{N}^+=\text{N}^-$ ), satisfying the above descriptors in the scaffold structure of noscapine pertaining to better antitumor activity. The molecules designed showed superior activity in comparison to the lead molecule, noscapine. In the third chapter, I have tried to look into the molecular insight of isotypes specific  $\beta$ -tubulin interaction of tubulin heterodimer with a panel of noscapinoids. Tubulin molecule, composed of  $\alpha$ - and  $\beta$ -tubulin, exist as various isotypes whose distribution and drug-binding properties are significantly different. The molecular structures of all the  $\beta$ -tubulin isotype specific tubulin heterodimers were modelled based on the crystal structure. Binding affinity of noscapinoids onto different  $\alpha\beta$ -tubulin isotypes was determined using molecular docking. I found that the binding score of a specific noscapinoid with each type of tubulin isotype is different. Inspired by the docking result their preferred binding mode and binding affinity with  $\alpha\beta_{\text{III}}$  (overexpression of  $\alpha\beta_{\text{III}}$  has been associated with resistance to a wide range of chemotherapeutic drugs for several human malignancies) was determined by performing 10 ns of MD simulation. An

## Chapter 1

important finding of these calculations was that both amino-noscapine and the clinical derivative, bromo-noscapine have the highest binding affinity against  $\alpha\beta_{III}$  as measured using MM-PBSA. Knowledge of the isotype specificity of noscapinoid may allow for development of novel therapeutic agents based on this drug. In chapter four, I presented many potent derivatives of noscapine that were designed *in silico* through structural modifications on the isoquinoline ring with improved predictive activity in comparison to noscapine as suggested by binding affinity calculations using MMGBSA and MMPBSA. Inspired by the predictive activity, these derivatives were chemically synthesized and experimentally evaluated for their biological activity as anticancer drugs. These derivatives were also experimentally found to have better tubulin binding activity, able to arrest mitotic cell division and inhibit cell proliferation with significantly higher efficiency than noscapine in a precise panel of cancer cells from different tissue origin. Toxicological evaluation of one of this series of compounds showed fails to reveal any detectable pathological abnormalities in normal tissues that are active in normal cell proliferation. The compound does not show any toxicity in the liver, lung, heart, brain and kidney. In addition, it does not have obvious side effects in tissues with frequently dividing cells, such as the spleen and duodenum. Therefore, we believe that the compounds designed in this study were safe and effective anticancer drug with a potential for the oral treatment cancer and holds great promise for further clinical studies. In the final chapter, I have summarized my results.

## REFERENCES

1. Zorn, K.C., Gofrit, O.N., Steinberg, G.D. et al. *Evolution of robotic surgery in the treatment of localized prostate cancer*. Curr Treat Options Oncol , 8 pp 197-210. 2007.
2. Medeiros, L.R., Rosa, D.D., Bozzetti, M.C., et al. *Laparoscopy versus laparotomy for benign ovarian tumour*. Cochrane Database Syst Rev, 2 pp 4751. 2009.
3. Luh, S.P. and Liu, H.P. *Video-assisted thoracic surgery--the past, present status and the future*. J Zhejiang Univ Sci B, 7 pp 118-28. 2006.
4. Gerber, D.E. and Chan, T.A. *Recent advances in radiation therapy*. Am Fam Physician, 78 pp 1254-62. 2008.
5. Desai, A. and Mitchison, T.J. *Microtubule polymerization dynamics*. Annu Rev Cell Dev Biol, 13 pp 83-117. 1997.
6. Howard, J. and Hyman, A.A. *Dynamics and mechanics of the microtubule plus end*. Nature, 422 pp 753-8. 2003.
7. Jordan, M.A. and Wilson, L. *Microtubules as a target for anticancer drugs*. Nat Rev Cancer, 4 pp 253-65. 2004.
8. Nogales, E., Wolf, S.G. and Downing, K.H. *Structure of the alpha beta tubulin dimer by electron crystallography*. Nature, 391 pp 199-203. 1998.
9. Chakarborty, S., Gupta, S., Sarkar, T., Poddar, A., Pena, J., Solana, R., Tarazona, R. and Bhattacharya, B. *The B-ring substituted at C-7 of colchicine and the alpha-C-terminus of tubulin communication through the "tail-body" interaction*. Proteins, 57(3) pp 602-609. 2004.
10. Rai, S.S. and Wolf, J. *The Cterminus of beta tubulin regulates vinblastine-induced tubulin polymerization*. Proceedings of National Academy of Sciences, USA, 95(8) pp 4253-4257. 1998.
11. Bhattacharyya, B., Panda, D., Gupta, S., et al. *Anti-mitotic activity of colchicine and the structural basis for its interaction with tubulin*. Med Res Rev, 28 pp 155-83. 2008.
12. Pasquier, E. and Kavallaris, M. *Microtubules: a dynamic target in cancer therapy*. IUBMB Life, 60 pp 165-70. 2008.
13. Wittmann, T., Hyman, A. and Desai, A. *The spindle: a dynamic assembly of microtubules and motors*. Nat Cell Biol, 3 pp E28-34. 2001.
14. Gelfand, V.I. and Bershadsky, A.D. *Microtubule dynamics: mechanism, regulation, and function*. Annu Rev Cell Biol, 7 pp 93-116. 1991.

15. McIntosh, J.R., Grishchuk, E.L. and West, R.R. *Chromosome-microtubule interactions during mitosis*. Annu Rev Cell Dev Biol, 18 pp 193-219. 2002.
16. Mitchison, T. and Kirschner, M. *Microtubule assembly nucleated by isolated centrosomes*. Nature, 312 pp 232-7. 1984.
17. Mitchison, T. and Kirschner, M. *Dynamic instability of microtubule growth*. Nature, 312 pp 237-42. 1984.
18. Margolis, R.L. and Wilson, L. *Microtubule treadmilling: what goes around comes around*. Bioessays, 20 pp 830-6. 1998.
19. Wilson, L. and Jordan, M.A. *Microtubule dynamics: taking aim at a moving target*. Chem Biol, 2 pp 569-73. 1995.
20. Farrell, K.W., Jordan, M.A., Miller, H.P., et al. *Phase dynamics at microtubule ends: the coexistence of microtubule length changes and treadmilling*. J Cell Biol, 104 pp 1035-46. 1987.
21. Margolis, R.L. and Wilson, L. *Microtubule treadmills--possible molecular machinery*. Nature, 293 pp 705-11. 1981.
22. Schulze, E. and Kirschner, M. *New features of microtubule behaviour observed in vivo*. Nature, 334 pp 356-9. 1988.
23. Mitchison, T. and Kirschner, M. *Cytoskeletal dynamics and nerve growth*. Neuron, 1 pp 761-72. 1988.
24. Koshland, D.E., Mitchison, T.J. and Kirschner, M.W. *Polewards chromosome movement driven by microtubule depolymerization in vitro*. Nature, 331 pp 499-504. 1988.
25. Kirschner, M.W. and Mitchison, T. *Microtubule dynamics*. Nature, 324 pp 621. 1986.
26. Mitchison, T., Evans, L., Schulze, E., et al. *Sites of microtubule assembly and disassembly in the mitotic spindle*. Cell, 45 pp 515-27. 1986.
27. Ye, K., Ke, Y., Keshava, N., et al. *Opium alkaloid noscapine is an antitumor agent that arrests metaphase and induces apoptosis in dividing cells*. Proc Natl Acad Sci USA, 95 pp 1601-6. 1998.
28. Williams, R.F., Mumford, C.L., Williams, G.A., et al. *A photoaffinity derivative of colchicine: 6'-(4'-azido-2'-nitrophenylamino) hexanoyldeacetylcolchicine. Photolabeling and location of the colchicine-binding site on the alpha-subunit of tubulin*. J Biol Chem 260 pp 13794-802. 1985.
29. Safa, A.R., Hamel, E. and Felsted, R.L. *Photoaffinity labeling of tubulin subunits with a photoactive analogue of vinblastine*. Biochemistry, 26 pp 97-102. 1987.
30. Horwitz, S.B. *Taxol (paclitaxel): mechanisms of action*. Ann Oncol, 5: S3-6.1994.

31. Jordan, A., Hadfield, J.A., Lawrence, N.J., et al. *Tubulin as a target for anticancer drugs: agents which interact with the mitotic spindle*. Med Res Rev, 18 pp 259-96. 1998.
32. Correia, J.J. and Lobert, S. *Physiochemical aspects of tubulin-interacting antimitotic drugs*. Curr Pharm Des, 7 pp 1213-28. 2001.
33. Ngan, V.K., Bellman, K., Panda, D., et al. *Novel actions of the antitumor drugs vinflunine and vinorelbine on microtubules*. Cancer Res, 60 pp 5045-51. 2000.
34. Shih, C. and Teicher, B.A. *Cryptophycins: a novel class of potent antimitotic antitumor depsipeptides*. Curr Pharm Des, 7 pp 1259-76. 2001.
35. Leoni, L.M., Hamel, E., Genini, D., et al. *Indanocine, a microtubule-binding indanone and a selective inducer of apoptosis in multidrug-resistant cancer cells*. J Natl Cancer Ins, 92 pp 217-24. 2000.
36. Schumacher, G. and Neuhaus, P. *The physiological estrogen metabolite 2-methoxyestradiol reduces tumor growth and induces apoptosis in human solid tumors*. J Cancer Res Clin Oncol, 127: 405-10. 2001.
37. Tahir, S.K., Han, E.K., Credo, B. et al. *A-204197, a new tubulin-binding agent with antimitotic activity in tumor cell lines resistant to known microtubule inhibitors*. Cancer Res, 61 pp 5480-5. 2001.
38. Schiff, P.B., Fant, J. and Horwitz, S.B. *Promotion of microtubule assembly in vitro by taxol*. Nature, 277 pp 665-7. 1979.
39. Schiff, P.B. and Horwitz, S.B. *Taxol assembles tubulin in the absence of exogenous guanosine 5'-triphosphate or microtubule-associated proteins*. Biochemistry, 20 pp 3247-52. 1981.
40. Cassidy, P.B., Moos, P.J., Kelly, R.C., et al. *Cyclooxygenase-2 induction by paclitaxel, docetaxel, and taxane analogues in human monocytes and murine macrophages: structure-activity relationships and their implications*. Clin Cancer Res, 8 pp 846-55. 2002.
41. Nogales, E. *A structural view of microtubule dynamics*. Cell Mol Life Sci, 56 pp 133-42. 1999.
42. Snyder, J.P., Nettles, J.H., Cornett, B., et al. *The binding conformation of Taxol in  $\beta$ -tubulin: A model based on electron crystallographic density*. PNAS, 98 pp 5312-5316. 2001.
43. Bacus, S.S., Gudkov, A.V., Lowe, M., et al. *Taxol-induced apoptosis depends on MAP kinase pathways (ERK and p38) and is independent of p53*. Oncogene, 20 pp 147-55. 2001.
44. Parness, J., Kingston, D.G., Powell, R.G., Harracksingh, C., et al. *Structure-activity study of cytotoxicity and microtubule assembly in vitro by taxol and related taxanes*. Biochem Biophys Res Commun, 105 pp 1082-9. 1982.

45. Rowinsky, E.K. *The development and clinical utility of the taxane class of antimicrotubule chemotherapy agents*. Annu Rev Med, 48 pp 353-74. 1997.
46. Bogdan, C. and Ding, A. *Taxol, a microtubule-stabilizing antineoplastic agent, induces expression of tumor necrosis factor alpha and interleukin-1 in macrophages*. J Leukoc Biol 52 pp 119-21. 1992.
47. Moos, P.J. and Fitzpatrick, F.A. *Taxane-mediated gene induction is independent of microtubule stabilization: induction of transcription regulators and enzymes that modulate inflammation and apoptosis*. Proc Natl Acad Sci USA, 95 pp 3896-901. 1998.
48. White, C.M., Martin, B.K., Lee, L.F., et al. *Effects of paclitaxel on cytokine synthesis by unprimed human monocytes, T lymphocytes, and breast cancer cells*. Cancer Immunol Immunother, 46 pp 104-12. 1998.
49. Napoleone, E., Zurlo, F., Latella, M.C. et al. *Paclitaxel downregulates tissue factor in cancer and host tumour-associated cells*. Eur J Cancer, 45 pp 4707. 2009.
50. Altaha, R., Fojo, T., Reed, E., et al. *Epothilones: a novel class of non-taxane microtubule-stabilizing agents*. Curr Pharm Des, 8 pp 1707-12. 2002.
51. Altmann, K.H. *Microtubule-stabilizing agents: a growing class of important anticancer drugs*. Curr Opin Chem Biol, 5 pp 424-31. 2001.
52. He, L., Orr, G.A. and Horwitz, S.B. *Novel molecules that interact with microtubules and have functional activity similar to Taxol*. Drug Discov Today, 6 pp 1153-1164. 2001.
53. Kowalski, R.J., Giannakakou, P., Gunasekera, S.P., et al. *The microtubule-stabilizing agent discodermolide competitively inhibits the binding of paclitaxel (Taxol) to tubulin polymers, enhances tubulin nucleation reactions more potently than paclitaxel, and inhibits the growth of paclitaxel-resistant cells*. Mol Pharmacol, 52 pp 613-22. 1997.
54. Madari, H., Panda, D., Wilson, L., et al. *Dicoumarol: a unique microtubule stabilizing natural product that is synergistic with Taxol*. Cancer Res, 63 pp 1214-20. 2003.
55. Pryor, D.E., O'Brate, A., Bilcer, G., et al. *The microtubule stabilizing agent laulimalide does not bind in the taxoid site, kills cells resistant to paclitaxel and epothilones, and may not require its epoxide moiety for activity*. Biochemistry, 41 pp 9109-15. 2002.
56. Hood, K.A., West, L.M., Rouwé, B., et al. *Peloruside A, a novel antimitotic agent with paclitaxel-like microtubule-stabilizing activity*. Cancer Res, 62 pp 3356-60. 2002.
57. Panda, D., Miller, H.P., Banerjee, A., et al. *Microtubule dynamics in vitro are regulated by the tubulin isotype composition*. Proc Natl Acad Sci USA, 91 pp 11358-62. 1994.
58. Rowinsky, E.K., Eisenhauer, E.A., Chaudhry, V., et al. *Clinical toxicities encountered with paclitaxel (Taxol)*. Semin Oncol, 20 pp 1-15. 1993.

59. Weiss, R.B., Donehower, R.C., Wiernik, P.H. et al. *Hypersensitivity reactions from taxol*. Journal of Clinical Oncology 1990; 8: 1263-1268
60. DeMario MD, Ratain MJ. Oral chemotherapy: rationale and future directions. J Clin Oncol, 16 pp 2557-67. 1998.
61. Bardelmeijer, H.A., Ouwehand, M., Beijnen, J.H. et al. *Efficacy of novel P-glycoprotein inhibitors to increase the oral uptake of paclitaxel in mice*. Invest New Drugs, 22 pp 219-29. 2004.
62. Huizing, M.T., Giaccone, G., van Warmerdam, L.J., et al. *Pharmacokinetics of paclitaxel and carboplatin in a dose-escalating and dose-sequencing study in patients with non-small-cell lung cancer*. J Clin Oncol, 15 pp 317-29. 1997.
63. Schellens, J.H., Malingré, M.M., Kruijtzter, C.M. et al. *Modulation of oral bioavailability of anticancer drugs: from mouse to man*. Eur J Pharm Sci, 12 pp 103-10. 2000.
64. Gerrits, C.J., Schellens, J.H., Creemers, G.J. et al. *The bioavailability of oral GII47211 (GG211), a new topoisomerase I inhibitor*. Br J Cancer, 76 pp 946-51. 1997.
65. Sparreboom, A., van Asperen, J., Mayer, U. et al. *Limited oral bioavailability and active epithelial excretion of paclitaxel (Taxol) caused by P-glycoprotein in the intestine*. Proc Natl Acad Sci USA, 94 pp 2031-5. 1997.
66. Checchi, P.M., Nettles, J.H., Zhou, J. et al. *Microtubule-interacting drugs for cancer treatment*. Trends Pharmacol Sci, 24 pp 361-5. 2003.
67. Jordan, M.A., Toso, R.J., Thrower, D. et al. *Mechanism of mitotic block and inhibition of cell proliferation by taxol at low concentrations*. Proc Natl Acad Sci USA, 90 pp 9552-6. 1993.
68. Wang, Y., O'Brate, A., Zhou, W., et al. *Resistance to microtubule-stabilizing drugs involves two events: beta-tubulin mutation in one allele followed by loss of the second allele*. Cell Cycle, 4 pp 1847-53. 2005.
69. Drukman, S. and Kavallaris, M. *Microtubule alterations and resistance to tubulin-binding agents (review)*. Int J Oncol, 21 pp 621-8. 2002.
70. Krishna, R. and Mayer, L.D. *Multidrug resistance (MDR) in cancer. Mechanisms, reversal using modulators of MDR and the role of MDR modulators in influencing the pharmacokinetics of anticancer drugs*. Eur J Pharm Sci, 11 pp 265-83. 2000.
71. Yamada, T., Mori, Y., Hayashi, R. et al. *Suppression of intestinal polyposis in Mdr1-deficient ApcMin/+ mice*. Cancer Res, 63 pp 895-901. 2003.

72. Wu, H., Hait, W.N. and Yang, J.M. *Small interfering RNA-induced suppression of MDR1 (P-glycoprotein) restores sensitivity to multidrug-resistant cancer cells*. Cancer Res, 63 pp 1515-9. 2003.
73. Giannakakou, P., Gussio, R., Nogales, E. et al. *A common pharmacophore for epothilone and taxanes: molecular basis for drug resistance conferred by tubulin mutations in human cancer cells*. Proc Natl Acad Sci USA, 97 pp 2904-9. 2000.
74. Cowan, N.J. and Dudley, L. *Tubulin isotypes and the multigene tubulin families*. Int Rev Cytol, 85 pp 147-73. 1983.
75. Luduena, R.F. *Multiple forms of tubulin: different gene products and covalent modifications*. Int Rev Cytol, 178 pp 207-275. 1998.
76. Joshi, H.C. and Cleveland, D.W. *Diversity among tubulin subunits: toward what functional end?* Cell Motil Cytoskeleton, 16 pp 159-63. 1990.
77. Kim, Y.S., Tseng, C.Y., Mane, J.Y., Winter, P., Johnson, L., Huzil, T., Izbicka, E., Luduena, R.F. & Tuszynski, J. *Quantitative analysis of the effect of tubulin isotype expression on sensitivity of cancer cell lines to a set of novel colchicine derivatives*. Molecular Cancer, 9 pp 131. 2010.
78. Roach, M.C., Boucher, V.L., Walss, C. et al. *Preparation of a monoclonal antibody specific for the class I isotype of beta-tubulin: the beta isotypes of tubulin differ in their cellular distributions within human tissues*. Cell Motil Cytoskeleton, 39 pp 273-85. 1998.
79. Banerjee, A. & Luduena, R.F. *Kinetics of colchicine binding to purified beta tubulin isotypes from bovine brain*. J Biol Chem, 267 pp 13335-13339. 1992.
80. Joshua, A., McCarroll, Gan P.P., Liu, M. & Kavallaris, M.  *$\beta$ III-Tubulin Is a Multifunctional Protein Involved in Drug Sensitivity and Tumorigenesis in Non-Small Cell Lung Cancer*. Clin Cancer Res, 70(12) pp 4995-5003. 2010.
81. English, D.P., Roque, D.M. & Santin, A.D. *Class III b-tubulin over expression in gynecologic tumors: implications for the choice of microtubule targeted agents*. Expert Review of Anticancer Therapy, 13(1) pp 63-74. 2013.
82. Burkhart, C.A., Kavallaris, M. and Band Horwitz, S. *The role of beta-tubulin isotypes in resistance to antimitotic drugs*. Biochim Biophys Acta, 1471 pp 1-9. 2001.
83. Mozzetti, S., Ferlini, C., Concolino, P. et al. *Class III B-Tubulin Overexpression Is a Prominent Mechanism of Paclitaxel Resistance in Ovarian Cancer Patients*. Clin Cancer Res, 11 pp 298-305. 2005.



84. Kavallaris, M., Tait, A.S., Walsh, B.J. et al. *Multiple microtubule alterations are associated with Vinca alkaloid resistance in human leukemia cells*. Cancer Res, 61 pp 5803-9. 2001.
85. Graf, W.D., Chance, P.F., Lensch, M.W. et al. *Severe vincristine neuropathy in Charcot-Marie-Tooth disease type 1A*. Cancer, 77 pp 1356–62 1996.
86. Warolin, C. and Pierre-Jean Robiquet. *Rev Hist Pharm*, 47(321) pp 97-110. 1999.
87. Idanpaan-Heikkila, J.E., Jalonen, K. and Vartiainen, A. *Evaluation of the antitussive effect of noscapine and codeine on citric acid cough in guinea-pigs*. Acta Pharmacol Toxicol, 25 pp 333-338. 1967.
88. Eagle, H. and Foley, G. *Cytotoxicity in Human Cell Cultures as a Primary Screen for the Detection of Anti-Tumor Agents*. Cancer Res, 18 pp 1017-1025. 1958.
89. Lettre, H. *Synergists and Antagonists of Mitotic Poisons*. Ann. N.Y. Academy of Science, 58 pp 1264. 1954.
90. Zhou, J., Gupta, K., Yao, J. et al. *Paclitaxel-resistant human ovarian cancer cells undergo c-Jun NH2-terminal kinase-mediated apoptosis in response to noscapine*. J Biol Chem, 277 pp 39777-85. 2002.
91. Mahmoudian, M. and Rahimi-Moghaddam P. *The anti-cancer activity of noscapine: a review*. Recent Pat Anticancer Drug Discov, 4 pp 92-7. 2009.
92. Landen, J.W., Lang, R., McMahon, S.J. et al. *Noscapine alters microtubule dynamics in living cells and inhibits the progression of melanoma*. Cancer Res, 62 pp 4109-14. 2002.
93. Ke, Y., Ye, K., Grossniklaus, H.E. et al. *Noscapine inhibits tumor growth with little toxicity to normal tissues or inhibition of immune responses*. Cancer Immunol Immunother, 49 pp 217-25. 2000.
94. Aneja, R., Zhou, J., Vangapandu, S.N. et al. *Drug-resistant T-lymphoid tumors undergo apoptosis selectively in response to an antimicrotubule agent, EM011*. Blood, 107 pp 2486-92. 2006.
95. Landen, J.W., Hau, V. and Wang, M. et al. *Noscapine crosses the blood-brain barrier and inhibits glioblastoma growth*. Clin Cancer Res, 10 pp 5187-201. 2004.
96. Aneja, R., Dhiman, N., Idnani, J. et al. *Preclinical pharmacokinetics and bioavailability of noscapine, a tubulin-binding anticancer agent*. Cancer Chemother Pharmacol, 60 pp 831-9. 2007.
97. Aggarwal, S., Ghosh, N.N., Aneja, R., Joshi, H.C. and Chandra, R. *A convenient synthesis of aryl-substituted N-carbamoyl/N-thiocarbamoyl narcotine and related compounds*. Helvetica Chimica Acta, 85 pp 2458-2462. 2002.

98. Aneja, R., Vangapandu, S.N., Lopus, M., Viswesarappa, V.G., Dhiman, N., Verma, A., Chandra, R., Panda, D. and Joshi, H.C. *Synthesis of microtubule-interfering halogenated noscapine analogs perturb mitosis in cancer cells followed by cell death*. Biochemistry and Pharmacology, 72 pp 415-426. 2006.
99. Zhou, J., Gupta, K., Aggarwal, S. et al. *Brominated derivatives of noscapine are potent microtubule-interfering agents that perturb mitosis and inhibit cell proliferation*. Mol Pharmacol, 63 pp 799-807. 2003.
100. Aneja, R., Vangapandu, S.N. and Joshi, H.C. *Synthesis and biological evaluation of a cyclic ether fluorinated noscapine analog*. Bioorganic Medicinal Chemistry, 14 pp 8352-8358. 2006.
101. Aneja, R., Vangapandu, S.N., Lopus, M., Chandra, R., Panda, D. and Joshi, H.C. *Development of a novel nitro-derivative of noscapine for the potential treatment of drug-resistant ovarian cancer and T-cell lymphoma*. Molecular Pharmacology, 69 pp 1801-1809. 2006.
102. Aneja, R., Lopus, M., Zhou, J., Vangapandu, S.N., Ghaleb, A., Yao, J., Nettles, J.H., Zhou, B., Gupta, M., Panda, D., Chandra, R. and Joshi, H.C. *Rational design of the microtubule-targeting anti-breast cancer drug EM015*. Cancer Research 66 pp 3782-3791. 2006.
103. Manchukonda, N.K., Naik, P.K., Santoshi, S., Lopus, M., Joseph, S., Sridhar, B. & Kantevari, S. *Rational Design Synthesis and Biological Evaluation of Third Generation  $\alpha$ -Noscapine Analogues as Potent Tubulin Binding Anti-Cancer Agents*. PLOS ONE, 8(10) pp 77970. 2013.
104. Workman, P. *How much gets there and what does it do?: The need for better pharmacokinetic and pharmacodynamic endpoints in contemporary drug discovery and development*. Current Pharmaceutical Design, 9 pp 891-902. 2003.
105. Brown, D. and Superti-Furga, G. *Rediscovering the sweet spot in drug discovery*. Drug Discovery Today, 8 pp 1067-1077. 2003.
106. Gomeni, R., Bani, M., D'Angeli, C., Corsi, M. and Bye, A. *Computer-assisted drug development (CADD): an emerging technology for designing first-time-in-man and proof-of-concept studies from preclinical experiments*. European Journal of Pharmaceutical Science, 13 pp 261-270. 2001.
107. Veselovsky, A.V. and Ivanov, A.S. *Strategy of computer-aided drug design*. Current Drug Targets Infectious Disorder, 3 pp 33-40. 2003

# **CHAPTER - 2**

## **QSAR BASED DESIGN OF NOVEL NOSCAPINOIDS AND THEIR BIOLOGICAL EVALUATION.**

## CHAPTER 2

**ABSTRACT**

An anti-cough medicine, noscapine [(S)-3-((R)4-methoxy-6-methyl-5,6,7,8-tetrahydro-[1,3]dioxolo[4,5-g]isoquinolin-5-yl)-6,7-dimethoxyiso-benzofuran-1(3H)-one], was discovered as a novel type of tubulin-binding agent that mitigates polymerization dynamics of microtubule polymers without changing overall subunit-polymer equilibrium. To obtain a systematic insight into structure activity relationship between the structural framework of noscapine scaffold and its anti-tumor activity, a QSAR model was developed taking a list of noscapinoids reported previously. All these derivatives were tested for their anti-tumor activity in identical condition using human acute lymphoblastic leukemia cells (CEM). The  $IC_{50}$  values of these analogs vary from 1.2 to 56.0  $\mu M$ . To develop the QSAR model, the biological active conformations of the compounds were obtained by performing geometrical optimization using semi-empirical quantum chemical calculations at 3-21G\* level. These conformations were screened out in reference to the experimentally obtained structure with NMR Analysis of Molecular Flexibility in Solution-NAMFIS, and crystal structure of noscapine. Genetic function approximation algorithm of variable selection was used to generate the QSAR model. The robustness of the QSAR model ( $R^2 = 0.942$ ) was analyzed by values of the internal cross-validated regression coefficient ( $R^2_{LOO} = 0.815$ ) for the training set and determination coefficient ( $R^2_{test} = 0.817$ ) for the test set. Validation was achieved by rational design of further novel and potent anti-tumor noscapinoid, 9-azido-noscapine and reduced-9-azido-noscapine. The experimentally determined value of  $pIC_{50}$  for both the compounds (5.585 M) turned out to be very close to predicted  $pIC_{50}$  (5.731 and 5.710 M).

## 2.1 INTRODUCTION

Noscapine (a phthalideisoquinoline), is an opium alkaloid, isolated from *Papaver somniferum* has been widely utilized as an antitussive agent [1]. While looking for orally available small tubulin-binding compounds with novel properties, noscapine was discovered as a stoichiometric tubulin-binding molecule that alters tubulin conformation upon binding, yet allows its polymerization into microtubules (MTs) [2]. Noscapine bound microtubules, however, are extremely sluggish in their dynamic instability property [3]. As a result of very slow MT-dynamics, noscapine blocks cell cycle progression at mitosis (prometaphase) leading eventually to apoptotic cell death in many cancer cell types [2,3]. Perhaps due to a different binding site on tubulin, noscapine synergizes with other tubulin-binding anti-cancer drug, paclitaxel, and retains activity against paclitaxel-resistant cell lines (1A9/PTX10; 1A9/PTX22) and epothilone-resistant cell line (1A9/A8) [4]. In addition, noscapine seems to be a poor substrate for the drug-pumps because it remains effective against multidrug-resistant cancer cells [5].

Although noscapine is cytotoxic in a variety of different cancer cell lines in the public library of the National Cancer Institute, USA (NCI 60-cell screen), the  $IC_{50}$  values remain in the high micromolar ranges (~21.1 to 100  $\mu$ M). Opportunities must now be explored to acquire better and more effective derivatives. Indeed, initial efforts in this area have been quite encouraging, in that some more effective derivatives of the lead compound, noscapine were developed [6-9]. This led us to build a reasonable quantitative structure activity relationship (QSAR) model. The QSAR model guided us in rationally designing the azido-derivatives of noscapine with superior activity. We synthesized 9-azido-noscapine and reduced 9-azido-noscapine and tested their biological activity against human lymphoblastoid cells (CEM) that corroborate with the QSAR evaluation. Thus results show that our QSAR model is robust and demonstrates successful predictive ability for further drug development.

## 2.2 MATERIALS AND METHODS

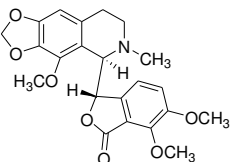
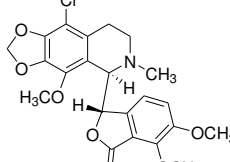
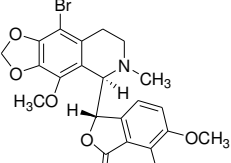
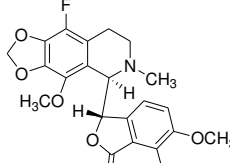
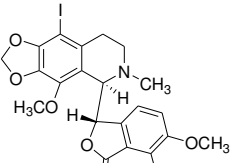
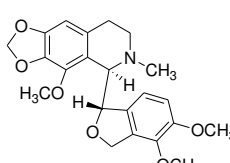
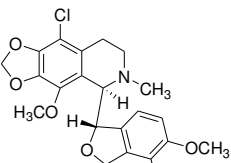
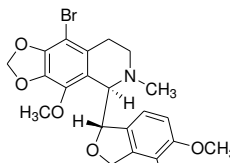
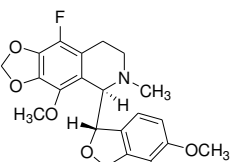
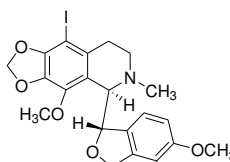
### 2.2.1 Data set

The data set in this study consists of 32 noscapine derivatives, collectively called as noscapinoids (Table 2.1) with different substitution on the isoquinoline and dimethoxy benzyl furanone ring systems of noscapine scaffold. All these compounds were obtained in synthetic form from Department of Cell Biology, Emory University School of Medicine, Georgia, USA and the compound **1** was purchased from Sigma-Aldrich. The halogenated derivatives of noscapine (Table 2.1: compounds **2-5**) were synthesized by substituting halogen groups (Br, Cl, F, and I) at C-9 of

## CHAPTER 2

the scaffold structure as previously described [6]. The cyclic ether halogenated analogs of noscapine (Table 2.1: compounds **6-10**) were synthesized by reducing an oxygen atom from the benzyl furanone ring, also described previously [7]. The nitro derivatives of noscapine (Table 2.1: compounds **11,12**) were synthesized by substituting a nitro group at C-9 [8]. One group of compound (Table 2.1: compounds **13-21**) contains aryl substituted N-carbamoyl/N-thiocarbamoyl noscapine analogs [9]. The other analogs (Table 2.1: compounds **22-32**) harboring changes in the two methoxy groups, the lactone ring of the isobenzofuranone system (the dioxolo ring and the methoxy group) as well as the methyl group in the isoquinoline ring system [9]. All test compounds used in this study were dissolved in DMSO as 10 mM stock.

Table 2.1. Chemical structures of noscapine and its congeners used in the present study along with their observed inhibitory activity of CEM (human lymphoblastoid) cancer cell line proliferation.

Sl No.	Compound structure	IC <sub>50</sub> (M)	Sl No.	Compound Structure	IC <sub>50</sub> (M)
1		16.59 x 10 <sup>-6</sup>	2		1.2 x 10 <sup>-6</sup>
3		1.9 x 10 <sup>-6</sup>	4		2.3 x 10 <sup>-6</sup>
5		38.9 x 10 <sup>-6</sup>	6		28.3 x 10 <sup>-6</sup>
7		45.2 x 10 <sup>-6</sup>	8		2.8 x 10 <sup>-6</sup>
9		15.5 x 10 <sup>-6</sup>	10		30.5 x 10 <sup>-6</sup>

## CHAPTER 2

11		$10.0 \times 10^{-6}$	12		$10.0 \times 10^{-6}$
13		$48.0 \times 10^{-6}$	14		$45.2 \times 10^{-6}$
15		$44.2 \times 10^{-6}$	16		$40.6 \times 10^{-6}$
17		$41.9 \times 10^{-6}$	18		$45.1 \times 10^{-6}$
19		$46.5 \times 10^{-6}$	20		$44.4 \times 10^{-6}$
21		$44.1 \times 10^{-6}$	22		$51.8 \times 10^{-6}$
23		$39.5 \times 10^{-6}$	24		$42.6 \times 10^{-6}$
25		$41.0 \times 10^{-6}$	26		$42.3 \times 10^{-6}$
27		$35.5 \times 10^{-6}$	28		$53.6 \times 10^{-6}$
29		$56.0 \times 10^{-6}$	30		$52.8 \times 10^{-6}$
31		$37.4 \times 10^{-6}$	32		$43.3 \times 10^{-6}$



### 2.2.2 In vitro cell proliferation assays

Each of these compounds had associated *in vitro* anti-tumor activities in variety of cancer types including a few in CEM (human lymphoblastoid) cancer cell lines. Therefore we have determined the biological activities of all compounds in one specific cell line and at similar experimental conditions (to minimize any biasness). We have used CEM cell lines as our assay system and were provided by Dr. William T. Beck (Cancer Center, University of Illinois at Chicago). Cell culture reagents were obtained from Mediatech, Cellgro. Cells were grown in RPMI-1640 medium supplemented with 10% fetal bovine serum, 1% penicillin/streptomycin, 2 mM l-glutamine at 37 °C in a humidified atmosphere with 5% CO<sub>2</sub>. Suspension cells were plated into 96-well plates at a density of  $5 \times 10^3$  cells per well and were treated with gradient concentrations of noscapinoids for 72 hours. Measurement of cell proliferation was performed with a colorimeter by 3-(4,5-dimethylthiazol-2-yl)-5-(3-carboxymethoxyphenyl)-2-(4-sulphophenyl)-2H-tetrazolium, inner salt (MTS) assay, using the CellTiter96 AQueous One Solution Reagent (Promega, Madison, WI). Cells were exposed to MTS for 3 hours and absorbance (optical density) was measured using a microplate reader (Molecular Devices, Sunnyvale, CA) at a wavelength of 490 nm. The percentage of cell survival as a function of drug concentration was then plotted to determine the IC<sub>50</sub> value. The negative logarithm of IC<sub>50</sub> value in molar concentrations ( $pIC_{50} = -(\log_{10} IC_{50})$ ) of these compounds was used as response for QSAR model building.

### 2.2.3 Molecular model building and optimization of noscapinoids structure

The scaffold structure of noscapine consists of 2 chiral centers leading to formation of 4 different stereoisomers. To determine the stable conformation of noscapine we have performed X-ray crystallographic study. The opium alkaloid noscapine was obtained from Sigma-Aldrich. It was dissolved in chloroform-methanol (50:50) and the crystal was made under vacuum. The formation of crystal was examined under microscope and its X-ray crystallographic structure was determined (Figure 2.1).

Data collection: *SMART* (Brunker, 2007); Cell refinement: *SAINT* (Brunker, 2007); data reduction: *SAINT*; program(s) used to solve structure: *SHELXS97* (Sheldrick, 2008); program(s) used to refine structure: *SHELXL97* (Sheldrick, 2008); molecular graphics; *SHELXTL* (Sheldrick, 2008). The details of the experimental methods are included in (Table 2.2).

## CHAPTER 2

Table 2.2. Crystal data and structure refinement for noscapine.

Empirical formula	C <sub>22</sub> H <sub>23</sub> N O <sub>7</sub>
Formula weight	413.41
Temperature	173(2) K
Wavelength	1.54178 Å
Crystal system	Orthorhombic
Space group	P2(1)2(1)2(1)
Unit cell dimensions	a = 7.8349(5) Å
$\alpha = 90^\circ$ .	$\beta = 90^\circ$ .
b = 15.2363(9) Å	$\gamma = 90^\circ$ .
c = 32.5640(19) Å	
Volume	3887.3(4) Å <sup>3</sup>
Z	8
Density (calculated)	1.413 Mg/m <sup>3</sup>
Absorption coefficient	0.884 mm <sup>-1</sup>
F(000)	1744
Crystal size	0.26 x 0.17 x 0.08 mm <sup>3</sup>
Theta range for data collection	2.71 to 69.50°.
Index ranges	-9 ≤ h ≤ 9, -18 ≤ k ≤ 18, -37 ≤ l ≤ 39
Reflections collected	42197
Independent reflections	7122 [R(int) = 0.0406]
Completeness to theta = 69.50°	98.8 %
Absorption correction	Semi-empirical from equivalents
Max. and min. transmission	0.9327 and 0.8028
Refinement method	Full-matrix least-squares on F <sup>2</sup>
Data / restraints / parameters	7122 / 0 / 542
Goodness-of-fit on F <sup>2</sup>	1.054
Final R indices [I > 2σ(I)]	R1 = 0.0393, wR2 = 0.1177
R indices (all data)	R1 = 0.0455, wR2 = 0.1268
Absolute structure parameter	-0.03(15)
Extinction coefficient	0.00194(18)
Largest diff. peak and hole	0.611 and -0.500 e.Å <sup>-3</sup>

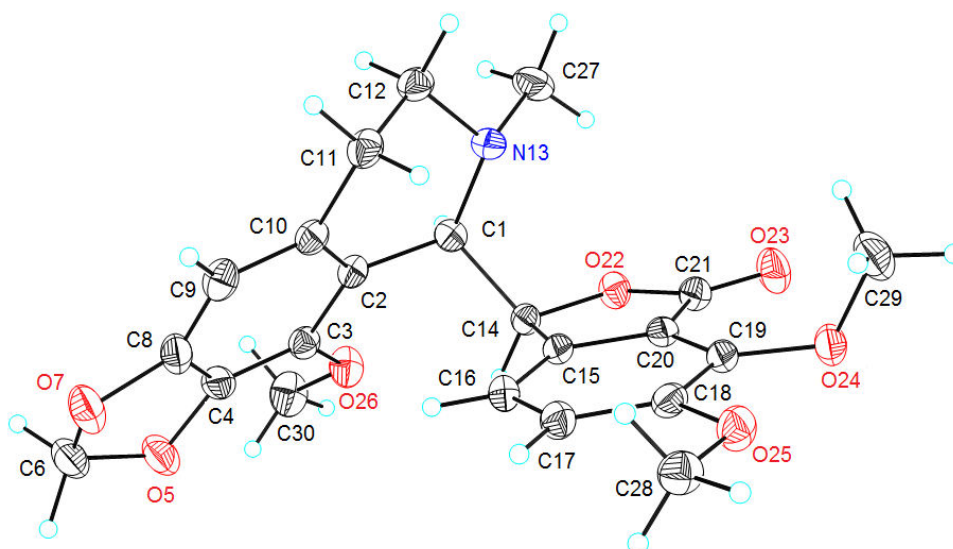


Figure 2.1. View of noscapine with the atom-labelling scheme. Displacement ellipsoids are drawn at 50% probability level.

In general the crystal structures of molecules are snap-shots of a dynamic process and could be a misleading representation of how they behave in solution. We have therefore used high resolution NMR spectroscopy to determine the range of dynamic structures of noscapine in solution and then calculate the probabilities of their existence. We have studied the noscapine conformation in solution with two-dimensional NMR spectroscopy. In particular we performed NOESY (Nuclear Overhauser and Exchange Spectroscopy) to calculate the distance between various protons in the noscapine structure. With this method, the nuclear overhauser effects between all spatially close protons on noscapine can be observed as cross peaks simultaneously (Figure 2.2). We calculated the distances between protons by method of Esposito and Pastore (1988). We then integrated the calculated distances with a methodology called NAMFIS (NMR Analysis of Molecular Flexibility In Solution). This method integrates NMR observables and force field structures to specify individual conformer populations and their relative percentages. In addition this program is capable of identifying multiple conformations consistent with the experimental NMR data. Our efforts have generated a series of conformers, out of which two are very reliable probabilities. Based on our data it seems that at any given time noscapine exists 86% in conformation I (blue , Figure2.3 (A) ) and 13% times in conformation II (yellow , Figure2.3 (A) ). In the more abundant conformation I two hydrophobic ring systems of noscapine are presented in an open configuration which resemble open palm relative to the collapsed two flat ring system.

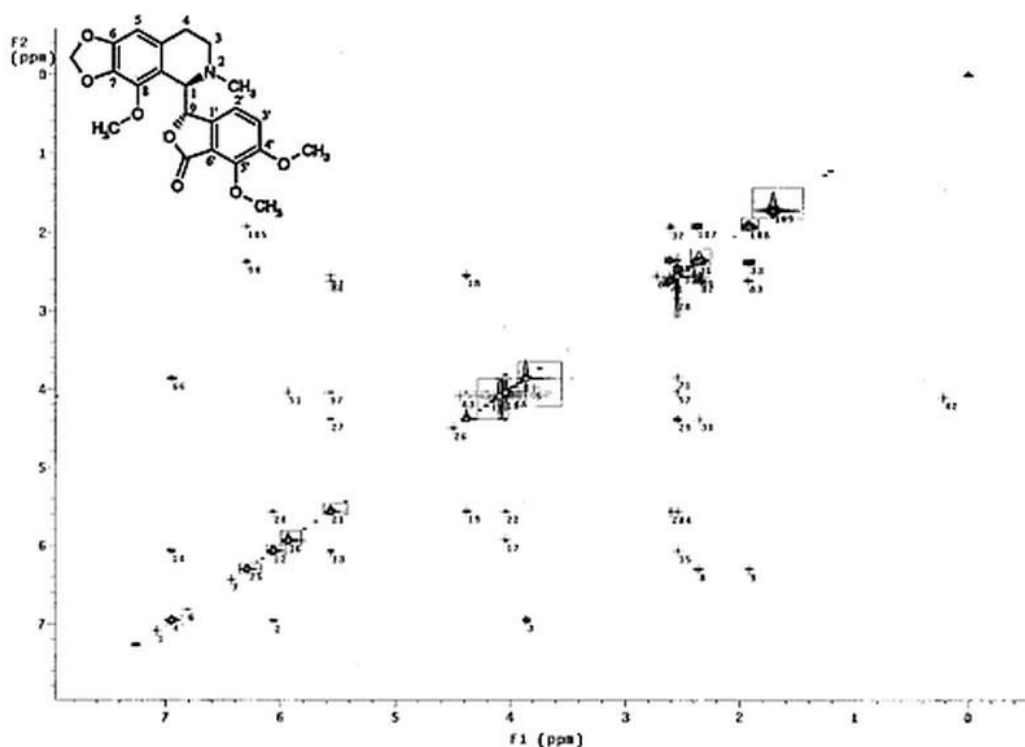


Figure 2.2. Two-dimensional NOESY spectrum of noscapine measured on 600 MHz NMR machine with two benzene ring protons as standard. (Inset) Noscapine structure with atomic numbering. The NOE in two-dimensional spectroscopy can be useful in determining precise distances between spatially closely located protons as cross-peaks. This technique has been productive in elucidating the structures of different noscapine conformers. The two axes represent a contrast between altered  $90^\circ$  pulses of magnetizations and the frequency labeled during the evolution time.

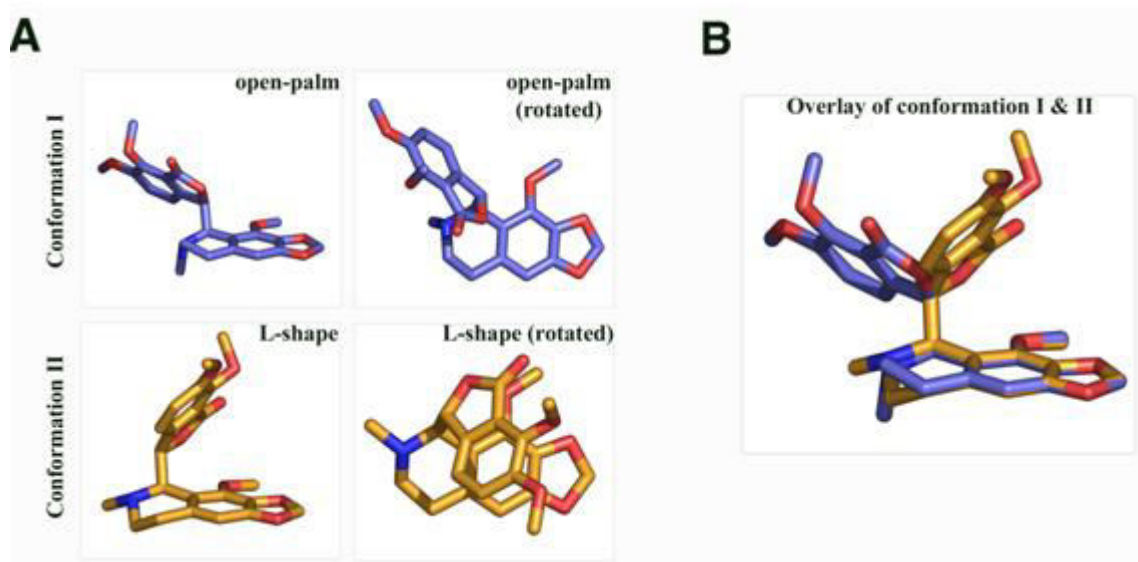


Figure 2.3 Two most probable noscapine conformations in solution derived from the NOESY spectroscopy followed by NAMFIS analysis. Please note that conformation I (top, blue in A) is an open-palm conformation, while conformation II (bottom, yellow in A) is a tilted L-shaped conformation. The rotated versions of these two conformations are shown on the right. (B). An overlay of the two conformations of noscapine as shown in A.

Both the crystal structure and NAMFIS have determined open palm conformation of noscapine. To generate similar structure of noscapine and its derivatives, we have initially built their molecular structures using the builder feature in Maestro (Schrödinger package, version 8.5). Each structure was assigned an appropriate bond order using ligprep (Schrödinger package, version 2.4) and a unique low-energy ring conformation with correct chirality was generated. All structures were subjected to molecular mechanics energy minimizations using Macromodel (Schrödinger package, version 9.8) with default settings. Partial atomic charges were assigned to the molecular structures using OPLS 2005 force field. Finally we have selected only the open palm conformation of noscapine and its derivatives for geometric optimization. To ensure that the geometry of the structure is fairly reasonable, we performed complete geometric optimization of these structures using Jaguar (Schrödinger package, version 7.7). We have used hybrid density functional theory with Becke's three-parameter exchange potential and the Lee-Yang-Parr correlation functional (B3LYP) and basis set 3-21G\* for geometrical optimization.

#### **2.2.4 Calculations of molecular descriptors**

Different classes of molecular descriptors were calculated from the structures obtained above. Briefly, quantum chemical descriptors including, heat of formation, dipole moment, highest occupied molecular orbital (HOMO), lowest unoccupied molecular orbital (LUMO) energies, and local charges were calculated by the molecular operating environment (MOE, version 2009-2010) software. Different topological, shape-based, physical, constitutional, and inductive descriptors were also calculated for each molecule by MOE software. MOE provides a number of calculation functions for descriptors, and has unique universal descriptors that enable a variety of properties to be modeled.

#### **2.2.5 Data processing and QSAR modeling**

The total number of molecular descriptors calculated initially was 422. All these molecular descriptors were categorized into different classes such as topological, shape, physical, sterimol and quantum. A systematic search in the order of missing value test, zero test, correlation coefficient and genetic function approximation (GFA) was performed to determine significant descriptors from each class of descriptor for QSAR model building. The calculated descriptors were collected in a data matrix (*D*) whose number of rows and columns were the number of molecules and descriptors, respectively. The descriptors were centered to zero mean and scaled to unit variance (auto scaling). Any parameter which is not calculated (missing value) for any number of the compounds in the data

set was rejected in the first step. Some of the descriptors were rejected because they contained a value of zero for all compounds and have been removed (zero tests). In order to minimize the effect of co-linearity and to avoid redundancy, the correlation of descriptors with each other was investigated, and those pairs with high co-linear relationships were determined. Among the co-linear descriptors, one with the lowest correlation with drug activity was removed from the data matrix. Among the remaining descriptors, the set of descriptors that gave statistically best QSAR models was selected using GFA [10] within the QSAR-evolution module (ga.svl) of the MOE program. This evolutionary genetic tool enables automated QSAR modeling “on the fly” and is available through the “SVL exchange”. The GFA algorithm starts with the creation of a population of randomly generated parameter sets. The algorithm was set up to discover descriptor-activity relationships consisting of linear polynomial terms. One hundred random initial equations with four variables were used (adding constants where necessary) to search for equations of unlimited length but with acceptable lack-of-fit scores [10]. New “child” equations were generated using the multiple linear regression (MLR) method. Child equations were “mutated” (i. e., changed at “birth”) 50% of the time after their generation by addition of randomly selected new terms. The number of generations of equation evolution required in the data set was gauged by the attainment of adjusted  $R^2$  values and minimal lack-of-fit scores. Creation of a consecutive generation involves crossovers between set contents, as well as mutations. The total number of crossovers was set to 50,000 with the auto-termination factor of 1,000 (meaning that the calculation was stopped when the “fitness function” value does not change during 1,000 crossovers). The equations were evaluated for statistical soundness by Friedman’s lack-of-fit score,  $R^2$ , adjusted  $R^2$ , least-squares error, and correlation coefficient after cross validation statistics. The Friedman’s lack of fit (LOF) score is expressed by the following equation:

$$\text{LOF} = \text{LSE} / \{1 - (c + dp)/m\} \quad (1)$$

where LSE is the least-square error, c is the number of basis functions in the model, d is smoothing parameters, p is the number of descriptors and m is the number of observations in the training set. The smoothing parameter, which controls the scoring bias between equations of different sizes, was set at default value of 1.0.

### 2.2.6 Validation of QSAR models

The predictive capability of the developed QSAR model was validated based on several statistical tests such as leave-one-out, leave-10%-out, leave-20%-out cross validation and Y-randomization test using a svl script (Qsarwizard.svl). The cross validation regression coefficient

( $R^2_{LOO}$ ) was calculated based on the PRESS (prediction error sum of squares) and SSY (Sum of squares of deviation of the experimental values,  $Y$ , from their mean) using following equation:

$$R^2_{LOO} = 1 - \frac{PRESS}{SSY} = 1 - \frac{\sum_{i=1}^n (Y_{exp} - Y_{pred})^2}{\sum_{i=1}^n (Y_{exp} - \bar{Y})^2} \quad (2)$$

where,  $Y_{exp}$ ,  $Y_{pred}$  and  $\bar{Y}$  are the experimental, predicted, and mean values of experimental activity of the training set compounds, respectively. The  $Y$ -randomization test was done by repeatedly shuffling the activity values of the data set and developing new QSAR models and then comparing the resulting score with the score of the original QSAR model generated from non-randomized activity values. This process was repeated 100 times. If the original QSAR model is statistically significant, its score should be significantly better than those from permuted data. We have used a parameter,  $R_p^2$ , which penalizes the model for the difference between squared mean correlation coefficient of randomized models ( $R_r^2$ ) and squared correlation coefficient of the nonrandomized model ( $R^2$ ). The  $R_p^2$  parameter was calculated by the following equation:

$$R_p^2 = R^2 \cdot \sqrt{R^2 - R_r^2} \quad (5)$$

The parameter,  $R_p^2$ , ensures that our QSAR models thus developed are not obtained by chance. We have assumed the value of  $R_p^2$  should be greater than 0.5 for an acceptable model.

The determination coefficient in prediction using the test set ( $R^2_{test}$ ) was calculated using the following equation [11,12].

$$R^2_{test} = 1 - \frac{\sum (Y_{pred_{test}} - Y_{exp_{test}})^2}{\sum (Y_{exp_{test}} - \bar{Y}_{exp_{train}})^2} \quad (3)$$

where  $Y_{pred_{test}}$  and  $Y_{exp_{test}}$  are the predicted values based on the QSAR equation (model response) and experimental activity of the test set compounds.  $\bar{Y}_{exp_{train}}$  is the mean activity value of the training set compounds. Further evaluation of the predictive ability of the QSAR model for the test set compounds was done by determining the value of  $rm^2$  by the following equation [11,12].

$$rm^2 = R^2_{test} \left( 1 - \sqrt{R^2_{test} - R^2_{test_0}} \right) \quad (4)$$

where  $R^2_{test}$  is the squared Pearson correlation coefficient for regression calculated using  $Y = a + bx$ ; 'a' is referred to as the y-intercept, 'b' is the slope value of regression line, and  $R^2_{test_0}$  is the squared

correlation coefficient for regression without using y-intercept and the regression equation was  $Y=bx$ .

To further check the inter-correlation between molecular descriptors used in the final QSAR model, we performed variance inflation factor (VIF) analysis. The VIF value was calculated from  $1/(1-R^2)$ , where  $R^2$  is the multiple correlation coefficient of one descriptor's effect regressed onto the remaining molecular descriptors. If the VIF value is larger than 10 for a descriptor its information could be hidden by other descriptors [11,12].

## 2.3 RESULTS AND DISCUSSIONS

### 2.3.1 Anti-tumor activity of noscapinoids

The anti-tumor activities ( $IC_{50}$ ) of 32 noscapinoids in the human lymphoblastoid cancer cell line (CEM) was determined to complete a reasonable data set that possess a variety of substituents with different hydrophobic and electronic properties while preserving the primary skeleton of noscapine (Table 2.1). This series of noscapinoids have a reasonably wide spectrum of anti-tumor activities (1.2  $\mu$ M to 56.0  $\mu$ M; statistically significant;  $F = 182.6$ ,  $p < 0.001$ ), as determined by MTS assay. The reasonable structural diversity as well as the resulting biological activity ( $IC_{50}$  in CEM) could produce QSAR models for accurate activity predictions. We used 22 structures as a training set for the development of our QSAR models to compute the biological activity for a test set of the remaining 10 structures.

### 2.3.2 Optimization of the structure of noscapinoids

The structure of noscapine can be viewed as “two flat planar plates” of its two ring systems (isoquinoline and isobenzofuranone) joined by a rotatable single C-C bond between two chiral centers of the molecule. This is much akin to two palms of the hand put together at an angle of approximately  $36^\circ$ , but rotating freely in space against each other producing a range of structures between two extremes of an L-shaped “closed-palm (two planar rings at approximately  $36^\circ$ )” and a completely extended outstretched “open-palm (two ring planes at approximately  $108^\circ$ )”. Noscapine might thus experience a diverse range of conformer states in solution. To get an insight into this, we used high-resolution 2D-NMR spectroscopy to determine the range of dynamic structure of noscapine in solution and then calculated the percentage of time spent in each conformer state. Out of many conformations generated, noscapine spends majority of its time (86%) in “open-palm” conformations. *Ab initio* quantum chemical calculations using B3LYP and basis set 3-21G\* level was used to find the optimum 3D geometry of the molecules. In order to prevent the structures



located at local minima, geometry optimization was iterated many times with different starting points for each molecule. The optimization was preceded by the Polak-Rebiere algorithm to reach to 0.01 root mean square gradient. In order to check the reliability of the geometry obtained, we compared the structural parameters of the noscapine (Figure 2.4c) with the conformation obtained from NAMFIS (Figure 2.4 b & Table 2.3) and crystal structure (Figure 2.1 and Table 2.3, Table 2.4 & Table 2.5). All calculations reproduced most of the structural parameters of the noscapine (Table 2.3). The overlaid 3D structures of molecules are shown in Figure 2.4d. The conformation of the noscapine and its congeners can clearly reveal an overall similar scaffold structure, specifically the isoquinoline and isobenzofuranone rings.

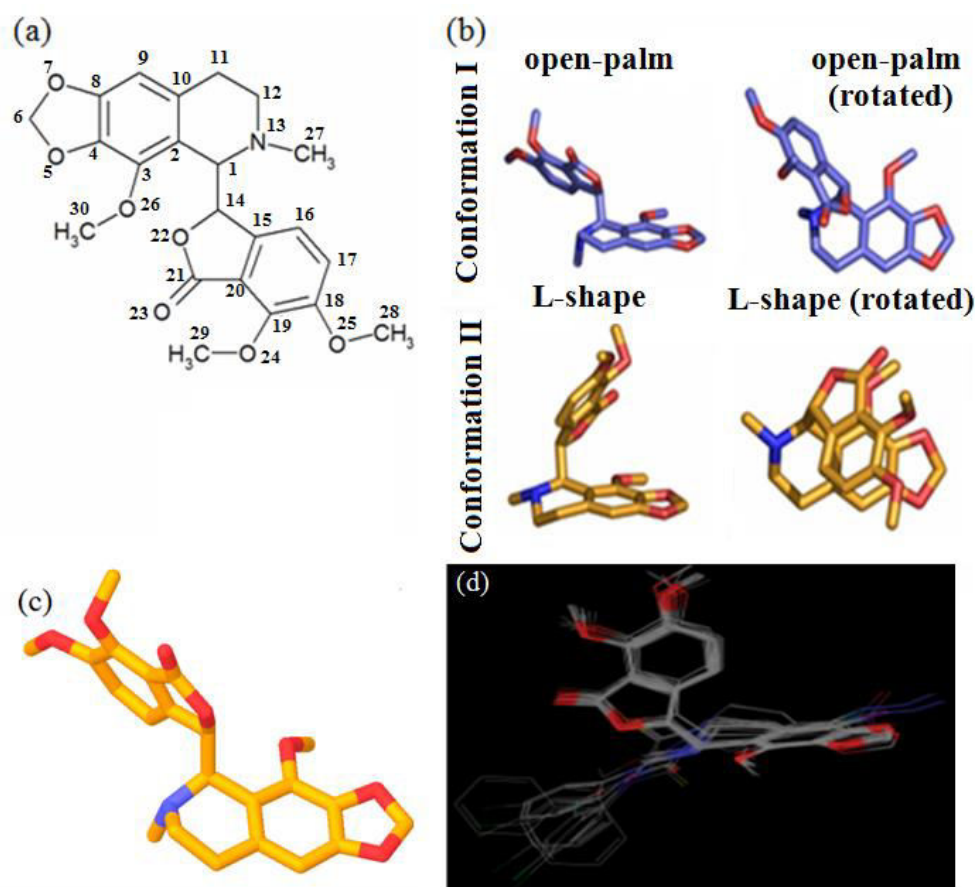


Figure 2.4. Elucidation of dynamic structure of noscapine. (a) Structure of noscapine with atomic numbers used in this study. (b) Two probable noscapine conformations in solution derived from the NOESY spectra followed by NAMFIS analysis: conformation I is an open-palm conformation (exists 86% of time in solution) and conformation II is a closed-palm conformation (a tilted L-shaped conformation that exists 13% of time in solution). The rotated versions of these two conformations are shown on the right. (c) The geometrically optimized Jaguar generated conformation of noscapine also comfortably revealed open-palm conformation. (d) Superposition of geometrically optimized conformations of noscapinoids (32 molecules) revealed similar scaffold. (For the purpose of aligning the scaffold structures, we have altered the displayed orientation from that of c.)

## CHAPTER 2

Table 2.3. Experimental and theoretical values of the isoquinoline and isobenzofuranone ring parameters (bond lengths in Å, bond angles and torsional angles in degrees). Atoms are numbered according to Figure 2.2a.

Parameters	Theoretical (3-21G*)	Crystal structure	Parameters	Theoretical (3-21G*)	Crystal structure
N13-C12	1.488	1.459	C18-C17	1.401	1.397
N13-C27	1.489	1.462	C17-C16	1.402	1.391
N13-C1	1.472	1.471	C16-C15	1.381	1.379
O5-C6	1.394	1.436	C12-N13-C27	111.1	110.18
O5-C4	1.360	1.387	C12-N13-C1	113.9	114.98
O7-C6	1.389	1.420	C27-N13-C1	113.5	111.57
O7-C8	1.351	1.378	C4-O5-C6	104.2	104.8
O26-C30	1.406	1.417	C8-O7-C6	104.7	105.3
O22-C21	1.347	1.374	C3-O26-C30	116.5	118.2
O22-C14	1.452	1.452	C21-O22-C14	113.8	111.63
O23-C21	1.189	1.198	O7-C6-O5	109.1	107.9
O24-C19	1.426	1.428	C9-C8-C4	123.8	122.5
O24-C29	1.384	1.382	C3-C4-C8	120.8	121.3
O25-C18	1.378	1.369	O26-C3-C4	124.0	125.7
O25-C28	1.433	1.426	C4-C3-C2	116.3	117.0
C4-C8	1.378	1.388	C10-C2-C3	121.7	120.6
C4-C3	1.376	1.379	C10-C2-C1	119.5	121.32
C3-O26	1.380	1.376	N13-C1-C2	112.7	115.14
C3-C2	1.411	1.415	N13-C1-C14	106.6	110.0
C2-C10	1.401	1.397	C2-C1-C14	108.1	107.53
C2-C1	1.521	1.516	N13-C12-C11	112.3	110.35
C12-C11	1.505	1.515	O23-C21-O22	125.6	122.8
C11-C10	1.497	1.504	O23-C21-C20	126.6	128.9
C10-C9	1.391	1.390	C19-C20-C15	122.5	122.0
C9-C8	1.369	1.368	C15-C20-C21	107.1	108.72
C1-C14	1.543	1.547	C20-C19-C18	117.7	117.58
C14-C15	1.496	1.502	C20-C19-O24	117.8	120.8
C21-C20	1.458	1.471	C17-C18-O25	125.2	124.1
C20-C15	1.381	1.392	C18-C17-C16	120.4	121.0
C20-C19	1.383	1.391	C19-O24-C29	102.2	104.8
C19-C18	1.409	1.399	C18-O25-C28	128.5	126.5
Parameters	Theoretical (3-21G*)	Experimental (NAMFIS)	Parameters	Theoretical (3-21G*)	Experimental (NAMFIS)
H14-H1	2.36	2.36	H12-H12	1.73	1.75
H9-H11	2.87	2.96	H11-H11	1.94	1.90
H1-NCH <sub>3</sub>	2.77	2.76	H16-H14	3.16	3.29
H17-OCH <sub>3</sub>	2.61	2.59	H14-OCH <sub>3</sub>	4.47	4.43
H12-H11	2.72	2.74	H6-H6	1.78	1.77

## CHAPTER 2

Table 2.4. Atomic coordinates ( $\times 10^4$ ) and equivalent isotropic displacement parameters ( $\text{\AA}^2 \times 10^3$ ) for noscapine.  $U(\text{eq})$  is defined as one third of the trace of the orthogonalized  $U_{ij}$  tensor.

	x	y	z	$U(\text{eq})$
C(1)	4429(3)	3256(2)	1617(1)	28(1)
C(2)	4946(3)	2311(2)	1692(1)	28(1)
C(3)	4392(3)	1904(2)	2059(1)	30(1)
C(4)	4737(3)	1021(2)	2103(1)	35(1)
O(5)	4275(3)	450(1)	2415(1)	48(1)
C(6)	5194(4)	-345(2)	2329(1)	49(1)
O(7)	5741(3)	-311(1)	1914(1)	50(1)
C(8)	5609(3)	558(2)	1801(1)	37(1)
C(9)	6193(3)	947(2)	1450(1)	36(1)
C(10)	5869(3)	1837(2)	1399(1)	30(1)
C(11)	6551(3)	2323(2)	1033(1)	35(1)
C(12)	6929(3)	3264(2)	1153(1)	35(1)
N(13)	5366(2)	3704(1)	1287(1)	32(1)
C(14)	2492(3)	3264(1)	1524(1)	27(1)
C(15)	1935(3)	2844(2)	1129(1)	28(1)
C(16)	2003(3)	1986(2)	996(1)	31(1)
C(17)	1333(3)	1777(2)	612(1)	33(1)
C(18)	591(3)	2421(2)	365(1)	31(1)
C(19)	474(3)	3289(2)	503(1)	30(1)
C(20)	1171(3)	3483(1)	885(1)	28(1)
C(21)	1170(3)	4320(2)	1111(1)	33(1)
O(22)	1917(2)	4166(1)	1486(1)	33(1)
O(23)	646(3)	5034(1)	1023(1)	47(1)
O(24)	-379(2)	3916(1)	282(1)	39(1)
O(25)	-129(2)	2260(1)	-11(1)	39(1)
O(26)	3513(2)	2411(1)	2333(1)	40(1)
C(27)	5726(4)	4617(2)	1392(1)	47(1)
C(28)	66(3)	1394(2)	-170(1)	39(1)
C(29)	515(4)	4236(2)	-70(1)	54(1)
C(30)	3645(4)	2204(2)	2756(1)	49(1)

## CHAPTER 2

Table 2.5. Anisotropic displacement parameters ( $\text{\AA}^2 \times 10^3$ ) for noscapine. The anisotropic displacement factor exponent takes the form:  $-2\pi^2 [h^2 a^{*2} U^{11} + \dots + 2 h k a^* b^* U^{12}]$ .

	U <sup>11</sup>	U <sup>22</sup>	U <sup>33</sup>	U <sup>23</sup>	U <sup>13</sup>	U <sup>12</sup>
C(1)	31(1)	30(1)	24(1)	-1(1)	2(1)	0(1)
C(2)	25(1)	31(1)	27(1)	0(1)	-2(1)	3(1)
C(3)	28(1)	35(1)	26(1)	2(1)	-2(1)	1(1)
C(4)	33(1)	39(1)	31(1)	9(1)	-4(1)	-4(1)
O(5)	59(1)	38(1)	47(1)	16(1)	1(1)	-2(1)
C(6)	56(2)	34(1)	58(2)	15(1)	-11(1)	-7(1)
O(7)	66(1)	29(1)	55(1)	4(1)	-11(1)	4(1)
C(8)	39(1)	27(1)	43(1)	1(1)	-11(1)	3(1)
C(9)	35(1)	38(1)	35(1)	-7(1)	-4(1)	7(1)
C(10)	26(1)	36(1)	27(1)	-2(1)	-3(1)	2(1)
C(11)	32(1)	43(1)	32(1)	0(1)	5(1)	8(1)
C(12)	29(1)	45(1)	32(1)	5(1)	3(1)	0(1)
N(13)	30(1)	34(1)	33(1)	4(1)	3(1)	-3(1)
C(14)	26(1)	26(1)	31(1)	2(1)	5(1)	4(1)
C(15)	23(1)	30(1)	30(1)	6(1)	2(1)	2(1)
C(16)	30(1)	28(1)	34(1)	4(1)	-3(1)	3(1)
C(17)	32(1)	29(1)	38(1)	0(1)	-2(1)	1(1)
C(18)	25(1)	38(1)	30(1)	2(1)	-3(1)	-3(1)
C(19)	24(1)	32(1)	32(1)	8(1)	3(1)	2(1)
C(20)	24(1)	28(1)	32(1)	4(1)	4(1)	0(1)
C(21)	31(1)	32(1)	36(1)	3(1)	2(1)	2(1)
O(22)	37(1)	27(1)	35(1)	-2(1)	3(1)	8(1)
O(23)	59(1)	27(1)	54(1)	4(1)	-6(1)	9(1)
O(24)	36(1)	42(1)	37(1)	14(1)	2(1)	9(1)
O(25)	42(1)	40(1)	35(1)	0(1)	-11(1)	-1(1)
O(26)	46(1)	49(1)	26(1)	4(1)	7(1)	11(1)
C(27)	47(1)	33(1)	62(2)	5(1)	5(1)	-10(1)
C(28)	39(1)	43(1)	33(1)	-2(1)	-2(1)	-4(1)
C(29)	61(2)	52(2)	50(2)	23(1)	9(1)	8(2)
C(30)	57(2)	62(2)	27(1)	1(1)	-1(1)	10(2)

### 2.3.3 QSAR modeling

The geometrically optimized structures of the molecules were used and a set of 422 molecular descriptors were calculated. It includes a set of shape and topological descriptors, described by means of the surface area, volume, topological indices and dihedral angle between the isoquinoline and isobenzofuranone rings. The electronic descriptors such as  $E_{\text{HOMO}}$ ,  $E_{\text{LUMO}}$ , local charges and dipole moments were derived from AM1 calculations. Indices of electronegativity ( $\chi = -0.5(E_{\text{HOMO}} - E_{\text{LUMO}})$ ), hardness ( $\eta = 0.5(E_{\text{HOMO}} - E_{\text{LUMO}})$ ), softness ( $S = 1/\eta$ ) and electrophilicity ( $\omega = \chi^2/2\eta$ ) were calculated from HOMO and LUMO energies [14]. Constitutional molecular descriptors were used to define the effect of different fragments of the molecules. From each class of molecular descriptors, significant descriptors were filtered out systematically as mentioned in

materials and method section, pertaining to QSAR model development. Multiple linear regression (MLR) analyses were employed for QSAR model development (Table 2.6).

Table 2.6. The results of multiple linear regression (MLR) analysis with different type of descriptors.

Sl. No.	MLR equations	Type of descriptors
1	$pIC_{50} = 4.737(0.077)*VDistEq - 2.386(0.6631)*weinerPath + 1.53(0.428)*BCUT\_SLOGP\_1 + 0.169(0.101)*GCUT\_SLOGP\_1$ N = 22, LOF = 0.203, $R^2 = 0.590$ , $R^2_{adj} = 0.545$ , $S = 0.373$ , PRESS = 4.264, F-test = 6.76, P = 0.001, $R^2_{cv} = 0.418$ , $RM^2 = 0.352$ , $R^2_{test} = 0.529$	Topology
2	$pIC_{50} = 4.793(0.076) + 3.897(1.118)*chi0v - 3.31(1.361)*chi1v + 0.967(2.395)*chi0 - 0.408(2.447)*Kier1 - 1.29(0.471)*KierA3$ N = 22, LOF = 0.203, $R^2 = 0.641$ , $R^2_{adj} = 0.547$ , $S = 0.373$ , PRESS = 4.261, F-test = 6.79, P = 0.001, $R^2_{cv} = 0.421$ , $RM^2 = 0.356$ , $R^2_{test} = 0.537$	Shape
3	$pIC_{50} = 4.761(0.073) - 1.62(0.456)*logS + 7.391(2.013)*MR - 9.349(1.779)*SMR - 0.124(0.113)*TPSA + 1.025(0.570)*vdw\_area - 0.797(0.392)*log p(o/w)$ N = 22, LOF = 0.202, $R^2 = 0.688$ , $R^2_{adj} = 0.584$ , $S = 0.357$ , PRESS = 5.845, F-test = 6.62, P = 0.001, $R^2_{cv} = 0.463$ , $RM^2 = 0.434$ , $R^2_{test} = 0.604$	Physical
4	$pIC_{50} = 4.696(0.067) + 0.188(0.082)*SMB2 - 2.431(0.578)*SMB4 + 2.152(0.511)*SMB5 + 0.243(0.154)*directional\_hyd\_sa + 0.115(0.147)*directional\_pol\_sa$ (N = 22, LOF = 0.140, $R^2 = 0.737$ , $R^2_{adj} = 0.663$ , $S = 0.322$ , PRESS = 3.302, F-test = 10.43, P = 0.0001, $R^2_{cv} = 0.552$ , $RM^2 = 0.572$ , $R^2_{test} = 0.617$ )	Sterimol
5	$pIC_{50} = 4.753(0.069) - 0.384(0.126)*Am1\_dipole + 0.291(0.103)*E\_rele + 0.106(0.098)*dipoleX + 22.766(6.369)*Electronegativity - 13.987(3.924)*Softness + 10.04(2.708)*Electrophilicity$ (N = 22, LOF = 0.140, $R^2 = 0.749$ , $R^2_{adj} = 0.665$ , $S = 0.321$ , PRESS = 4.056, F-test = 8.94, P = 0.0001, $R^2_{cv} = 0.449$ , $RM^2 = 0.554$ , $R^2_{test} = 0.679$ )	Quantum
6	$pIC_{50} = 4.746(0.034) - 0.586(0.075)*softness + 0.664(0.253)*vdw\_area - 0.317(0.288)*KierA3 + 0.241(0.071)*SMB2 + 0.101(0.108)*directional\_hyd\_sa - 0.167(0.06)*directional\_pol\_sa$ (N = 22, LOF = 0.123, $R^2 = 0.942$ , $R^2_{adj} = 0.914$ , $S = 0.159$ , PRESS = 1.199, F-test = 34.42, P = 0.0001, $R^2_{cv} = 0.815$ , $RM^2 = 0.900$ , $R^2_{test} = 0.817$ )	All descriptor

At first the QSAR equation was derived using the topology descriptors. This initial equation does not have a high statistical quality. The QSAR equation developed from shape descriptors revealed better structure-activity relationships (equation 2) than that of topology descriptors (equation 1). Among the chemical descriptors that define the shape of the molecules: chi0 (atomic connectivity index, order 0), chi0v and chi1v (atomic valence connectivity indices, order 0 and 1 respectively), first kappa shape index and third alpha modified shape index were used by the equation. Similarly the molecular descriptors defining the physical properties of the molecules: log S (log of the aqueous solubility), MR (molecular refractivity), TPSA (polar surface area calculated

using group contributions to approximate the polar surface area), vdw\_area (area of van der Waals surface) and log P (log of the octanol/water partition coefficient) were used by the QSAR equation 4. The parameters such as log S, vdw\_area and log P have been considered as the descriptors for the hydrophobic effect. The molar refractivity is a constitutive-additive property that is calculated by the Lorenz-Lorentz formula. The high standard error and low correlation coefficient for QSAR equations (1, 2 and 3) revealed that the anti-tumour activity of the molecules is not correlated by the individual topology, shape and physical descriptors. However, the QSAR equations developed based on sterimol and quantum descriptors of the molecules have improved the predictive value (equations 4 and 5) with correlation coefficient of 0.737 and 0.749 and standard error of 0.322 and 0.312, respectively. The sterimol descriptors calculate a set of six parameters: L, B1, B2, B3, B4 and B5 for the whole molecule. The parameter 'L' is measured along the substitution axis and B1-B4 are measured orthogonal to the substitution axis as shown in Figure 2.5.

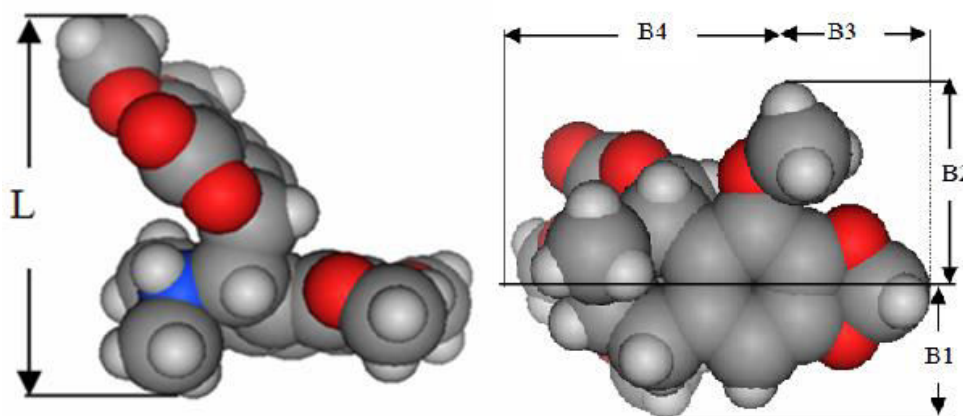


Figure 2.5. Schematic representations of different steriomolecular parameters used in the study.

Sterimol descriptors were calculated using a svl script (sterimol.svl). The descriptors such as directional\_pol\_sa and directional\_hyd\_sa used in equation 4, describe the directionality of polar and hydrophobic characters and compute the amounts of polar and hydrophobic atomic accessible surface for a structure [15]. Both descriptors were calculated using a svl script (q\_surfare.svl). The quantum mechanical descriptors were calculated using MOPAC distributed with MOE. Electronegativity and electrophilicity parameters have positive coefficient value. Softness parameter has negative coefficient value. Together, these parameters indicate strong dependence of biological activity (anti-tumor) on the electronic features. The indices of electronegativity, electrophilicity and softness were calculated from the difference between the HOMO and LUMO energies. The QSAR equation (5) developed including these descriptors had high correlation ( $R^2 = 0.749$ ) with biological activity. It should be noted that the correlation of the HOMO or LUMO energies alone, however,

show low  $R^2$  values (0.187 and 0.235) with biological activity. The final QSAR model (equation 6; Table 2.6) was obtained when all the above descriptors were combined together. It consists of only six descriptors: softness (electronic descriptor), vdw\_area (physical descriptor), KierA3 (shape index) and B2, directional\_hyd\_sa, directional\_pol\_sa (sterimol descriptor). The best significant relationship for the biological activity has been deduced to be:

$$pIC_{50} = 4.746 (0.034) - 0.586 (0.075) * \text{softness} + 0.664 (0.253) * \text{vdw\_area} - 0.317 (0.288) * \text{KierA3} + 0.241 (0.071) * \text{SMB2} + 0.101 (0.108) * \text{directional\_hyd\_sa} - 0.167 (0.06) * \text{directional\_pol\_sa}$$

$$(N = 22, \text{LOF} = 0.123, R^2 = 0.942, R^2_{adj} = 0.914, S = 0.159, \text{PRESS} = 1.199, F\text{-test} = 34.42, P = 0.0001, R^2_{LOO} = 0.815, RM^2 = 0.900, R^2_{test} = 0.817)$$

where  $n$  is the number of compounds in the training set,  $R^2$  is the squared correlation coefficient,  $S$  is the estimated standard deviation about the regression line,  $R^2_{adj}$  is the square of the adjusted correlation coefficient for degrees of freedom,  $F$ -test is the measure of variance that compares 2 models differing by one or more variables to determine if the complexity of the model correlates positively with its reliability (the model is supposed to be good if the  $F$  test is above a threshold value), and  $R^2_{LOO}$  is the square of the correlation coefficient of the cross-validation using the leave-one-out (LOO) cross-validation technique.

The QSAR model developed in this study is statistically best fitted ( $R^2 = 0.942$ ,  $R^2_{LOO} = 0.815$ ,  $F$ -test = 34.42) and consequently used for the prediction of anti-tumor activities ( $pIC_{50}$ ) of training and test sets of molecules as reported in Tables 2.7 and 2.8. The quality of the prediction models for the training set compounds is shown in Figure 2.6.

The  $R^2$  and  $R^2_{LOO}$  values (0.942 and 0.815) of the model corroborates with the criteria for a highly predictive QSAR model [11,12]. The standard error of estimate for the model was 0.159 that is an indicator of the robustness of the fit, and suggested that the predicted  $pIC_{50}$  based on QSAR model is reliable. The developed model was further validated by  $Y$ -randomization test. In general, QSAR model with  $R^2_p$  values greater than 0.5 is considered statistically robust, whereas the lower  $R^2_p$  values (less than 0.5) point to a chance occurrence. The values of  $R^2_p$  for all 100 models were found well above the stipulated value of 0.5 ( $R^2_p$ : 0.683 to 0.814). Therefore, the QSAR model is highly predictive.

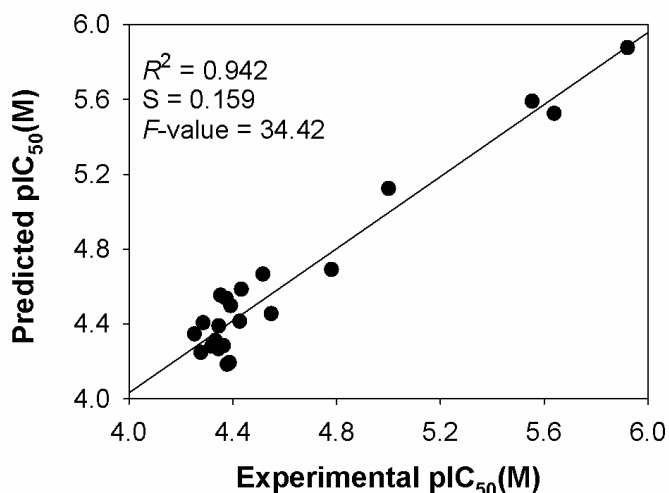


Figure 2.6. Relationship between predicted and experimental biological activities of training set compounds as per QSAR equation (6). Biological activities are  $pIC_{50} = -\log (IC_{50})$  in molar concentrations.

Table 2.7. Predicted anti-tumor activity of the training set compounds in Table 2.1 according to the QSAR models (using equations 2-6, Table 2.6).

Compound number	Experimental $pIC_{50}(M)$	Predicted $pIC_{50}(M)$				
		$pIC_{50}^2$	$pIC_{50}^3$	$pIC_{50}^4$	$pIC_{50}^5$	$pIC_{50}^6$
1	4.780	5.137	4.897	4.915	5.132	4.692
2	5.921	5.331	4.706	5.332	5.607	5.877
4	5.638	5.779	4.723	5.431	5.261	5.525
5	4.410	4.989	4.651	4.623	4.243	4.586
6	4.548	4.669	4.844	4.713	4.618	4.456
7	4.345	4.429	4.469	4.560	4.313	4.269
8	5.553	4.945	4.851	5.335	5.240	5.591
10	4.516	4.529	4.948	4.865	4.714	4.667
11	5.000	5.079	4.785	4.891	5.175	5.124
13	4.319	4.397	4.518	4.527	4.301	4.283
16	4.392	4.535	4.586	4.581	4.250	4.499
17	4.378	4.230	4.466	4.298	4.372	4.185
18	4.346	4.334	4.627	4.272	4.217	4.390
19	4.333	4.239	4.568	4.503	4.142	4.313
20	4.353	4.251	4.813	4.130	4.394	4.554
22	4.286	4.616	5.099	4.280	4.232	4.407
25	4.387	3.980	5.257	4.406	3.993	4.195
26	4.374	4.676	5.332	4.690	4.239	4.538
29	4.252	4.392	5.256	3.927	4.289	4.347
30	4.277	4.186	5.152	4.488	4.374	4.249
31	4.427	4.747	5.111	4.255	4.430	4.415
32	4.364	4.584	4.717	3.709	4.513	4.285

<sup>2,3,4,5,6</sup>Based on QSAR equation 2,3,4,5 and 6 developed in the study.



Table 2.8. Predicted anti-tumor activity of the test set compounds in Table 2.1 according to the QSAR models (using equations 2-6, included in table 2.6 ).

Compound number	Experimental $pIC_{50}$ (M)	Predicted $pIC_{50}$ (M)				
		$pIC_{50}^2$	$pIC_{50}^3$	$pIC_{50}^4$	$pIC_{50}^5$	$pIC_{50}^6$
3	5.721	5.100	5.153	5.103	5.736	5.736
9	4.810	4.905	5.192	5.048	4.816	4.841
12	5.000	4.744	5.078	5.034	5.016	5.267
14	4.345	4.624	4.242	4.635	4.769	4.586
15	4.355	4.527	4.620	4.512	4.449	4.711
21	4.356	4.633	4.527	4.487	4.224	4.158
23	4.403	4.554	4.171	4.414	4.541	4.266
24	4.371	4.827	4.571	4.845	4.229	4.786
27	4.450	4.565	4.067	4.250	3.657	4.447
28	4.271	4.695	4.303	4.464	4.240	4.201

<sup>2,3,4,5,6</sup>Based on QSAR equation 2,3,4,5 and 6 developed in the study.

The inter-correlation of the descriptors used in the final model was very low (below 0.6) and thus the model is statistically significant. It is necessary that the descriptors involved in the equation should not be inter-correlated with each other. To further check the inter-correlation of descriptors VIF analysis was performed. VIF values of these descriptors are: 3.268 (softness), 4.525 (vdw\_area), 4.651 (KierA3), 4.608 (SMB2), 2.849 (directional\_hyd\_sa), and 2.740 (directional\_pol\_sa). Based on the VIF analysis it was found that the descriptors used in the final model have very low inter-correlation [11,12]. Satisfied with the robustness of the QSAR model developed using the training set we next applied the QSAR model to an external data set of noscapine analogs comprising the test set. Table 2.8 presents the predicted  $pIC_{50}$  values of the test set based on QSAR model. The overall root mean square error (RMSE) between the experimental and the predicted  $pIC_{50}$  value was 0.193 that revealed good predictability. The squared correlation coefficient between experimental and predicted  $pIC_{50}$  values for the test set is also significant ( $R^2 = 0.817$ ). Figure 2.5 shows the quality of the fit. The estimated correlation coefficient between experimental and predicted  $pIC_{50}$  values with intercept ( $R^2$ ) and without intercept ( $R^2_0$ ) are 0.942 and 0.940, respectively. The value of  $[(R^2 - R^2_0)/R^2] = (0.942-0.940)/0.942 = 0.0021$  is also less than the stipulated value of 0.1 [11,12]. Values of  $R^2_{test} = 0.817$  and  $rm^2 = 0.90$  were in the acceptable range thereby indicating the good external predictability of the QSAR model [11,12].

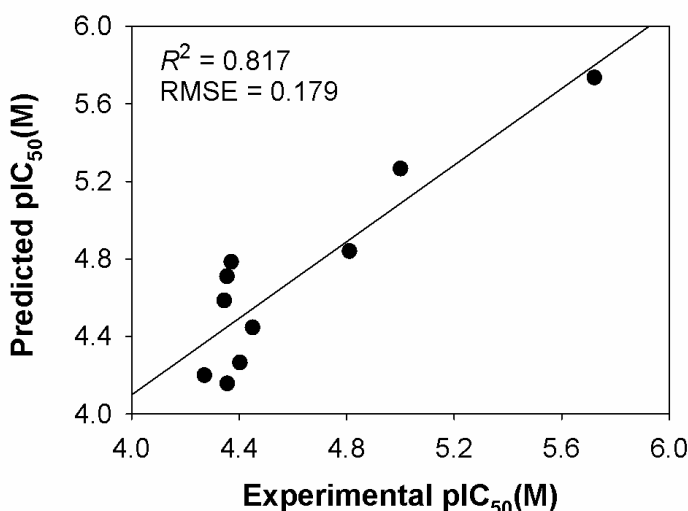


Figure 2.7. Relationship between predicted and experimental biological activities of test set compounds as per QSAR equation (6). Biological activities are  $pIC_{50} = -\log(IC_{50})$  in molar concentrations.

The appearance of the electronic descriptors such as electronegativity and electrophilicity in equation 5 as well as softness in equation 6 (calculated from HOMO and LUMO energies) demonstrates that these descriptors significantly influence the anti-tumor activity of noscapinoids. They favor columbic interaction between ligands and receptor. Therefore, the developed QSAR models guided us to substitute a functional group such as “azido” ( $N^-=N^+=N^-$ ), satisfying the above descriptors in the scaffold structure of noscapine pertaining to better anti-tumor activity. To begin to test this, we build two noscapine derivatives using molecular builder: 9-azido noscapine and reduced-9-azido noscapine (Table 2.9) and predicted their biological activities by using QSAR model. Both molecules deduced to have superior activity in comparison to the lead molecule, noscapine. To experimentally test the predictability of our QSAR model we chemically synthesized both the molecules (Figure 2.8)

#### 2.3.4 Synthesis of novel 9-azido-noscapine

Both 9-azido-noscapine and reduced 9-azido-noscapine were synthesized from noscapine (**1**) and reduced noscapine (**4**) as starting materials, respectively. The reduced noscapine (**4**) itself was synthesized from noscapine (**1**) as described previously [7]. Both synthetic schemes involved their respective intermediates, 9-bromo-noscapine and reduced 9-bromo-noscapine (Figure 2.6).

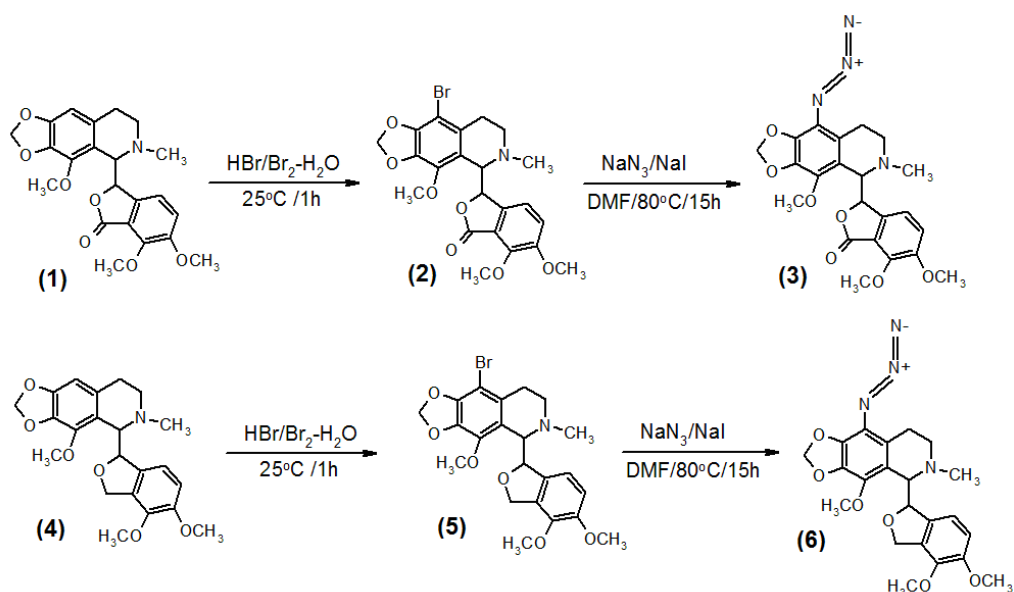


Figure 2.8. Synthesis of 9-azido-noscapine and reduced 9-azido-noscapine.

(a) Synthesis of 9-azido-noscapine [(*S*)-3-((*R*)-9-azido-4-methoxy-6-methyl-5,6,7,8-tetrahydro-[1,3]dioxolo[4,5-*g*]isoquinolin-5-yl)-6,7-dimethoxyisobenzofuran-1(3*H*)-one]

Twenty grams of noscapine (**1**) (48.4 mmol) was dissolved by adding minimum amount of 48% hydrobromic acid solution (~40 ml) in a flask. Freshly prepared bromine water (~250 ml) was added drop wise to the reaction mixture until an orange precipitate appeared. The reaction mixture was then stirred at room temperature for 1 hour, neutralized to pH 10.0 using ammonia solution to obtain a precipitate. The solid precipitate was then re-crystallized in ethanol to yield 9-bromonoscapine (**2**): yield, 82%; melting point (mp), 169 to 170°C; IR, 2945 (m), 2800 (m), 1759 (s), 1612 (m), 1500 (s), 1443 (s), 1263 (s), 1091 (s), 933 (w)  $\text{cm}^{-1}$ .  $^1\text{H}$  NMR ( $\text{CDCl}_3$ , 400 MHz),  $\delta$  7.04 (d, 1H,  $J = 7$  Hz), 6.32 (d, 1H,  $J = 7$  Hz), 6.03 (s, 2H), 5.51 (d, 1H,  $J = 4$  Hz), 4.55 (d, 1H,  $J = 4$  Hz), 4.10 (s, 3H), 3.98 (s, 3H), 3.89 (s, 3H), 2.52 (s, 3H), 2.8 to 1.93 (m, 4H);  $^{13}\text{C}$  NMR ( $\text{CDCl}_3$ , 100 MHz),  $\delta$  167.5, 151.2, 150.5, 150.1, 148.3, 140.0, 135.8, 130.8, 120.3, 120.4, 120.1, 105.3, 100.9, 100.1, 87.8, 64.4, 56.1, 56.0, 55.8, 51.7, 41.2, 27.8. Mass spectrometry: fast atom bombardment ions (FAB),  $m/z$  (relative abundance percentage), 494 (93.8), 492 (100), 300 (30.5), 298 (35.4); matrix-assisted laser desorption ionization (MALDI),  $m/z$  491.37 ( $\text{M}^+$ ), 493.34; electrospray ionization/tandem mass spectrometry, parent ion masses, 494, 492; daughter ion masses (intensity, percentage): 433 (51), 431 (37), 300 (100), 298 (93.3); high resolution mass spectrometry (HRMS-ESI),  $m/z$  calculated for  $\text{C}_{22}\text{H}_{23}\text{BrNO}_7$  ( $\text{M}+1$ ), 493.3211; experimentally determined, 493.3215 ( $\text{M}+1$ ).

Sodium azide (2.641 g, 40.63 mmol) and sodium iodide (0.609 g, 4.063 mmol) were added to a 20 ml solution of the above compound **2** (4.063 mmol) in DMF and the reaction mixture was

## CHAPTER 2

stirred at 80 °C for 15 hours. Then, the solvent was removed *in vacuo* and the resultant residue was dissolved in chloroform (40 ml), washed with water (2 x 40 ml), dried over sodium sulfate and concentrated to obtain the compound 3, which was re-crystallized in ethanol:hexane (10:90): yield, 89%; mp 177.2 to 178.1 °C; IR: 1529, 1362 cm<sup>-1</sup>; <sup>1</sup>H NMR (CDCl<sub>3</sub>, 400 MHz): δ 7.05 (d, 1H, *J* = 7.0 Hz), 6.4 (d, 1H, *J* = 7.0 Hz), 6.01 (s, 2H), 5.85 (d, 1H, *J* = 4.4 Hz), 4.40 (d, 1H, *J* = 4.4 Hz), 4.15 (s, 3H), 3.88 (s, 3H), 3.84 (s, 3H), 2.75-2.62 (m, 2H), 2.60-2.56 (m, 2H), 2.51 (s, 3H); <sup>13</sup>C NMR (CDCl<sub>3</sub>, 100 MHz): δ 169.2, 157.7, 152.6, 147.9, 142.2, 140.5, 135.0, 134.0, 123.5, 121.8, 119.7, 119.3, 114.1, 100.5, 87.4, 64.1, 56.7, 56.5, 56.2, 51.4, 39.2, 27.2; HRMS (ESI): *m/z* calculated for C<sub>22</sub>H<sub>23</sub>N<sub>4</sub>O<sub>7</sub> (M+1), 455.4335; experimentally determined, 455.4452 (M+1).

(b) Synthesis of reduced 9-azido-noscapine [((*S*)-3-((*R*)-9-azido-4-methoxy-6-methyl-5,6,7,8-tetrahydro-[1,3]dioxolo[4,5-*g*]isoquinolin-5-yl)-6,7-dimethoxyisobenzofuran-1(3*H*))]:

The synthetic scheme was quite parallel to the one described above. Briefly, reduced noscapine (**4**) (20.0 g, 48.8 mmol) was dissolved by slowly adding minimal 48% hydrobromic acid (~40 ml) in a flask, freshly prepared bromine water (~250 ml) drop wise until a precipitate appeared. Reaction mixture was stirred at room temperature for 1 hour, neutralized with ammonia solution to pH 10.0 to obtain solid precipitate of reduced 9-bromo-noscapine (**5**), which was then also re-crystallized in ethanol. (Yield, 80%; mp 113-114 °C; IR: 2950 (m), 2852 (m), 1635 (w), 1616 (m), 1450 (s), 1267 (s), 1226 (s), 1078 (s), 1035 (s) cm<sup>-1</sup>; <sup>1</sup>H NMR (CDCl<sub>3</sub>, 400 MHz), δ 6.73 (d, 1H, *J* = 8 Hz), 6.11 (d, 1H, *J* = 8 Hz), 6.08 (s, 2H), 5.78 (s, 2H), 5.33 (dd, 1H, *J* = 12 Hz), 5.05 (dd, 1H, *J* = 12 Hz), 4.90 (s, 1H), 3.86 (s, 6H), 3.83 (s, 3H), 3.42 to 3.19 (m, 2H), 2.99 (s, 3H), 2.82-2.80 (m, 2H); <sup>13</sup>C NMR (CDCl<sub>3</sub>, 100 MHz), δ 151.8, 151.6, 149.7, 148.8, 136.3, 135.8, 132.9, 131.1, 120.9, 121.5, 114.4, 106.0, 101.2, 97.9, 69.3, 65.2, 56.9, 56.6, 56.0, 52.5, 41.3, 27.9; MS (FAB): *m/z* (relative abundance, %), 480 (100), 478 (100), 462 (8), 460 (8.3), 300 (18), 298 (19), 179 (12.5); MALDI: *m/z* 478.5 (M)<sup>+</sup>, 480.5; ESI: parent ion mass, 480, 478; daughter ion masses (intensity, %), 462 (74), 460 (52.5), 447 (21), 445 (16.6), 431 (83.3), 429 (66.6), 300 (79), 298 (74.7), 193 (11), 191 (23.5), 179 (100); HRMS (ESI): *m/z* calculated for C<sub>22</sub>H<sub>25</sub>BrNO<sub>6</sub> (M+1), 479.3345; experimentally determined, 479.3329 (M+1). )

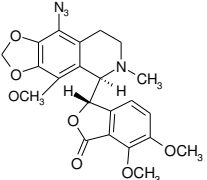
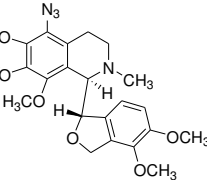
To obtain reduced 9-azido-noscapine (**6**), compound (**5**) was used as the starting material, and parallel procedure was followed as described above for the synthesis of 9-azido-noscapine (**3**). Yield for compound 6 was 84%; mp 121 to 122 °C; IR: 1320, 1153 cm<sup>-1</sup>; <sup>1</sup>H NMR (CDCl<sub>3</sub>, 400 MHz): δ 6.74 (d, 1H, *J* = 8.0 Hz), 6.19 (d, 1H, *J* = 8.0 Hz), 6.06 (s, 2H), 5.48 (s, 2H), 4.88 (dd, 1H, *J* = 12 Hz), 4.77 (dd, 1H, *J* = 12 Hz), 4.75 (s, 1H), 3.82 (s, 6H), 3.79 (s, 3H), 3.38 to 3.15 (m, 2H),

2.95 (s, 3H), 2.78-2.80 (m, 2H);  $^{13}\text{C}$  NMR ( $\text{CDCl}_3$ , 100 MHz),  $\delta$  153.5, 151.2, 149.3, 148.4, 135.9, 135.4, 132.5, 130.7, 120.5, 121.1, 114.0, 105.6, 100.8, 97.5, 68.9, 64.8, 56.5, 56.2, 55.6, 52.1, 40.9, 27.5; HRMS (ESI):  $m/z$  calculated for  $\text{C}_{22}\text{H}_{23}\text{N}_4\text{O}_6$  (M+1), 441.4469; experimentally determined, 441.4453 (M+1).

### 2.3.4 Anti-tumor activity of newly designed noscapinoids

The biological activity of the synthesized derivatives was experimentally determined in CEM cells using MTS assay described in the method section. As guided by our QSAR model, we chose to substitute an 'azido' group at C-9 position of noscapine scaffold (Fig 2.4a) producing 9-azido noscapine and also chose to reduce the ketone group of 9-azido-noscapine on its isobenzofuronone ring conjuring up a reduced 9-azido-noscapine. The predicted (5.731 and 5.710 M) and experimental (5.585 M)  $p\text{IC}_{50}$  values are included in Table 2.9. The experimental results (with extremely small deviations of 0.146 M and 0.125 M) show that our model has a highly predictive power for the further design of better noscapinoids for anti-cancer drug discovery and development.

Table 2.9. Predicted biological activity ( $p\text{IC}_{50}$ ) obtained from the QSAR models (using equations 2-6, included in supplemental data S2) and experimental biological activity for the designed set of noscapinoids.

Structure of the compound	Experimental $\text{IC}_{50}$ (M)	Experimental $p\text{IC}_{50}$ (M)	Predicted $p\text{IC}_{50}$ (M)				
			$p\text{IC}_{50}^2$	$p\text{IC}_{50}^3$	$p\text{IC}_{50}^4$	$p\text{IC}_{50}^5$	$p\text{IC}_{50}^6$
 (9-azido-noscapine)	$2.6 \times 10^{-6}$	5.585	5.166	4.541	5.340	5.607	5.731
 (Reduced 9-azido-noscapine)	$2.6 \times 10^{-6}$	5.585	5.629	4.624	5.626	5.709	5.710

## 2.4 CONCLUSION

In this chapter I have systematically investigated the relationship between the well characterized structure and its anti-tumor activity by synthesizing strategic derivatives of noscapinoids. Geometrically optimized structures were in agreement with NMR Analysis of

## CHAPTER 2

Molecular Flexibility in Solution—NAMFIS and crystal structures. To obtain quantitatively the effects of various structural parameters of the noscapine derivatives on their biological activity, QSAR analysis with different types of molecular descriptors was operated. We used genetic function approximation algorithm of variable selection and generated robust QSAR models with high predictability for the external data set. The QSAR model guided us towards designing two more derivatives, 9-azido-noscapine and reduced 9-azido-noscapine. The activity of these new compounds was predicted using the developed QSAR model, which motivated us further towards synthesis of the compound. Validation of the model was achieved by experimentally determining value of  $pIC_{50}$  for both the compounds (5.585 M) which turned out to be very close to predicted  $pIC_{50}$  (5.731 and 5.710 M). We thus believe that this model would perform as a good rapid screening tool to uncover new and more potent anti-tumor drugs based on noscapine derivatizations.

## REFERENCES

1. Wulff O. *Prolonged antitussive action of a resin-bound noscapine preparation*. J Pharma Sci, 54 pp 1058-1060. 1965.
2. Ye, K., Ke, Y., Keshava, N., Shanks, J., Kapp, J.A., Tekmal, R.R., Petros, J. & Joshi, H.C. *Opium alkaloid noscapine is an antitumor agent that arrests metaphase and induces apoptosis in dividing cells*. Proc Natl Acad Sci, 95 pp 2280-2286. 1998.
3. Zhou, J., Panda, D., Landen, J.W., Wilson, L. & Joshi, H.C. *Minor alteration of microtubule dynamics causes loss of tension across kinetochore pairs and activates the spindle checkpoint*. J Biol Chem, 277 pp 17200-17208. 2002.
4. Zhou, J., Gupta, K., Aggarwal, S., Aneja, R., Chandra, R., Panda, D. & Joshi, H.C. *Brominated derivatives of noscapine are potent microtubule-interfering agents that perturb mitosis and inhibit cell proliferation*. Mol Pharmacol, 63 pp 799-807. 2003.
5. Aneja, R., Liu, M., Yates, C., Gao, J., Dong, X., Zhou, B., Vangapandu, S.N., Zhou, J. & Joshi, H.C. *Multidrug resistance-associated protein-over expressing teniposide-resistant human lymphomas undergo apoptosis by a tubulin-binding agent*. Cancer Res, 68 pp 1495-1503. 2008.
6. Aneja, R., Vangapandu, S.N., Lopus, M., Viswesarappa, V.G., Dhiman, N., Verma, A., Chandra, R., Panda, D. & Joshi, H.C. *Synthesis of microtubule-interfering halogenated noscapine analogs perturb mitosis in cancer cells followed by cell death*. Biochem Pharmacol, 72 pp 415-426. 2006.
7. Aneja, R., Vangapandu, S.N. & Joshi, H.C. *Synthesis and biological evaluation of a cyclic ether fluorinated noscapine analog*. Bioorg Med Chem, 14 pp 8352-8358. 2006.
8. Aneja, R., Vangapandu, S.N., Lopus, M., Chandra, R., Panda, D. & Joshi, H.C. *Development of a novel nitro-derivative of noscapine for the potential treatment of drug-resistant ovarian cancer and T-cell lymphoma*. Mol Pharmacol, 69 pp 1801-1809. 2006.
9. Aggarwal, S., Ghosh, N.N., Aneja, R., Joshi, H.C. & Chandra, R. *A convenient synthesis of aryl-substituted N-carbamoyl/N-thiocarbamoyl narcotine and related compounds*. Helvetica Chimica Acta, 85 pp 2458-2462. 2002.
10. Friedman, J. *MultiVariate AdaptiVe Regression Splines*; Technical Report No. 102, Laboratory for computational statistics, Department of Statistics; Stanford University: Stanford, CA, Nov 1988 (revised Aug 1990).

## CHAPTER 2

11. Naik, P.K., Alam, A., Malhotra, A. & Rizvi, O. *Molecular Modeling and Structure-activity relationship of the podophyllotoxin and its congeners*. J Biomol Screen, 15 pp 528-540.2010.
12. Naik, P.K., Sindhura, Y., Singh, T. & Singh, H. *Quantitative structure-activity relationship (QSAR) of the insecticides: the development of predictive in vivo insecticide activity models*. SAR QSAR in Env Res, 20 pp 551-556. 2009.
13. Cicero, D.O., Barbato, G. & Bazzo, R. *NMR Analysis of Molecular Flexibility in Solution: A new method for the study of complex distributions of rapidly exchanging conformations*. J Am Chem Soc, 117 pp 1027-1033. 1995.
14. Thanikaivelan, P., Subramanian, V., Rao, J.R. & Nair, B.U. *Application of quantum chemical descriptor in quantitative structure activity and structure property relationship*. Chem Phys Lett, 323 pp 59–70. 2000.
15. Ertl, P., Rohde, B. & Selzer, P. *Fast calculation of molecular polar surface area as a sum of fragment-based contributions and its application to the prediction of drug transport properties*. J Med Chem, 43 pp 3714 - 3717.2000.



# CHAPTER – 3

**MOLECULAR INSIGHTS INTO THE INTERACTIONS OF  
NOSCAPINOIDS WITH  $\beta$ -TUBULIN SPECIFIC ISOTYPES OF  
 $\alpha\beta$ -TUBULIN HETERODIMER.**



## Abstract

Noscapine and its derivatives were demonstrated to bind stoichiometrically to tubulin, alter its dynamic instability upon binding and thus effectively inhibit the cellular proliferation of a wide variety of cancer cells including many drug-resistant variants. The tubulin molecule is composed of  $\alpha$ - and  $\beta$ -tubulin, which exist as various isotypes whose distribution and drug-binding properties are significantly different. Although the noscapinoids bind to a site overlapping with colchicine, their interaction is more biased towards  $\beta$ -tubulin. In fact, their precise interaction and binding affinity with specific isotypes of  $\beta$ -tubulin in tubulin heterodimer has never been addressed. In this study, the binding affinity of a panel of noscapinoids with each type of tubulin is investigated computationally. We found that the binding score of a specific noscapinoid with each type of tubulin isotype is different. Specifically, amino-noscapine has the highest binding score of -6.432, -7.179, -7.416 and -7.317 kcal/mol with  $\alpha\beta_I$ ,  $\alpha\beta_{II}$ ,  $\alpha\beta_{III}$  and  $\alpha\beta_{IV}$  isotypes, respectively. Similarly **10** showed higher binding affinity of -6.792 kcal/mol with  $\alpha\beta_V$ , whereas **8** had the highest binding affinity of -7.182, -7.136 and -7.236 kcal/mol, respectively with  $\alpha\beta_{VI}$ ,  $\alpha\beta_{VII}$  and  $\alpha\beta_{VIII}$  isotypes. More importantly, both amino-noscapine and the clinical derivative, bromo-noscapine have the highest binding affinity of -46.23 and -38.09 kcal/mol against  $\alpha\beta_{III}$  (overexpression of  $\alpha\beta_{III}$  has been associated with resistance to a wide range of chemotherapeutic drugs for several human malignancies) as measured using MM-PBSA. Knowledge of the isotype specificity of noscapinoids may allow for development of novel therapeutic agents based on this class of drugs.

### 3.1 INTRODUCTION

Microtubules are highly dynamic cytoskeletal polymers composed of  $\alpha$ - and  $\beta$ - tubulin heterodimers that regulate various physiological functions such as cell division, maintenance of intracellular transport, positioning of cellular organelles and cellular motility [1,2]. The crucial roles microtubules play in cell division, the segregation of chromosomes, make them an attractive target for cancer chemotherapy. A number of tubulin-binding molecules with anti-mitotic properties such as taxanes, vinca alkaloids and podophyllotoxin have been discovered in recent years [2-10].

Tubulin is encoded by multiple genes that represent multiple isotypes of  $\alpha$ - and  $\beta$ -tubulin. These isotypes are expressed in a tissue specific manner in the body [11,12] and are known to play specific biological functions and exhibit different kinetics and dynamics of microtubule assembly. The differential expression of  $\beta$ -tubulin isotypes is included in Table 3.1.

Table 3.1. Tissue distribution of  $\beta$ -tubulin isotypes in normal cells.[21]

Isotype	Organ expression	Cellular expression
$\beta_I$	Constitutive	Most cells
$\beta_{II}$	Brain, nerves, muscle; rare elsewhere	Restricted to particular cell types
$\beta_{III}$		Neurons only
		Sertoli cells
	Colon (very slight amounts)	Epithelial cells only
$\beta_{IV}$	Brain only	Neurons and glia
$\beta_V$	Unknown	Unknown
$\beta_{VI}$	Blood , bone marrow, spleen	Erythroid cells, platelets
$\beta_{VII}$	Brain	Unknown
$\beta_{VIII}$	Unknown	Unknown

It is known that although there may be a dominant form of  $\beta$ -tubulin within a certain organ, other isotypes are also found in lower amounts within the same organ. The percentage of each isotype may change when tissue turns cancerous as cancerous cells are capable of altering the normal levels of expression of tubulin isotypes and hence deregulate the tissue specific pattern; particularly  $\beta_{III}$  overexpression has been associated with aggressive drug resistant cancer cells [13-19]. Other isotypes are also dysregulated in cancerous cells in comparison to noncancerous cells [11,12,20-24]. It is possible that this property can be exploited in sophisticated drug design strategies aimed to more effectively eliminate cancer cells. The change in tubulin isotype distribution could be exploited such that a specific drug could be chosen to maximize cancer cell death while simultaneously minimizing damage to healthy tissues.

Recent reports suggest that differential expression of  $\alpha$ - and  $\beta$ -tubulin isotypes by mammalian tissues results in differential binding affinities of anti-mitotic agents [25-26], preferring one isotype slightly over the other. Varied expression of tubulin isotypes also affects the sensitivity of cancer cells of different tissue origin to the tubulin binding agents. Although current anti-tubulin drugs bind to all of these isotypes, they showed better responses against specific types of cancer cells that are overexpressing a particular type of isotype [22,26,27]. For example, the vinca alkaloids bind best to  $\beta_{II}$ , providing an explanation as to their efficacy in leukemia and Hodgkin's lymphoma, since these cancer cells well express  $\beta_{II}$  while normal lymphocytes do not. Moreover, overexpression of some isotypes in cancer cells has been linked to resistance towards anti-mitotic drugs [28-30]. As an example overexpression of  $\beta_{III}$  in cancer cells such as ovarian, breast and non-small-cell lung cancer has been linked to resistance to paclitaxel [28]. Similarly overexpression of class  $\beta_V$  in cancer cells also leads to resistance to taxane-based chemotherapy [29]. Therefore it is of utmost importance to design tubulin binding drugs that can bind ubiquitously onto different tubulin isotypes and are lethal to cancer cells but not to normal cells.

Screening for similar new microtubule-targeting agents that possess functional groups similar to colchicine and podophyllotoxin, led to discovery of noscapine that binds to the tubulin heterodimer and perturbed the secondary conformation of tubulin, as a result lead to mitotic arrest. However, unlike the majority of the microtubule-targeting agents, noscapine does not significantly alter the ability of tubulin to form microtubules [30]. Investigating the mechanism behind this discrepancy, it was found that noscapine arrests cancer cells by altering the dynamic instability of microtubules, primarily by increasing the time spent in the attenuated states of dynamic instability [30-42]. Also it was observed that cancer cells of different tissue origin that have altered expression of  $\beta$ -tubulin isotypes are sensitive to these tubulin binding agents albeit differently [42-49]. Moreover, noscapine can efficiently inhibit paclitaxel resistant human ovarian cancer cells (1A9PTX10 and 1A9PTX22) that possess mutation to  $\beta$ -tubulin [49]. A number of noscapine analogs have been reported in recent years as having superior efficacy in retard to inhibition of cancer cell proliferation, while having negligible effects on normal cells [32-36,43,44,46]. Furthermore, owing to its relatively non-toxic and safe profile, we have rationally designed many derivatives of noscapine with enhanced tubulin binding affinity [42-45].

Noscapine and its derivatives bind to a site at the interface of  $\alpha$ - and  $\beta$ -tubulin but are more biased to  $\beta$ -tubulin [47-49]. Contrastingly different isotypes of  $\alpha$ -tubulin are also reported. However, the comparative analysis of isotypes of  $\alpha$ -tubulin did not reveal any mismatches in the amino acids present in or near (within 12 Å) of the noscapinoids binding site (Figure 3.1).

Furthermore, binding of noscapinoids is more biased towards  $\beta$ -tubulin whereas the  $\alpha$ -tubulin contributes very little in the binding. Hence the  $\alpha$ -tubulin isotypes are not considered in this study.

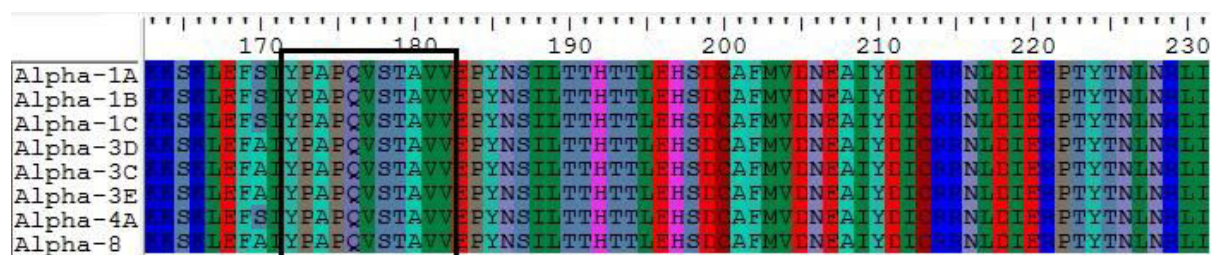


Figure 3.1. Multiple sequence alignment of the stretches of amino acids located in or near the 12 Å of the binding site of noscapinoids in  $\alpha$ -tubulin in the tubulin heterodimer. The figure clearly shows there is no much difference in sequences in or near the binding site (enclosed on black box).

The  $\beta$ -tubulin isotypes consist of 421 amino acid residues (excluding their C-termini) and approximately 1–20% of the residues differ between the isotypes. The binding of noscapinoids is stronger towards  $\beta$ -tubulin than  $\alpha$ -tubulin. Thus any substitution or changes in amino acids on and near the binding site of noscapinoids that exists in  $\beta$ -tubulin would significantly affect the binding affinity and responses of noscapine derivatives, so it would be more appropriate to consider the isotypes of  $\beta$ -tubulin for study of interaction of noscapinoids with different tubulin isotypes. The presence of both numerous structures of tubulin and sequences of multiple isotypes of tubulin offers an opportunity to create a library of structures of human  $\beta$ -tubulin isotypes using homology modelling pertaining to investigate the key biochemical characteristics.

Of particular interest in this chapter we have made an effort to investigate the mechanistic details of differential activity of noscapinoids across cancer types that are reported to have different proportions  $\beta$ -tubulin isotypes. Towards this end, we have used noscapine and some of its derivatives for the computational analysis of binding interaction with tubulin heterodimers made up of  $\alpha$ - and isotype-specific  $\beta$ -tubulin. Understanding of molecular interactions of these agents with tubulin isotypes would be important to improve the efficacy of noscapinoids towards a specific cancer type.

## 3.2 MATERIALS AND METHODS

### 3.2.1 Isotypes of $\beta$ -tubulin and sequence analysis

To investigate the binding affinity of noscapine and its derivatives onto isotype-specific  $\beta$ -tubulin, we have constructed tubulin heterodimers comprised of  $\alpha$ -tubulin and different isotypes of  $\beta$ -tubulin. The protein sequences of eight human  $\beta$ -tubulin isotypes ( $\beta_I$  to  $\beta_{VIII}$ ) reported previously were downloaded from the NCBI database. The representative sequences of  $\beta$ -isotypes:  $\beta_I$  (gi:18088719),  $\beta_{II}$  (gi:29788768),  $\beta_{III}$  (gi: 1297274),  $\beta_{IV}$  (gi: 135470),  $\beta_V$  (gi:14201536),  $\beta_{VI}$  (gi:

62903515),  $\beta_{VII}$  (gi:1857526) and  $\beta_{VIII}$  (gi:42558279) were to build molecular structure of tubulin hetero-dimers. These sequences of  $\beta$ -tubulin isotypes were aligned and compared using a multiple sequence alignment program (Bioedit version 7.1.9) [50].

### 3.2.2 Template preparation and homology modeling of tubulin isotypes

The co-crystallized structure of the colchicine-tubulin complex (PDB ID: 1SA0, resolution 3.58 Å) was used as a template for homology modeling of tubulin isotypes. Because of its low resolution the crystal structure possesses several errors: (a) the residues were not sequentially numbered in  $\beta$  chain (B chain), as an example 45<sup>th</sup> residue was numbered as 47<sup>th</sup> residue and 361<sup>st</sup> residue was numbered as 370<sup>th</sup> residue (Figure 3.2); (b) some of the amino acids between 37 to 47 ( $\alpha$ -tubulin) and 275 to 284 ( $\beta$ -tubulin) were found to be missing (Figure 3.3 & 3.4). In order to remove the errors in the crystal structure we have renumbered its amino acids and the gaps were filled by homology modeling based on PDB ID: 3DU7 (C-chain) and PDB ID: 3RYC (D-chain) respectively as templates using Prime (version 3.0, Schrödinger).

ATOM	3553	N	LEU	B	44		ATOM	6002	N	PRO	B	360
ATOM	3554	CA	LEU	B	44		ATOM	6003	CA	PRO	B	360
ATOM	3555	C	LEU	B	44		ATOM	6004	C	PRO	B	360
ATOM	3556	O	LEU	B	44		ATOM	6005	O	PRO	B	360
ATOM	3557	CB	LEU	B	44		ATOM	6006	CB	PRO	B	360
ATOM	3558	CG	LEU	B	44		ATOM	6007	CG	PRO	B	360
ATOM	3559	CD1	LEU	B	44		ATOM	6008	CD	PRO	B	360
ATOM	3560	CD2	LEU	B	44		ATOM	6009	N	ARG	B	369
ATOM	3561	N	GLU	B	47		ATOM	6010	CA	ARG	B	369
ATOM	3562	CA	GLU	B	47		ATOM	6011	C	ARG	B	369
ATOM	3563	C	GLU	B	47		ATOM	6012	O	ARG	B	369
ATOM	3564	O	GLU	B	47		ATOM	6013	CB	ARG	B	369
ATOM	3565	CB	GLU	B	47		ATOM	6014	CG	ARG	B	369
ATOM	3566	CG	GLU	B	47		ATOM	6015	CD	ARG	B	369
ATOM	3567	CD	GLU	B	47		ATOM	6016	NE	ARG	B	369
ATOM	3568	OE1	GLU	B	47		ATOM	6017	CZ	ARG	B	369
ATOM	3569	OE2	GLU	B	47		ATOM	6018	NH1	ARG	B	369
							ATOM	6019	NH2	ARG	B	369

REMARK 999 THE RESIDUES IN CHAIN B ARE NOT SEQUENTIALLY  
 REMARK 999 NUMBERED. RESIDUES 44 AND 47, AND RESIDUES  
 REMARK 999 360 AND 369 ARE COVALENTLY BOUND.

Figure 3.2. Snapshots of pdb file 1SA0 showing errors in numbering in  $\beta$  chain: 47<sup>th</sup> number after 44<sup>th</sup> and 369<sup>th</sup> number after 360<sup>th</sup> and a statement in remark mentioning that residues are not sequentially numbered and residues 44<sup>th</sup> and 47<sup>th</sup> and residues 360<sup>th</sup> and 369<sup>th</sup> are covalently bound.

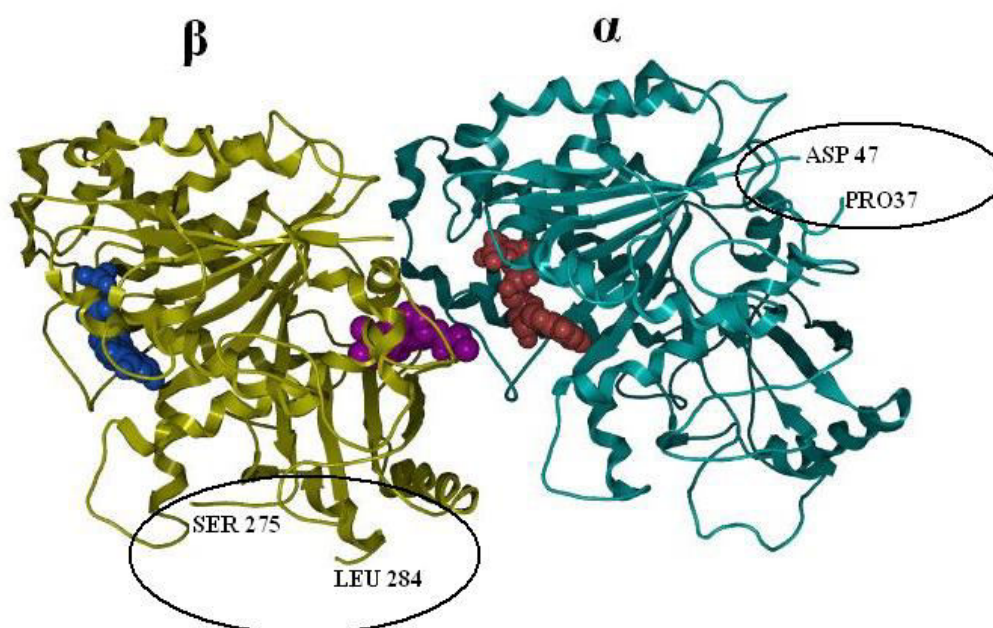


Figure 3.3. Representation of gaps (missing residues) in the crystal structure (1SA0) of tubulin dimer along with ligand colchicine (pink), GTP (Brown) and GDP (blue). The gaps (encircled) and the end residues of gaps ASP47 and PRO37 in  $\alpha$  chain and SER275 and LEU384 in  $\beta$  chain are shown in the figure.

ATOM	264	N	PRO A	37	ATOM	5378	N	SER B	275	
ATOM	265	CA	PRO A	37	ATOM	5379	CA	SER B	275	
ATOM	266	C	PRO A	37	ATOM	5380	C	SER B	275	
ATOM	267	O	PRO A	37	ATOM	5381	O	SER B	275	
ATOM	268	CB	PRO A	37	ATOM	5382	CB	SER B	275	
ATOM	269	CG	PRO A	37	ATOM	5383	OG	SER B	275	
ATOM	270	CD	PRO A	37	ATOM	5384	N	LEU B	284	
ATOM	271	N	ASP A	47	ATOM	5385	CA	LEU B	284	
ATOM	272	CA	ASP A	47	ATOM	5386	C	LEU B	284	
ATOM	273	C	ASP A	47	ATOM	5387	O	LEU B	284	
ATOM	274	O	ASP A	47	ATOM	5388	CB	LEU B	284	
ATOM	275	CB	ASP A	47	ATOM	5389	CG	LEU B	284	
					ATOM	5390	CD1	LEU B	284	
					ATOM	5391	CD2	LEU B	284	
					ATOM	6524	N	ALA B	428	
					ATOM	6525	CA	ALA B	428	
					ATOM	6526	C	ALA B	428	
					ATOM	6527	O	ALA B	428	
					ATOM	6528	CB	ALA B	428	
					TER	6529		ALA	428	

Residues 38th to 46th and missing in A chain

Residues 276th to 283th missing in B chain also the residues 429th to 435th residue missing as the chain is chain terminating at 428th residue

Figure 3.4. Screen shot of missing residues in  $\alpha$  (A) and  $\beta$  (B) chain shown in the pdb file (1SA0). Residues 38<sup>th</sup> to 46<sup>th</sup> missing in  $\alpha$  chain and residues 267<sup>th</sup> to 283<sup>th</sup> missing in  $\beta$  chain also the C terminal end residues of the sequence 429<sup>th</sup> to 435<sup>th</sup> residue is missing in the  $\beta$  chain.

The modelled structure obtained was energy minimized using OPLS 2005 force field with Polak-Ribiere Conjugate Gradient (PRCG) algorithm, which was stopped either after 5000 steps or after the energy gradient converged below 0.001 kcal/mol using MacroModel (version 9.9, Schrödinger). The structure was further refined by performing an all atom molecular dynamics



(MD) simulation in explicit water using GROMACS 4.5.4 software [51] and the GROMOS96 force field on a time scale of 10 ns. By enclosing the molecule in a dodecahedron solvated with the SPC216 water model provided in the GROMACS package, three-dimensional periodic boundary conditions were imposed and the structure was energy minimized using 1000 steps of steepest descent minimization. To achieve the system electro neutrality, 32 Na<sup>+</sup> counter ions were added to the system and the results locally minimized using 100 steps of steepest descent. The electrostatic term was described using the Particle Mesh Ewald algorithm [52]. For the calculation of the coulombic and van der Waals interactions at 1.0 nm, the LINCS [53] algorithm was used to constrain all bond lengths and cut-off distances. At 300 K and normal pressure we equilibrated the system by 100 ps of MD runs with position restraints on the protein to allow the relaxation of the solvent molecules. With a coupling time of 0.1 ps at the default setting, the system was coupled to the external bath by the Berendsen thermostat. The final MD calculations were performed for 10 ns with a time step of 2 fs. A total of 5000 frames were generated in the MD trajectories, out of which the last 2000 frames were used to generate an average structure of the tubulin. The overall quality of the model, stereochemical values and non-bonded interactions were evaluated using PROCHECK [54, 55], ERRAT [56] and VERIFY3D [57].

The homology models of different tubulin isotypes were built based on the above prepared and refined structure of tubulin (PDB ID: 1SA0) as template using Prime (version 3.0, Schrödinger). Furthermore, the modeled structures were refined by performing an all atom MD simulation of 10 ns as described previously. The quality of the modelled structures of tubulin isotypes were evaluated using PROCHECK, ERRAT and VERIFY3D.

### 3.2.3 Ligand preparation

Molecular structures of noscapine and its derivatives (Figure 3.5) that had been previously demonstrated to be tubulin binding agents [33-36,43,44,47,58] were built using the molecular builder of Maestro (version 9.2, Schrödinger). All these structures were energy minimized using Macromodel (version 9.9, Schrödinger) and OPLS 2005 force field with PRCG algorithm (1000 steps of minimization and an energy gradient of 0.001). Appropriate bond order for each structure was assigned using Ligprep (version 2.5, Schrödinger). Furthermore, these molecular structures were geometrically optimized using hybrid density functional theory with Becke's three-parameter exchange potential and the Lee-Yang-Parr correlation functional (B3LYP) [59,60] with basis set 3-21G\* (61-63). Jaguar (version 7.7, Schrödinger, LLC) was used for the geometrical optimization of the ligands.

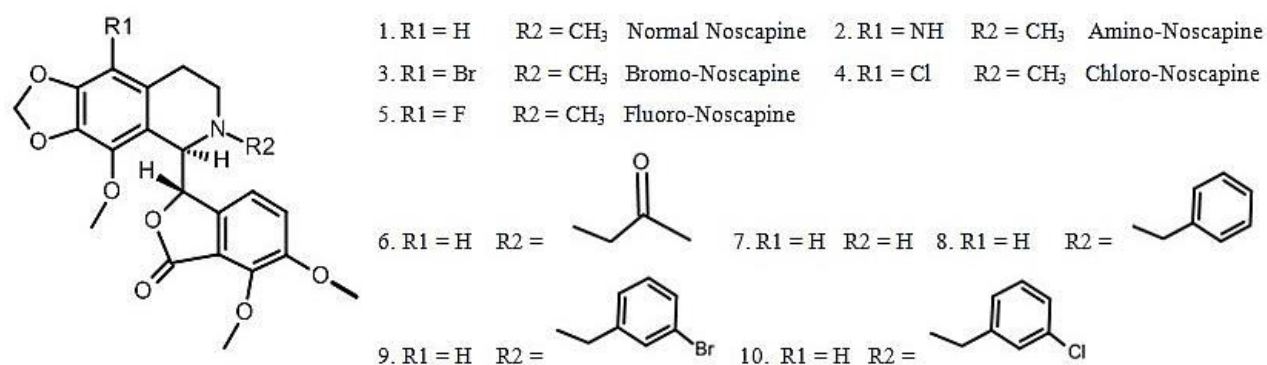


Figure 3.5. Chemical structure of noscapine and its derivatives used in the study. These derivatives were previously demonstrated to be tubulin-binding agents.

### 3.2.4 Prediction and analysis of noscapinoid binding pocket

Different binding sites were predicted and analyzed for the modeled  $\alpha\beta$ -tubulin isotypes using SiteMap (version 2.4, Schrodinger). However, only the noscapinoid binding site [48] (at the interface between  $\alpha$ - and  $\beta$ -tubulin) for each protein structure which is in agreement with the predicted noscapinoid binding site and partially supported by experimental study [48] was selected for comparative analysis and predicting the binding affinity of noscapinoids. The best way to understand the noscapinoid binding site is to obtain a co-crystal structure with tubulin, which is not yet possible so far. Alternatively, only one piece of experimental evidence (competition interaction of Br-noscapine with colchicine binding) is so far reported that revealed a binding site of noscapinoid at or near the colchicine binding site of tubulin [48]. The binding site residues (comprised of 16 amino acids) which are in agreement with the predicted noscapinoids binding site [48] from each of the tubulin isotypes were extracted and superimposed for comparative analysis.

### 3.2.5 Molecular docking of ligands

Molecular docking of noscapinoids (Figure 3.5) onto tubulin isotypes was performed using “Extra Precision” (XP) algorithm of Glide docking (version 5.7, Schrödinger) [64,65]. The noscapinoid binding pocket on different  $\alpha\beta$ -tubulin isotypes was defined using a concentric grid box at the centroid of the noscapinoid binding site using the Glide grid-receptor generation program [65]. A bounding box of size 12Å x 12Å x 12Å was defined in order to confine the mass center of the docked ligand. The larger enclosing box of size 12Å x 12Å x 12Å was also chosen so that it occupied all the atoms of the docked poses. All the ligands were then docked into the binding site using Glide XP (extra precision) and evaluated using a Glide XP<sub>Score</sub> function [64,65]. For the ligand docking stage, a scale factor of 0.4 for van der Waals radii was applied to atoms of protein with absolute partial charges less than or equal to 0.25. Out of the 10,000 poses that were sampled,

1000 were taken through minimization (conjugate gradients) and the 30 structures having the lowest energy conformations were further evaluated for a favorable Glide docking score. The single best conformation for each ligand was considered for further analysis. The residues within 12 Å of the docked ligands were extracted and analyzed for differences in molecular interactions with respect to tubulin isotypes.

### 3.2.6 Molecular dynamics simulations of the docked complexes

To specifically investigate the binding affinity of amino-noscapine (the most potent derivative in our library), bromo-noscapine (the clinical derivative) and noscapine (the lead molecule) onto the  $\alpha\beta_{III}$  isotype, I have calculated their binding free energy. Towards this end, the complex of  $\alpha\beta_{III}$  isotype with amino-noscapine, bromo-noscapine and noscapine, obtained after Glide docking was used as an initial conformation for MD simulation. The MD simulation was performed in AMBER 11.0 [66] software suite and the force fields used were AMBER ff99SB [67] for the protein and general AMBER (GAFF) [68] for the ligands. To solvate the system, TIP3P water model was used in an octahedral box with a distance of 15 Å between the wall of the box and the closest atom of the complex. To neutralize the system 31 Na<sup>+</sup> ions were added as counter ions. The molecular systems were first energy minimized with 500 steps of steepest descent energy minimization, followed by 500 steps of conjugate gradient energy minimization so as to remove the bad contacts in the structure; this was done in 3 consecutively rounds. With the force constants of 10 and 2 kcal<sup>-1</sup>Å<sup>-2</sup> respectively, positional restraints were applied to the whole system for the first and second round to allow for relaxation of the solvent molecules. In the third round the whole system was minimized without restraint. Finally a 10 ns MD simulation was carried out following 200 ps of equilibration at 300 K. With a time step of 2 fs a total of 5000 frames were generated. SHAKE algorithm [69] was applied for all the bonds involving hydrogen bonds. The non-bonded cut off distance was 10 Å. The particle mesh Ewald (PME) method [52] was applied to treat long-range electrostatics interactions. The temperature of the system was regulated using the langevin thermostat. All equilibration and subsequent MD stages were carried out in an isothermal isobaric (NPT) ensemble using a Berendsen barometer [69-71] with a target pressure of 1 bar, recording trajectories every 2 ps.

### 3.2.7 Calculation of binding free energy

We have used molecular mechanics generalized Born surface area (MM-GBSA) and molecular mechanics Poisson Boltzmann (MM-PBSA) [72, 73] to calculate the binding free energy implemented in AMBER 11.0 [66]. For this calculation a total of 1000 snapshots generated from

the last 2 ns of the MD trajectory for each molecular species were considered. The binding free energy was computed as the difference between the energy of the complex with the combination energy of the receptor and ligand for each frame for a total of 1000 frames that were generated. The binding free energy was then calculated for each molecular species as

$$\Delta G_{\text{bind}} = G_{\text{complex}} - (G_{\text{receptor}} + G_{\text{ligand}}).$$

The free energy,  $G$  for each species was calculated by the following scheme using the MM-PBSA and MM-GBSA methods [72-76].

$$G = E_{\text{gas}} + G_{\text{sol}} - TS$$

$$E_{\text{gas}} = E_{\text{int}} + E_{\text{ele}} + E_{\text{vdw}}$$

$$G_{\text{ele, PB (GB)}} = E_{\text{ele}} + G_{\text{PB (GB)}}$$

$$G_{\text{sol}} = G_{\text{sol-np}} + G_{\text{PB (GB)}}$$

$$G_{\text{sol-np}} = \gamma \text{SAS}$$

Here,  $E_{\text{gas}}$  is the gas-phase energy;  $E_{\text{int}}$  is the internal energy;  $E_{\text{ele}}$  and  $E_{\text{vdw}}$  are the coulomb and van der Waals energies, respectively.  $E_{\text{gas}}$  was calculated using the ff99SB molecular mechanics force field.  $G_{\text{sol}}$  is the solvation free energy and can be split into polar and non-polar contributions.  $G_{\text{PB(GB)}}$  is the polar solvation contribution calculated by solving the GB and PB equations.  $G_{\text{ele, PB(GB)}}$  is the polar interaction contribution.  $G_{\text{sol-np}}$  is the nonpolar solvation contribution and was estimated via the solvent-accessible surface area (SAS), which was determined using a water probe radius of 1.4 Å.  $T$  and  $S$  are the temperature and the total solute entropy, respectively.

### 3.2.8 Per residue energy contribution with ligands

To achieve the detailed view of the  $\alpha\beta_{\text{III}}$  isotype and noscapinoids interaction, I have computed the binding free-energy contribution of each residue using the MM-GBSA model. The binding energy of each ligand-residue pair includes three energy terms: the van der Waals contribution ( $\delta E_{\text{vdw}}$ ), the electrostatic contribution ( $\delta E_{\text{ele}}$ ) and the solvation contribution ( $\delta E_{\text{sol}}$ ). All the energy components were calculated using the same frames obtained from MD trajectories that were used for calculation of binding free energy. The contribution of each residue to the binding free energy was obtained by summing up the contribution of each atom of the given residue.

## 3.3 RESULTS AND DISCUSSIONS

### 3.3.1 Sequence analysis of isotype specific $\beta$ -tubulin

Different isotypes of  $\beta$ -tubulin ( $\beta_{\text{I}}\text{-}\beta_{\text{VIII}}$ ) encoded by different genes exhibited tissue restricted expression patterns. Cancer cells especially express a variety of isotypes and are not limited to the isotypes that are expressed in non-cancerous cells from which they are derived. There

are several examples of this pattern. As an example,  $\beta_{II}$  was over-expressed in leukemia and Hodgkin's lymphoma [21]. HeLa cell line shows maximum expression of  $\beta_I$  with a little expression of  $\beta_{III}$  and even less expression of  $\beta_{II}$  and  $\beta_{IV}$  [26]. Similarly both A549 and CEM cell lines over-expresses  $\beta_{III}$ , while  $\beta_{II}$  is over expressed in the MCF-7 cell line in comparison to all other  $\beta$ -tubulin isotypes [26].

The protein sequences of eight human  $\beta$ -tubulin isotypes ( $\beta_I$  to  $\beta_{VIII}$ ) reported previously [21] were downloaded from the NCBI database. The representative sequences of each isotype were compared by multiple sequence alignment using bioedit [50]. The sequences were observed to have mismatches at different positions with an identity score ranging from 77-94. In particular the mismatches were mostly concentrated in the region of residues 160-370 that constitutes the noscapinoid binding site [48]. No clear consensus in amino acids was observed at four different positions (236, 239, 315, 316, 351 and 368) within the noscapinoid binding site with reference to the crystal structure of  $\alpha\beta$ -tubulin (PDB ID: 1SA0) (Table 3.2). As an example, Ala315 is substituted by Threonine in both  $\beta_{III}$  and  $\beta_V$  as well as Cysteine in  $\beta_{VI}$ , whereas Val316 is substituted by Isoleucine in  $\beta_{II}$  and  $\beta_{VI}$  to  $\beta_{VIII}$  (Table 3.2). Furthermore, the sequence analysis of the amino acids within 12 Å of noscapinoid binding pocket also reveals many differences in and near the binding site (Figure 3.6). Differences in binding site residues among  $\alpha\beta$ -tubulin isotypes may contribute to differences in binding energy with noscapinoids.



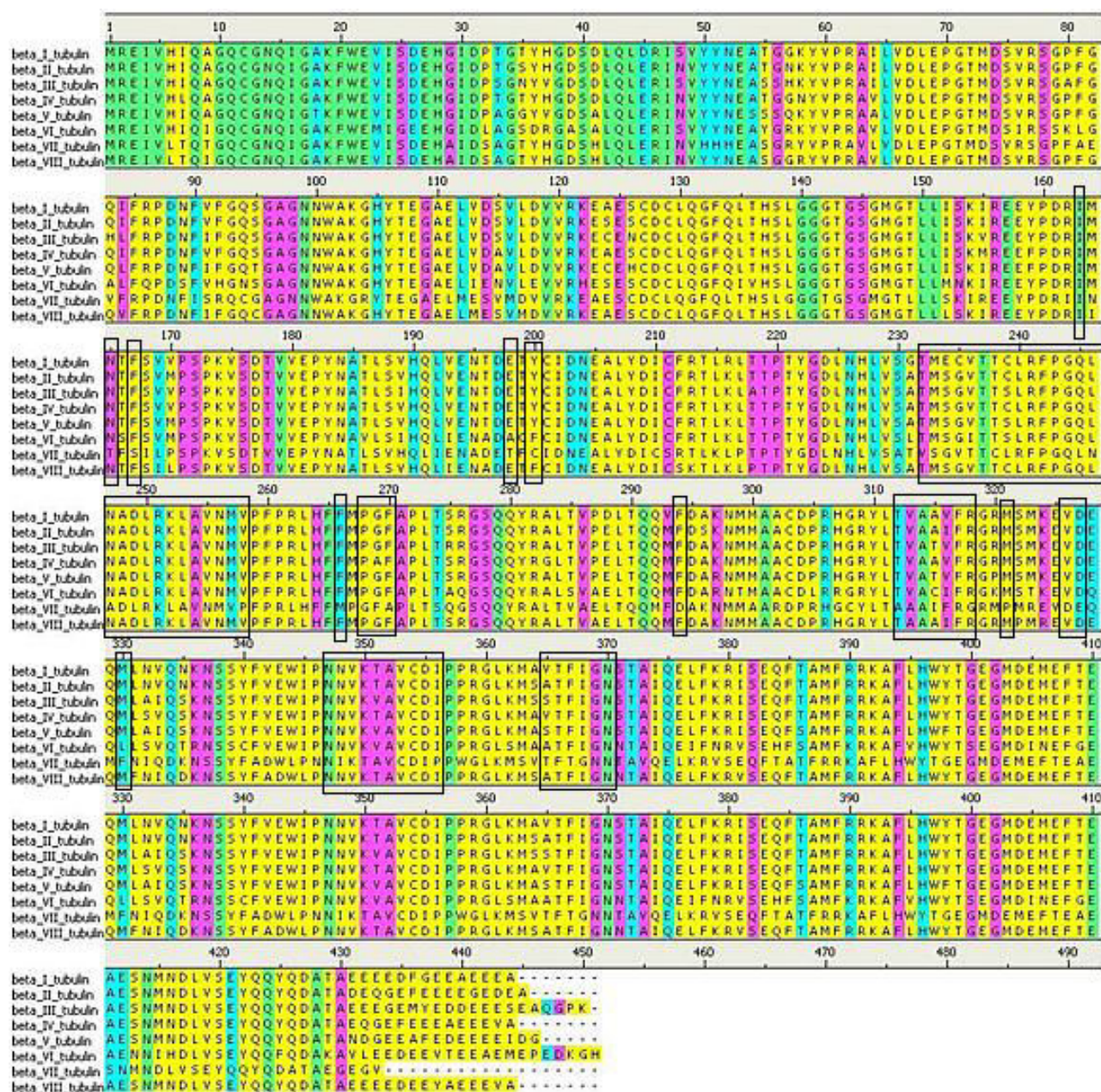


Figure 3.6. Multiple sequence alignment of  $\beta_I$ - $\beta_{VIII}$  isotypes showing mismatches at certain places. All the isotypes are comprised of different lengths of amino acid sequences. Green colour represents identical residues, cyan represents strongly similar, pink represents weakly similar and yellow represents very strongly dissimilar residues. The amino acids located in or near 12.0 Å of the noscapinoid binding site (marked in the boxes) show mismatches at certain places.

Table 3.2. Mismatches in amino acids comprising the noscapinoid binding site among different  $\beta$  isotypes in comparison to the template (1SA0). There are six positions (such as 236,239,315,316,351 and 368) where there are no clear consensuses in residues over all the  $\beta$ -isotypes.

Isotype	Amino acid position															
	179(A)	235	236	237	239	246	248	252	253	314	315	316	350	351	366	368
1SA0	Thr	Gly	Val	Thr	Cys	Leu	Ala	Lys	Leu	Ala	Ala	Val	Lys	Thr	Thr	Ile
$\beta_I$	Thr	Gly	Val	Thr	Cys	Leu	Ala	Lys	Leu	Ala	Ala	Val	Lys	Thr	Thr	Ile
$\beta_{II}$	Thr	Gly	Val	Thr	Cys	Leu	Ala	Lys	Leu	Ala	Ala	Ile	Lys	Thr	Thr	Ile
$\beta_{III}$	Thr	Gly	Val	Thr	Ser	Leu	Ala	Lys	Leu	Ala	Thr	Val	Lys	Val	Thr	Ile
$\beta_{IV}$	Thr	Gly	Val	Thr	Cys	Leu	Ala	Lys	Leu	Ala	Ala	Val	Lys	Thr	Thr	Ile
$\beta_V$	Thr	Gly	Val	Thr	Ser	Leu	Ala	Lys	Leu	Ala	Thr	Val	Lys	Val	Thr	Ile
$\beta_{VI}$	Thr	Gly	Ile	Thr	Ser	Leu	Ala	Lys	Leu	Ala	Cys	Ile	Lys	Val	Thr	Ile
$\beta_{VII}$	Thr	Gly	Val	Thr	Cys	Leu	Ala	Lys	Leu	Ala	Ala	Ile	Lys	Thr	Thr	Thr
$\beta_{VIII}$	Thr	Gly	Val	Thr	Cys	Leu	Ala	Lys	Leu	Ala	Ala	Ile	Lys	Thr	Thr	Ile

### 3.3.2 Template preparation and homology modeling of $\alpha\beta$ -tubulin isotypes

The x-ray crystal structures of tubulin heterodimers composed of  $\alpha$ - and isotypes specific  $\beta$ -tubulin are not available. Thus it is necessary to build these structures for comparative analysis. Crystal structure of tubulin (PDB ID: 1SA0) has been used as template for the homology modeling. The missing amino acids in the template structure were filled using homology model building (Figure 3.7, 3.8 3.9 & 3.10).

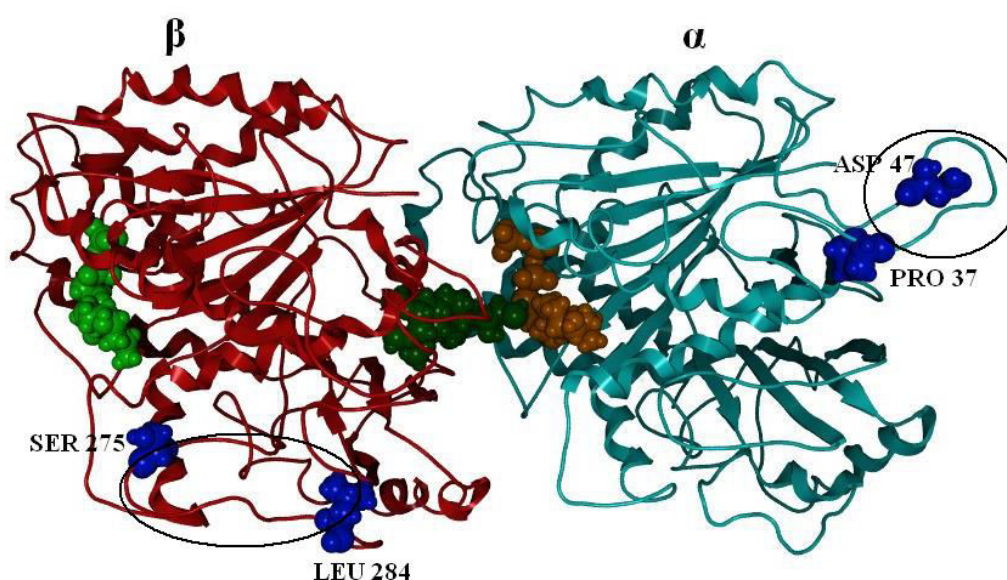


Figure 3.7. Modeled tubulin dimer along with ligand colchicine (dark green), GTP (Brown) and GDP (light green) having no gaps as is evident from the figure gap between the end residues of gaps ASP 47 and PRO 37 in  $\alpha$  chain and SER 275 and LEU 284 in  $\beta$  chain are filled there is a loop there (encircled portion).



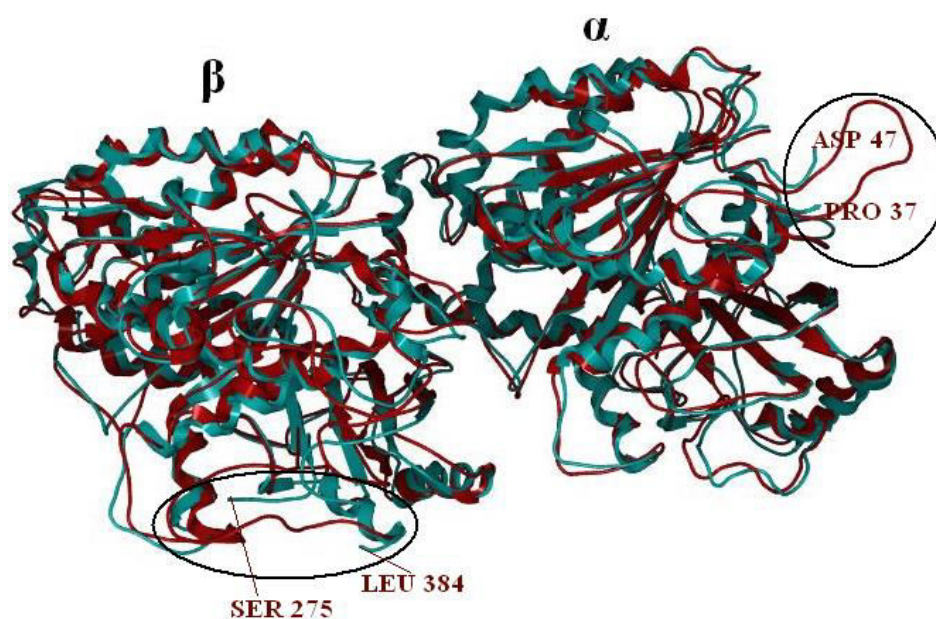


Figure 3.8. Figure showing the superimposition of the 1SA0 template(green) and the modeled tubulin dimer(red). (gap filled shown in encircled region).

ATOM	522	CA	PRO	A	37	4.458	117.671	77.072	Filled gap of A chain residue 38 to 46
ATOM	537	CA	SER	A	38	5.521	115.015	74.393	
ATOM	548	CA	ASP	A	39	3.902	113.329	71.311	
ATOM	560	CA	LYS	A	40	2.423	109.749	71.338	
ATOM	582	CA	THR	A	41	5.410	108.232	73.174	
ATOM	596	CA	ILE	A	42	3.526	105.231	74.433	
ATOM	615	CA	GLY	A	43	3.716	102.874	71.402	
ATOM	622	CA	GLY	A	44	-0.085	102.454	71.235	
ATOM	629	CA	GLY	A	45	-3.146	102.883	73.472	
ATOM	636	CA	ASP	A	46	-2.917	102.425	77.265	Filled gap of B chain residue 276 to 283
ATOM	648	CA	ASP	A	47	-4.921	103.592	80.383	
ATOM	10873	CA	SER	B	275	-24.386	157.364	127.141	
ATOM	10884	CA	ARG	B	276	-24.485	160.560	129.253	
ATOM	10908	CA	GLY	B	277	-20.839	159.984	130.405	
ATOM	10915	CA	SER	B	278	-18.634	157.727	132.698	
ATOM	10926	CA	GLN	B	279	-15.301	155.820	132.456	
ATOM	10943	CA	GLN	B	280	-14.737	153.324	129.590	
ATOM	10960	CA	TYR	B	281	-13.264	149.979	128.668	
ATOM	10981	CA	ARG	B	282	-13.727	146.326	129.826	
ATOM	11005	CA	ALA	B	283	-14.208	143.576	127.152	
ATOM	11015	CA	LEU	B	284	-11.608	141.280	125.297	
ATOM	11034	CA	THR	B	285	-9.111	139.583	128.106	

Figure 3.9. Typical snapshots of pdb file showing Ca coordinates of the filled gap in  $\alpha$ (A) chain residue 38 to 46 and  $\beta$ (B) chain residue 276 to 283.



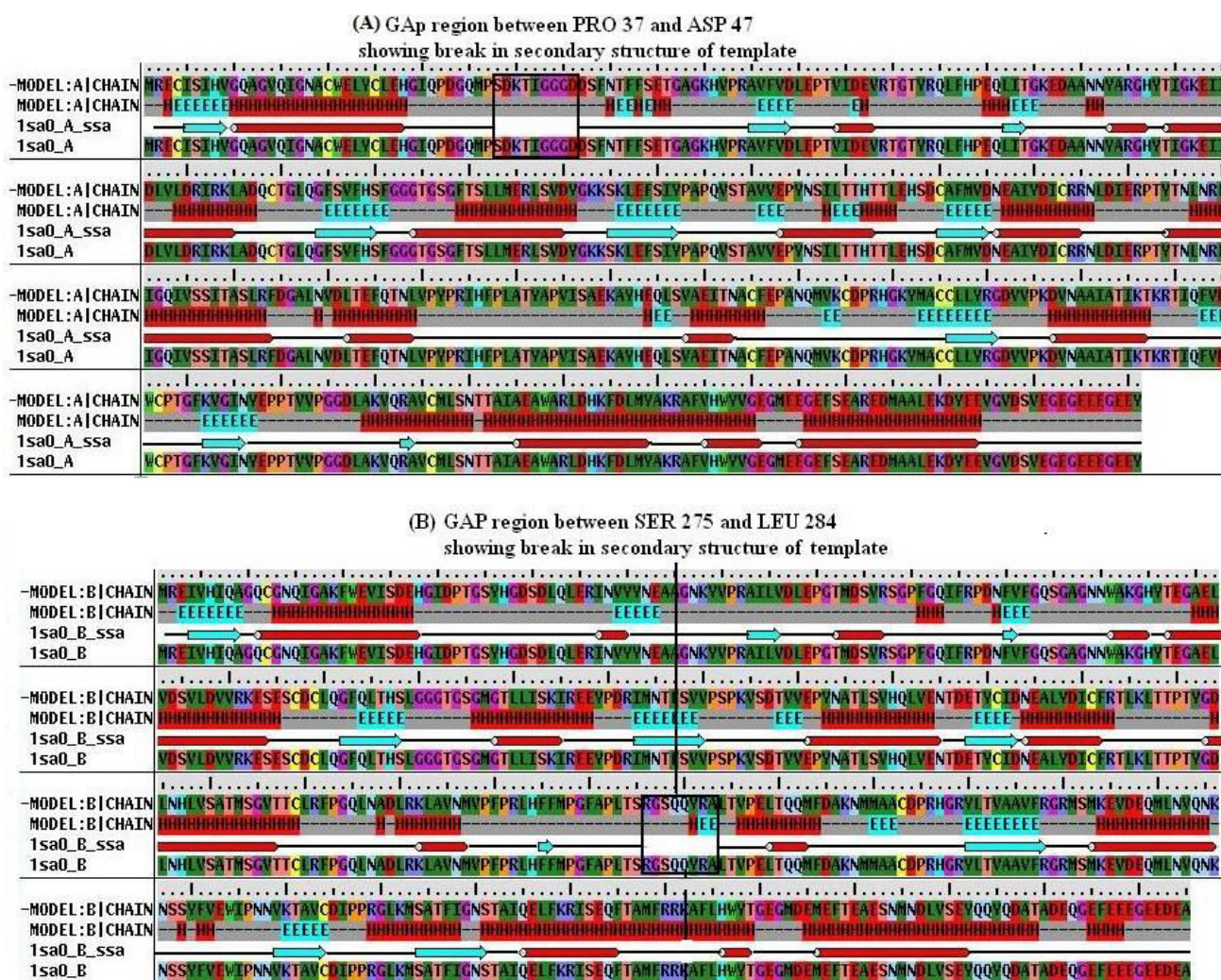


Figure 3.10. (a) Pairwise alignment between sequences of modeled structure of chain A and template 1SA0 chain A along with secondary structure alignment, template secondary structure has a gap between PRO37 and ASP47 due to missing residues in template structure.(b) Pairwise alignment between sequences of modeled structure of chain B and template 1SA0 chain B along with secondary structure alignment , template secondary structure has a gap between SER 275 and LEU 284 due to missing residues in template structure.

The structure was further refined using MD simulation for a period of 10 ns. Various structure validation programs such as an ERRAT score of 88.402 and a VERIFY 3D score of 95.25% indicated a good quality structure for the template. The PROCHECK results also showed 94.8% of backbone angles were in allowed regions with G-factors of - 0.12. Ramachandran plot [55] analysis revealed only 1.6% of residues in the disallowed region and 2.3% of residues in generously allowed regions (Figure 3.11a&b).

(a) Errat score 88.402

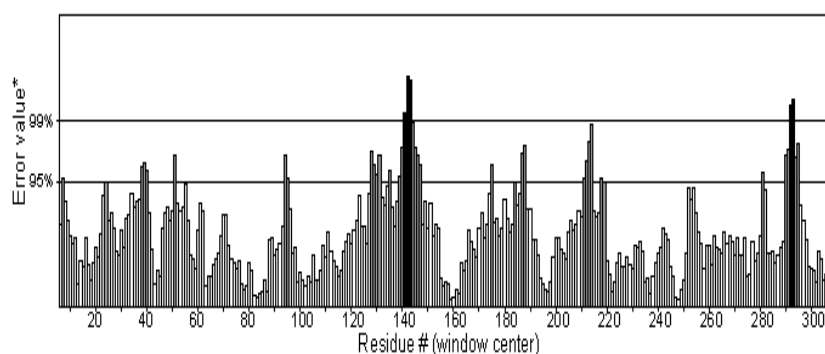
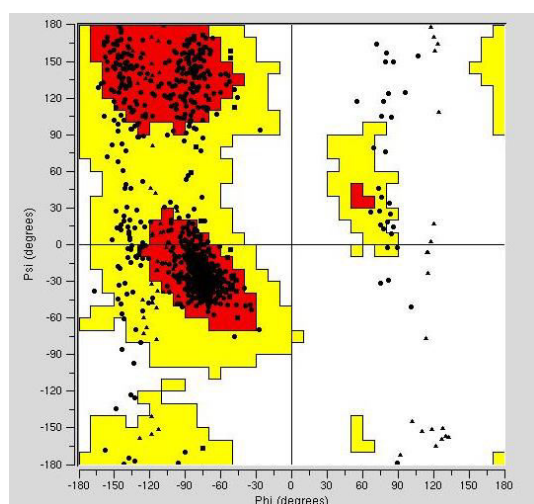


Figure 3.11(a). Structure validation program Errat shows a score of 88.402 which indicates good quality of the template structure.(a portion of the residue window is represented)

(b)



<b>Residues in most favoured regions</b>	<b>94.8%</b>
<b>Residues in generously allowed regions</b>	<b>2.3%</b>
<b>Residues in disallowed regions</b>	<b>1.6%</b>

(c)

**95.25% of atoms have 3D-ID score > 0.2**

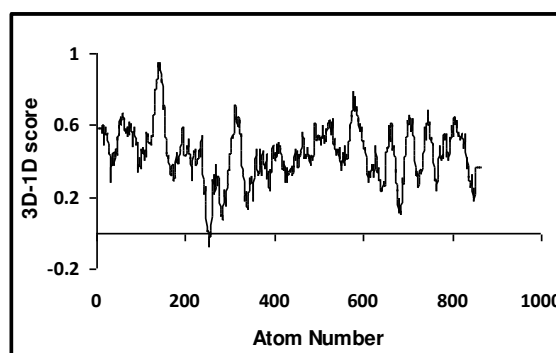


Figure 3.11(b). Ramachandran plot analysis using PROCHECK also showed 94.8% of backbone angles were in allowed regions with G-factors of - 0.12 and only 1.6% residues in the disallowed region and 2.3% residues in generously allowed regions.(c) VERIFY 3D score of 95.25% indicated a good quality structure to the template.

Thus the overall quality of the template structure was very good for homology modeling of  $\alpha\beta$ -tubulin isotypes. The molecular structures of these  $\alpha\beta$ -tubulin isotypes were built based on the prepared template structure and further refined using an MD simulation run of 10 ns. The equilibration of the MD trajectories was monitored based on the convergence of plots of root-mean-

square deviations (RMSDs) of C $\alpha$  carbon atoms of  $\alpha\beta$ -tubulin isotypes during 10 ns of MD simulation starting from the initial modelled structure (Figure 3.12).

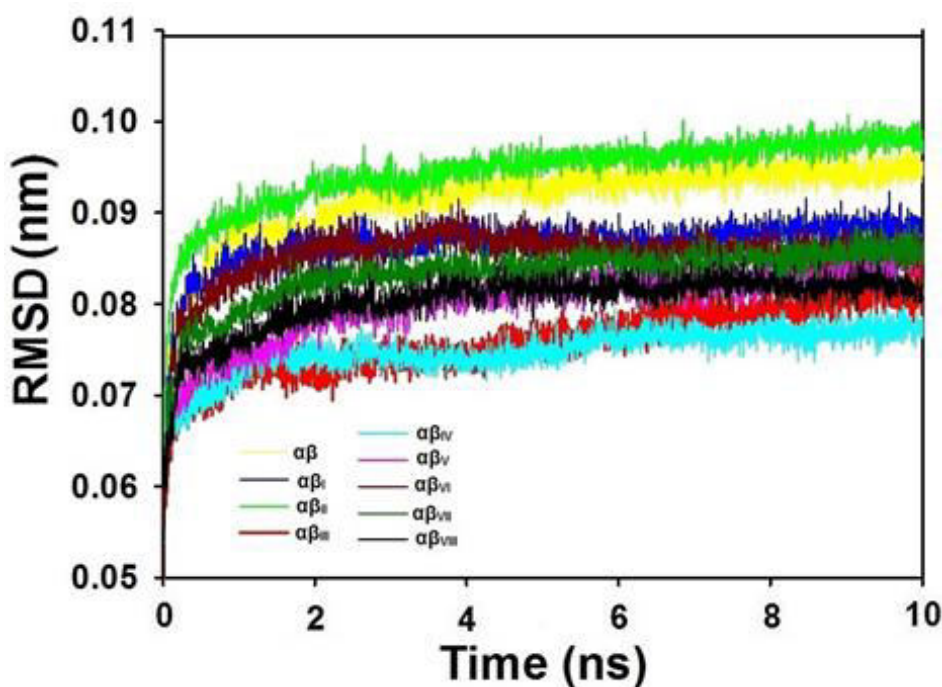


Figure 3.12. Time series of the root-mean-square deviations (RMSD) for the C $\alpha$  carbon atoms of template ( $\alpha\beta$ ) and all the 8 tubulin isotypes ( $\alpha\beta_I$  to  $\alpha\beta_{VIII}$ ) during 10 ns of MD simulation starting from the initial structure. The relative fluctuation in the RMSD of the C $\alpha$  atoms is very small after the initial equilibration ( $\sim 5$  ns) demonstrating the convergence of the simulation. A 10 ns MD simulation was carried out with a time step of 2 fs following 200 ps of equilibration at 300 K. A total of 5000 frames were generated and the last 2000 frames were used to generate the average structure for each  $\alpha\beta$ -tubulin isotype.

As can be seen from Figure 3.12, the relative fluctuation in the RMSD of the C $\alpha$  atoms is very small after the initial equilibration ( $\sim 5$  ns), demonstrating the convergence of the simulation. A total of 5000 frames were generated out of which the last 2000 frames were used to generate an average structure of the  $\alpha\beta$ -tubulin isotypes. These modeled structures were of good quality with the ERRAT scores ranging from 88-95 and VERIFY 3D score within 97% - 99%. The Ramachandran plot analysis also revealed good quality structures with the percentage of residues in disallowed regions ranging from only 1.2% - 1.6%. The modeled  $\alpha\beta$ -tubulin isotypes showed significant structural similarity with the template protein (1SA0) with an RMSD value in the range of 1.082 – 1.251 Å (Figure 3.13). However, pairwise comparative analysis of these  $\alpha\beta$ -tubulin isotypes showed RMSD values in the range of 0.963-1.511 Å (Table 3.3).



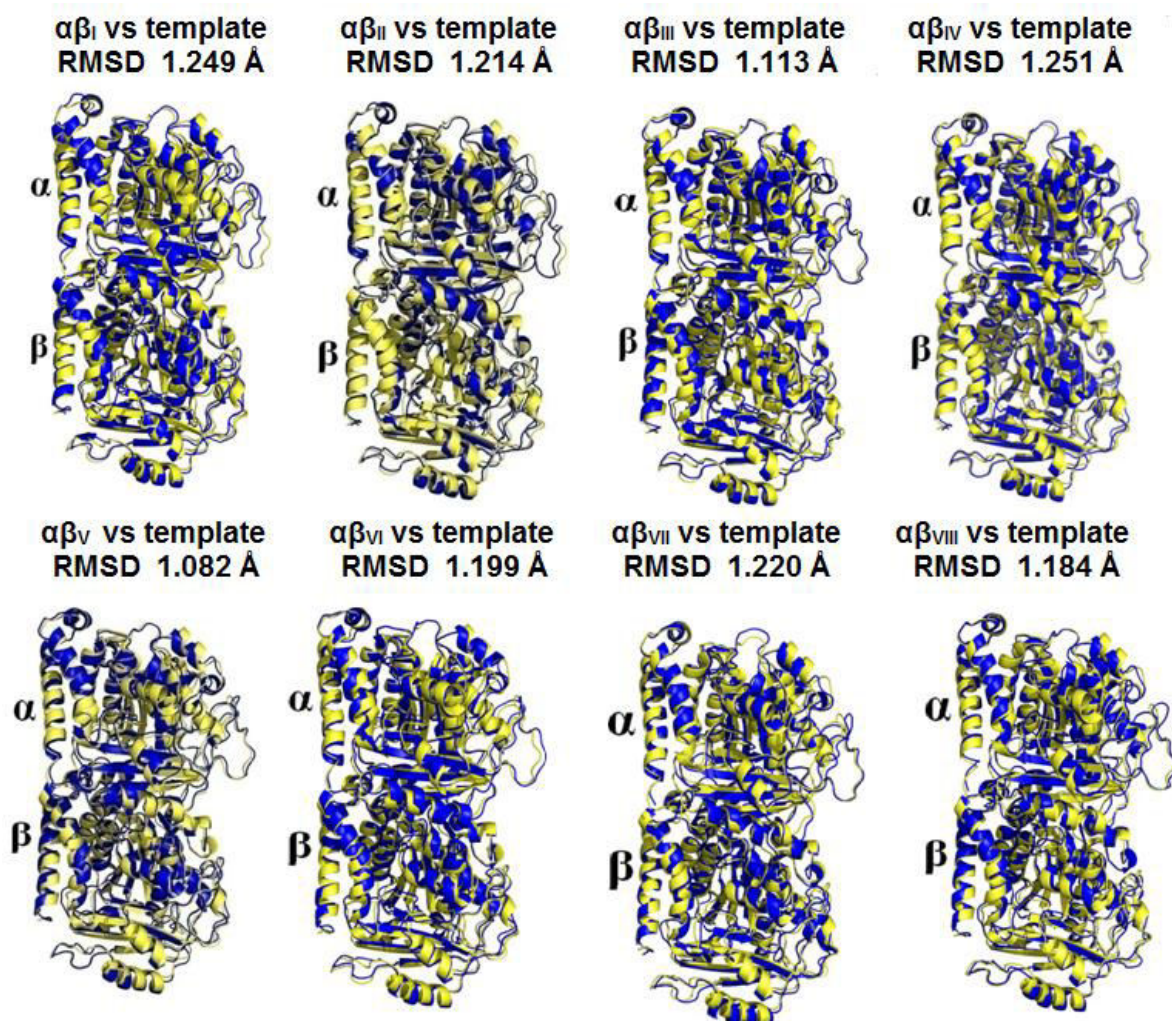


Figure 3.13. Superimposition of  $\alpha\beta$ -tubulin isotypes ( $\alpha\beta_I$  to  $\alpha\beta_{VIII}$ , blue) with the template structure (1SA0, yellow). The RMSD values ranges from 1.082-1.251 Å.

Table 3.3. All-vs-all structure comparison of the  $\alpha\beta$ -tubulin isotypes. The values are root mean square deviation (RMSD) calculated by superimposition of the structures.

Isotypes	$\alpha\beta_I$	$\alpha\beta_{II}$	$\alpha\beta_{III}$	$\alpha\beta_{IV}$	$\alpha\beta_V$	$\alpha\beta_{VI}$	$\alpha\beta_{VII}$	$\alpha\beta_{VIII}$
$\alpha\beta_I$	0							
$\alpha\beta_{II}$	0.963	0						
$\alpha\beta_{III}$	1.200	1.136	0					
$\alpha\beta_{IV}$	1.145	1.139	1.127	0				
$\alpha\beta_V$	1.261	1.318	1.055	1.177	0			
$\alpha\beta_{VI}$	1.481	1.461	1.244	1.257	1.130	0		
$\alpha\beta_{VII}$	1.511	1.423	1.139	1.337	1.359	1.339	0	
$\alpha\beta_{VIII}$	1.351	1.277	0.943	1.216	1.152	1.244	1.054	0

The structure comparison of all the isotypes among themselves revealed significant variations among the isotype Figure (3.14a-h).  $\alpha\beta_I$ -tubulin isotype is showing maximum variation with  $\alpha\beta_{VI}$ -tubulin isotype and minimum variation with  $\alpha\beta_{II}$ -tubulin isotype with an RMSD of 1.511 Å and 0.963 Å respectively.  $\alpha\beta_{II}$ -tubulin isotype is showing maximum variation with  $\alpha\beta_{VI}$ -tubulin isotype and minimum variation with  $\alpha\beta_{III}$ -tubulin isotype with an RMSD of 1.461 Å and 0.963 Å respectively.  $\alpha\beta_{III}$ -tubulin isotype is showing maximum variation with  $\alpha\beta_{VI}$ -tubulin isotype and minimum variation with  $\alpha\beta_{VIII}$ -tubulin isotype with an RMSD of 1.244 Å and 0.943 Å respectively.  $\alpha\beta_{IV}$ -tubulin isotype is showing maximum variation with  $\alpha\beta_{VII}$ -tubulin isotype and minimum variation with  $\alpha\beta_{III}$ -tubulin isotype with an RMSD of 1.127 Å and 1.337 Å respectively.  $\alpha\beta_V$ -tubulin isotype is showing maximum variation with  $\alpha\beta_{VII}$ -tubulin isotype and minimum variation with  $\alpha\beta_{III}$ -tubulin isotype with an RMSD of 1.359 Å and 1.055 Å respectively.  $\alpha\beta_{VI}$ -tubulin isotype is showing maximum variation with  $\alpha\beta_I$ -tubulin isotype and minimum variation with  $\alpha\beta_V$ -tubulin isotype with an RMSD of 1.481 Å and 1.130 Å respectively.  $\alpha\beta_{VII}$ -tubulin isotype is showing maximum variation with  $\alpha\beta_I$ -tubulin isotype and minimum variation with  $\alpha\beta_{VIII}$ -tubulin isotype with an RMSD of 1.481 Å and 1.130 Å respectively.  $\alpha\beta_{VIII}$ -tubulin isotype is showing maximum variation with  $\alpha\beta_I$ -tubulin isotype and minimum variation with  $\alpha\beta_{III}$ -tubulin isotype with an RMSD of 1.351 Å and 0.943 Å respectively.  $\alpha\beta_I$  and  $\alpha\beta_{VII}$  are the most different structures among all the  $\alpha\beta$ -tubulin isotypes.  $\alpha\beta_I$  and  $\alpha\beta_{II}$  have come up as least different of all the  $\alpha\beta$ -tubulin isotypes. Since the overall structures of all the  $\alpha\beta$ -tubulin isotypes are significantly different which is expected to affect the structure of the noscapinoid binding site of these isotypes. These differences motivated us for the comparative analysis of the noscapinoids binding site in different isotypes.



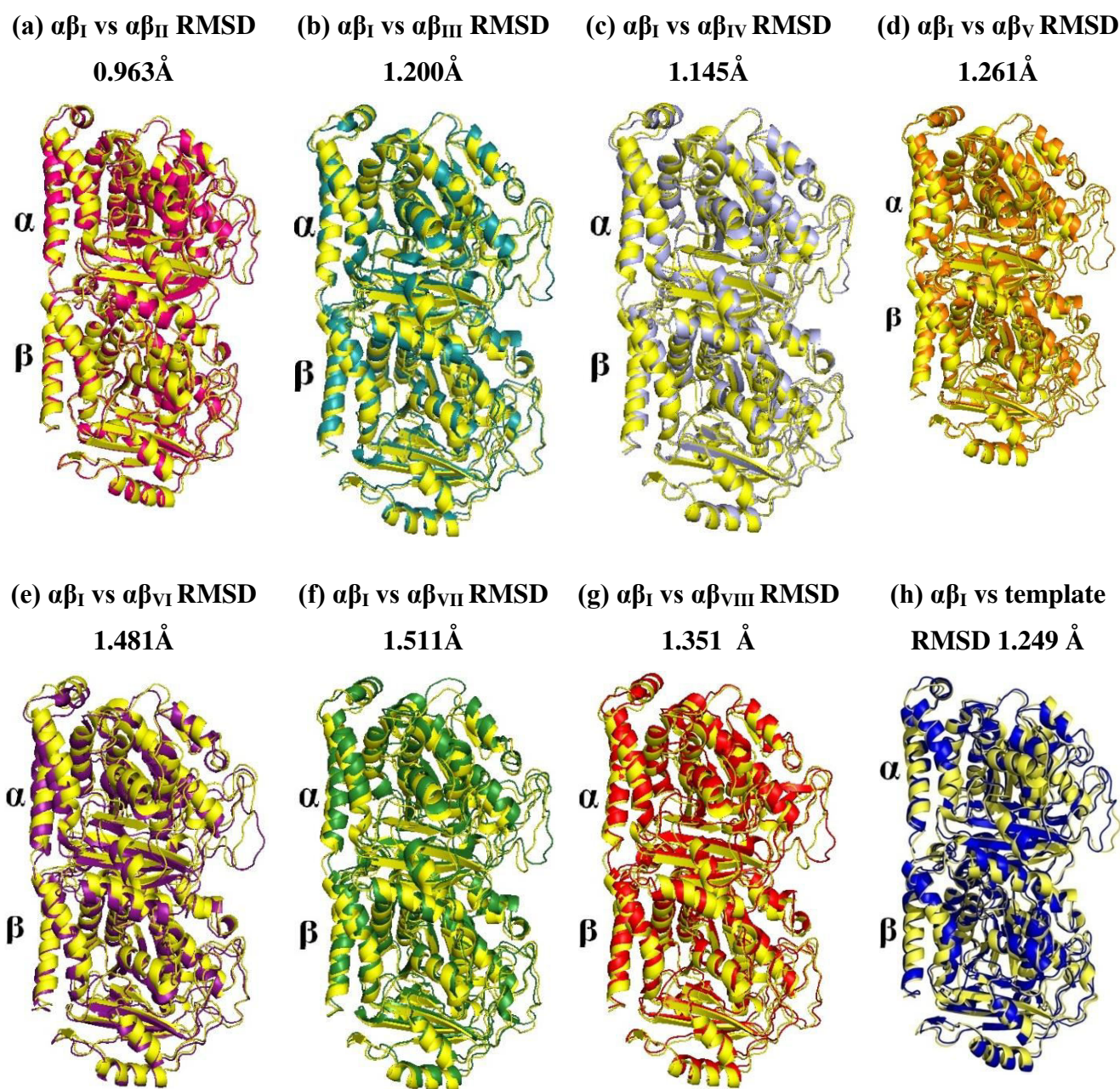


Figure 3.14 (a). Superimposition of  $\alpha\beta_I$ -tubulin isotype(yellow) with different  $\alpha\beta$ -tubulin isotypes ( $\alpha\beta_{II}$  to  $\alpha\beta_{VIII}$ , different colours) (a-g) and (h)  $\alpha\beta_I$ -tubulin isotype(blue) with template structure (1SA0, yellow). The RMSD values ranges from 0.963-1.511 Å.  $\alpha\beta_I$ -tubulin isotype is showing maximum variation with  $\alpha\beta_{VI}$ -tubulin isotype and minimum variation with  $\alpha\beta_{II}$ -tubulin isotype with an RMSD of 1.511 Å and 0.963 Å respectively.



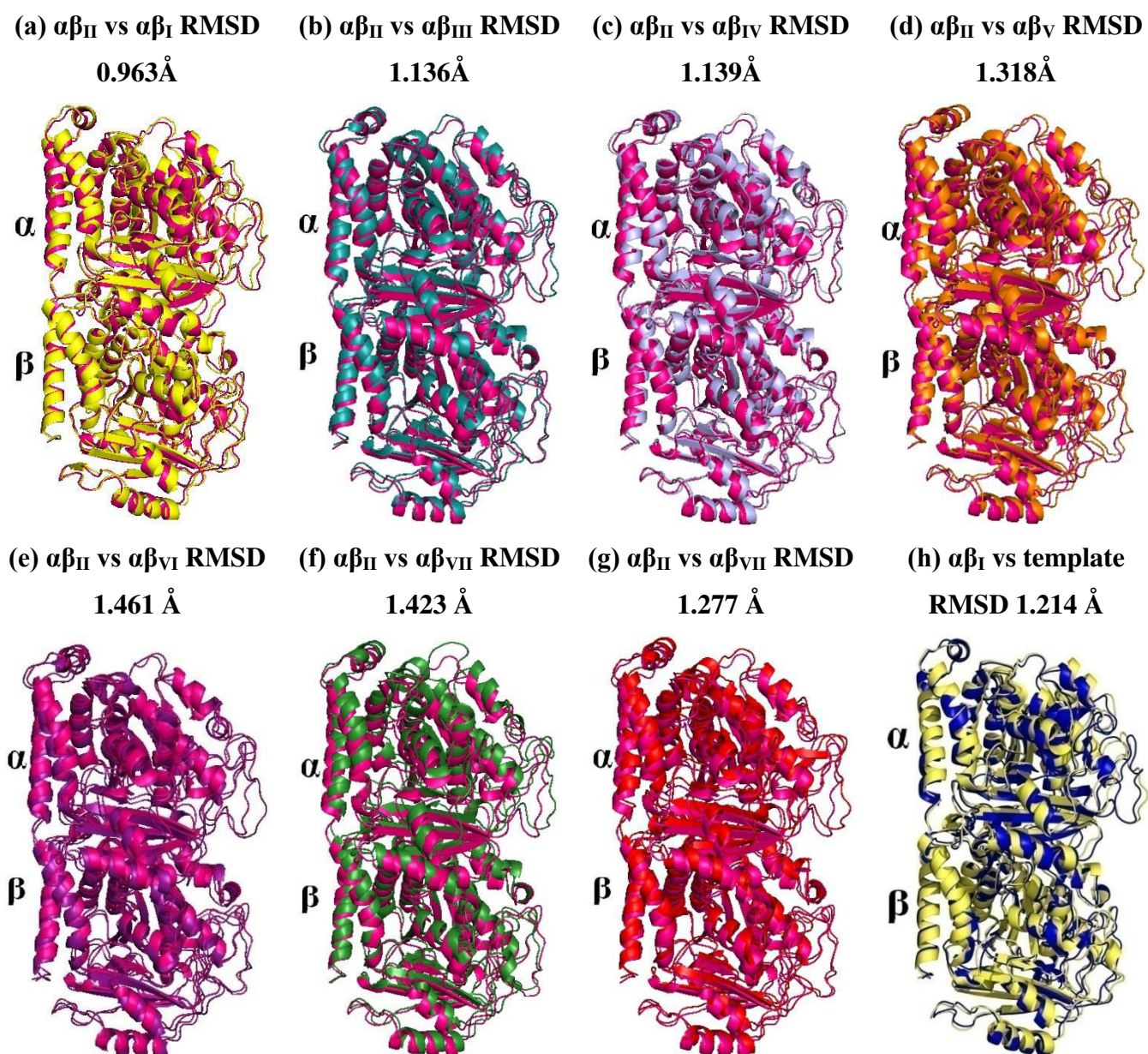


Figure 3.14(b). Superimposition of  $\alpha\beta_{II}$ -tubulin isotype(pink) with different  $\alpha\beta$ -tubulin isotypes ( $\alpha\beta_I$  to  $\alpha\beta_{VII}$ , different colours) (a-g) and (h)  $\alpha\beta_{II}$ -tubulin isotype(blue) with template structure (1SA0, yellow). The RMSD values ranges from 0.963-1.461 Å.  $\alpha\beta_{II}$ -tubulin isotype is showing maximum variation with  $\alpha\beta_{VI}$ -tubulin isotype and minimum variation with  $\alpha\beta_{II}$ -tubulin isotype with an RMSD of 1.461 Å and 0.963 Å respectively.



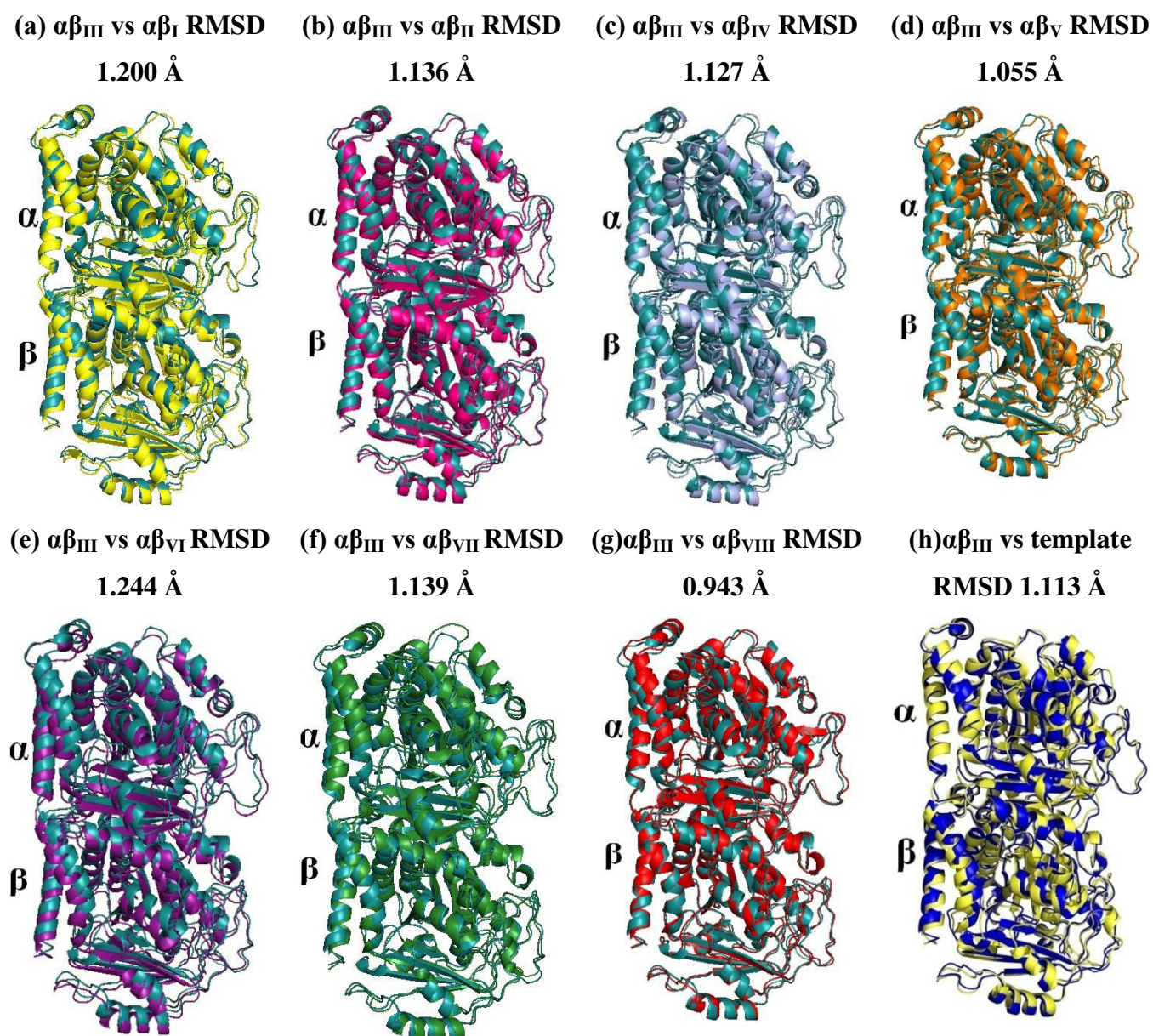


Figure 3.14(c). Superimposition of  $\alpha\beta_{III}$ -tubulin isotype(dark cyan) with different  $\alpha\beta$ -tubulin isotypes ( $\alpha\beta_I$  to  $\alpha\beta_{VIII}$ , different colours) (a-g) and (h)  $\alpha\beta_{III}$ -tubulin isotype(blue) with template structure (1SA0, yellow). The RMSD values ranges from 0.943-1.244 Å.  $\alpha\beta_{III}$ -tubulin isotype is showing maximum variation with  $\alpha\beta_{VI}$ -tubulin isotype and minimum variation with  $\alpha\beta_{VIII}$ -tubulin isotype with an RMSD of 1.244 Å and 0.943 Å respectively.



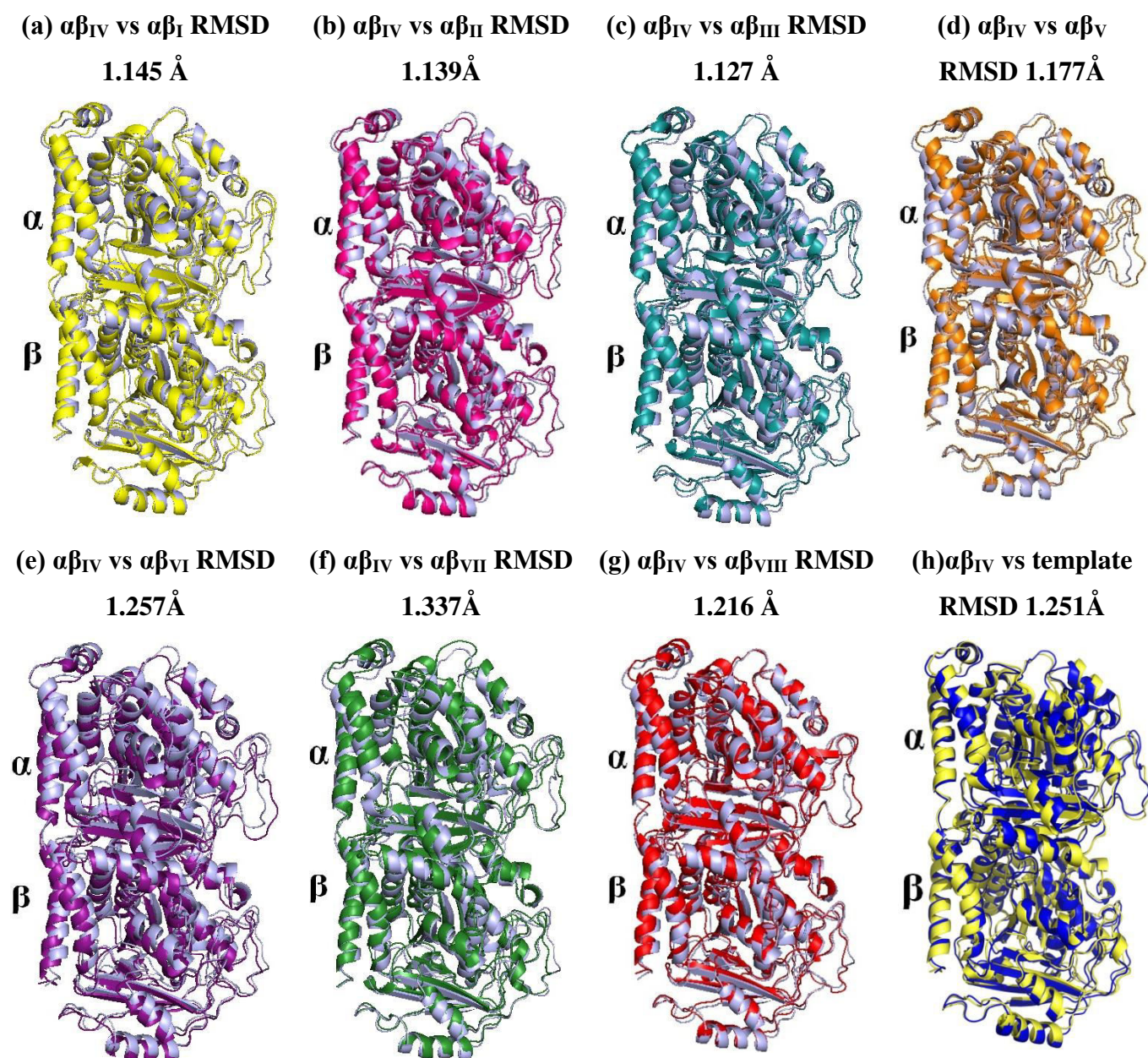


Figure 3.14(d). Superimposition of  $\alpha\beta_{IV}$ -tubulin isotype(light blue) with different  $\alpha\beta$ -tubulin isotypes ( $\alpha\beta_I$  to  $\alpha\beta_{VIII}$ , different colours) (a-g) and (h)  $\alpha\beta_{IV}$ -tubulin isotype(blue) with template structure (1SA0, yellow). The RMSD values ranges from 1.127-1.337 Å.  $\alpha\beta_{IV}$ -tubulin isotype is showing maximum variation with  $\alpha\beta_{VII}$ -tubulin isotype and minimum variation with  $\alpha\beta_{III}$ -tubulin isotype with an RMSD of 1.127Å and 1.337 Å respectively.



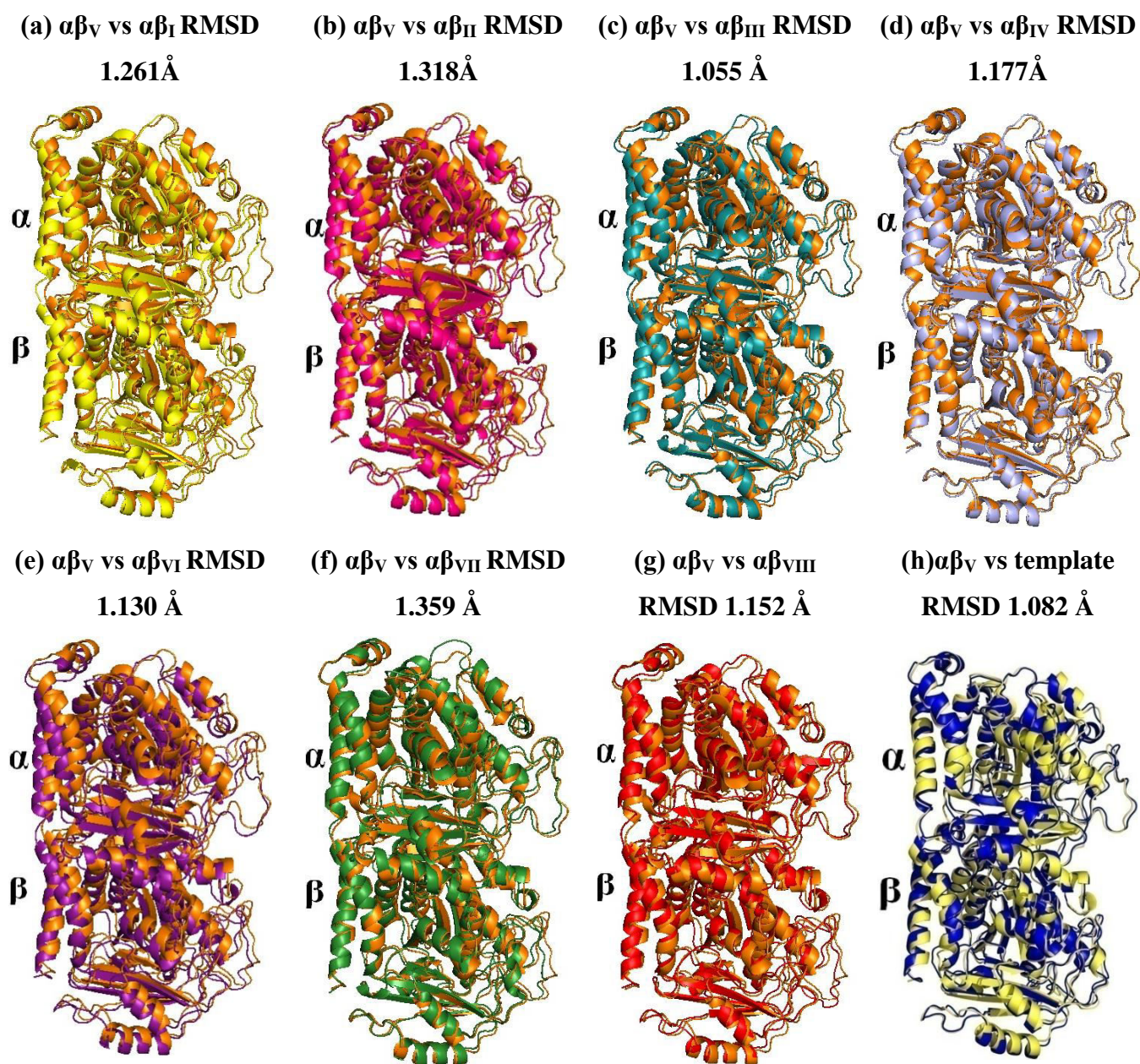


Figure 3.14(e). Superimposition of  $\alpha\beta_V$ -tubulin isotype(brown) with different  $\alpha\beta$ -tubulin isotypes ( $\alpha\beta_I$  to  $\alpha\beta_{VIII}$ , different colours) (a-g) and (h)  $\alpha\beta_V$ -tubulin isotype(blue) with template structure (1SA0, yellow). The RMSD values ranges from 1.055-1.359 Å.  $\alpha\beta_V$ -tubulin isotype is showing maximum variation with  $\alpha\beta_{VII}$ -tubulin isotype and minimum variation with  $\alpha\beta_{III}$ -tubulin isotype with an RMSD of 1.359Å and 1.055 Å respectively.



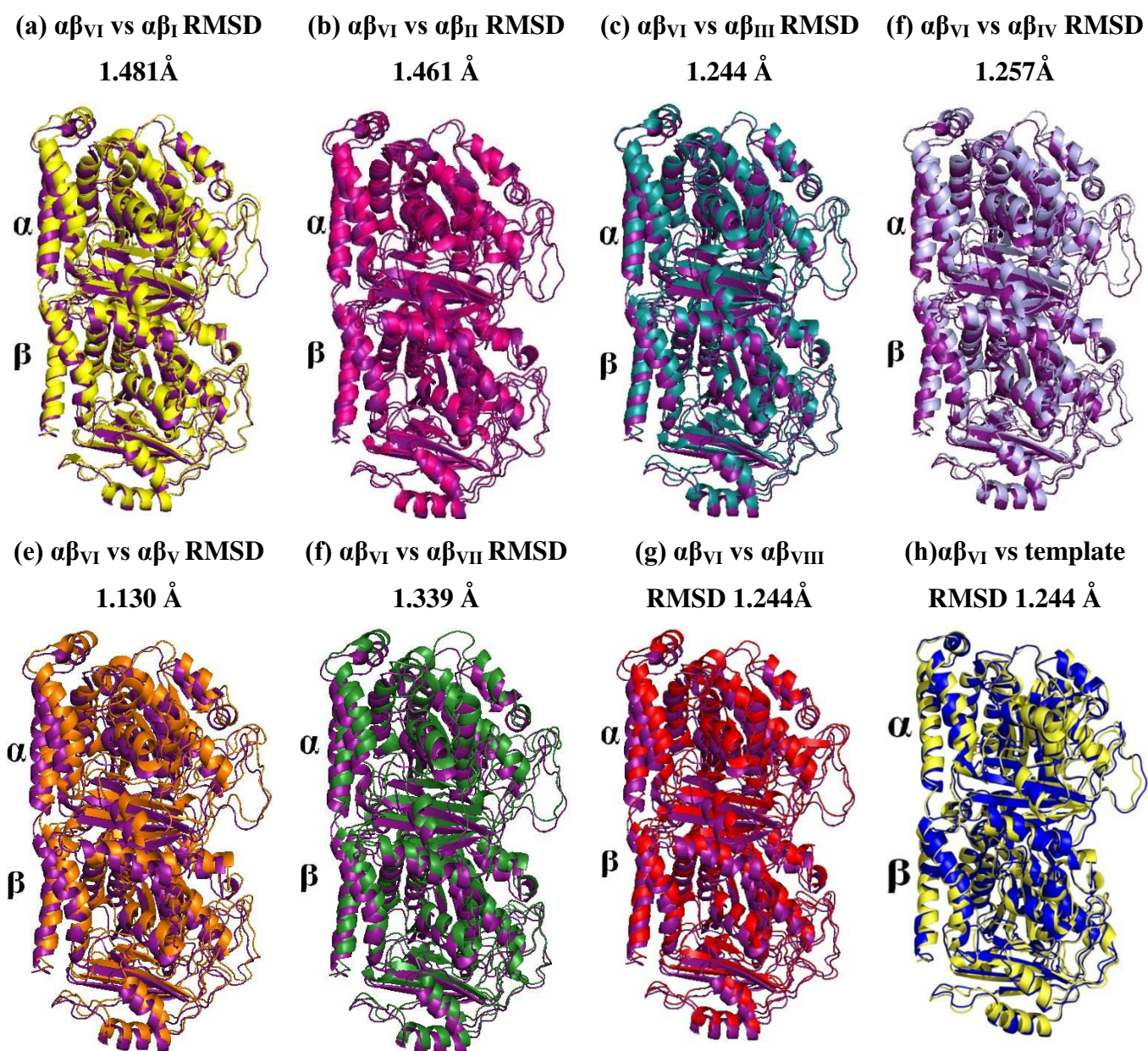


Figure 3.14(f). Superimposition of  $\alpha\beta_{VI}$ -tubulin isotype(purple) with different  $\alpha\beta$ -tubulin isotypes ( $\alpha\beta_I$  to  $\alpha\beta_{VIII}$ , different colours) (a-g) and (h)  $\alpha\beta_{VI}$ -tubulin isotype(blue) with template structure (1SA0, yellow). The RMSD values ranges from 1.130-1.481 Å.  $\alpha\beta_{VI}$ -tubulin isotype is showing maximum variation with  $\alpha\beta_I$ -tubulin isotype and minimum variation with  $\alpha\beta_V$ -tubulin isotype with an RMSD of 1.481 Å and 1.130 Å respectively.



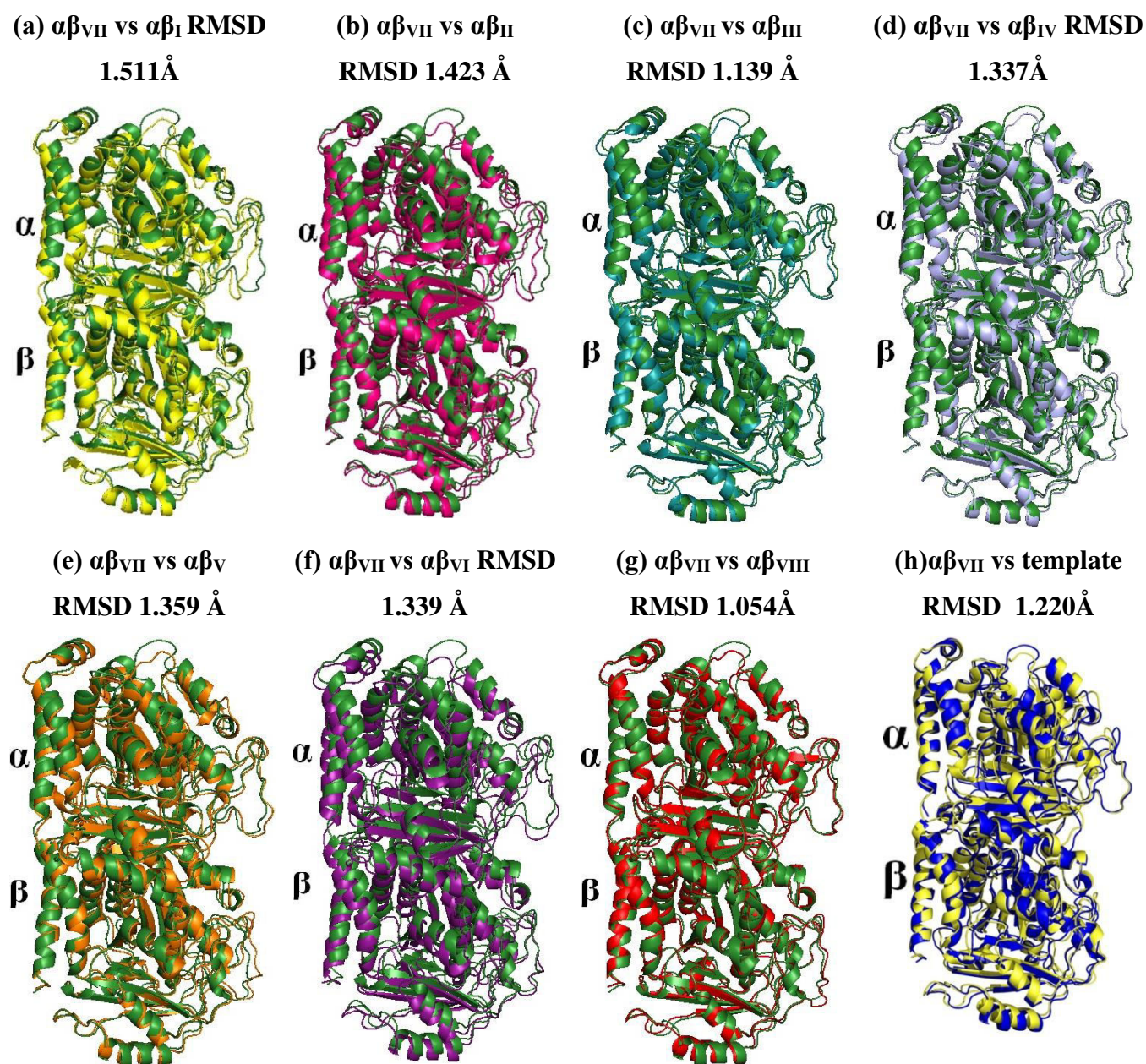


Figure 3.14(g). Superimposition of  $\alpha\beta_{VII}$ -tubulin isotype(green) with different  $\alpha\beta$ -tubulin isotypes ( $\alpha\beta_I$  to  $\alpha\beta_{VIII}$ , different colours) (a-g) and (h)  $\alpha\beta_{VII}$ -tubulin isotype(blue) with template structure (1SA0, yellow). The RMSD values ranges from 1.054-1.511 Å.  $\alpha\beta_{VII}$ -tubulin isotype is showing maximum variation with  $\alpha\beta_I$ -tubulin isotype and minimum variation with  $\alpha\beta_{VIII}$ -tubulin isotype with an RMSD of 1.481 Å and 1.130 Å respectively.



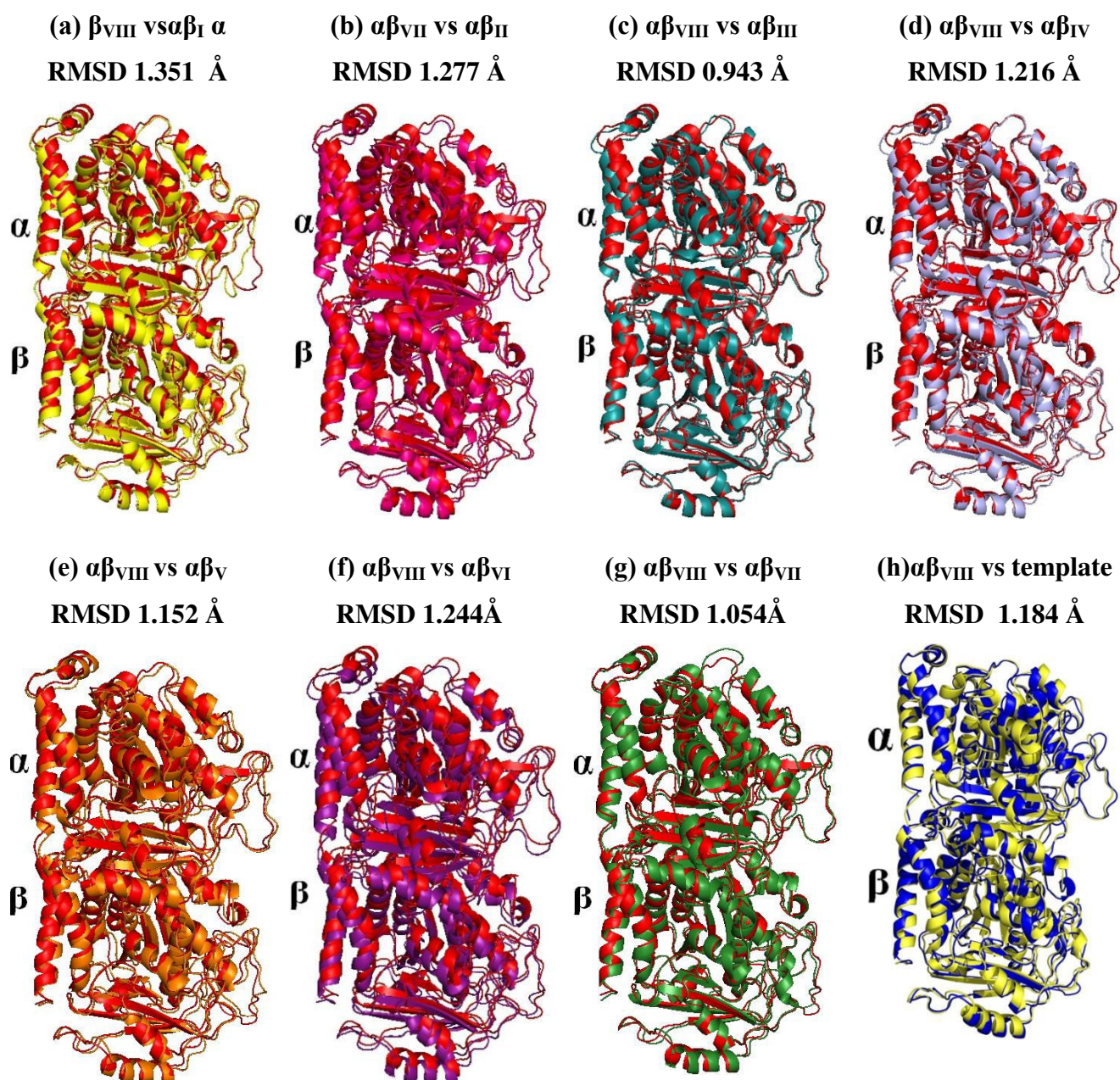


Figure 3.14(h). Superimposition of  $\alpha\beta_{VIII}$ -tubulin isotype(red) with different  $\alpha\beta$ -tubulin isotypes ( $\alpha\beta_I$  to  $\alpha\beta_{VII}$ , different colours) (a-g) and (h)  $\alpha\beta_{VIII}$ -tubulin isotype(blue) with template structure (1SA0, yellow). The RMSD values ranges from 0.943-1.351 Å.  $\alpha\beta_{VIII}$ -tubulin isotype is showing maximum variation with  $\alpha\beta_I$ -tubulin isotype and minimum variation with  $\alpha\beta_{III}$ -tubulin isotype with an RMSD of 1.351 Å and 0.943 Å respectively.

### 3.3.3 Computational prediction and analysis of noscapinoid binding site

To ascertain the impact of the structural differences among the  $\alpha\beta$ -tubulin isotypes on their noscapinoid binding site, I did a comparative analysis of the noscapinoid binding site. Different binding sites were predicted and analyzed for the modeled  $\alpha\beta$ -tubulin isotypes using SiteMap (version 2.4, Schrodinger). However, in the absence of co-crystal structure of noscapinoid with tubulin, only the noscapinoid binding site [48] (at the interface between  $\alpha$ - and  $\beta$ -tubulin) which is in agreement with the predicted noscapinoid binding site and partially supported by experimental study [48] was selected for comparative analysis and predicting the binding affinity of noscapinoids. The binding site residues (comprised of 16 amino acids) which are in agreement with the predicted noscapinoids binding site [48] from each of the tubulin isotypes were extracted and superimposed for comparative analysis. The noscapinoid binding site [48] from different  $\alpha\beta$ -tubulin isotypes were characterized using Sitemap based on various physico-chemical properties included in Table 3.4. The sitemap scores for all the  $\alpha\beta$ -tubulin isotypes ranging from 0.576 ( $\alpha\beta_I$ ) to 0.820 ( $\alpha\beta_{II}$ ) suggest an overall better accommodation of the noscapinoids within the binding site. However, due to various substitutions of amino acids within the binding site region, differences in various parameters among the isotypes were noticed. Similarly, the binding sites among the  $\alpha\beta$ -tubulin isotypes also differed in their ability to accommodate the solvent molecules as measured by exposure and enclosure scores. Apropos to this finding, the binding affinity of the noscapinoids may differ with different  $\alpha\beta$ -tubulin isotypes. All-vs-all comparison of the amino acids within 12 Å of binding site, measured by RMSD score, showed significant variations among the isotypes (Table 3.5).

Table 3.4. Physico-chemical properties of the noscapinoid bind site of different  $\alpha\beta$ -tubulin isotypes. The differences in binding site are due to the different composition of the binding site residues within and near the binding site region.

Isotype	SiteScore (a.u)	Volume(Å) <sup>3</sup>	Exposure (a.u)	Enclosure (a.u)	Contact (a.u)	Phobic (kcal/mol)	Philic (kcal/mol)	Balance (a.u)	don/acc (a.u)
$\alpha\beta_I$	0.576	138.23	0.654	0.653	0.772	0.806	0.86	0.936	0.898
$\alpha\beta_{II}$	0.820	160.87	0.5	0.663	0.867	1.053	0.61	1.737	0.710
$\alpha\beta_{III}$	0.660	109.76	0.705	0.620	0.656	0.469	0.53	0.883	1.418
$\alpha\beta_{IV}$	0.743	171.16	0.550	0.593	0.741	0.886	0.62	1.439	1.438
$\alpha\beta_V$	0.634	122.45	0.629	0.629	0.805	0.611	0.80	0.762	1.261
$\alpha\beta_{VI}$	0.698	134.80	0.680	0.596	0.769	1.166	0.54	2.145	0.943
$\alpha\beta_{VII}$	0.735	126.91	0.426	0.663	0.905	1.343	0.58	2.299	1.641
$\alpha\beta_{VIII}$	0.588	91.581	0.561	0.653	0.814	0.749	0.80	0.938	2.279

Table 3.5. All-vs-all comparison of the amino acids within 12 Å diameter of noscapinoid binding site of the different  $\alpha\beta$ -tubulin isotypes. The variation in the structure is measured by RMSD score after superimposition.

Isotypes	$\alpha\beta_I$	$\alpha\beta_{II}$	$\alpha\beta_{III}$	$\alpha\beta_{IV}$	$\alpha\beta_V$	$\alpha\beta_{VI}$	$\alpha\beta_{VII}$	$\alpha\beta_{VIII}$
$\alpha\beta_I$	0							
$\alpha\beta_{II}$	0.881	0						
$\alpha\beta_{III}$	1.110	0.750	0					
$\alpha\beta_{IV}$	0.865	0.662	0.761	0				
$\alpha\beta_V$	1.251	0.861	0.620	1.046	0			
$\alpha\beta_{VI}$	1.340	1.049	1.148	1.205	1.345	0		
$\alpha\beta_{VII}$	0.945	0.868	0.926	0.947	1.032	1.352	0	
$\alpha\beta_{VIII}$	1.066	0.655	0.701	0.746	0.808	1.144	0.969	0

The RMSD score was found to be maximum between  $\alpha\beta_I$  -  $\alpha\beta_{VI}$ ,  $\alpha\beta_{VI}$  -  $\alpha\beta_V$  and  $\alpha\beta_{VI}$  -  $\alpha\beta_{VII}$  with values of 1.340, 1.345 and 1.352 Å, respectively. However, the binding site between  $\alpha\beta_{II}$  and  $\alpha\beta_{VIII}$  showed minimum differences with an RMSD of 0.655 Å. Furthermore, the noscapinoid binding site consisted of 16 amino acids [48] and extracted from  $\alpha\beta$ -tubulin isotypes revealed significant differences as shown in Figure 3.15 and Figure 16(a-h).



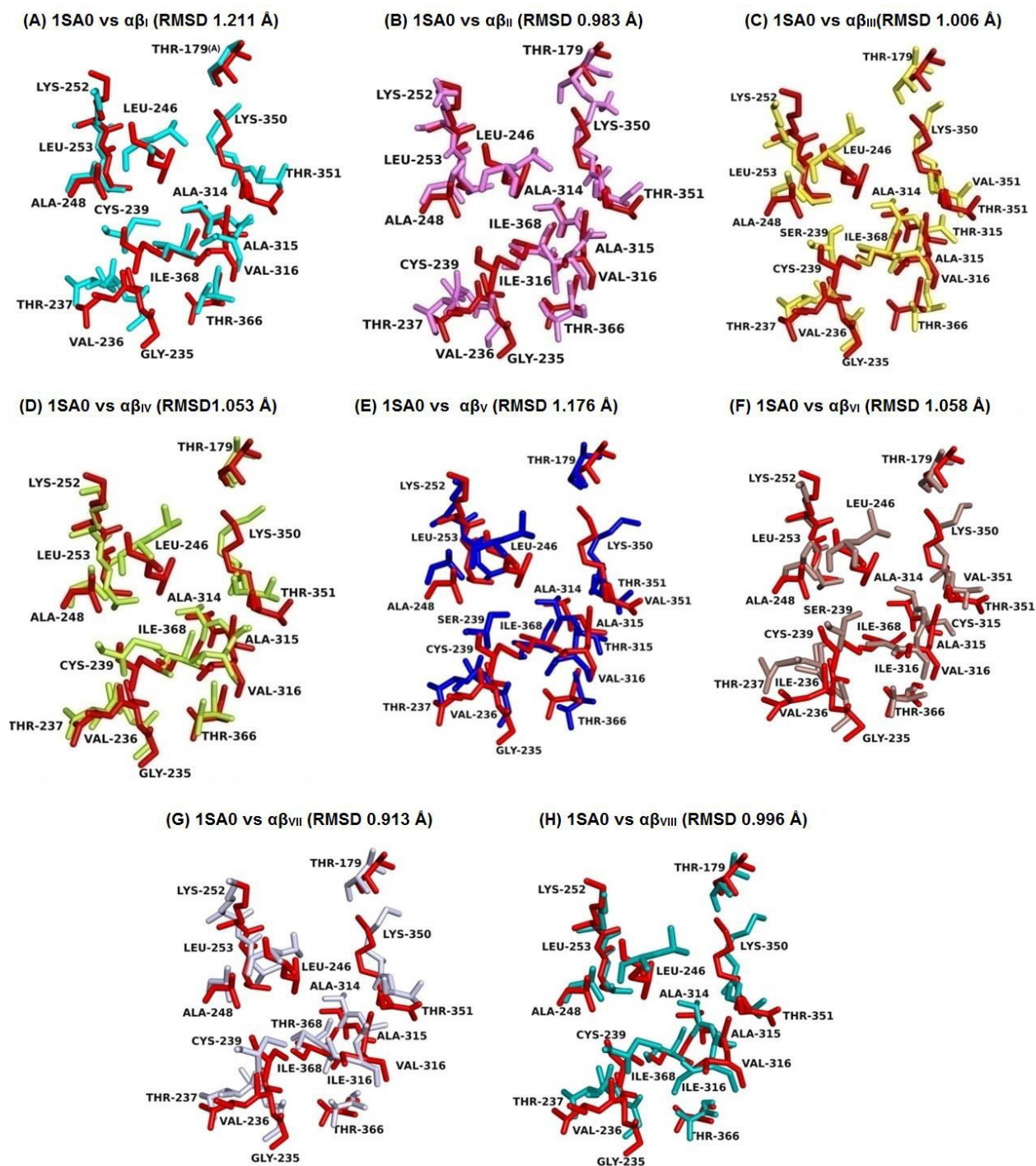


Figure 3.15. Superimposition of the noscapinoid binding site [48] of the template structure (1SA0) in red and all the 8 isotypes of tubulin ( $\alpha\beta_I$ - $\alpha\beta_{VIII}$ ) represented in different colours. The figure clearly shows the differences between the binding sites of the isotypes due to change in residues at different positions. The differences in conformation and composition of binding sites of different  $\alpha\beta$ -tubulin isotypes with the template structure suggested difference in the overall environment of the binding site that may affect the binding affinity of noscapinoids with these isotypes.



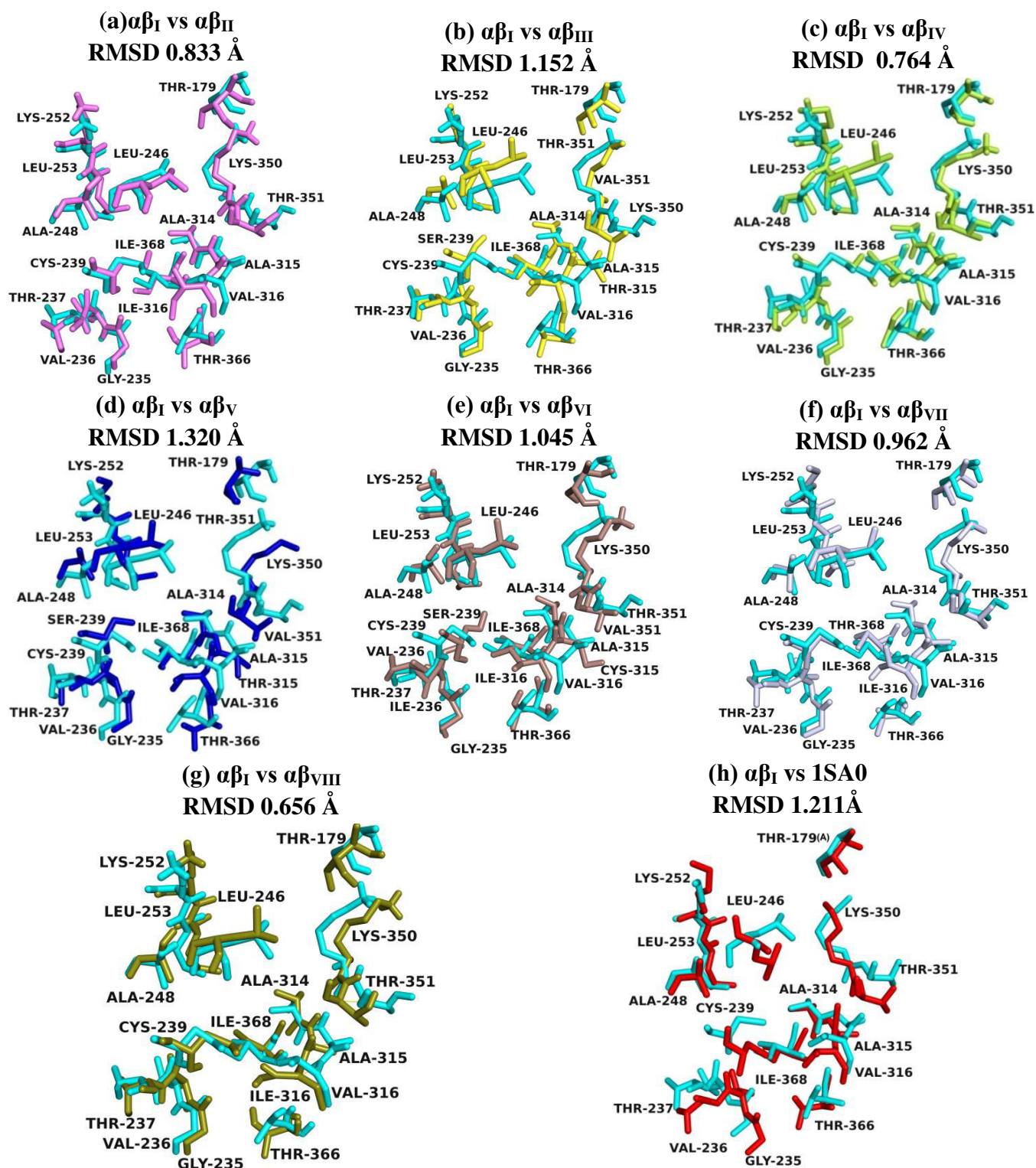


Figure 3.16(a). Superimposition of the noscapinoid binding site of the  $\alpha\beta_I$ -tubulin structure in cyan and all the other isotypes of tubulin represented in different colours and the template structure 1SA0 (red). The figure clearly shows the differences between the binding sites of the isotypes due to change in residues at different positions. Binding site of  $\alpha\beta_I$  differs least with  $\alpha\beta_{VIII}$  and most with  $\alpha\beta_V$  with an RMSD of 0.656 Å and 1.320 Å respectively.

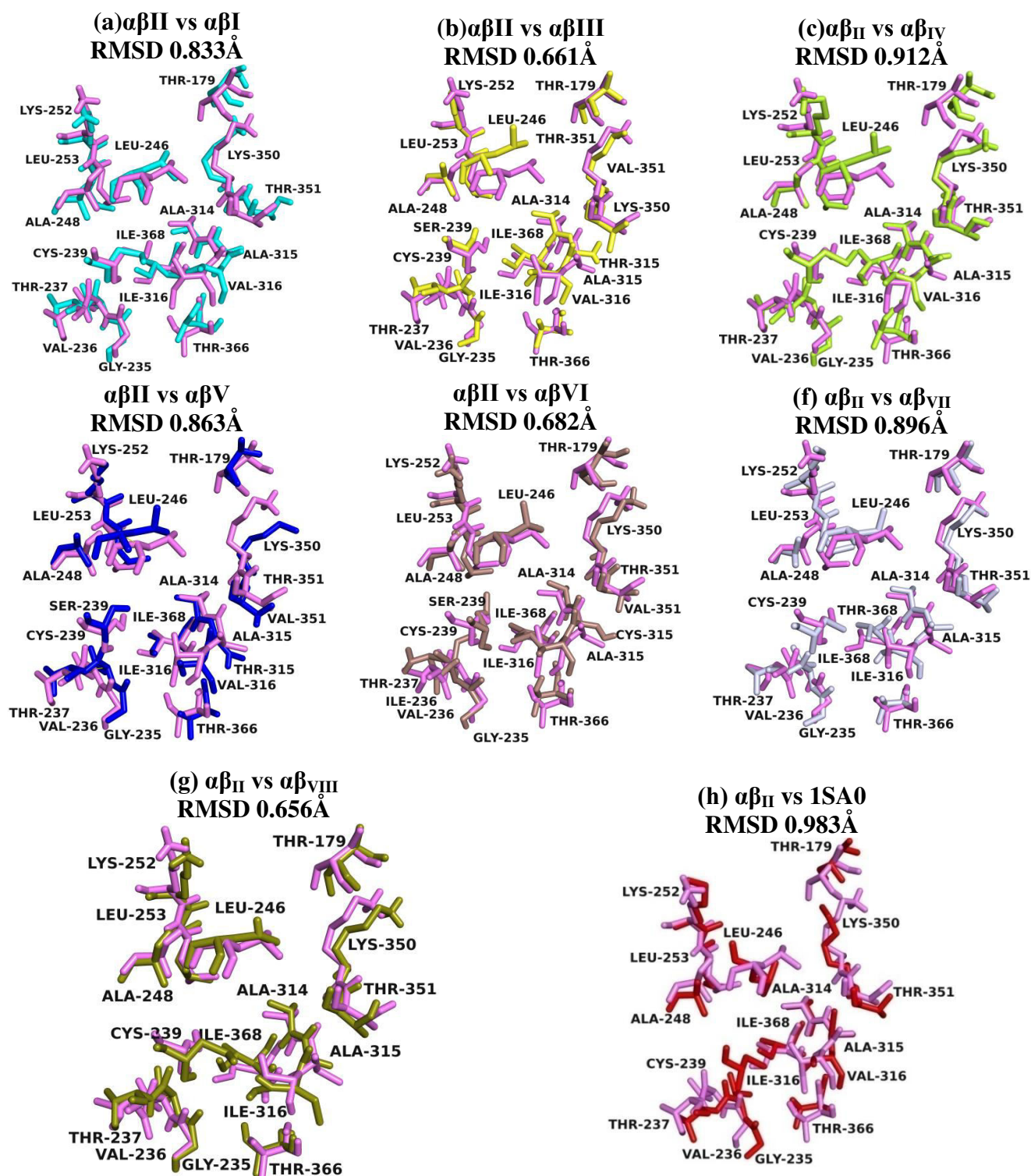


Figure 3.16(b). Superimposition of the noscapinoid binding site of the  $\alpha\beta_{II}$ -tubulin structure in light pink and all the other isotypes of tubulin represented in different colours and the template structure 1SA0(red). The figure clearly shows the differences between the binding sites of the isotypes due to change in residues at different positions. Binding site of  $\alpha\beta_{II}$  differs least with  $\alpha\beta_{VIII}$  and most with  $\alpha\beta_{IV}$  with an RMSD of 0.656 Å and 0.912 Å respectively.



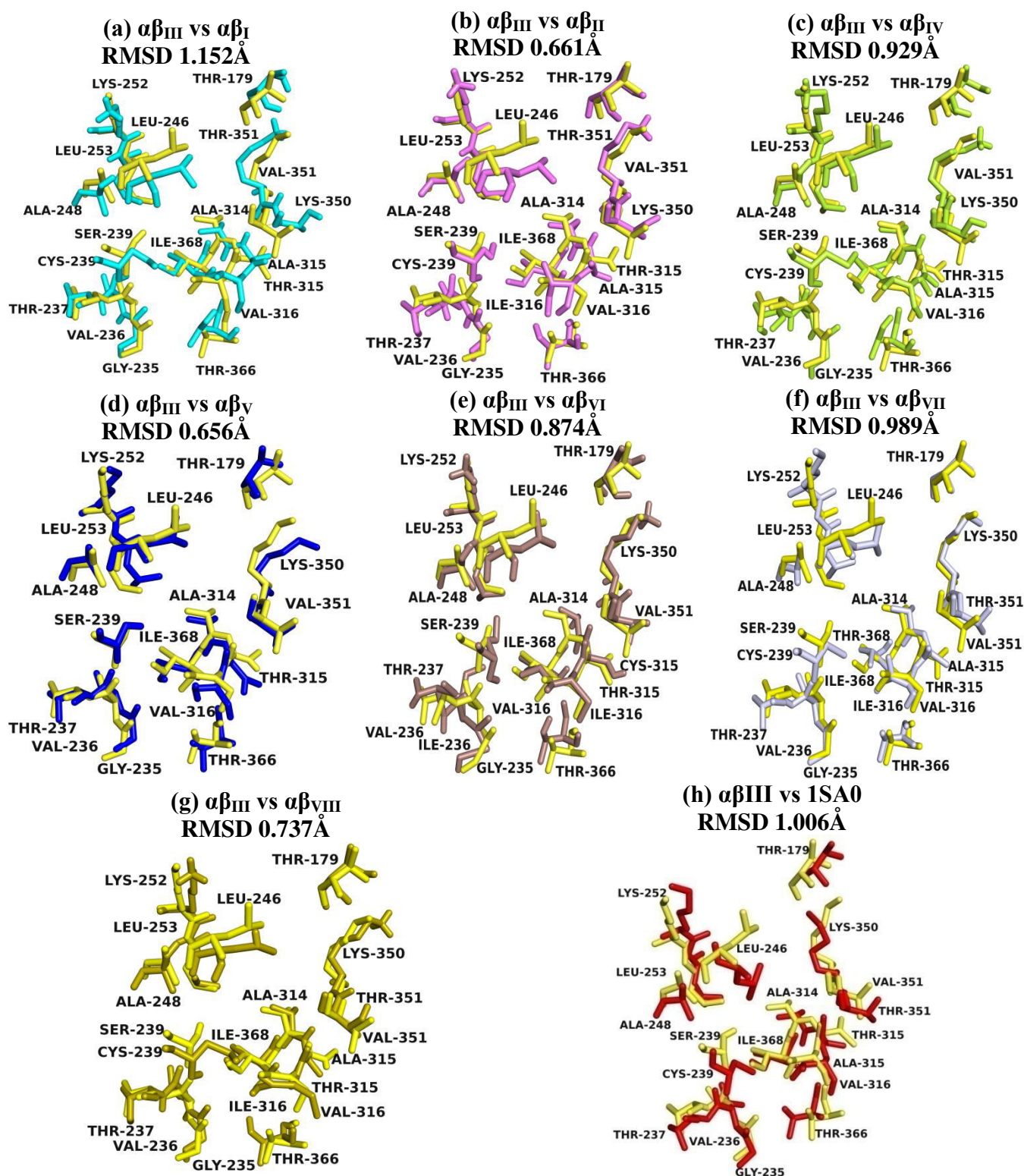


Figure 3.16(c). Superimposition of the noscapinoid binding site of the  $\alpha\beta_{III}$ -tubulin structure in yellow and all the other isotypes of tubulin represented in different colours and the template structure 1SA0(red). The figure clearly shows the differences between the binding sites of the isotypes due to change in residues at different positions. Binding site of  $\alpha\beta_{III}$  differs least with  $\alpha\beta_V$  and most with  $\alpha\beta_I$  with an RMSD of 0.656Å and 1.152Å respectively.

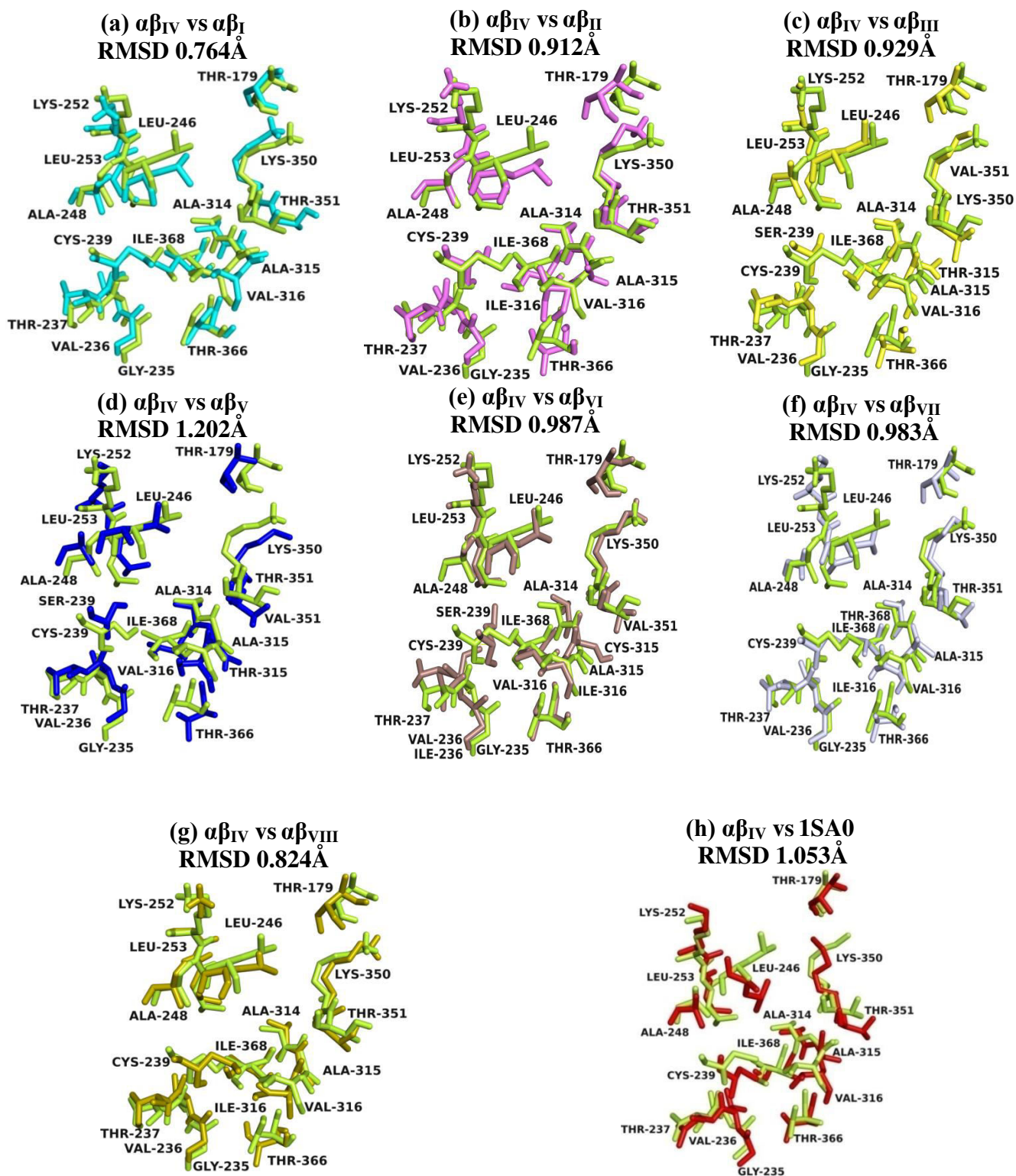


Figure 3.16(d). Superimposition of the noscapinoid binding site of the  $\alpha\beta_{IV}$ -tubulin structure in light green and all the other isoforms of tubulin represented in different colours and the template structure 1SA0 (red). The figure clearly shows the differences between the binding sites of the isoforms due to change in residues at different positions. Binding site of  $\alpha\beta_{IV}$  differs least with  $\alpha\beta_I$  and most with  $\alpha\beta_V$  with an RMSD of 0.764Å and 1.202Å respectively.



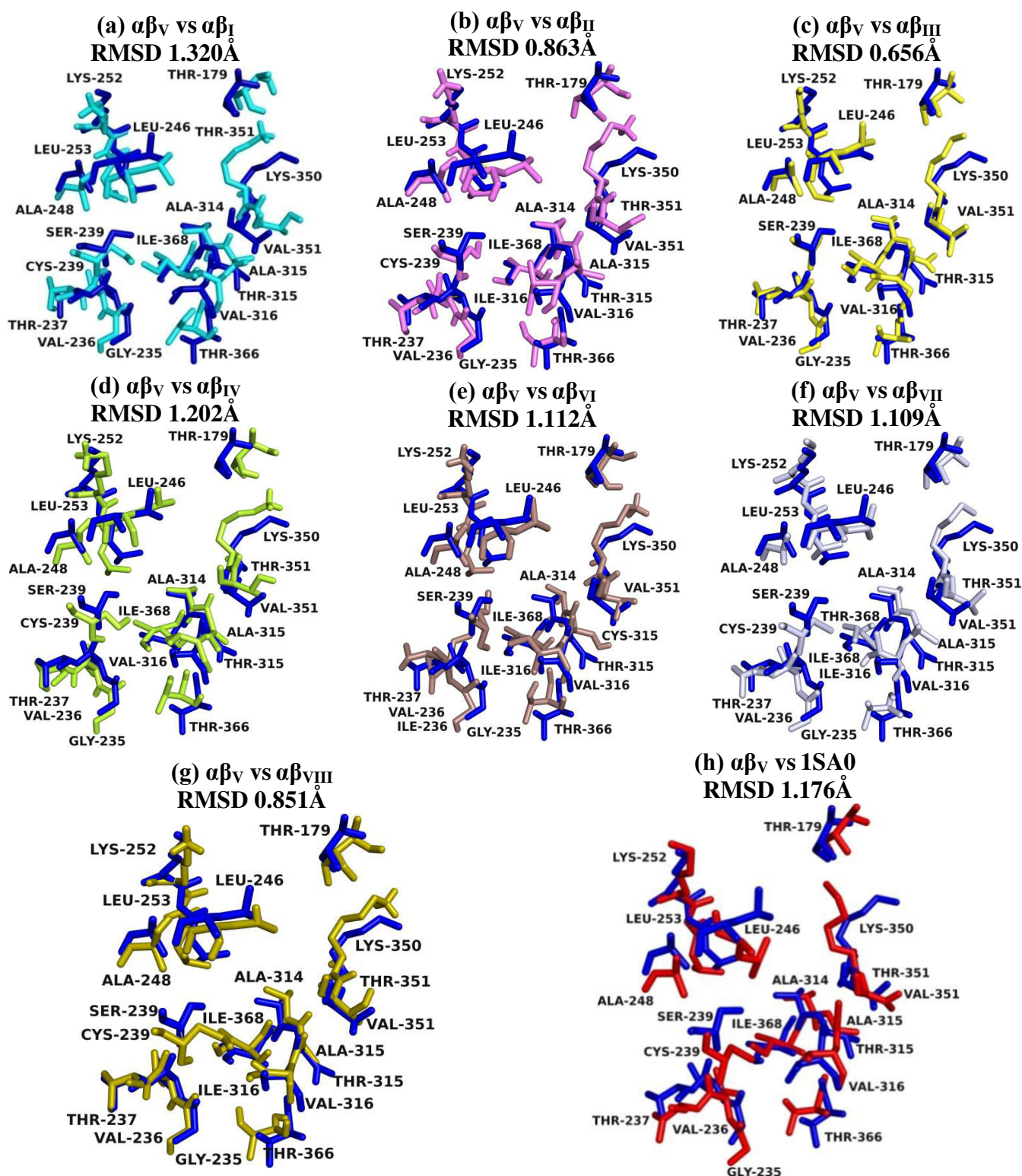
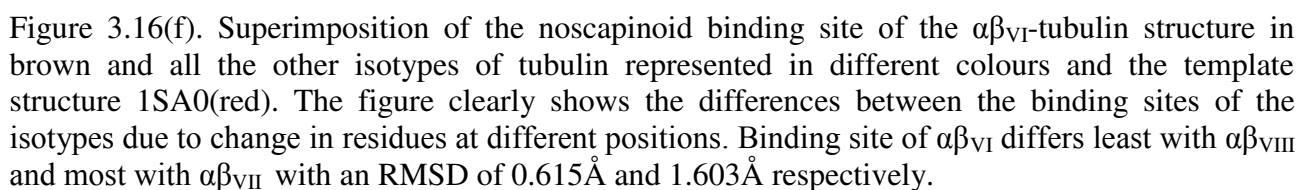


Figure 3.16(e). Superimposition of the noscapinoid binding site of the  $\alpha\beta_V$ -tubulin structure in blue and all the other isoforms of tubulin represented in different colours and the template structure 1SA0(red). The figure clearly shows the differences between the binding sites of the isoforms due to change in residues at different positions. Binding site of  $\alpha\beta_V$  differs least with  $\alpha\beta_{III}$  and most with  $\alpha\beta_I$  with an RMSD of 0.656Å and 1.320Å respectively.





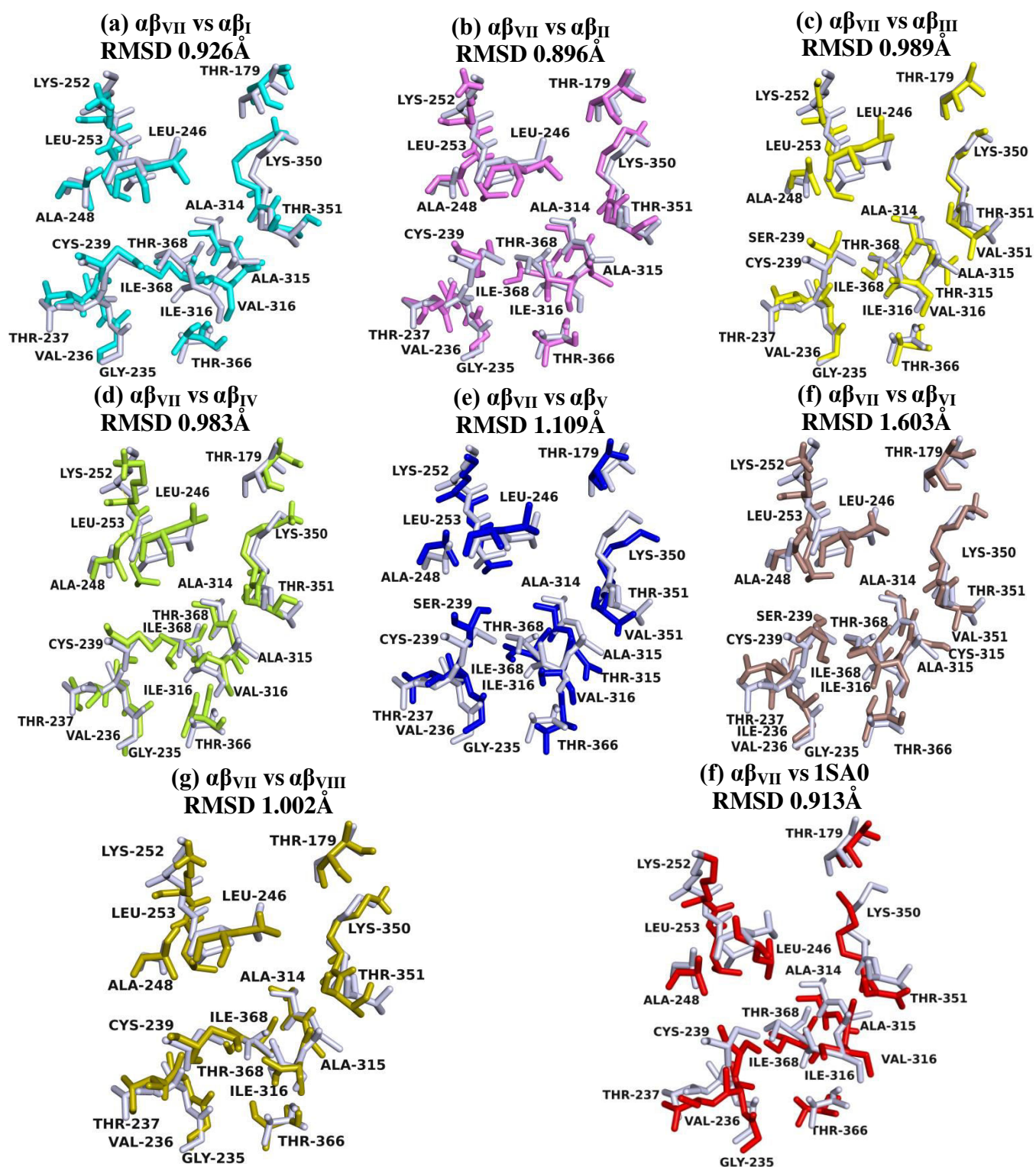


Figure 3.16(g). Superimposition of the noscapinoid binding site of the  $\alpha\beta_{VII}$ -tubulin structure in grey and all the other isotypes of tubulin represented in different colours and the template structure 1SA0(red). The figure clearly shows the differences between the binding sites of the isotypes due to change in residues at different positions. Binding site of  $\alpha\beta_{VII}$  differs least with  $\alpha\beta_{II}$  and most with  $\alpha\beta_{VI}$  with an RMSD of 0.896Å and 1.603Å respectively.

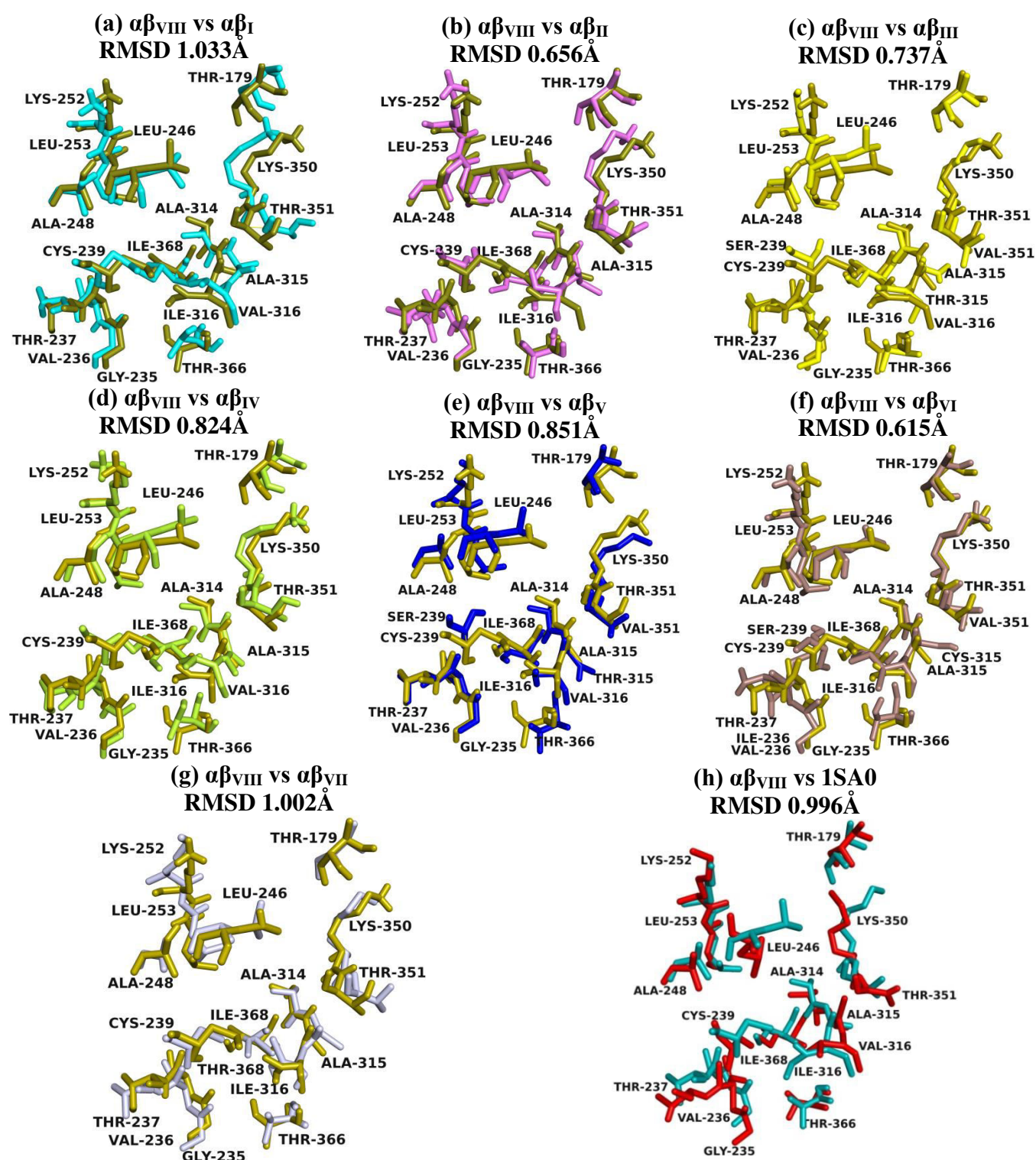


Figure 3.16(h). Superimposition of the noscapinoid binding site of the  $\alpha\beta_{VIII}$ -tubulin structure in olive green and all the other isotypes of tubulin represented in different colours and the template structure 1SA0(red). The figure clearly shows the differences between the binding sites of the isotypes due to change in residues at different positions. Binding site of  $\alpha\beta_{VIII}$  differs least with  $\alpha\beta_{VI}$  and most with  $\alpha\beta_I$  with an RMSD of 0.615Å and 1.033Å respectively.



The differences in conformation and composition of binding site among  $\alpha\beta$ -tubulin isotypes suggested differences in the overall environment of the binding site that may affect the binding affinity of noscapinoids.

### 3.3.4 Binding affinity of noscapinoids to different tubulin isotypes

To determine the binding affinity of noscapinoids at the noscapinoid binding site among different  $\alpha\beta$ -tubulin isotypes, we have docked a set of well characterized noscapinoids, **1-10** using Glide-XP docking. The Glide docking program validates different positions, orientations and conformations of ligands in the receptor binding site in a systematic manner and returns the best docked poses of various ligands in the binding pocket. All the noscapinoids showed significant differences in binding score (Table 3.6) with respect to different  $\alpha\beta$ -tubulin isotypes.

Table 3.6. Docking results (Glide XP) of noscapinoids with different  $\alpha\beta$ -tubulin isotypes. All the noscapinoids binds well with different isotypes. However, each noscapinoid showed different docking score with respect to different  $\alpha\beta$ -tubulin isotypes. Overall the amino-noscapine and the clinical derivative, bromo-noscapine showed better docking score against  $\alpha\beta_{III}$ -tubulin isotype in comparison to other isotypes.

ISOTYPE	Docking score(kcal/mol)									
	1	2	3	4	5	6	7	8	9	10
$\alpha\beta_I$	-5.278	-6.432	-5.601	-5.803	-5.213	-5.448	-5.039	-5.765	-6.328	-6.261
$\alpha\beta_{II}$	-6.671	-7.179	-6.897	-6.530	-6.851	-5.802	-6.327	-7.152	-7.147	-7.090
$\alpha\beta_{III}$	-5.278	-7.416	-7.242	-5.764	-5.496	-6.202	-5.151	-7.149	-7.126	-7.136
$\alpha\beta_{IV}$	-5.963	-7.317	-6.415	-6.617	-5.598	-3.084	-5.984	-6.312	-7.188	-6.364
$\alpha\beta_V$	-6.286	-5.453	-5.477	-6.270	-5.368	-6.280	-4.290	-6.086	-5.723	-6.792
$\alpha\beta_{VI}$	-5.903	-5.831	-5.763	-5.832	-6.560	-5.330	-7.148	-7.182	-7.010	-6.874
$\alpha\beta_{VII}$	-6.041	-6.351	-5.233	-6.506	-7.102	-4.547	-5.853	-7.136	-3.518	-6.371
$\alpha\beta_{VIII}$	-7.111	-6.804	-6.539	-6.068	-5.416	-5.706	-6.779	-7.236	-7.108	-7.205

Moreover, the binding affinity of a specific noscapinoid was also found to be different with respect to different  $\alpha\beta$ -tubulin isotypes. As an example, amino-noscapine (**2**) showed higher binding score of -6.432, -7.179, -7.416 and -7.417 kcal/mol with  $\alpha\beta_I$ ,  $\alpha\beta_{II}$ ,  $\alpha\beta_{III}$  and  $\alpha\beta_{IV}$ , respectively in comparison to the rest of the compounds. Similarly **10** showed the higher binding affinity of all the noscapinoids of -6.792 kcal/mol against  $\alpha\beta_V$ . Moreover, **8** showed highest binding affinities of -7.182, -7.136 and -7.236 kcal/mol, respectively against  $\alpha\beta_{VI}$ ,  $\alpha\beta_{VII}$  and  $\alpha\beta_{VIII}$ . The simplest reason could be the differences in binding mode of noscapinoids among different isotypes mainly because of the differences in binding site amino acids. In a representative example, analysis of the binding mode of amino-noscapine across various  $\alpha\beta$ -tubulin isotypes revealed variation in hydrogen bonding (H-bond) patterns within the binding pocket of different  $\alpha\beta$ -tubulin isotypes (Figure 3.17).

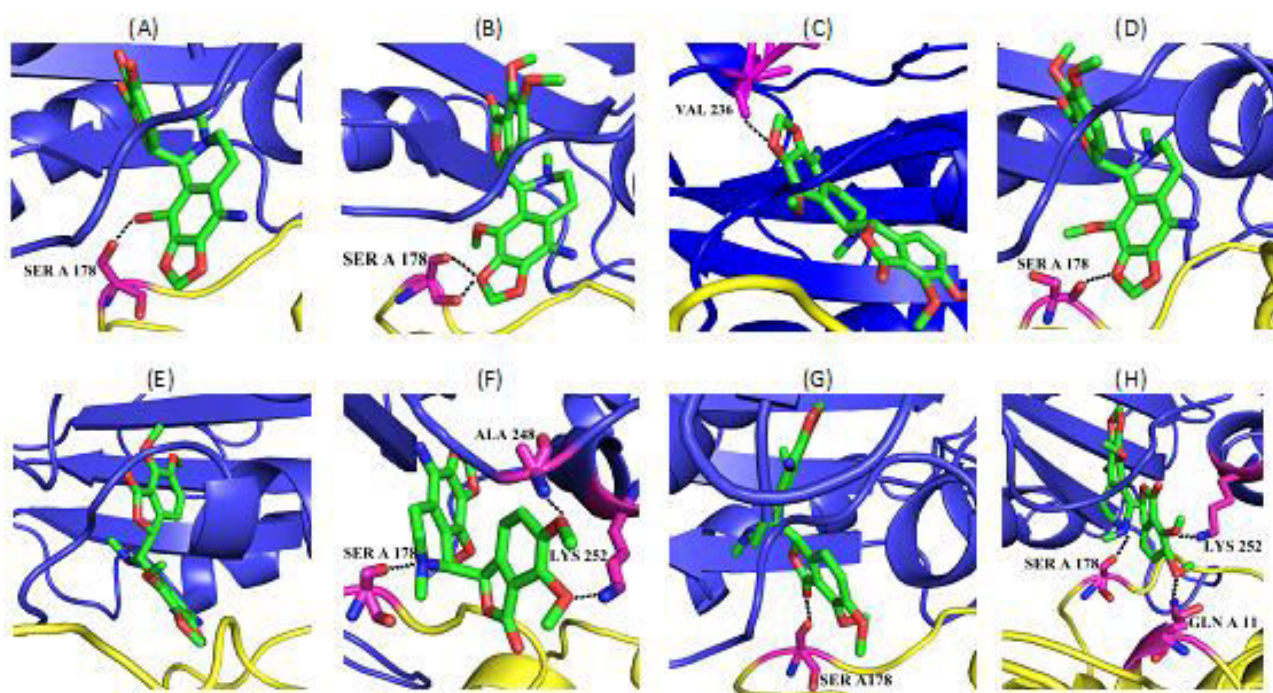


Figure 3.17. The hydrogen bonding pattern of amino-noscapine with respect to (A)  $\alpha\beta_I$ -tubulin isotype, showing one hydrogen bond with Ser178 of  $\alpha$ -chain; (B)  $\alpha\beta_{II}$ -tubulin isotype, showing two hydrogen bonds with Ser178 of  $\alpha$ -chain; (C)  $\alpha\beta_{III}$ -tubulin isotype, showing one hydrogen bond with Val236 of  $\beta$ -chain; (D)  $\alpha\beta_{IV}$ -tubulin isotype, showing a hydrogen bond with Ser178 of  $\alpha$ -chain; (E)  $\alpha\beta_V$ -tubulin isotype, showing no hydrogen bond with any of the chains; (F)  $\alpha\beta_{VI}$ -tubulin isotype, showing a hydrogen bond with Ser178 of  $\alpha$ -chain, Ala248 and Lys252 of  $\beta$ -chain; (G)  $\alpha\beta_{VII}$ -tubulin isotype, showing a hydrogen bond with Ser178 of  $\alpha$ -chain; (H)  $\alpha\beta_{VIII}$ -tubulin isotype, showing a hydrogen bond with Ser178 of  $\alpha$ -chain, Gln11 of  $\alpha$ -chain and Lys252 of  $\beta$ -chain.

Only one H-bond is formed between the amino-noscapine and SerA178 in the binding pocket of  $\alpha\beta_I$ ,  $\alpha\beta_{IV}$  and  $\alpha\beta_{VII}$ . In contrast SerA178 forms two H-bonds with amino-noscapine in the binding pocket of  $\alpha\beta_{II}$ . Similarly amino-noscapine forms only one H-bond with ValB236 in the binding pocket of  $\alpha\beta_{III}$ ; three H-bonds with AlaB248, SerA178 and LysB252 in the binding pocket of  $\alpha\beta_{VI}$  as well as three H-bonds with SerA178, LysB252 and GlnA11 in the binding pocket of  $\alpha\beta_{VIII}$ . To gain more information about the interaction of noscapinoids with all the  $\alpha\beta$ -tubulin isotypes, we have calculated the per residue van der Waals ( $E_{vdw}$ ) and electrostatic ( $E_{ele}$ ) energy contribution of the residues within 12 Å of docked ligands. In a representative example with amino-noscapine (Figure 3.18) the binding site amino acids showed significant contribution of  $E_{vdw}$  and  $E_{ele}$  energy with amino-noscapine across all the  $\alpha\beta$ -tubulin isotypes.

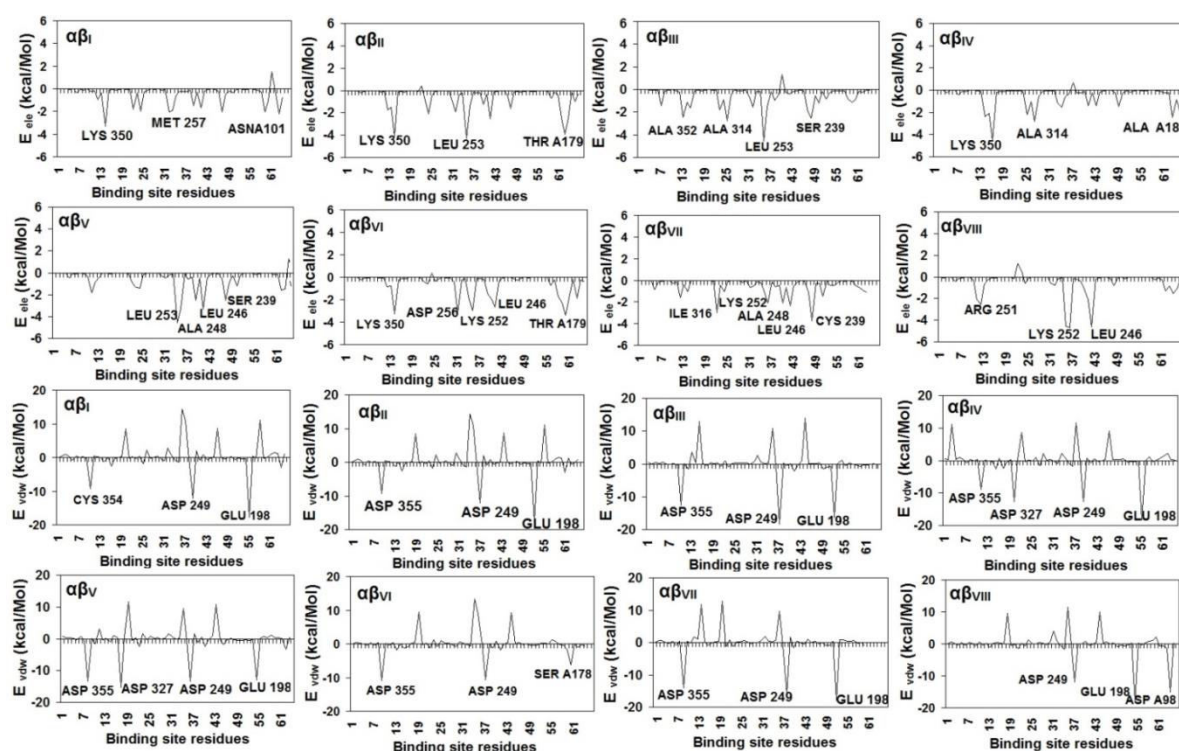


Figure 3.18. Differences in the electrostatic and van der Waals energy contribution of residues within the 12 Å diameter of noscapinoid binding site. In this representative figure only the docked amino-noscapine with respect to  $\beta_{I-VIII}$ -tubulin isotypes are considered. It clearly shows that binding site residues contribute differently to the electrostatic and van der Waals binding energy with amino-noscapine with respect to different  $\beta$ -isotypes. As an example, GluA198 and Asp249 from all of the 8  $\alpha\beta$  isotypes (except  $\alpha\beta_{VI}$ ) have an appreciable  $E_{vdw}$  energy contribution ( $\leq -10$  kcal/mol), whereas, Asp355 of  $\alpha\beta_{II-VII}$  contributed  $\leq -10$  kcal/mol  $E_{vdw}$  energy. Similarly, Cys354 of  $\alpha\beta_I$  contributed  $\approx -10$  kcal/mol only, whereas Asp327 of  $\alpha\beta_{IV}$  and  $\alpha\beta_V$  contributed strong  $E_{vdw}$  energy ( $\leq -15$  kcal/mol). Furthermore, the binding site residues of different  $\alpha\beta$ -tubulin isotypes also contributed different  $E_{ele}$  energy with amino-noscapine. Precisely Leu253 of  $\alpha\beta_{II}$ ,  $\alpha\beta_{III}$  and  $\alpha\beta_V$  significantly contributed  $E_{ele}$  energy ( $\leq -4$  kcal/mol). In contrast, Lys350 of  $\alpha\beta_I$ ,  $\alpha\beta_{II}$ ,  $\alpha\beta_{IV}$  and  $\alpha\beta_{VI}$  contributed only  $\leq -3$  kcal/mol  $E_{ele}$  to the binding of amino-noscapine. In case of  $\alpha\beta_{VII}$  Ile316 and Cys239 contributed most to electrostatic energy with  $E_{ele}$  of  $\leq -3$  kcal/mol, whereas in  $\alpha\beta_{VIII}$  Lys252 and Leu246 showed maximum contribution of  $E_{ele}$  ( $\leq -5$  kcal/mol).

Specifically two amino acids, GluA198 and AspB249 of all the 8  $\alpha\beta$  isotypes (except  $\alpha\beta_{VI}$ ) have an appreciable  $E_{vdw}$  energy contribution ( $\leq -10$  kcal/mol) with the binding of amino-noscapine. Similarly, the binding site residues of different  $\alpha\beta$  isotypes also contributed different  $E_{ele}$  energy with amino-noscapine (Figure 3.18). The differences in the energy contribution among different isotypes can be explained as a result of substitution of amino acids of one kind by the other in and near the binding pocket. The differential binding affinity and mode of interaction of noscapinoids suggests different specificity of noscapinoids across different  $\alpha\beta$ -tubulin isotypes. This might be the reason that cancer cells of different tissue origin showed different sensitivities to noscapinoids as reported previously using NCI 60 cell lines [35,42,43,46]. It should also be noted

that these cell lines over-express some isotypes. As an example, both A549 and CEM cell lines over-expresses  $\beta_{III}$ , while  $\beta_{II}$  is over-expressed in MCF-7 cell line in comparison to all other  $\beta$ -tubulin isotypes [26]. These results suggest that the reason for differential activity of noscapinoids against different cancer cell types may be also because of the differential expression of  $\beta$ -tubulin isotypes.

### 3.3.5 $\alpha\beta_{III}$ isotype as a potential target for anti-tumor drug development

Overexpression of  $\alpha\beta_{III}$  has been associated with resistance to a wide range of chemotherapeutic drugs for several human malignancies. It has also been associated with drug sensitivity and tumor progression [13-18]. Out of the different  $\alpha\beta$ -tubulin isotypes, researchers have already realized that  $\alpha\beta_{III}$  would be an excellent target for anti-tumor drugs [26, 13-18] and have attempted to use rational drug design to create a  $\alpha\beta_{III}$ -specific drug. The seco-taxoid, IDN 5390 [26] was explicitly designed to bind to the taxane binding site on  $\alpha\beta_{III}$ . This drug is very effective against paclitaxel resistant cell lines that overexpress  $\alpha\beta_{III}$ . To test whether the most potent noscapine derivative, amino-noscapine in our library and the clinical derivative, bromo-noscapine have a higher binding affinity with  $\alpha\beta_{III}$ -tubulin than noscapine, the focus has been narrowed down to tubulin targets to this isotype only. Targeting to  $\alpha\beta_{III}$  by noscapinoids may lead to improvement of both efficacy and specificity of treatment. Infact both amino-noscapine and bromo-noscapine showed highest docking score of -7.416 and -7.242 kcal/mol against this isotype in comparison to others. In a representative example amino-noscapine fitted well into the binding pocket of  $\alpha\beta_{III}$  as shown in Figure 3.19. Paclitaxel and vinblastine which are both very successful in chemotherapy favour  $\alpha\beta_{II}$  over  $\alpha\beta_{III}$ . They also suffer from side effects as  $\alpha\beta_{II}$  is very abundant in the nervous system and a few other tissues. In contrast  $\alpha\beta_{III}$  is less abundant in other tissues and has already been proven to be a very promising molecular target for cancer therapy. The ability of noscapinoids to target  $\alpha\beta_{III}$  more specifically could be a reason for its unique properties in comparison to other tubulin binding agents.

Inspired by the docking result we determined the preferred binding mode and binding affinity of these two compounds and the lead compound noscapine with  $\alpha\beta_{III}$  by performing 10 ns of MD simulation. The equilibration of the MD trajectories was monitored based on the convergence of plots of RMSDs of C $\alpha$  carbon atoms of tubulin during 10 ns of MD simulation starting from the docked complex (Figure 3.20).



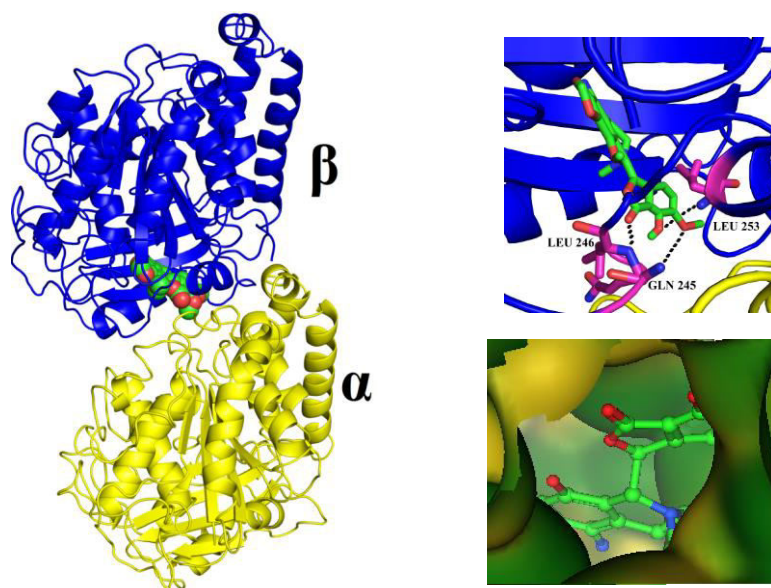


Figure 3.19. Typical snapshot of binding mode of amino-noscapine with tubulin obtained after MD simulation. Panel (A) show the docked poses of amino-noscapine (space field) bound to  $\alpha\beta_{III}$  at noscapine binding site. Panel (B) show the enlarged view the hydrogen bonding pattern of amino-noscapine with respect to  $\alpha\beta_{III}$ -tubulin isotype after MD simulation. Three hydrogen bonds contributing in the interaction of amino-noscapine with the binding site amino acids such as Gln245, Leu246 and Leu253 are shown in the figure. Panel (C) show the fitting of amino-noscapine with the binding site of  $\alpha\beta_{III}$ -tubulin isotype.

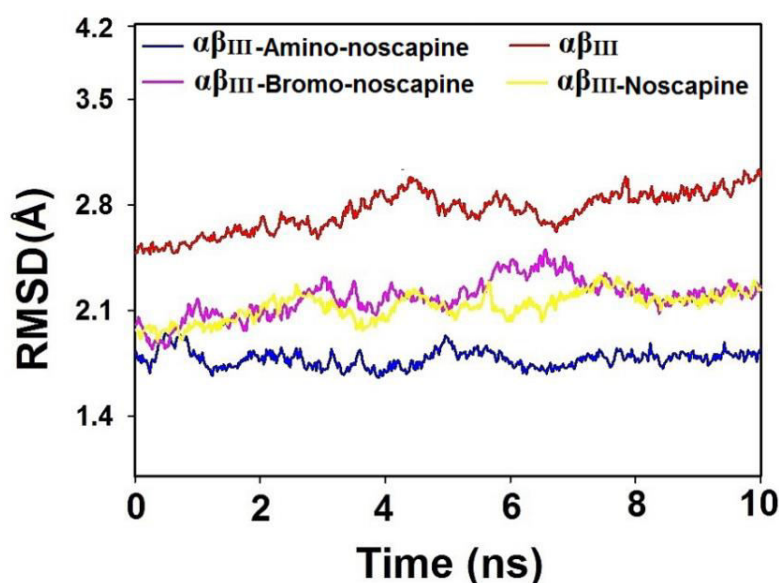


Figure 3.20. The root-mean square deviations (RMSD) of C $\alpha$  carbon atoms of tubulin during 10 ns of MD simulation, starting from the docking complexes of  $\alpha\beta_{III}$  with amino-noscapine, bromo-noscapine and noscapine. The relative fluctuation in the RMSD of the C $\alpha$  atoms is very small after ~8 ns of the simulation, demonstrating the convergence of the simulation. A 10 ns MD simulation was carried out with a time step of 2 fs, a total of 5000 frames were generated and the last 1000 frames from each molecular species were used to generate the average structure.

A total of 5000 frames were generated for each molecular system out of which the last 1000 frames were used to generate the average structure of the tubulin-drug complexes for the MM-GBSA and MM-PBSA calculation. The root mean square fluctuations (RMSF) of the residues within and around the noscapinoid binding site (13-393) of  $\alpha\beta_{III}$  in the free form and in complex with noscapinoids were also calculated to reveal the flexibility of these residues. Different levels of flexibility were noticed in the bound form of  $\alpha\beta_{III}$  with different noscapinoids (Figure 3.21).

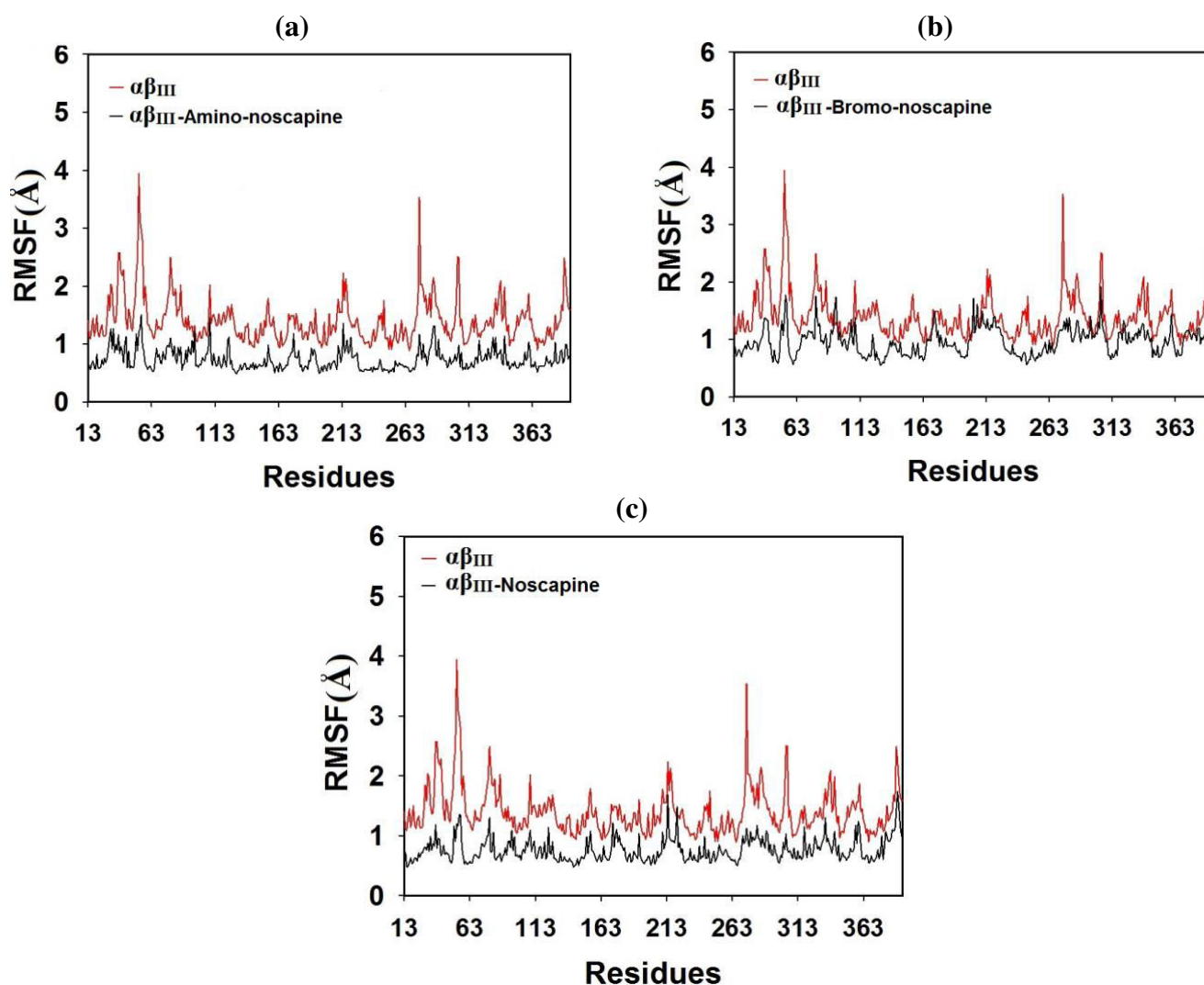


Figure 3.21. Root mean square fluctuation (RMSF) of residues around the ligand binding site of  $\alpha\beta_{III}$  (13-393) in complexed with (a) amino-noscapine, (b) bromo-noscapine and (c) noscapine. Different levels of flexibility of these residues were noticed in the bound form of tubulin with different noscapinoids. Most of the residues in the binding site showed flexibilities less than 2 Å in case of amino-noscapine, bromo-noscapine and noscapine compared to the free  $\alpha\beta_{III}$  isotype, indicating that these residues seem to be more rigid as a result of binding.

Most of the residues in the binding site showed flexibilities less than 2 Å in the case of  $\alpha\beta_{III}$  when bound to noscapine, amino-noscapine and bromo-noscapine compared to free  $\alpha\beta_{III}$ . The

RMSF of the bound form in comparison to the free form indicates that binding site residues become more rigid as a result of binding of the noscapinoids.

### 3.3.6 Binding affinity calculations

The calculated binding free energy ( $\Delta G_{\text{bind}}$ ) and its components based on MM-PBSA and MM-GBSA of noscapine, amino-noscapine and bromo-noscapine with  $\alpha\beta_{\text{III}}$  were summarized in Table 3.7.

Table 3.7. Binding free energy and its components (kcal/mol) for the receptor,  $\alpha\beta_{\text{III}}$  heterodimer and noscapine derivatives.

Energy components (kcal/mol)	Noscapine	Bromo-noscapine	Amino-noscapine
$\Delta E_{\text{ele}}$	-325.4	-337.2	-348.8
$\Delta E_{\text{vdw}}$	-56.22	-60.86	-57.42
$\Delta E_{\text{gas}}$	-381.6	-398.0	-406.2
$\Delta G_{\text{sol-np}}$	-6.530	-6.120	-6.370
$\Delta G_{\text{PB}}$	357.9	370.0	375.6
$\Delta G_{\text{solv,PB}}$	353.6	365.9	371.5
$\Delta G_{\text{ele,PB}}$	32.49	32.89	26.76
$\Delta G_{\text{bind, PB}}$	<b>-28.02</b>	<b>-32.05</b>	<b>-34.70</b>
$\Delta G_{\text{GB}}$	349.3	366.0	366.4
$\Delta G_{\text{solv,GB}}$	342.7	359.9	360.0
$\Delta G_{\text{ele, GB}}$	23.87	28.88	17.52
$\Delta G_{\text{bind, GB}}$	<b>-38.86</b>	<b>-38.09</b>	<b>-46.23</b>

All the three ligands showed better binding affinity with  $\alpha\beta_{\text{III}}$  in the pattern of amino-noscapine (-34.70 and -46.23 kcal/mol), bromo-noscapine (-32.05 and -38.09 kcal/mol) and noscapine (-28.02 and -38.86 kcal/mol) based on both MM-PBSA and MM-GBSA calculations. Non polar solvation terms ( $\Delta G_{\text{sol-np}}$ ) which correspond to the burial of solvent-accessible surface-area upon binding, contributes significantly to the binding of ligands. Similarly the intermolecular van der Waals ( $\Delta E_{\text{vdw}}$ ) also contributed significantly to the binding, whereas the polar solvation term ( $\Delta G_{\text{solv,PB(GB)}}$ ) counteracted binding of these ligands. Although the gas-phase electrostatic value ( $\Delta E_{\text{gas}}$ ) favors the binding of the noscapinoids, the overall electrostatic interaction energy ( $\Delta G_{\text{ele,PB(GB)}}$ ) is positive and thus unfavorable for the binding. This may be due to a large desolvation penalty of charged and polar groups that are not sufficiently compensated for by complex formation.

### 3.3.7 Per residue energy contribution to noscapinoid binding

All the three ligands (noscapine, bromo-noscapine and amino-noscapine) were well accommodated into the binding site of  $\alpha\beta_{III}$ , at the interface between  $\alpha$ - and  $\beta$ - tubulin, however, their binding interactions with the amino acids inside the binding cavity are distinct as shown in Figure 3.22.

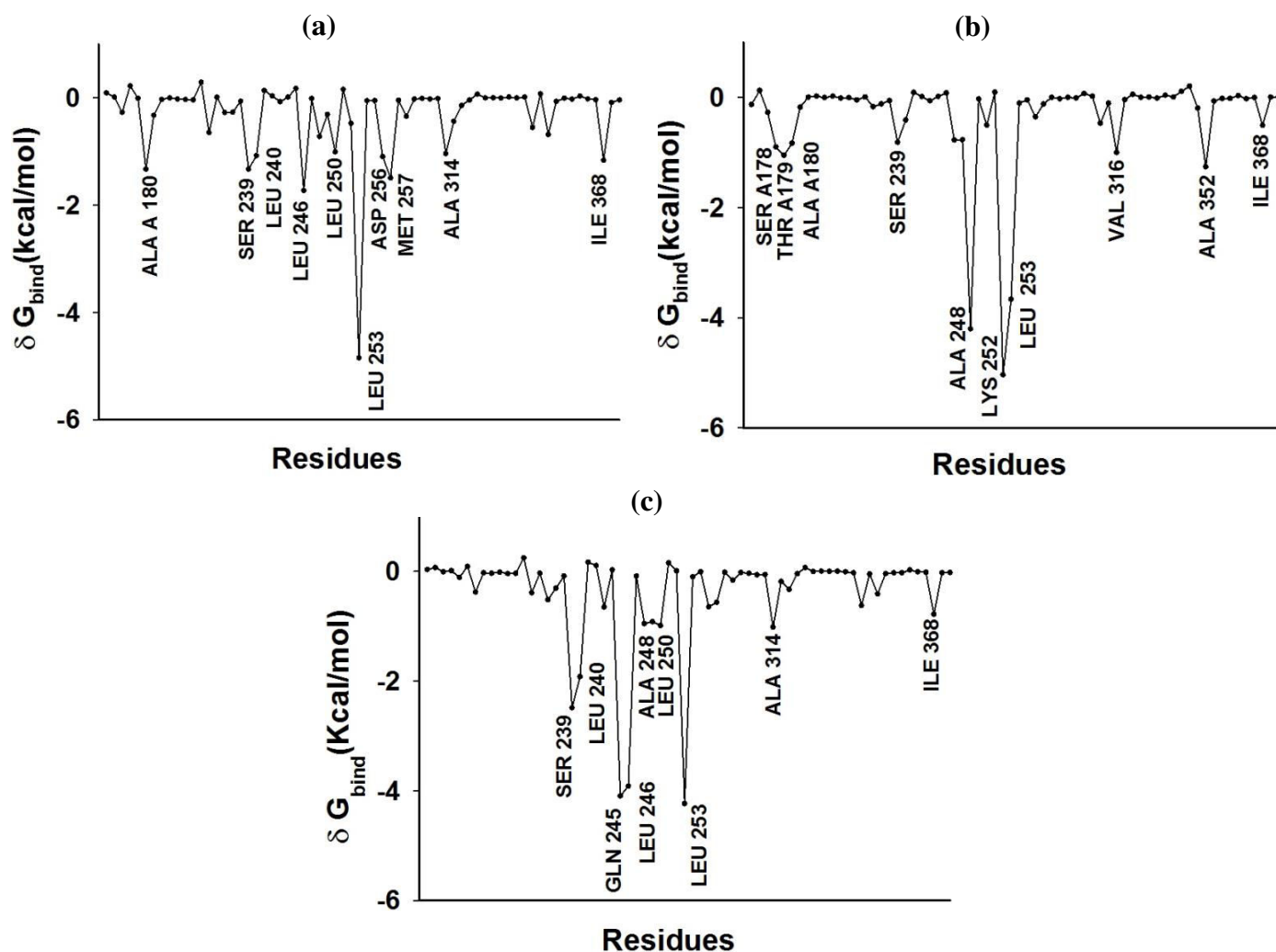


Figure 3.22. Per residue binding free energy ( $\delta G_{bind}$ ) contribution of  $\alpha\beta_{III}$  for the binding of (a) noscapine, (b) bromo noscapine and (c) amino-noscapine. The amino acids within 12 Å of the binding site were only considered.

Per residue contribution of binding free energy is an efficient way to investigate the details of protein–ligand interactions at the atomic level. We have identified the residues that have the greatest impact, in terms of total energy ( $\delta G_{bind}$ ) contribution (per residue contribution  $\leq -1$  kcal/mol), of the  $\alpha\beta_{III}$  with the noscapinoids. For the binding of noscapine, residue Leu253 showed the largest contribution of  $\leq -4$  kcal/mol to the binding energy, while 9 other binding site residues (AlaA180, Ser239, Leu240, Leu246, Leu250, Asp256, Met257, Ala314 and Ile368) contributed



energy  $\leq -1$  kcal/mol. For the binding of bromo-noscapine, residues Ala248 and Lys252 showed the largest contribution of  $\leq -4$  kcal/mol, whereas three other amino acids ThrA178, Val316 and Ala352 contributed  $\leq -1$  kcal/mol energy. Similarly, for the amino-noscapine, Gln245, Leu253 and Leu246 showed largest contribution of  $\approx -4$  kcal/mol, while Ser239 and Leu240 contributed  $\leq -2$  kcal/mol energy.

To determine the detailed contribution of each important residue, the summations of the per residue interaction free energy ( $\delta E_{\text{total}}$ ) was split into van der Waals ( $\delta E_{\text{vdw}}$ ), electrostatic ( $\delta E_{\text{elec}}$ ) and polar solvation ( $\delta E_{\text{sol,GB}}$ ) energies. The energy contributions from the selected residues are shown in Figure 3.23.

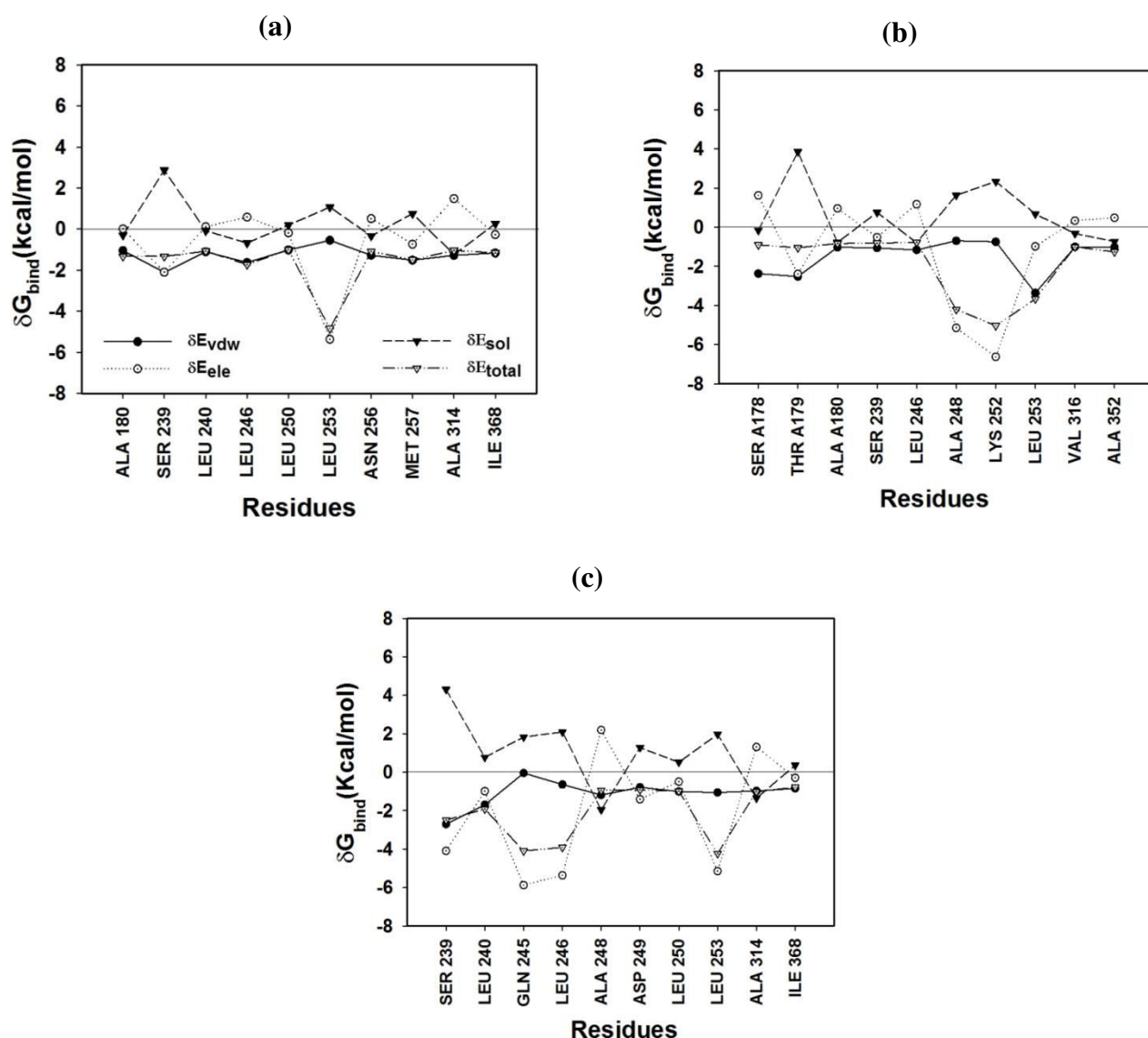


Figure 3.23. Energy decomposition of the key residues (contributing  $\delta G_{\text{bind}} < -1.0$  kcal/mol) in  $\alpha\beta_{\text{III}}$  that are involve in the binding of (a) noscapine, (b) bromo-noscapine and (c) amino-noscapine.

In the  $\alpha\beta_{III}$ -noscaphine complex, Leu253 has significant  $\delta E_{elec}$  contribution energy ( $\leq -5$  kcal/mol), leading to formation of one H-bond (Table 3.8). However, for  $\alpha\beta_{III}$ -bromo noscaphine complex, two amino acids such as Ala248 and Lys252 have appreciable  $\delta E_{elec}$  contribution energy ( $\leq -5$  kcal/mol), leading to formation of two H-bonds (Table 3.8), while Leu253 has the strongest attraction interaction (with  $\delta E_{vdw} \leq -3.35$  kcal/mol) with bromo-noscaphine. Similarly, for  $\alpha\beta_{III}$ -amino noscaphine complex, three amino acids such as Gln245, Leu246 and Leu253 have maximum  $\delta E_{elec}$  energy contribution ( $\leq -5$  kcal/mol), leading to formation of three H-bonds (Table 3.8), while Ser239 contributed better  $\delta E_{vdw}$  energy ( $\leq -2.7$  kcal/mol) with amino-noscaphine. The results also revealed that most of the residues while binding to the noscapinoids showed a minor contribution in  $\delta E_{vdw}$  energy ( $\leq -1.0$  kcal/mol).

Table 3.8. Hydrogen bonding (H-bond) patterns between the residues of  $\alpha\beta_{III}$  with amino-noscaphine, bromo-noscaphine and noscaphine.

Donor	Acceptor	Distance
<b>Amino noscaphine</b>		
GlnB245 N2	Lig O25	2.7 Å
LeuB246 N	Lig O23	3.4 Å
Leu B253 N	Lig O24	2.8 Å
<b>Bromo noscaphine</b>		
AlaB248 N	Lig O23	2.84 Å
LysB252 N2	Lig O24	3.66 Å
<b>Noscaphine</b>		
LeuB253 N	Lig O23	2.78 Å

### 3.4 CONCLUSION

In this study, the binding affinity of a panel of Noscapinoids with each type of tubulin is investigated computationally. It was found out that among tubulin heterodimers, composed of different  $\beta$ -tubulin isotypes, the binding site of noscapinoids varied significantly. Due to various substitutions of amino acids within the binding site region, differences in various physico-chemical and structural parameters among the isotypes were noticed. It was found out that the binding score of a specific noscapinoid with each type of tubulin isotype is different, owing to the differences in the binding site. Specifically, amino Noscaphine has the highest binding score of - with  $\alpha\beta_I$ ,  $\alpha\beta_{II}$ ,  $\alpha\beta_{III}$  and  $\alpha\beta_{IV}$  isotypes, respectively. To get an insight into how the most efficient noscapinoids till now behave with different isotypes, the binding affinities have been compared and it was found out that both amino-noscaphine and bromo-noscaphine showed highest docking score of -7.416 and -7.242 kcal/mol against this isotype in comparison to others. It has already been proved that  $\alpha\beta_{III}$  is less abundant in other tissues and a very promising molecular target for cancer therapy. The ability of

noscapinoids to target  $\alpha\beta_{III}$  more specifically could be a reason of its unique properties in comparison to other tubulin binding agents. More importantly, after narrowing down the focus on the interaction of noscapinoids with  $\alpha\beta_{III}$  tubulin isotype it has been found that both amino noscapine and the clinical derivative, bromo noscapine have the highest binding affinity of -46.23 and -38.09 kcal/mol against  $\alpha\beta_{III}$  (overexpression of  $\alpha\beta_{III}$  has been associated with resistance to a wide range of chemotherapeutic drugs for several human malignancies and has been established as the best molecular target so far) as measured using MM-PBSA. The interaction analysis revealed that amino acids, Ser 239, Leu253, Ile 368, consistently contribute to the binding energy for all the three ligands, indicating their importance in interaction with the ligands targeted towards  $\alpha\beta_{III}$ -tubulin isotype. The information gained in this study could pave a way for more efficient design of novel Noscapinoid, which could be specifically targeted towards cancer cells. Knowledge of the isotype specificity of Noscapinoid may allow for development of novel therapeutic agents based on this drug.

## REFERENCES

1. Stanton, R.A., Gernert, K.M., Nettles, J.H. & Aneja, R. *Drugs That Target Dynamic Microtubules: A new Molecular Perspective*. Med Res Rev, 31(3) pp 443-481. 2011.
2. Weisenberg, R.C., Borisy, G.G. & Taylor, E.W. *The colchicine-binding protein of mammalian brain and its relation to microtubules*. Biochemistry, 7 pp 4466–4479. 1968.
3. Checchi, P.M., Nettles, J.H., Zhou, J., Snyder, J.P. & Joshi, H.C. *Microtubule-interacting drugs for cancer treatment*. Trends Pharmacol Sci, 24(7) pp 361–365. 2003.
4. Panda, D., Jordan, M.A., Chu, K.C. & Wilson, L. *Differential effects of vinblastine on polymerization and dynamics at opposite microtubule ends*. J Biol Chem, 271 pp 29807–29812. 1996.
5. Coderch, C., Morreale, A. & Gago, F. *Tubulin-based Structure-affinity Relationships for Antimitotic Vinca Alkaloids*. Anti-Cancer Agents in Medicinal Chemistry, 12 pp 219-225. 2012.
6. Yvon, A.M., Wadsworth, P. & Jordan, M.A. *Taxol suppresses dynamics of individual microtubules in living human tumor cells*. Mol Biol Cell, 10 pp 947–959. 1999.
7. Downing, K.H. *Structural basis for the interaction of tubulin with proteins and drugs that affect microtubule dynamics*. Annu Rev Cell Dev Biol, 16 pp 89–111. 2000.
8. Elie-Caille, C., Severin, F., Helenius, J., Howard, J., Muller, D.J. & Hyman, A.A. *Straight GDP-tubulin protofilaments form in the presence of taxol*. Curr Biol, 17 pp 1765–1770. 2007.
9. Rao, S. He, L., Chakravarty, S. Ojima, I., Orr, G.A. & Horwitz, S.B. *Characterization of the Taxol binding site on the microtubule Identification of Arg(282) in beta-tubulin as the site of photoincorporation of a 7-benzophenone analogue of Taxol*. J Biol Chem, 274 pp 37990–37994. 1999.
10. Alam, M.A. & Naik, P.K. *Molecular modelling evaluation of the cytotoxic activity of podophyllotoxin analogues*. J Comput Aided Mol Des, 23 pp 209-225. 2009.
11. Luduena, R.F. *Multiple forms of tubulin: different gene products and covalent modifications*. Int Rev Cytol, 178 pp 207-275. 1998.
12. Banerjee, A. & Luduena, R.F. *Kinetics of colchicine binding to purified beta tubulin isotypes from bovine brain*. J Biol Chem, 267 pp 13335-13339. 1992.
13. Wang, Y., Sparano, J.A., Fineberg, S., Stead, L., Sunkara, J., Horwitz, S.B. & McDaid, H.M. *High Expression of Class III  $\beta$ -Tubulin Predicts Good Response to Neoadjuvant Taxane and Doxorubicin/Cyclophosphamide-Based Chemotherapy in Estrogen Receptor–Negative Breast Cancer*. Clin Breast Cancer, 13(2) pp 103–108. 2013.

14. Mozzetti, S., Ferlini, C., Concolino, P. et al. *Class III B-Tubulin Overexpression Is a Prominent Mechanism of Paclitaxel Resistance in Ovarian Cancer Patients*. Clin Cancer Res, 11 pp 298-305. 2005.
15. Joshua. A., McCarroll, Gan P.P., Liu, M. & Kavallaris, M.  *$\beta$ III-Tubulin Is a Multifunctional Protein Involved in Drug Sensitivity and Tumorigenesis in Non–Small Cell Lung Cancer*. Clin Cancer Res, 70(12) pp 4995-5003. 2010.
16. Nicoletti, M.I., Valoti, G., Giannakakou, P. et al. *Expression of  $\beta$ -Tubulin Isoforms in Human Ovarian Carcinoma Xenografts and in a Sub-Panel of Human Cancer Cell Lines from the NCI-Anticancer Drug Screen: Correlation with Sensitivity to Microtubule Active Agents*. Clin Cancer Res, 7 pp 2912 – 2922. 2001.
17. Se`ve, P., Issac, S. Tr`edan, O. et al. *Expression of Class III B-Tubulin Is Predictive of Patient Outcome in Patients with Non Small Cell Lung Cancer Receiving Vinorelbine-Based Chemotherapy*. Clin Cancer Res, 11 pp 5481 – 5486. 2005.
18. Zhang, Y., Yang, H., Liu, J. et al. *High expression levels of class III  $\beta$ -tubulin in resected non-small cell lung cancer patients are predictive of improved patient survival after vinorelbine-based adjuvant chemotherapy*. Oncology letters, 6 pp 220 – 226. 2013.
19. Khan, I. & Luduena, R. *Different effects of vinblastine on the polymerization of isotypically purified tubulins from bovine brain*. In Vest New Drugs, 21 pp 3–13. 2003.
20. Huzil, J.T., Luduena, R.F. & Tuszynski, J. *Comparative modelling of human beta-tubulin isoforms and implications for drug binding*. Nanotechnology, 17 pp S90-S100. 2006.
21. Mane, J.Y., Klobukowski, M.J., Huzil, T. & Tuszynski, J. *Free Energy Calculations on the Binding of Colchicine and Its Derivatives with the  $\alpha/\beta$ -Tubulin Isoforms*. J Chem Inf Model, 48 (9) pp 1824-1832. 2008.
22. Derry, W.B., Wilson, L., Khan, I.A., Luduena, R.F. & Jordan, M. A. *Taxol differentially modulates the dynamics of microtubules assembled from unfractionated and purified beta-tubulin isoforms*. Biochemistry, 36 pp 3554-3562. 1997.
23. Gan, P.P., Pasquier, E. & Kavallaris, M. *Class III beta-tubulin mediates sensitivity to chemotherapeutic drugs in non small cell lung cancer*. Cancer Res, 67 pp 9356-9363. 2000.
24. Choi, J.W., Kim, Y. & Le, J.H. *Expression of  $\beta$ -tubulin isoforms in urothelial carcinoma of the bladder*. World J Urol, DOI 101007/s00345-012-0993-z .2012.
25. English, D.P., Roque, D.M. & Santin, A.D. *Class III b-tubulin over expression in gynecologic tumors: implications for the choice of microtubule targeted agents*. Expert Review of Anticancer Therapy, 13(1) pp 63-74. 2013.

26. Kim, Y.S., Tseng, C.Y., Mane, J.Y., Winter, P., Johnson, L., Huzil, T., Izbicka, E., Luduena, R.F. & Tuszyński, J. *Quantitative analysis of the effect of tubulin isotype expression on sensitivity of cancer cell lines to a set of novel colchicine derivatives*. Molecular Cancer, 9 pp 131. 2010.
27. Das, L., Bhattacharya, B. & Basu, G. *Rationalization of paclitaxel insensitivity of yeast  $\beta$ -tubulin and human  $\beta$ III-tubulin isotype using principal component analysis*. BMC Research Notes, 5 pp 395. 2012.
28. Kanakkanthara, A., Northcote, P.T. & Miller, J.H.  *$\beta$ II-Tubulin and  $\beta$ III-Tubulin Mediate Sensitivity to Peloruside A and Laulimalide but not Paclitaxel or Vinblastine in Human Ovarian Carcinoma Cells*. Mol Cancer Ther, 11(2) pp 393–404. 2011.
29. Christoph, D.C., Kasper, S., Gauler, T.C., Loesch, C., Engelhard, M., Theegarten, D., Poettgen, C., Hepp, R., Peglow, A., Loewendick, H., Welter, S., Stamatis, G., Hirsch, F.R., Schuler, M., Eberhardt, W.E. & Wohlschlaeger, J.  *$\beta$ V-tubulin expression is associated with outcome following taxane-based chemotherapy in non-small cell lung cancer*. British Journal of Cancer, 107 pp 823–830. 2012.
30. Ye, K., Ke, Y., Keshava, N., Shanks, J., Kapp, J.A., Tekmal, R.R., Petros, J. & Joshi, H.C. *Opium alkaloid Noscapine is an antitumor agent that arrests metaphase and induces apoptosis in dividing cells*. Proc Natl Acad Sci USA, 95 pp 1601-1606. 1998.
31. Bulduk, I. & Taktak, F. *Isolation and Characterization of Antitumor Alkaloid from Poppy Capsules (*Papaversomniferum*)*. J Chemistry doi 10.1155/2013/493870 . 2013.
32. Al-Yahya, Hassan, M. A. *Noscapine*. Anal Profiles Drug Subst, 11 pp 407-61.
33. Segal, M.S., Goldstein, M.M. & Attinger, E.O. *The Use of Noscapine (Narcotine) as an Antitussive Agent*. CHEST, 32 pp 305-309. 1957.
34. Joshi, H.C., Salil, A., Bughani, U. & Naik, P.K. *Noscapinoids: a new class of anticancer drugs demand bio-technological intervention*, Medicinal Plant Biotechnology, Ed Arora R CAB e-Books CABI (H ISBN 9781845936785) .2010.
35. Mahmoudian, M. & Rahimi-Moghaddam, P. *The anti-cancer activity of noscapine: A review*. Recent Pat Anticancer Drug Discov, 4(1) pp 92-97. 2009.
36. Aneja, R., Asress, S., Dhiman, N., Awasthi, A., Rida, P.C., Arora, S.K., Zhou, J., Glass, J.D. & Joshi, H.C. *Non-toxic melanoma therapy by a novel tubulin-binding agent*. Int J Cancer, 126 pp 256-265. 2010.



37. Aneja, R., Dhiman, N., Idnani, J., Awasthi, A., Arora, S.K., Chandra, R. & Joshi, H.C. *Preclinical pharmacokinetics and bioavailability of Noscapine a tubulin-binding anticancer agent*. Cancer Chemother Pharmacol, 60 pp 831-839. 2007.
38. Jackson, T., Chougule, M.B., Ichite, N., Patlolla, R.R. & Singh, M. *Antitumor activity of noscapine in human non-small cell lung cancer xenograft model*. Cancer Chemotherapy and Pharmacology, 63 (1) pp 117-126. 2008.
39. Yong, K., Ye, K., Grossniklanus, H.E., Archer, D.R., Joshi, H.C. & Kapp, J.A. *Noscapine inhibits tumor growth with little toxicity to normal tissues or inhibition of immune responses*. Cancer Immunol Immunother, 49 pp 217-225. 2000.
40. Landen, J., Lang, W.R., McMahon, S.J., Rusan, N.M., Yvon, A.M., Adams, A.W., Sorcinelli, M.D., Campbell, R., Bonaccorsi, P., Ansel, J.C., Archer, D.R., Wadsworth, P., Armstrong, C.A. & Joshi, H.C. *Noscapine alters microtubule dynamics in living cells and inhibits the progression of melanoma*. Cancer Res, 62 pp 4109-4114. 2002.
41. Zhou, J., Panda, D., Landen, J.W., Wilson, L. & Joshi, H.C. *Minor alteration of microtubule dynamics causes loss of tension across kinetochore pairs and activates the spindle checkpoint*. J Biol Chem, 277 pp 17200-17208. 2002.
42. Aneja, R., Vangapandu, S.N., Lopus, M., Viswesarappa, V.G., Dhiman, N., Verma, A., Chandra, R., Panda, D. & Joshi, H.C. *Synthesis of microtubule-interfering halogenated Noscapine analogues that perturb mitosis in cancer cells followed by cell death*. Biochem Pharmacol, 72 pp 415-426. 2006.
43. Zhou, J., Gupta, K., Aggarwal, S., Aneja, R., Chandra, R., Panda, D. & Joshi, H.C. *Brominated derivatives of Noscapine are potent microtubule-interfering agents that perturb mitosis and inhibit cell proliferation*. Mol Pharmacol, 63 pp 799-807. 2003.
44. Jhaveri, N., Cho, H., Torres, S., Wang, W., Schöenthal, A.H., Petasis, N.A., Louie, S.G., Hofman, F.M. & Chen, T.C. *Noscapine inhibits tumor growth in TMZ-resistant gliomas*. Cancer Lett, 31 pp 245-52. 2011.
45. Aneja, R., Vangapandu, S.N., Lopus, M., Chandra, R., Panda, D. & Joshi, H.C. *Development of a novel nitro-derivative of Noscapine for the potential treatment of drug-resistant ovarian cancer and Tcell lymphoma*. Mol Pharmacol 69 & 1801-1809. 2006.
46. Naik, P.K., Chatterji, B.P., Vangapandu, S.N., Aneja, R., Chandra, R., Kanteveri, S. & Joshi, H.C. *Rational design synthesis and biological evaluations of amino-Noscapine: A high affinity tubulin-binding noscapinoids*. J Comput Aided Drug Design, 25 pp 443-454. 2011.

47. Santoshi, S., Naik, P.K. & Joshi, H.C. *Rational design of novel anti-microtubule agent (9-azido-Noscapine) from quantitative structure activity relationship (QSAR) evaluation of noscapinoids.* J Biomol Screening, 16 pp 1047-1058. 2011.
48. Naik, P.K., Santoshi, S., Rai, A. & Joshi, H.C. *Molecular modelling and competition binding study of Br- Noscapine and colchicine provide insight into noscapinoid-tubulin binding site.* J Mol Graphics and Model, 29 pp 947-955. 2011.
49. Zhou, J., Gupta, K., Yao, J., Ye, K., Panda, D., Giannakakou, P. & Joshi, H.C. *Paclitaxel-resistant Human ovarian cancer cells undergo v-Jun NH<sub>2</sub>-terminal kinase-mediated Apoptosis in response to Noscapine.* The journal of biological chemistry, 277(42) pp 39777-39785. 2002.
50. Hall, T.A. *BioEdit: a user-friendly biological sequence alignment editor and analysis program for Windows 95/98/NT.* Nucleic Acids Symposium Series, 41 pp 95-98. 1999.
51. Berendsen, H.J.C., Spoel, V.D. & Drunen, V.R. *GROMACS: A message passing parallel molecular dynamics implementation.* Computer Physics Communications. 91 pp 43-56. 1995.
52. Daren, T., York, D. & Pedersen, L. *Particle mesh Ewald: An N-log(N) method for Ewald sums in large systems.* Journal of Chemical Physics 98 pp 10089-10092. 1993.
53. Hess, B., Bekker, H., Berendsen, H.J.C. & Fraaije, J.G.E.M. *LINCS: A linear constraint solver for molecular simulations.* J Comput Chem, 18 pp 1463-1472. 1997.
54. Laskowski, R.A., MacArthur, M.W., Moss, D.S. & Thornton, J.M. *PROCHECK: a program to check the stereochemical quality of protein structures.* J App Crystal, 26 pp 283-291. 1993.
55. Ramachandran, G.N., Ramakrishnan, C. & Sasisekharan, V. *Stereochemistry of polypeptide chain configurations.* J Mol Biol, 7 pp 95-99. 1963.
56. Colovos, C. & Yeates, T.O. *Verification of protein structures: Patterns of non-bonded atomic interactions.* Protein Sci, 2 pp 1511-1519. 1993.
57. Eisenberg, D., Luthy, R. & Bowie, J.U. *VERIFY3D: assessment 694 of protein models with three-dimensional profiles.* Methods Enzymol, 277 pp 396-404. 1997.
58. Manchukonda, N.K., Naik, P.K., Santoshi, S., Lopus, M., Joseph, S., Sridhar, B. & Kantevari, S. *Rational Design Synthesis and Biological Evaluation of Third Generation  $\alpha$ -Noscapine Analogues as Potent Tubulin Binding Anti-Cancer Agents.* PLOS ONE, 8(10) pp 77970. 2013.
59. Lee, C., Yang, W. & Parr, R.G. *Development of the Colle-Salvetti correlation-energy formula into a functional of the electron density.* Phys Rev B, 37 pp 785-789. 1988.
60. Becke, A.D. *A new mixing of Hartree-Fock and local density-functional theories.* J Chem Phys, 98 pp 1372-1377. 1993.

61. Binkley, J.S., Pople, J.A. & Hehre, W.J. *Self-consistent molecular orbital methods 21 Small split-valence basis sets for first-row elements*. J Am Chem Soc, 102 pp 939-947. 1980.
62. Gordon, M.S., Binkley, J.S., Pople, J.A., Pietro, W.J. & Hehre, W.J. *Self-consistent molecular-orbital methods 22 Small split-valence basis sets for second-row elements*. J Am Chem Soc, 104 pp 2797-2803. 1982.
63. Pietro, W.J., Francl, M.M., Hehre, W.J., Defrees, D.J., Pople, J.A. & Binkley, J.S. *Self-consistent molecular orbital methods 24 Supplemented small split-valence basis sets for second-row elements*. J Am Chem Soc, 104 pp 5039-5048. 1982.
64. Friesner, R.A., Banks, J.L., Murphy, R.B., Halgren, T.A., Klicic, J.J., Mainz, D.T., Repasky, M.P., Knoll, E.H., Shelley, M., Perry, J.K., Shaw, D.E., Francis, P. & Shenkin, P.S. *Glide: a new approach for rapid accurate docking and scoring 1 method and assessment of docking accuracy*. J Med Chem, 47 pp 1739–1749. 2004.
65. Halgren, T.A., Murphy, R.B., Friesner, R.A., Beard, H.S., Frye, L.L., Pollard, W.T. & Banks, J.L. *Glide: a new approach for rapid accurate docking and scoring 2 Enrichment factors in database screening*. J Med Chem, 47 pp 1750-1759. 2004.
66. Case, D.A., Walker, R.C. et al. *AMBER 11 University of California San Francisco*. 2010.
67. Cornell, W.D., Cieplak, P., Bayly, C.I., Gould, I.R., Merz, K.M., Jr Ferguson, D.M., Spellmeyer, D.C., Fox, T., Caldwell, J.W. & Kollman, P.A. *A second generation force field for the simulation of proteins nucleic acids and organic molecules*. J Am Chem Soc, 117 pp 5179–5197. 1995.
68. Wang, J.M., Wolf, R.M., Caldwell, J.W., Kollman, P.A. & Case, D.A. *Development and testing of a general amber force field*. J Comput Chem, 25 pp 1157–1174. 2004.
69. Ryckaert, J.P., Ciccotti, G. & Berendsen, H.J.C. *Numerical integration of the Cartesian equations of motion of a system with constraints: molecular dynamics of n-alkanes*. J Comput Phys, 23 pp 327–341. 1977.
70. Hornak, V., Abel, R., Okur, A., Strockbine, B., Roitberg, A. & Simmerling, C. *Comparison of multiple Amber force fields and development of improved protein backbone parameters*. Protein, 65 pp 712-25. 2006.
71. Berendsen, H.J.C., Postma, J. P., van, M., Gunsteren, W.F., DiNola, A. & Haak, J.R. *Molecular dynamics with coupling to an external bath*. J Chem Phys, 81 pp 3684 – 3691. 1984.
72. Srinivasan, J., Cheatham, T.E., Cieplak, P., Kollman, P.A. & Case, D.A. *Continuum Solvent Studies of the Stability of DNA RNA and Phosphoramidate–DNA Helices*. J Am Chem Soc, 120 pp 9401–9409. 1998.

73. Kollman, P.A., Massova, I., Reyes, C., Kuhn, B., Huo, S., Chong, L., Lee, M., Lee, T., Duan, Y., Wang, W., Donini, O., Cieplak, P., Srinivasan, J., Case, D.A. & Cheatham, T.E. *Calculating structures and free energies of complex molecules: combining molecular mechanics and continuum models*. Acc Chem Res, 33 pp 889-97. 2000.
74. Shen, X.L., Kamimura, M.T., Wei, J., Gao, Q.Z. *Computer-aided de novo ligand design and docking/molecular dynamics study of Vitamin D receptor agonists*. J Mol Model, 18 pp 203–212. 2012.
75. Niu, X., Gao, X., Wang, H., Wang, X. & Wang, S. *Insight into the dynamic interaction between different flavonoids and bovine serum albumin using molecular dynamics simulations and free energy calculations*. J Mol Model, 19 pp 1039–1047. 2013.
76. Guo, J., Wang, X., Sun, H., Liu, H. & Yao, X. *The molecular basis of IGF-II/IGF2R recognition: acombined molecular dynamics simulation free-energy calculation and computational alanine scanning study*. J Mol Model, 18 pp 1421-1430. 2012.

# **CHAPTER - 4**

**RATIONAL DESIGN OF BIARYL PHARMACOPHORE  
SUBSTITUTED NOSCAPINE DERIVATIVES AS POTENT  
TUBULIN BINDING ANTICANCER AGENTS.**





**ABSTRACT**

In pursuit of developing novel noscapinoid with improved anti-cancer activity, I have used structure based drug design approach. I have strategically designed a series of noscapine derivatives by substituting biaryl pharmacophore (a major structural constituent of many of the microtubule-targeting natural anticancer compounds) onto the scaffold structure of noscapine. Molecular interaction of these derivatives with  $\alpha\beta$ -tubulin heterodimer was investigated by molecular docking, molecular dynamics simulation, and binding free energy calculation. The predictive binding affinity indicates that the newly designed noscapinoids bind to tubulin with a greater affinity. The predictive binding free energy ( $\Delta G_{\text{bind,pred}}$ ) of these derivatives (ranging from -5.568 to -5.970 kcal/mol) based on linear interaction energy (LIE) method with a surface generalized Born (SGB) continuum solvation model showed improved binding affinity with tubulin compared to the lead compound, natural  $\alpha$ -noscapine (-5.505 kcal/mol). Guided by the computational findings, these new biaryl type  $\alpha$ -noscapine congeners were synthesized from 9-bromonoscapine using optimized Suzuki reaction conditions for further experimental evaluation. The derivatives showed improved inhibition of the proliferation of human breast cancer cells (MCF-7), human cervical cancer cells (HeLa) and human lung adenocarcinoma cells (A549) compared to natural noscapine. The cell cycle analysis in MCF-7 further revealed that these compounds alter the cell cycle profile and cause mitotic arrest at G2/M phase more strongly than noscapine. Tubulin binding assay revealed higher binding affinity to tubulin, as suggested by dissociation constant ( $K_d$ ) of  $126 \pm 5.0 \mu\text{M}$  for **5a**,  $107 \pm 5.0 \mu\text{M}$  for **5c**,  $70 \pm 4.0 \mu\text{M}$  for **5d**, and  $68 \pm 6.0 \mu\text{M}$  for **5e** compared to noscapine ( $K_d$  of  $152 \pm 1.0 \mu\text{M}$ ). In fact, the experimentally determined value of  $\Delta G_{\text{bind,expt}}$  (calculated from the  $K_d$  value) are consistent with the predicted value of  $\Delta G_{\text{bind,pred}}$  calculated based on LIE-SGB. Based on these results, one of the derivatives (**5e**) of this series was used for further toxicological evaluation. Treatment of mice with a daily dose of 300 mg/kg and a single dose of 600 mg/kg indicate that the compound does not induce detectable pathological abnormalities in normal tissues. Also there was no significant difference in hematological parameters between the treated and untreated groups. Hence the newly designed noscapinoid, **5e** is an orally bioavailable, safe and effective anticancer agent with a potential for the treatment of cancer and might be a candidate for clinical evaluation.

## 4.1 INTRODUCTION

The critical role that microtubules play in cell division makes them a suitable target for the development of chemotherapeutic drugs against the rapidly dividing cancer cells. This has been demonstrated by extensive use of several vinca alkaloids (that depolymerize and decrease polymer mass of microtubules) and taxanes (that polymerize and bundle microtubules) [1,2] for the treatment of a variety of human cancers. However, their clinical success has been limited by the emergence of drug resistance as well as discomforting toxicities such as gastrointestinal (diarrhea, nausea, vomiting), myelosuppression (leucopenia), alopecia and peripheral neuropathies due to the blockage of axonal transport [3-5]. Besides, their high lipophilicity demands use of co-solvents like cremophor, which are associated with undesirable side effects. These shortcomings have prompted to search for novel microtubule-targeting compounds that display favorable toxicity profiles, have better therapeutic indices and superior pharmacological profiles.

It is crucial that microtubule dynamics must be aptly regulated for error-free progression through mitosis. As a result the compounds that either accelerated or suppressed microtubule dynamics are correlated with impaired mitotic spindle function and inhibition of cell proliferation [6]. Previously it has been demonstrated that noscapine and its derivatives (noscapinoids) suppresses the dynamic instability of microtubule, thereby block cell cycle progression at mitosis, followed by apoptotic cell death in a wide variety of cancer cell types [7-10]. Furthermore, it has been shown that noscapine and its clinical derivative (EM011, 9-bromo-noscapine) regresses human xenografts of lymphomas, melanoma and breast tumors implanted in nude mice with little or no toxicity to the kidney, heart, liver, bone marrow, spleen, or small intestine and does not inhibit primary humoral immune responses in mice [7,11-13]. In addition, the water solubility and feasibility for oral administration also represent valuable advantages of noscapine over many other anti-microtubule drugs [14-16]. Hence among the various anti-mitotic agents that perturb microtubule dynamics, noscapinoids constitute an emerging class of compounds receiving considerable attention. In an attempt to improve the therapeutic activity of noscapine, we have recently designed several noscapine analogues with better therapeutic indices [17-20].

On the other hand, colchicine also perturbs the assembly dynamics of microtubules by interacting with tubulin and remained as useful lead candidate for generation of anticancer agents. However, due to toxic side effects use of colchicines as anticancer agent is limited. Later reports examined several natural and synthetic compounds such as Steganacin, Eupomatiolne, Bufalvin, Wuwezi B and C,  $\alpha$ -DDB, Bicyclol (Figure 4.1) with colchicine like architecture and were found to possess potential anticancer activity. The observed anticancer activity was attributed to the

pharmacophoric biaryl like structural features. Previously this pharmacophore feature has been used to synthesized biaryl based anticancer agents to act as antitumor agents with inhibition of tubulin assembly [21]. With these observations, we envisaged that embedding the biaryl pharmacophore onto the natural noscapine could lead to new hybrid analogues for evaluation as anticancer agents.

As a proof of concept, in this study we computationally designed six derivatives of noscapine (Figure 4.2) by substituting biaryl pharmacophore onto the scaffold structure of noscapine. Their binding affinity with tubulin was evaluated based on molecular dynamic simulation followed by rescoring using MM-PBSA (molecular mechanics Poisson Boltzmann surface area) and MM-GBSA (molecular mechanics generalized Born surface area). All the designed noscapine analogues showed good predictive binding affinity with tubulin. Inspired from the molecular modeling calculations, we have synthesized these new derivatives from 9-bromonoscapine exploring optimized Suzuki reaction conditions and evaluated their biological activity. These new derivatives exhibited higher binding affinity for tubulin as evidenced by tryptophan quenching assay compared to the lead molecule, noscapine, and significantly inhibited proliferation of cancer cells. They displayed much lower  $IC_{50}$  values in comparison to noscapine in the three human cancer cell lines (MCF-7, a breast epithelial cancer cell line; HeLa, a cervix cell line and A549, a lung cancer cell line). The precise mechanism of action of these compounds involved a selective arrest of cell cycle progression at the G2/M phase in rapidly dividing cancer cells. Further, toxicity evaluation of one of the representative compound from this series with mice revealed no evidence of toxicity. Our results indicate that the biaryl pharmacophore substituted noscapine derivatives are potential candidates for clinical evaluation.

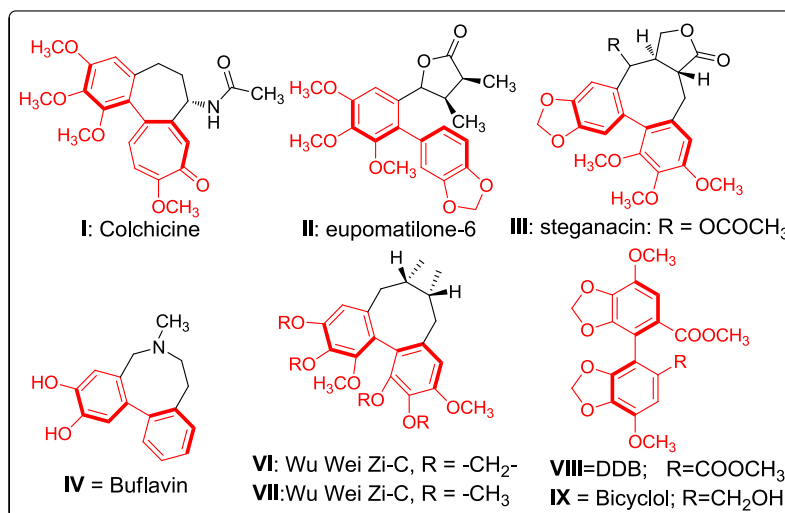


Figure 4.1. Natural and synthetic analogues that are acting as microtubule targeting agents consist of biaryl (red) pharmacophore as major structural constituent. This pharmacophore feature is crucial for their biological activity.

## 4.2 MATERIALS AND METHODS

## 4.2.1 Computational design of noscapine derivatives and structure optimization

Referring to the chemical structure of many of the natural products (Colchicine, Steganacin, Eupomatiolne, Bufalvin, WuweziB and C,  $\alpha$ -DDB, Bicyclol) that are acting as microtubule targeting agents, we rationally designed a series of noscapine derivatives by substituting biaryl pharmacophore onto the scaffold structure of noscapine. These natural products consist of biaryl pharmacophore (Figure 4.1) as major structural constituent which is crucial for their biological activity. Molecular structures of the newly designed noscapine derivatives **5a-f** (Figure 4.2) as well as the previously reported derivatives (used as training set, Figure 4.3) were built using molecular builder of Maestro (version 9.2, Schrödinger). All these structures were energy minimized using MacroModel (version 9.9, Schrödinger) and OPLS 2005 force field with PRCG algorithm (1000 steps of minimization and energy gradient of 0.001). Each structure was assigned an appropriate bond order using Ligprep (version 2.5, Schrödinger, LLC). Complete geometrical optimization of these structures was carried out using hybrid density functional theory (DFT) with Becke's three-parameter exchange potential and the Lee-Yang-Parr (B3LYP) correlation functional [22,23] and using basis set 3-21G\* [24-26]. Jaguar (version 7.7, Schrödinger, LLC) was used for the geometrical optimization of the ligands.

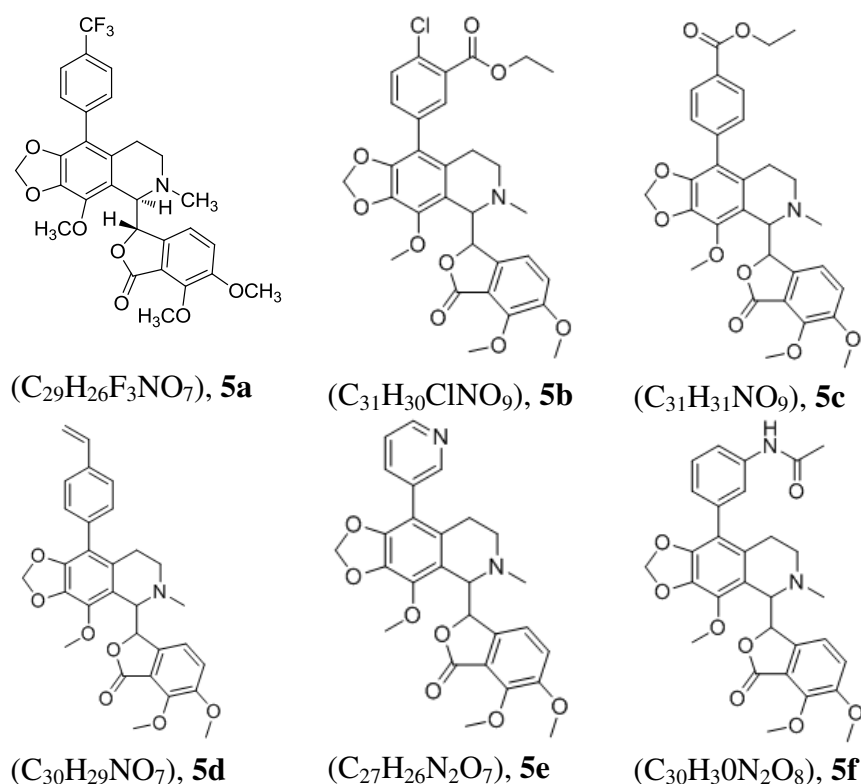


Figure 4.2. Molecular structure of newly designed noscapinoids, **5a-f** in this study. These molecules are rationally designed by substituting biaryl pharmacophore from the natural and synthetic analogues that are acting as microtubule targeting agents onto the scaffold structure of noscapine.

### 4.2.2 Protein preparation

The X-ray crystallographic structure of colchicine-tubulin complex (PDB ID: 1SA0, resolution 3.58Å) was used for molecular docking of noscapine derivatives. The detail of the preparation of tubulin complex from its available low resolution X-ray crystallographic structure is described in chapter 3. Briefly, a complex consisting of  $\alpha$ - and  $\beta$ - tubulin was only retained. Missing hydrogen atoms to the structure were added using Maestro (version 9.2, Schrödinger). The hydrogen bond network of the complex was optimized using multi-step Schrödinger's protein preparation wizard (PPrep). The missing amino acids from 37 to 47 ( $\alpha$ -tubulin) and 275 to 284 ( $\beta$ -tubulin) in the co-crystallized structure were filled using Prime (version 3.0, Schrödinger) based on templates such as PDB ID: 3DU7 (C-chain) and PDB ID: 3RYC (D-chain) respectively. Furthermore, all atoms molecular dynamic (MD) simulation of protein structure in explicit water was carried out using GROMACS[27-29] 4.5.4 and GROMOS96 force field for 10 ns to refine the protein structure. A total of 5000 frames were generated in the MD trajectories, out of which the last 2000 frames were used to generate an average structure of the tubulin. The overall quality of the model, stereochemical values and non-bonded interactions were evaluated using PROCHECK[30], ERRAT[31] and VERIFY3D[32]. The PROCHECK results showed 94.8% of backbone angles are in allowed regions with G-factors of -0.12. Ramachandran plot analysis[33] revealed only 1.6% residues in the disallowed region and 2.3% residues in generously allowed regions. The ERRAT score was 88.402 that is within the range of high quality model. Similarly, the VERIFY 3D score of 95.25% indicates a good quality model.

### 4.2.3 Molecular docking

The receptor-grid file was generated at the centroid of the noscapinoid binding site [34] using Glide (version 5.7, Schrödinger). A bounding box of size 12Å x 12Å x 12Å was defined in tubulin and centered on the mass center of binding site in order to confine the mass center of the docked ligand. The larger enclosing box of size 12Å x 12Å x 12Å which occupied all the atoms of the docked poses was also defined. The scale factor of 0.4 for van der Waals radii was applied to atoms of protein with absolute partial charges less than or equal to 0.25. All the ligands were then docked into the binding site using Glide XP (extra precision) and evaluated using a Glide XP<sub>Score</sub> function [35,36].

### 4.2.4 Molecular dynamics simulations

The best docked complexes of each selected compound, **5a-5f** with tubulin were used as initial conformation for MD simulation. The MD simulation was performed with the AMBER 11.0 software suite [37] using AMBER ff99SB force field [38]. Each molecular system was solvated

with ~32,300 TIP3P water molecules in a truncated octahedral box and neutralized by adding 32 Na<sup>+</sup> ions. The molecular system was energy minimized in three consecutive rounds, each of which consisted of 500 steps of steepest descent followed by 500 steps of conjugate gradient energy minimization method, so as to remove the bad contacts in the structure. With the force constants of 10 and 2 kcal<sup>-1</sup>Å<sup>-2</sup> respectively, positional restraints were applied to the whole system for the first and second round, to allow for relaxation of the solvent molecules. In the third round the whole system was minimized without restraint. Finally, a 10 ns MD simulation was carried out with a time step of 2 fs following 200 ps of equilibration at 300 K. SHAKE algorithm [39] was applied for all the bonds involving hydrogen bonds. The non bonded cut off distance was 10 Å, and the Particle Mesh Ewald (PME) method [28] was applied to treat long-range electrostatics interactions. The temperature of the system was regulated using the langevin thermostat. All equilibration and subsequent MD stages were carried out in an isothermal isobaric (NPT) ensemble using Berendsen barometer [40, 41] with a target pressure of 1 bar and trajectories was recorded every 1 ps.

#### 4.2.5 Binding affinity of 5a-5f using MM-PBSA and MM-GBSA

Binding affinity of newly designed compounds, **5a-5f** with tubulin was evaluated based on both molecular mechanics Poisson Boltzmann surface area (MM-PBSA) and molecular mechanics Generalized Born surface area (MM-GBSA) [42, 43] calculation using AMBER 11.0 [38]. For this calculation a total of 1000 snapshots generated from the last 2 ns of the MD trajectory for each molecular species were considered. The binding affinity ( $\Delta G_{\text{bind}}$ ) of the molecular species for each frame was then calculated as the difference between the energy of complex with the combination energy of receptor and ligand as follows.

$$\Delta G_{\text{bind}} = G_{\text{complex}} - (G_{\text{receptor}} + G_{\text{ligand}})$$

The free energy,  $G$  for each species was calculated as described previously using the MM-PBSA and MM-GBSA methods [42, 43].

$$G = E_{\text{gas}} + G_{\text{sol}} - TS$$

$$E_{\text{gas}} = E_{\text{int}} + E_{\text{ele}} + E_{\text{vdw}}$$

$$G_{\text{ele,PB(GB)}} = E_{\text{ele}} + G_{\text{PB(GB)}}$$

$$G_{\text{sol}} = G_{\text{sol-np}} + G_{\text{PB(GB)}}$$

$$G_{\text{sol-np}} = \gamma \text{SAS}$$

Here,  $E_{\text{gas}}$  is the gas-phase energy;  $E_{\text{int}}$  is the internal energy;  $E_{\text{ele}}$  and  $E_{\text{vdw}}$  are the coulomb and van der Waals energies, respectively [4,45,46].  $E_{\text{gas}}$  was calculated using the ff99SB molecular mechanics force field.  $G_{\text{sol}}$  is the solvation free energy which is decomposed into polar and non-polar contributions.  $G_{\text{PB(GB)}}$  is the polar solvation contribution calculated by solving the PB and GB equations [42, 43].  $G_{\text{ele,PB(GB)}}$  is the polar interaction contribution.  $G_{\text{sol-np}}$  is the non-polar solvation



contribution and was estimated via the solvent-accessible surface area (SAS), which was determined using a water probe radius of 1.4 Å. T and S are the temperature and the total solute entropy, respectively.

#### 4.2.6 Ligand-residue interaction decomposition

The energy contribution of each residue with the noscapinoids, **5a-5f** within the binding cavity of  $\alpha$ - and  $\beta$ - tubulin dimer was analyzed using MM-GBSA decomposition process utilizing MM-GBSA module in Amber 11.0. The binding energy of each ligand-residue pair includes three energy terms: the van der Waals contribution ( $\Delta E_{vdw}$ ), the electrostatic contribution ( $\Delta E_{ele}$ ) and the solvation contribution ( $\Delta E_{sol}$ ). All the energy components are calculated using the same frames obtained from MD trajectories that were used for calculation of binding affinity.

#### 4.2.7 Calculating predictive binding free energies of 5a-f towards tubulin using LIE-SGB method

The free energy of binding ( $\Delta G_{bind}$ ) of the newly designed library of noscapinoids, with tubulin was determined using linear interaction energy method (LIE) with a surface generalized Born (SGB) continuum solvation model proposed by Jorgensen [47] based on the experimental  $\Delta G_{bind}$  data of training set molecules (Figure 4.3). Liaison package (version 5.6, Schrödinger, LLC) was used to estimate the binding free energy based on empirical scoring function:

$$\Delta G_{bind} = \alpha \left( \langle U_{vdw}^b \rangle - \langle U_{vdw}^f \rangle \right) + \beta \left( \langle U_{elec}^b \rangle - \langle U_{elec}^f \rangle \right) + \gamma \left( \langle U_{cav}^b \rangle - \langle U_{cav}^f \rangle \right) \quad (1)$$

Here  $\langle \rangle$  represent the ensemble average,  $b$  represents the bound form of the ligand,  $f$  represents the free form of the ligand, and  $\alpha$ ,  $\beta$ , and  $\gamma$  are the coefficients.  $U_{vdw}$ ,  $U_{elec}$ , and  $U_{cav}$  are the van der Waals, electrostatic, and cavity energy terms in the SGB continuum solvent model. The cavity energy term,  $U_{cav}$ , is proportional to the exposed surface area of the ligand. Various energy parameters included in equation 1 were calculated from the best docked complexes of these ligands by energy minimization based on Hybrid Monte Carlo simulation and Truncated Newton sampling technique using the OPLS-2005 force field. The system was initially heated to 300 K with a relaxation time of 15 ps. A residue-based cut off of 12 Å was set for the non-bonding interactions. With a maximum of 100 steps of minimization the system was heated for 10 ps and finally Hybrid Monte Carlo simulation was performed for 15 ps. The  $\alpha$ ,  $\beta$ , and  $\gamma$  LIE fitting parameters were determined using Minitab statistical package (version 14.0, Minitab Inc.) by fitting the experimental binding affinities of training set molecules.

The experimental free energy of binding for the reported noscapinoids was calculated from their respective dissociation constant ( $K_d$ ) values using the relation:

$$\Delta G_{bind} = RT \ln K_d$$

Where  $R$  is gas constant (0.00199 kcal/mol) and  $T$  is temperature (298 K). The  $K_d$  values of the noscapinoids used in training set were obtained from earlier published work [18, 20, 48, 49] by measuring concentration dependent tubulin-binding curves derived from escalating concentrations of the compounds followed by Schatchard plots. Based on the predictive binding free energy using LIE-SGB, a set of six newly designed derivatives **5a-5f** (Figure 4.2), which have better binding free energy than the lead molecule were finally selected.

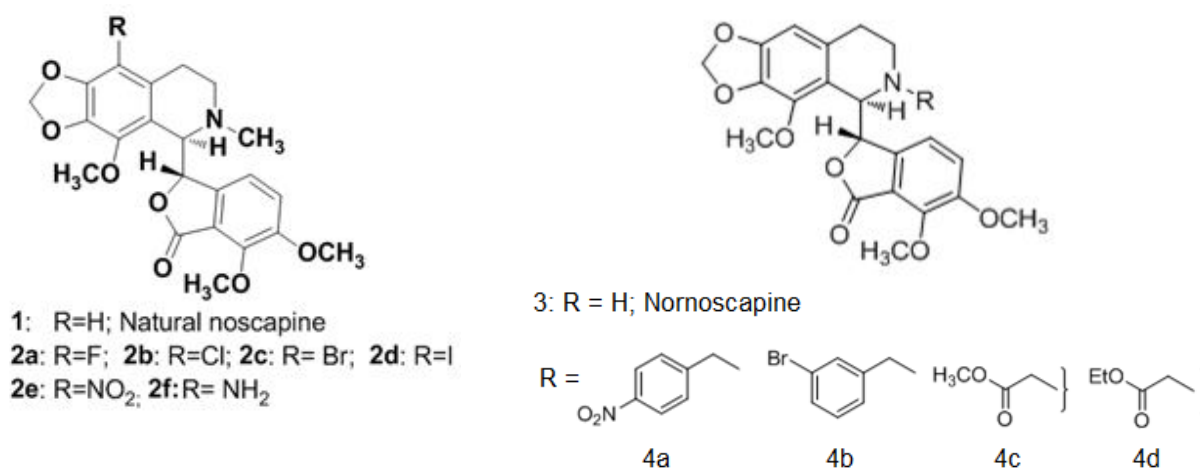


Figure 4.3. Molecular structure of previously reported noscapinoids used in the training set.

#### 4.2.8 Chemical synthesis of noscapinoids 5a-f

Inspired by the computational prediction, these analogues were chemically synthesized for further experimental evaluation.

##### 4.2.8.1 General methods and reagents

Reagents and all solvents were analytically pure and were used without further purification. All reactions were carried out in oven-dried flasks with magnetic stirring. All the experiments were monitored by analytical thin layer chromatography (TLC) performed on silica gel GF254 pre-coated plates. After elution, the plates were visualized under UV illumination at 254 nm for UV active materials. Staining with PMA and charring on a hot plate achieved further visualization. Solvents were removed in vacuo and heated on a water bath at 35 °C. Silica gel finer than 200 meshes was used for column chromatography. Columns were packed as slurry of silica gel in hexane and equilibrated with the appropriate solvent/solvent mixture prior to use. The compounds were loaded neat or as a concentrated solution using the appropriate solvent system. Applying pressure with an air pump assisted the elution. Yields refer to chromatographically and spectroscopically homogeneous materials unless otherwise stated. Appropriate names for all the new compounds were given with the help of ChemBioOffice 2010. Melting points were measured with a Fischer-Johns melting point apparatus and are uncorrected. Infrared spectroscopy (IR) spectra were

recorded as neat liquids or KBr pellets and absorptions are reported in  $\text{cm}^{-1}$ . Optical rotations were measured with a Roudolph Digipol 781 Polarimeter at 25 °C. Nuclear magnetic resonance (NMR) spectra were recorded on 300 (Bruker) and 500 MHz (Varian) spectrometers in appropriate solvents using tetramethylsilane (TMS) as an internal standard or the solvent signals as secondary standards and the chemical shifts are shown in  $\delta$  scales. Multiplicities of NMR signals are designated as s (singlet), d (doublet), t (triplet), q (quartet), br (broad), m (multiplet, for unresolved lines), etc.  $^{13}\text{C}$  NMR spectra were recorded on 75 MHz spectrometer. High-resolution mass spectra (HRMS) were obtained by using ESI-QTOF mass spectrometry. Purity of all the compounds (> 96%) used for biological screening were determined by analytical HPLC (SPD-M20A, make: Shimadzu) using ODS column eluted with gradient mixture of acetonitrile-water. Natural  $\alpha$ -noscapine was purchased from Sigma-Aldrich and is used as such. The synthetic approach for the preparation of newly designed noscapine derivatives, **5a-f** is depicted in Figure 4.4.

#### 4.2.8.2 General procedure for the chemical synthesis of **5a-f** analogues

In a oven dried round bottom flask 9-bromonoscapine 200 mg (0.4072 mmoles), Boronic acid (0.8145 mmoles),  $\text{Pd}(\text{PPh}_3)_4$  (0.04886 mmoles), Sodium bicarbonate (0.8145 mmoles) were taken. 10mL of ethanol, toluene(1:1) mixture was added. Reaction mixture was heated at 120°C for 48 hours. Reaction mixture was cooled to room temperature solvents were removed at reduced pressure extracted with dichloromethane (3x25mL) dried over anhydrous sodium sulphate concentrated to give crude product which is purified by column chromatography (25% EtOAc in Hexanes) to give compounds **5a-g** as colorless solid.

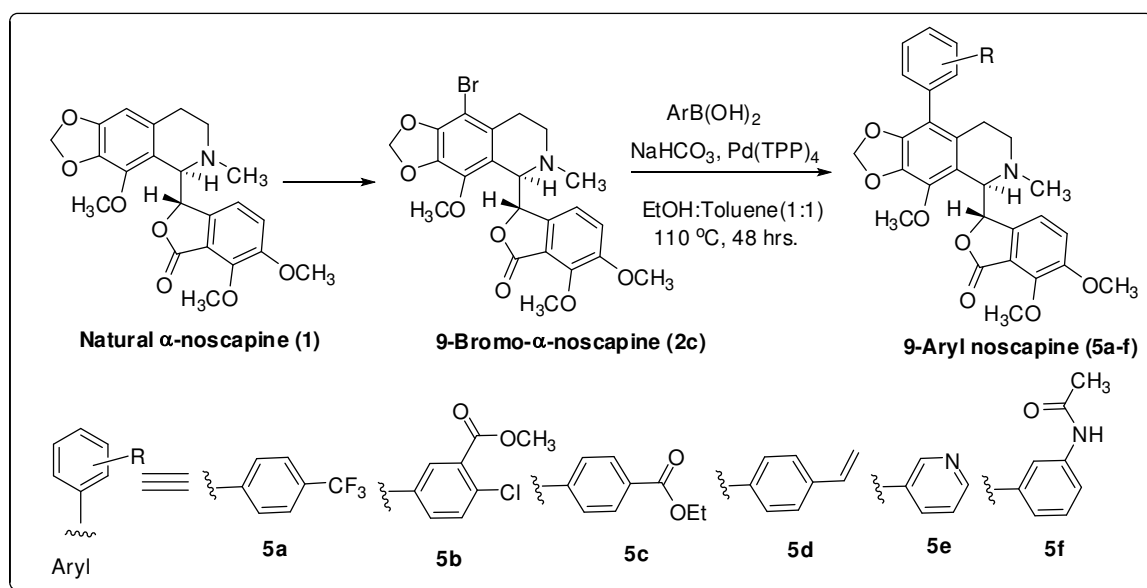


Figure 4.4 Optimized Suzuki coupling reaction conditions for synthesis of noscapine derivatives **5a-f**.

**6,7-dimethoxy-3-(4-methoxy-6-methyl-9-(4-(trifluoromethyl)phenyl)-5,6,7,8-tetrahydro-[1,3]dioxolo[4,5-g]isoquinolin-5-yl)isobenzofuran-1(3H)-one (5a).**

Yield:65%; MP:135°C. <sup>1</sup>H NMR (CDCl<sub>3</sub>, 300MHz) δ 7.60-7.40(m, 4H), 6.97(d, J=8.12, 4H), 6.05(d, J=8.30, 1H), 6.02(d, J=1.32, 1H), 5.93(d, J=1.32Hz, 1H), 5.44(d, J=4.15, 1H), 4.46(d, J=4.34, 1H), 4.14(s, 3H), 4.10(s, 3H), 3.89(s, 3H), 2.65-2.51(m, 4H), 2.20-2.00(m, 2H), 1.70-1.56(m, 1H). <sup>13</sup>C NMR (CDCl<sub>3</sub>, 75MHz) δ 167.9, 152.4, 147.5, 146.0, 140.5, 140.0, 134.9, 133.2, 128.7, 126.7, 126.6, 124.1, 120.5, 118.1, 117.2, 114.7, 100.9, 81.8, 62.2, 61.0, 59.5, 56.5, 50.7, 46.7, 29.6, 27.2. IR(KBr) 3413, 2948, 1765, 1614, 1497, 1422, 1237, 1158, 1120, 1039, 946, 806, 732, 701 cm<sup>-1</sup>. MS(EI) m/z 580 (M+Na)<sup>+</sup>; HRMS(ESI) Calcd for C<sub>29</sub>H<sub>26</sub>NO<sub>7</sub> F<sub>3</sub>Na(M+Na)<sup>+</sup>: 580.1559, found: 580.1568

**Ethyl 2-chloro-5-(5-(4,5-dimethoxy-3-oxo-1,3-dihydroisobenzofuran-1-yl) - 4-methoxy-6-methyl-5,6,7,8-tetrahydro-[1,3]dioxolo[4,5-g]isoquinolin-9-yl)benzoate (5b).**

Yield:70%; MP:152°C. <sup>1</sup>H NMR (CDCl<sub>3</sub>, 300MHz) δ 7.64(d, J=2.07Hz, 1H), 7.454(d, J=8.30, 1H), 7.34-7.27(m, 1H), 7.02(d, J=8.12, 1H), 6.16-6.05(d, J=7.93Hz, 1H), 6.00(s, J= 1H), 5.92(s, 1H), 4.49-4.34(m 3H), 4.10(s, 6H), 3.91(s, 3H), 2.72-2.53(m, 4H), 2.26-2.09(m, 2H), 1.66(s, 1H), 1.42(t, J=7.17Hz, 3H), <sup>13</sup>C NMR (CDCl<sub>3</sub>, 75MHz) 167.9, 165.6, 152.3, 147.6, 146.0, 140.8, 140.1, 133.7, 132.9, 132.5, 130.8, 130.5, 130.3, 120.4, 118.1, 117.7, 117.6, 114.1, 100.9, 81.8, 62.9, 61.6, 61.0, 59.5, 56.8, 50.5, 46.6, 26.9, 14.1. IR(KBr) 3418, 2922, 2853, 2795, 1756, 1633, 1597, 1498, 1363, 1274, 1159, 1036, 940, 813, 728, 506cm<sup>-1</sup>. MS (ESI) m/z 618 (M+Na)<sup>+</sup>; HRMS(ESI) Calcd for C<sub>31</sub>H<sub>30</sub>NO<sub>9</sub>ClNa (M+Na)<sup>+</sup>: 618.1506, found : 618.1476

**Ethyl 4-(5-(4,5-dimethoxy-3-oxo-1,3-dihydro isobenzofuran-1-yl)-4-methoxy-6-methyl-5,6,7,8-tetrahydro-[1,3]dioxolo[4,5-g]isoquinolin-9-yl)benzoate (5C)**

Yield:67%; MP: 143°C. <sup>1</sup>H NMR (CDCl<sub>3</sub>, 300MHz) δ 8.09(d, J=8.49Hz, 2H), 7.33(d, J=8.30Hz, 2H), 7.03(d, J=8.30Hz, 1H), 6.16(d, J=8.12Hz, 1H), 6.00(d, J=1.32, 1H), 5.93(d, J=1.32Hz, 1H), 5.54(d, J=4.15Hz, 1H), 4.49(d, J=4.34 1H), 4.40(q, J=7.17, 2H), 4.12(s 3H), 4.11(s 3H), 3.91(s, 3H), 2.67-2.52(m, 4H), 2.27-2.11(m, 2H), 1.76-1.65(m, 1H), 1.41(t, J=7.17, 3H). <sup>13</sup>C NMR (CDCl<sub>3</sub>, 75MHz) δ 167.9, 166.2, 152.3, 147.7, 146.0, 140.9, 140.0, 138.9, 133.7, 130.6, 130.0, 129.3, 120.5, 118.1, 117.7, 115.4, 100.9, 81.8, 62.2, 61.1, 60.9, 59.5, 56.9, 56.7, 46.7, 27.0, 14.3. IR(KBr) 3413, 2915, 1767, 1697, 1616, 1498, 1464, 1443, 1381, 1306, 1262, 1165, 1088, 1034, 1012, 821, 621cm<sup>-1</sup>. MS(ESI) m/z 584 (M+Na)<sup>+</sup>; HRMS (ESI) Calcd for C<sub>31</sub>H<sub>31</sub>NO<sub>9</sub>Na (M+Na)<sup>+</sup>: 584.1896, found: 584.1881.

**6,7-dimethoxy-3-(4-methoxy-6-methyl-9-(4-vinylphenyl)-5,6,7,8-tetrahydro-[1,3]dioxolo[4,5-g]isoquinolin-5-yl)isobenzofuran-1(3H)-one (5d)**

Yield:60%; MP:120°C. <sup>1</sup>H NMR (CDCl<sub>3</sub>, 300 MHz) δ 7.40(d, J=8.20Hz, (d, J=8.24, 2H), 7.17(d, J=8.04, 2H), 6.97(d, J=8.14, 1H), 6.74-6.66(dd, J=10.86, 17.45 1H), 6.10(s, 1H), 5.98(s, 1H),

5.91(s, 1H), 5.74(d, J=17.55, 1H), 5.48(s, 1H), 5.25(d, J= 4.15Hz, 1H), 4.47(s, 1H), 4.10(s, 1H), 3.90(s, 3H), 2.66-2.54(m, 4H), 2.27-2.13(m, 2H), 1.77-1.64(m, 1H).  $^{13}\text{C}$  NMR (75 MHz,  $\text{CDCl}_3$ )  $\delta$  157.9, 152.2, 147.7, 146.0, 143.6, 140.9, 139.6, 136.7, 133.7, 133.5, 130.7, 130.1, 126.0, 120.4, 117.8, 116.1, 114.2, 100.8, 81.9, 62.3, 61.1, 59.5, 56.9, 50.8, 46.6, 27.0, 23.2, 29.6. MS(ESI)  $m/z$  538( $\text{M}+\text{Na}$ ) $^+$ : HRMS(ESI) Calcd for  $\text{C}_{30}\text{H}_{29}\text{NO}_7\text{Na}(\text{M}+\text{Na})^+$ : 538.1841, found: 538.1848.

**6,7-dimethoxy-3-(4-methoxy-6-methyl-9-(pyridin-3-yl)-5,6,7,8-tetrahydro-[1,3]dioxolo[4,5-g]isoquinolin-5-yl)isobenzofuran-1(3H)-one (5e)**

Yield:62%; MP:193°C.  $^1\text{H}$  NMR ( $\text{CDCl}_3$ , 500MHz)  $\delta$  8.52(s, 1H), 8.43(s, 1H), 7.56(d, J=7.6Hz, 1H), 7.30(t, J=6.6Hz, 1H), 6.12(d, J=7.6Hz, 1H), 5.99(s, 1H), 5.92(s, 1H), 5.43(d, J=4.7Hz, 1H), 4.43(d, J=4.7Hz, 1H), 4.11(s, 3H), 4.08(s, 3H), 3.88(s, 3H), 2.67-2.60(m, 1H), 2.55(s, 3H), 2.22-2.14(m, 2H), 1.79-1.69(m, 1H). IR  $\text{C}^{13}$  NMR 167.9, 152.3, 150.7, 147.6, 146.4, 140.7, 140.2, 137.3, 133.7, 130.7, 123.1, 120.4, 118.2, 117.5, 100.9, 81.8, 62.2, 61.0, 59.4, 56.8, 50.6, 46.6, 26.8. (KBr) 3412, 2938, 1756, 1637, 1497, 1445, 1273, 1082, 1032, 943, 815, 714,  $\text{cm}^{-1}$ . MS(ESI)  $m/z$ : 513 ( $\text{M}+\text{Na}$ ) $^+$ ; HRMS (ESI) Calcd for  $\text{C}_{27}\text{H}_{26}\text{N}_2\text{O}_7\text{Na}(\text{M}+\text{Na})^+$ : 513.1637, found: 513.1615

**N-(3-(5-(4,5-dimethoxy-3-oxo-1,3-dihydroisobenzofuran-1-yl)-4-methoxy-6-methyl-5,6,7,8-tetrahydro-[1,3]dioxolo[4,5-g]isoquinolin-9-yl)phenyl)acetamide (5f)**

Yield:55%; MP:240°C.  $^1\text{H}$  NMR ( $\text{CDCl}_3$ , 300MHz)  $\delta$  7.68(s, 1H), 7.46-7.28(m, 1H), 7.25-7.12(d, J=8.30 1H), 7.07-6.93(d, J=7.17, 1H), 6.23-6.10(d, J=8.30Hz, 1H), 5.98(s, 1H), 5.91(s, 1H), 5.54(d, J=3.96Hz, 1H), 4.50(d J=3.96, 1H), 4.10(s, 6H), 3.94(s, 3H), 2.54(s, 5H), 2.27-2.10(m, 4H), 1.77-1.60(m, 1H)  $^{13}\text{C}$  NMR ( $\text{CDCl}_3$ , 75MHz)  $\delta$  168.4, 152.2, 147.3, 145.9, 140.6, 139.5, 138.2, 134.9, 133.6, 130.8, 128.5, 125.5, 121.3, 120.2, 118.3, 117.9, 117.6, 116.3, 100.8, 82.1, 62.1, 61.0, 59.4, 56.4, 50.8, 46.7, 27.0, 24.4. IR (KBr) 3329, 2920, 2791, 1739, 1682, 1586, 1548, 1503, 1384, 1274, 1086, 1037, 797, 620  $\text{cm}^{-1}$ . MS(ESI)  $m/z$  569 ( $\text{M}+\text{Na}$ ) $^+$ ; HRMS (ESI) Calcd for  $\text{C}_{30}\text{H}_{30}\text{N}_2\text{O}_8\text{Na}(\text{M}+\text{Na})^+$ : 569.1899, found: 569.1920.

#### 4.2.8.3 X-ray Crystallography

X-ray data for the compounds **5b** was collected at room temperature using a Bruker Smart Apex CCD diffractometer with graphite monochromated  $\text{MoK}\alpha$  radiation ( $\lambda=0.71073\text{\AA}$ ) with  $\omega$ -scan method [50]. Preliminary lattice parameters and orientation matrices were obtained from four sets of frames.

Integration and scaling of intensity data was accomplished using SAINT program [50]. The structure was solved by direct methods using SHELXS97 [51] and refinement was carried out by full-matrix least-squares technique using SHELXL97 [51]. Anisotropic displacement parameters were included for all non-hydrogen atoms. All H atoms were located in difference Fourier maps

and subsequently geometrically optimized and allowed for riding atoms, with C-H = 0.93- 0.97 Å, with  $U_{\text{iso}}(\text{H}) = 1.5U_{\text{eq}}(\text{C})$  for methyl H or  $1.2U_{\text{eq}}(\text{C}, \text{N})$ . The methyl groups were allowed to rotate but not to tip. The absolute configuration of the procured material was known in advance and was confirmed by unambiguous refinement of the absolute structure parameter [52] for **5b**.

Crystal data for **5b**:  $\text{C}_{31}\text{H}_{30}\text{ClNO}_9$ ,  $M = 596.01$ , colorless block,  $0.21 \times 0.18 \times 0.12 \text{ mm}^3$ , monoclinic, space group  $P2_1$  (No. 4),  $a = 12.9325(12)$ ,  $b = 8.2237(7)$ ,  $c = 13.3317(12) \text{ Å}$ ,  $\beta = 92.1170(10)^\circ$ ,  $V = 1416.9(2) \text{ Å}^3$ ,  $Z = 2$ ,  $D_c = 1.397 \text{ g/cm}^3$ ,  $F_{000} = 624$ , CCD Area Detector, MoK $\alpha$  radiation,  $\lambda = 0.71073 \text{ Å}$ ,  $T = 294(2)\text{K}$ ,  $2\theta_{\text{max}} = 50.0^\circ$ , 13429 reflections collected, 4953 unique ( $R_{\text{int}} = 0.0232$ ). Final  $\text{Goof} = 1.107$ ,  $RI = 0.0461$ ,  $wR2 = 0.1294$ ,  $R$  indices based on 4644 reflections with  $I > 2\sigma(I)$  (refinement on  $F^2$ ), 384 parameters, 1 restraint,  $\mu = 0.193 \text{ mm}^{-1}$ . Absolute structure parameter =  $0.12(10)$  [52].

Complete experimental details, copies of  $^1\text{H}$ ,  $^{13}\text{C}$  NMR and mass spectra (ESI and HR-MS) of synthesized products **5a-f**; single crystal X-ray diffraction data for compounds **5b**, **5c**, **5e** are included in the Appendix Section.

## 4.2.9 Experimental evaluation

### 4.2.9.1 In vitro cell proliferation assays (MTS assay)

Cell culture reagents were obtained from Sigma and Invitrogen. MCF-7, a human breast epithelial cancer cell line; HeLa, a human cervix cell line and A549, a human lung cancer cell line were obtained from the National Repository of Animal Cell Culture, National Centre for Cell Sciences, Pune (NCCS), India. The cell lines were maintained in Dulbecco's Modification of Eagle's Medium 1X (DMEM) with 4.5 g/L glucose and L-glutamine (Sigma) supplemented with 10% fetal bovine serum (Invitrogen) and 1% penicillin/streptomycin (Invitrogen).

A panel of three human cancer cell lines of different tissue of origin (MCF-7, HeLa and A549) were seeded into 96-well plates at a density of  $5 \times 10^3$  cells per well and were treated with increasing gradient concentrations of noscapinoids, **5a-5f** for 72 hours. Measurement of cell proliferation was performed colorimetrically by 3-(4,5-dimethylthiazol-2-yl)-5-(3-carboxymethoxyphenyl)-2-(4-sulphophenyl)-2H-tetrazolium, inner salt (MTS) assay, using the CellTiter96 AQueous One Solution Reagent (Sigma). Cells were exposed to MTS for 3 hours and absorbance was measured using a microplate reader (Molecular Devices, Sunnyvale, CA) at an optical density (OD) of 490 nm. The percentage of cell survival as a function of drug concentration was then plotted to determine the  $\text{IC}_{50}$  value, which stands for the drug concentration needed to prevent cell proliferation by 50%.



#### 4.2.9.2 DAPI staining

Nuclear morphology of cells treated with the noscapinoids was evaluated by staining the cells with DAPI and imaging with fluorescence microscopy. Briefly, MCF-7 cells ( $2 \times 10^3$  cells) were grown on poly-L-lysine coated coverslips in 6-well plates and were treated with the compounds at 25  $\mu$ M for 72 hours. After incubation, coverslips were fixed in cold methanol and washed with PBS, stained with DAPI, and mounted on slides. Images were captured using a BX60 fluorescence microscope (Olympus, Tokyo, Japan) with an 8-bit camera (Dage-MTI, Michigan City, IN) and IP Lab software (Scanalytics, Fairfax, VA). Apoptotic cells were identified by features characteristic of apoptosis (e.g. nuclear condensation, formation of membrane blebs and apoptotic bodies).

#### 4.2.9.3 Tubulin Binding Assay

Tubulin was isolated and purified from bovine brain by cycles of temperature-dependent polymerization and depolymerization as described previously [53] followed by phosphocellulose chromatography [53,54]. The concentration of the tubulin was determined by the method of Bradford using BSA as the standard [55]. Purified tubulin was quickly frozen as drops in liquid nitrogen and stored at  $-80^\circ\text{C}$  until used.

Fluorescence titration for determining the tubulin binding affinity of noscapinoids, **5a-5f** was performed as described previously [56]. In brief, the compounds (in a gradient concentration of 0-200  $\mu$ M) were incubated with 2  $\mu$ M tubulin in PEM buffer (100 mM PIPES, pH 6.8, 3 mM  $\text{MgSO}_4$ , and 1 mM EGTA) for 45 min at  $37^\circ\text{C}$ . The relative intrinsic fluorescence intensity of tubulin was then monitored in a Varian Cary Eclipse Fluorescence Spectrophotometer (Agilent Technologies, CA, USA) using a quartz cuvette of 0.3 cm path length. The samples were excited at 295 nm and the emission peaks at 335 nm were recorded. The fluorescence emission intensity of noscapinoids at this excitation wavelength was negligible. We used a 0.3-cm path-length cuvette to minimize the inner filter effects caused by the absorbance of the compound. In addition, the inner filter effects were corrected using a formula  $F_{\text{corrected}} = F_{\text{observed}} \cdot \text{anti-log} [(A_{\text{ex}} + A_{\text{em}})/2]$ , where  $A_{\text{ex}}$  is the absorbance at the excitation wavelength and  $A_{\text{em}}$  is the absorbance at the emission wavelength. The dissociation constant ( $K_d$ ) was determined by the formula:  $1/B = K_d/[\text{free ligand}] + 1$ , where B is the fractional occupancy and [free ligand] is the concentration of the ligand. The fractional occupancy (B) was determined by the formula  $B = \Delta F/\Delta F_{\text{max}}$ , where  $\Delta F$  is the change in fluorescence intensity when tubulin and its ligand are in equilibrium and  $\Delta F_{\text{max}}$  is the value of maximum fluorescence change when tubulin is completely bound with its ligand.  $\Delta F_{\text{max}}$  was calculated by plotting  $1/\Delta F$  versus  $1/[\text{free ligand}]$ . Two independent experiments were performed for each compound.

#### 4.2.9.4 Cell cycle analysis

The flow cytometric evaluation of the cell cycle status was performed as described previously [57]. Briefly, cancer cells (MCF-7) were incubated with 25  $\mu$ M concentration of the noscapinoids, **5c-f**. Cells were sampled at 3 time periods 24h, 48h and 72h and analysed using flow cytometry. After the incubation,  $2 \times 10^6$  cells were centrifuged, washed twice with cold phosphate buffered saline (PBS) and fixed in 70% ethanol. Tubes containing the cell pellets were stored at 4 °C for at least 24 h. The pellets were resuspended in 30  $\mu$ l of phosphate/citrate buffer (0.2 M  $\text{Na}_2\text{HPO}_4$ /0.1 M citric acid, pH 7.5) at room temperature for 30 min and centrifuged at  $1000 \times g$  for 10 min and the supernatant was discarded. The pellets were washed twice with 5 ml PBS and stained with propidium iodide (0.5 ml; 0.1% in 0.6% Triton-X in PBS) and 0.5 ml of RNase A (2 mg/ml) for 45 minutes in the dark. Samples were then analyzed on a FACS Calibur flow cytometer (Beckman Coulter Inc., Fullerton, CA).

#### 4.2.9.4 Toxicological evaluation of noscapinoids.

##### 4.2.9.4.1 Animals

The representative molecule (**5e**) which showed better activity was used for toxicity analysis in animal. All experimental protocols involved in this study were approved by Institutional Animal Ethics Committee, DIHAR, DRDO and followed by the guidelines of “Committee for the Purpose of Control and Supervision of Experiments on Animals” of Govt. of India. Three months old male and female Sprague-Dawley rats weighing approximately  $300 \pm 20$  g (Male) &  $250 \pm 10$  g (Female) were used for the experiments. Water and Food pellets (Lipton pvt Ltd, India) were given *ad libitum*. Animals were maintained in the animal house at 12 h light: 12 h dark cycle (Light 7AM-7PM). Temperature and humidity were maintained at 24-28°C and 55-60%, respectively.

##### 4.2.9.4.2 Drug treatment (Preparation of Drug and Pharmacological Administration)

One of the molecules (**5e**) which showed the best activity among the newly designed analogues was further evaluated for toxicological analysis. Adult male and female Sprague–Dawley rats (n=30) were divided into six experimental groups (5 rats/group) for the study (Table 4.1). Group 1 & Group 2 served as control for male and female rats respectively. Two oral doses of compound **5e** such as 25 mg/kg body weight (for sub-acute) and 50 mg/kg body weight (for acute) were administrated to four groups of rats for toxicological evaluation as included in Table 4.1. The above doses were determined as 10 times and 20 times of effective oral dose of the lead compound, noscapine as reported previously. The compound was dissolved in 0.1% DMSO in distilled water and administrated orally using the feeding cannula. The animals were continuously monitored for

food and water intake and body weights on daily and every second day basis respectively. Both the doses were well tolerated and mice did not show any signs of discomfort.

#### 4.2.9.4.3 Histology and hematology

At the end of the experiment, animals in group 1-4 were sacrificed on day 28, whereas animals in group 5 and 6 were sacrificed on day 14. Blood was collected from the normal or treated mice on the day of sacrifice directly from the heart in heparinized tubes and analyzed on a complete blood count instrument (CDC Technologies, Oxford, CT). For histological studies, mice of different groups were anesthetized with sodium pentobarbital and were perfused with 4% paraformaldehyde in PBS (pH 7.4). The vital organs such as brain, duodenum, liver, lungs, kidney, heart and spleen were removed, post fixed in 4% paraformaldehyde in PBS and further processed for histopathological analysis. Tissues were embedded in paraffin, sectioned using a microtome and 5  $\mu$ m sections were stained with hematoxylin and eosin. The stained sections were analyzed for microscopic evaluation at magnification 200x and 400x using bright field microscope (Olympus, CX31, Japan).

Table 4.1. Grouping of the experimental animals as acute, sub-acute and vehicle (control) treatment and the dosage and duration of dosage.

Groups	No. of animals	Sex	Dose/Day	Duration of Dose	Frequency
1) Vehicle treated (control)	5	Male	0.1% DMSO	28 days	Daily
2) Vehicle treated (control)	5	Female	0.1% DMSO	28 days	Daily
3) Sub-acute	5	Male	25 mg/kg	28 days	Daily
4) Sub-acute	5	Female	25 mg/kg	28 days	Daily
5) Acute	5	Male	50 mg/kg	01 day	Once
6) Acute	5	Female	50 mg/kg	01 day	Once

### 4.3 RESULTS AND DISCUSSIONS

The effectiveness of the lead compound, noscapine was improved to many folds by synthesizing many potent derivatives. These derivatives were proven to have increased tubulin binding affinity by decreasing the dissociation constant ( $K_d$ ) between tubulin-drug complex from 144  $\mu$ M of noscapine to 86  $\mu$ M by nitro noscapine, 80  $\mu$ M by F-noscapine, 54  $\mu$ M by Br-noscapine, 40  $\mu$ M by Cl-noscapine, 22  $\mu$ M by I-noscapine and 14  $\mu$ M by amino-noscapine [48,49,18]. Availability of structure activity data of some noscapinoids allowed us to develop a reasonable predictive model for predicting the binding affinity of newly designed derivatives and screening. In continuation of our efforts to develop new derivatives of noscapine for improving the anti-cancer activity profile, in this manuscript we have developed a series of 9-aryl noscapinoids **5a-f**.

It is known from the literature that natural  $\alpha$ -noscapine share binding characteristics similar to colchicine (I), having biaryl configuration [53]. However, due to toxic side effects, use of colchicine as anticancer agent is limited [54]. Later reports identified other natural products II-IX (Figure 4.1) with biaryl ring (red color) architecture as effective antimitotic agents affecting the tubulin-microtubule equilibrium. Jain et al [55] explored this phenomenon and developed nitrovinyl biaryl analogs as anti-mitotic agents and has shown to inhibit tubulin polymerization. Inspired by this we rationalize to design novel biaryl type  $\alpha$ -noscapine congeners by hybridizing biaryl ring architecture in to the natural  $\alpha$ -noscapine skeleton to evaluate them as anticancer agents. The design strategy adopted is depicted in Figure 4.5.

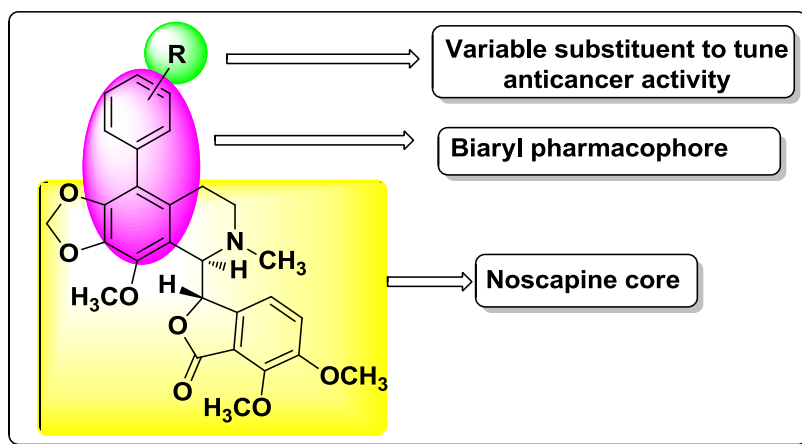


Figure 4.5 Design strategy for new biaryl type  $\alpha$ -noscapine congeners

#### 4.3.1 Binding mode and binding affinity of designed noscapinoids

The molecular interaction and binding affinities of designed noscapinoids, **5a-5f** onto tubulin were calculated applying molecular docking in combination with LIE-SGB as well as MM-PBSA and MM-GBSA calculations. The initial structure of tubulin was obtained from the PDB database; gap filled based on homology model building and refined using MD simulation. The relative fluctuation in the root-mean-square deviations (RMSDs) of the  $C\alpha$  atoms of tubulin ( $\alpha\beta$  heterodimer) is very small after the initial equilibration ( $\sim 4$  ns), demonstrating the convergence of the simulation (Figure 4.6)

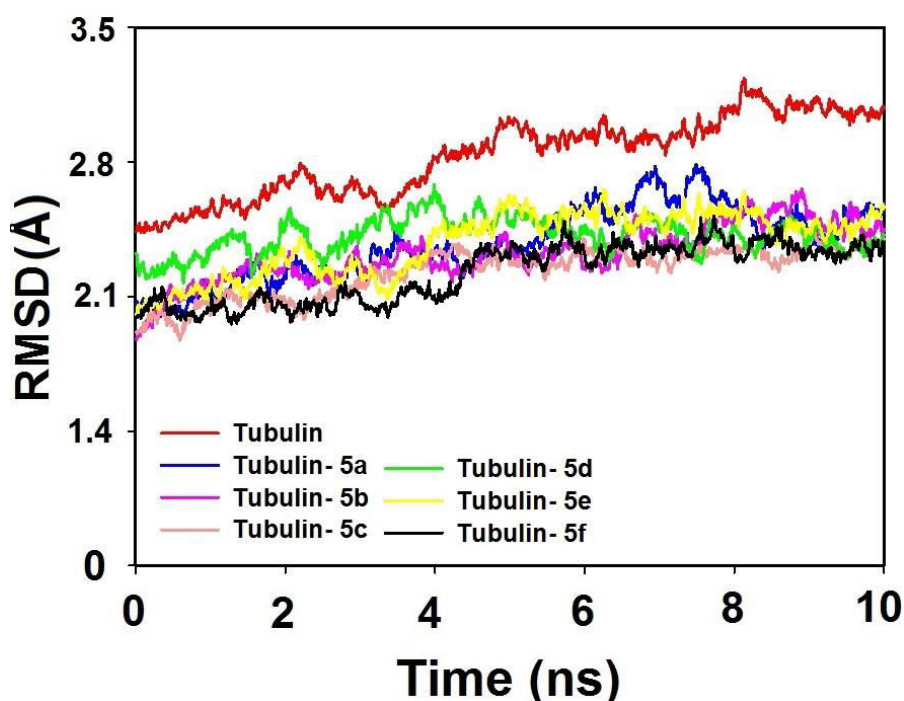


Figure 4.6 The root-mean square deviations (RMSD) of C $\alpha$  carbon atoms of tubulin during 10 ns of MD simulation of tubulin–ligand complexes with respect to initial structure as a function of time. The relative fluctuation in the RMSD of the C $\alpha$  atoms is very small after  $\sim$ 8 ns of the simulation, demonstrating the convergence of the simulation. A 10 ns MD simulation was carried out with a time step of 2 fs, a total of 5000 frames were generated and the last 1000 frames from each molecular species were used to generate the average structure.

Noscapinoids, newly designed in this study (Figure 4.2) and the previously reported (Figure 4.3) were docked into the reported binding site of noscapinoids [34] using Glide XP (extra precision) and evaluated using a Glide XP Score function. The Glide XP<sub>score</sub> of the training set molecules (Table 4.2) shows a positive correlation with the experimental  $\Delta G_{\text{bind}}$  ( $R^2 = 0.368$ ). The newly designed noscapinoids, **5a-f** showed better docking scores ranging from -8.466 kcal/mol to -6.085 kcal/mol than the parent compound, noscapine (-5.505 kcal/mol) (Table 4.3). Some of the derivatives even showed better docking score in comparison to the previously reported noscapinoids.

Table 4.2. Molecular docking results (Glide XP) as well as calculated energies based on LIE-SGB model of training set noscapine derivatives: van der Waals (vdw), electrostatic (elec), cavity (cav), predicted and experimental binding free energy ( $\Delta G_{\text{bind}}$ ).

Ligand	Glide XP <sub>score</sub> (kcal/mol)	$\langle U_{\text{vdw}} \rangle$ (kcal/mol)	$\langle U_{\text{elec}} \rangle$ (kcal/mol)	$\langle U_{\text{cav}} \rangle$ (kcal/mol)	K <sub>d</sub> value ( $\mu\text{M}$ )	Experimental $\Delta G_{\text{bind}}$ (kcal/mol)	Predicted $\Delta G_{\text{bind}}$ (kcal/mol)
1	-5.505	-52.06	43.32	1.720	$152 \pm 1.0$	-5.214	-5.194
2a	-5.684	-47.65	119.8	1.432	$81 \pm 8.0$	-5.587	-5.951
2b	-6.152	-59.54	68.27	2.12	$40 \pm 8.0$	-6.006	-6.063
2c	-6.437	-58.92	87.54	1.59	$54 \pm 9.1$	-5.827	-6.355
2d	-5.463	-58.13	83.35	1.059	$22 \pm 4.0$	-6.360	-5.755

2e	-6.228	-57.71	129.2	1.846	86 ± 6.0	-5.551	-5.835
2f	-5.279	-59.48	63.57	1.324	14 ± 1.0	-6.628	-6.540
3	-5.639	-53.28	87.36	0.823	68 ± 0.7	-5.691	-5.416
4a	-6.087	-63.42	41.26	0.824	91 ± 8.0	-5.518	-5.394
4b	-7.252	-62.62	76.32	1.232	38 ± 4.0	-6.036	-5.795
4c	-5.712	-61.82	41.32	0.698	79 ± 8.0	-5.602	-5.128
4d	-5.402	-56.95	7.851	0.756	228 ± 10.0	-4.973	-5.078

$\langle U_{\text{vdw}} \rangle$ ,  $\langle U_{\text{elec}} \rangle$  and  $\langle U_{\text{cav}} \rangle$  energy terms represents the ensemble average energy terms calculated as the difference between bound and free state of the ligands and its environment. Experimental  $\Delta G_{\text{bind}}$  was calculated from the dissociation constant ( $K_d$  value) using the relationship:  $\Delta G_{\text{bind}} = RT \ln K_d$  where  $T = 298$  K and  $R = 0.00199$  (kcal/mol.K). Predicted  $\Delta G_{\text{bind}}$  was calculated using (LIE-SGB empirical equation:  $\Delta G_{\text{bind}} = 0.0762 \langle U_{\text{vdw}} \rangle - 0.00965 \langle U_{\text{elec}} \rangle - 0.520 \langle U_{\text{cav}} \rangle$ ).

Table 4.3. Molecular docking results (Glide XP) as well as calculated energies based on LIE-SGB model of newly designed noscapinoids (**5a-5f**): van der Waals (vdw), electrostatic (elec), cavity (cav), predicted and experimental binding free energy ( $\Delta G_{\text{bind}}$ ).

Ligand	Glide XP <sub>score</sub> (kcal/mol)	$\langle U_{\text{vdw}} \rangle$ (kcal/mol)	$\langle U_{\text{elec}} \rangle$ (kcal/mol)	$\langle U_{\text{cav}} \rangle$ (kcal/mol)	Predicted $\Delta G_{\text{bind}}$ (kcal/mol)	$K_d$ value ( $\mu\text{M}$ )	Experimental $\Delta G_{\text{bind}}$ (kcal/mol)
5a	-6.085	-60.57	41.82	1.05	-5.568	126 ± 5.0	-5.325
5b	-6.397	-60.68	50.47	1.62	-5.954	-	-
5c	-6.833	-59.44	53.78	1.23	-5.689	107 ± 5.0	-5.422
5d	-6.845	-63.89	63.01	0.49	-5.732	71 ± 4.0	-5.665
5e	-7.717	-63.21	61.54	1.07	-5.965	68 ± 6.0	-5.691
5f	-7.466	-67.39	44.45	0.78	-5.970	-	-

Experimental  $\Delta G_{\text{bind}}$  was calculated from the dissociation constant ( $K_d$  value) using the relationship:  $\Delta G_{\text{bind}} = RT \ln K_d$  where  $T = 298$  K and  $R = 0.00199$  (kcal/mol.K). Predicted  $\Delta G_{\text{bind}}$  was calculated using LIE-SGB empirical equation:  $\Delta G_{\text{bind}} = 0.0762 \langle U_{\text{vdw}} \rangle - 0.00965 \langle U_{\text{elec}} \rangle - 0.520 \langle U_{\text{cav}} \rangle$ .

### 4.3.2 MM-PBSA and MM-GBSA calculation

To estimate the free energy change that describes the binding of newly designed noscapinoids, **5a-5f** with tubulin we calculated the difference between the free energy of the complex and that of the respective binding partners based on MM-PBSA and MM-GBSA methods. Energy values were calculated as the average value out of 1000 snapshots generated from the last 2 ns of the MD trajectory for each tubulin-noscapinoid complex. The convergence of the MD trajectories was monitored by plotting root mean square deviation (RMSD) of the backbone  $C_\alpha$  atoms with respect to time. In fact the relative fluctuation of the RMSD value is very small after ~ 8 ns suggesting the stability of the system (Figure 4.6). Furthermore, the root mean square fluctuations (RMSF) of the residues of tubulin involved in the interaction with the ligands (within 20 Å diameters) in the bound form and in the free form were calculated to reveal the flexibility of these residues (Figure 4.7).



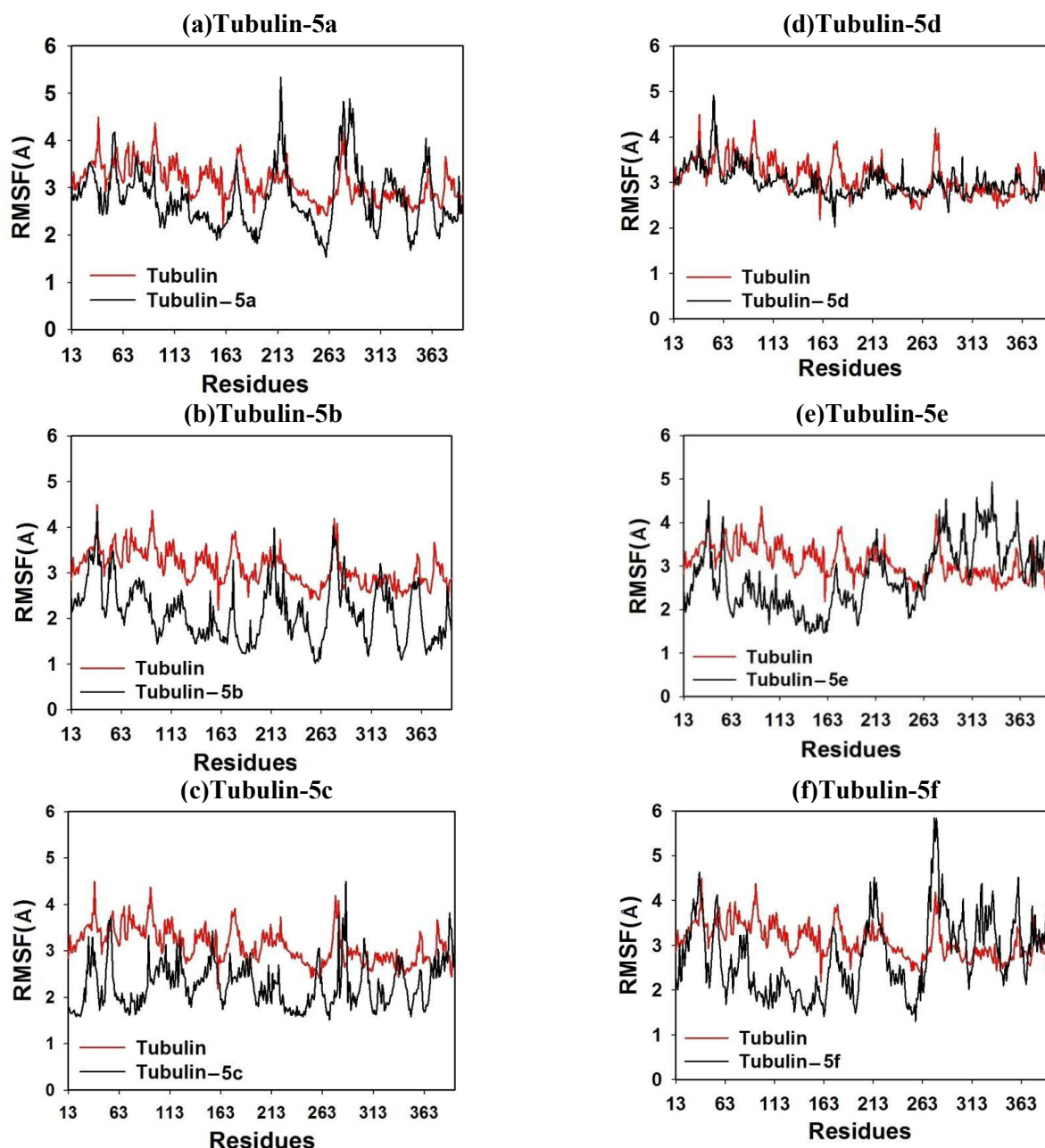


Figure 4.7. Root mean square fluctuation (RMSF) of the residues of tubulin within 20 Å diameter (includes 13-393 residues) of the docked ligands in the bound form and in the unbound form of tubulin heterodimer. Different levels of flexibility of these residues were noticed in the bound form of tubulin with different noscapinoids. Most of the residues in the binding site showed flexibilities less than 5 Å in case of tubulin bound to noscapinoids as compared to the free tubulin heterodimer, indicating that these residues seem to be more rigid as a result of binding.

In fact the RMSF values of these residues in the bound form were slightly lower compared to free form, indicating that these residues seem to be more rigid as a result of binding to noscapinoids. Different levels of flexibility of these residues have also noticed in the bound form of tubulin across various ligands (Figure 4.7). This may be because of subtle differences in the mode of molecular interactions of noscapinoids that perhaps account for their net effect on the binding free energy change with tubulin. All the noscapinoids, **5a-5f** are well accommodated into the

binding site, at the interface between  $\alpha$ - and  $\beta$ - tubulin (Figure 4.8). However, their binding modes inside the binding cavity are distinct as shown in Figure 4.9. The binding mode was represented in two steps: (a) receptor residues that have strong interactions with the ligand, such as a favorable hydrogen-bonding interactions, and (b) receptor residues that are close to the ligand, but whose interactions with the ligand are weak or diffuse, such as hydrophobic interaction. The differences in binding modes of these noscapinoids, **5a-5f** are not only due to various substitutions of functional groups in the scaffold structure but also because of differential contribution in binding free energy of amino acids involved in the interactions.

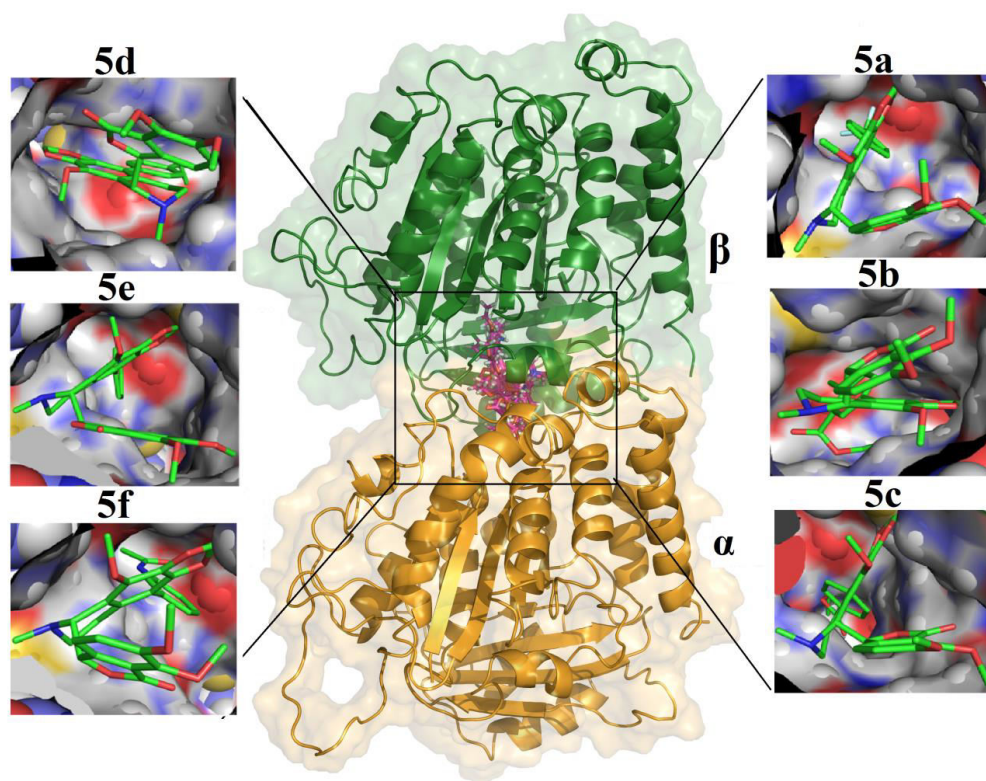


Figure 4.8. The newly designed noscapinoids **5a-5f** are well accommodated in the noscapinoid binding site at the interface between  $\alpha$ - and  $\beta$ - tubulin. Snapshot of the ligands **5a-f** are obtained from the MM-GBSA calculation. The binding site is represented as Macromodel surface according to residue charge (electropositive charge, blue; neutral, yellow and electronegative charge, red) as implemented in Pymol.

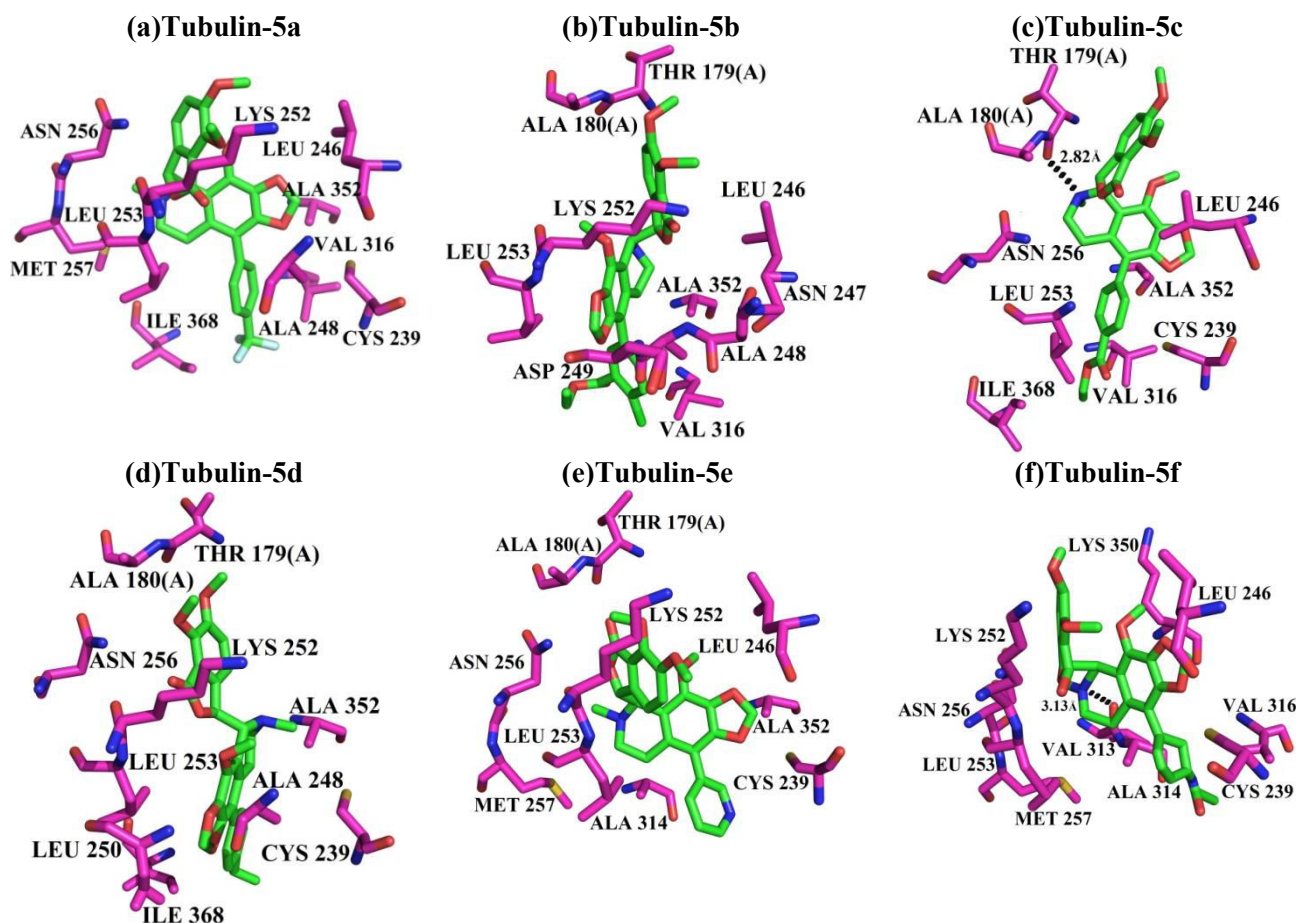


Figure 4.9. Typical snapshot of the binding mode of noscapinoids **5a-5f** with tubulin. The hydrogen bonds formed (if any) are represented as dotted lines. The noscapinoid **5c** forms one hydrogen bond with Thr179 of the  $\alpha$  chain. The nitrogen atom N1 of the upper isoquinalone ring hydrogen bonds with oxygen atom of Thr 179 with a distance of 2.82Å. The noscapinoid **5f** forms one hydrogen bond with Val 313 of the  $\beta$  chain. The nitrogen atom N1 of the upper isoquinalone ring hydrogen bonds with oxygen atom of Val 313 with a distance of 3.13Å. The other noscapinoids however do not involve any hydrogen bonds. The difference in binding modes of these noscapinoids is due to various substitutions in the scaffold structure.

Binding free energy of individual amino acid involved in the interaction with these ligands was calculated based on MM-GBSA calculation [42, 43] and plotted in Figure 4.10. As an example ten residues make considerable contributions to the binding energy of **5a**, each yielding < -1.0 kcal/mol of free energy (Figure 4.10a). Similarly 10, 9, 10, 10 and 11 residues contribute considerable binding energy with noscapinoids **5b-f** respectively, each yielding < -1.0 kcal/mol of free energy (Figure 4.10b-f). The analysis reveals that Leu253 is consistently important contributor to the binding energy among all the noscapinoids. Furthermore, to determine the detailed contribution of each important residue, the binding energy was decomposed into several other components (the electrostatic, van der Waals, solvation and total contribution) and plotted in Figure 4.11.



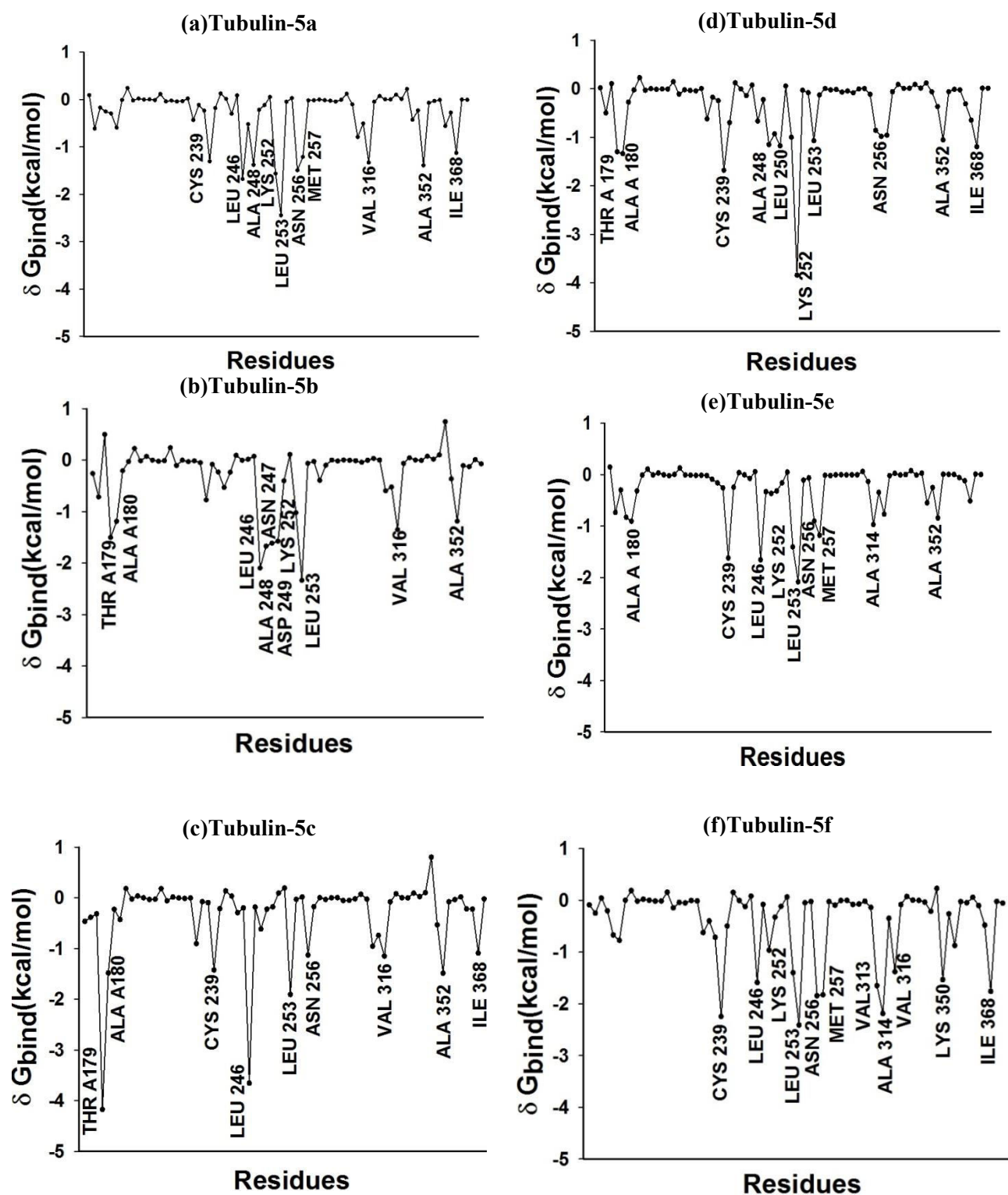


Figure 4.10. Total binding energy ( $\delta G_{\text{bind}}$ ) contribution on per residue basis in tubulin-drug complexes. The residues within 12 Å of the docked ligand were only considered.

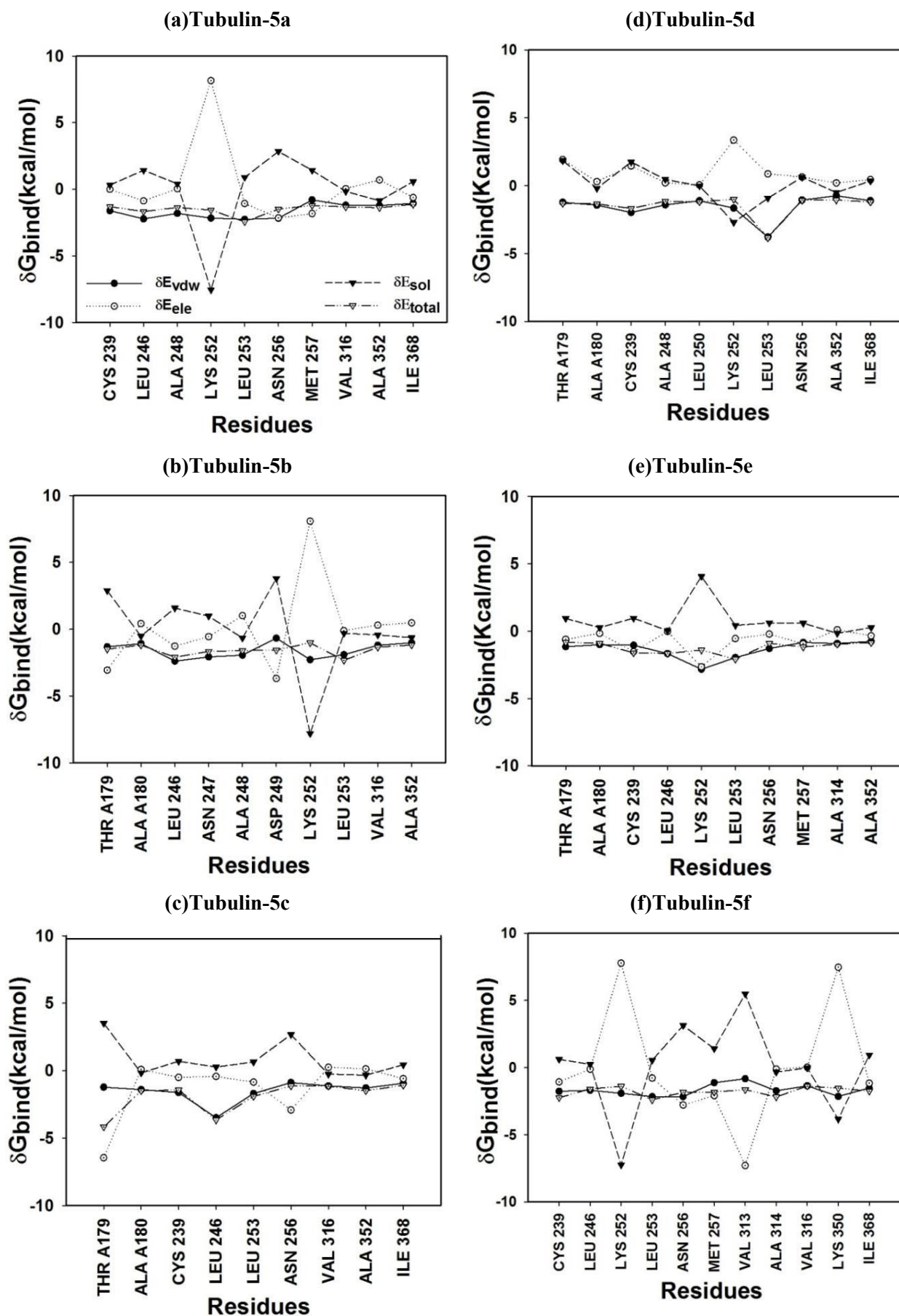


Figure 4.11. Decomposition of the binding energy on per residue basis of the key residues (contributing  $\Delta G_{bind} < -1.0$  kcal/mol) in tubulin-drug complexes.

As an example, in the tubulin-**5a** complex, Lys 252 has an appreciable solvation energy ( $\delta E_{\text{sol}}$ ) contribution, with a  $\delta E_{\text{sol}}$  of  $\leq -7$  kcal/mol, while electrostatic interaction ( $\delta E_{\text{ele}}$ ) shows unfavorable contributions at  $>6$  kcal/mol, as a result the total energy contributions of Lys 252 is weak (Figure 4.11a). For tubulin-**5b** complex, the residue Asp 249 has large electrostatic contribution ( $\delta E_{\text{ele}} \leq -4$  kcal/mol), while the residue Lys 252 has large solvation contribution ( $\delta E_{\text{sol}} \leq -7$  kcal/mol). Apropos to this Asp 249 has an unfavorable solvation contribution ( $\delta E_{\text{sol}} \geq 15$  kcal/mol) and Lys 252 has an unfavorable electrostatic contribution ( $\delta E_{\text{ele}} \geq 7$  kcal/mol) to the complex, resulting in weak contributions to the total energy for both the residues. Similarly, for tubulin-**5c** complex, the electrostatic interactions of Thr 178 and Asn 256 are -6.5 kcal/mol and -3.0 kcal/mol, respectively, which suggest that both are key residues in the binding of **5c**. In the tubulin-**5d** complex, Lys 252 has the strongest solvation energy contribution ( $\delta E_{\text{sol}} \leq -4$  kcal/mol), while the residues Lys 252 and Lys 350 contributed maximum of solvation energy ( $\delta E_{\text{sol}} \leq -7$  kcal/mol and  $\leq -4$  kcal/mol respectively) towards the binding of **5f** with tubulin.

### 4.3.3 Binding affinity calculations

The total calculated binding free energy ( $\Delta G_{\text{bind}}$ ) of the noscapinoids, **5a-5f** with tubulin and their detailed energy contributions calculated according to the MM-PBSA and MM-GBSA approaches are summarized in Table 4.4. The calculated  $\Delta G_{\text{bind}}$  based on both the methods, MM-PBSA and MM-GBSA, indicate that all the newly designed noscapinoids bind to tubulin with a greater affinity in the following order of magnitude: **5e** > **5f** > **5d** > **5c** > **5b** > **5a**. Both the intermolecular van der Waals ( $\Delta E_{\text{vdw}}$ ) and the electrostatic ( $\Delta E_{\text{ele}}$ ) interactions are significant contributions to the binding, whereas the polar solvation terms ( $\Delta G_{\text{PB(GB)}}$ ) counteract binding. In contrast non polar solvation terms ( $\Delta G_{\text{sol-np}}$ ), which correspond to the burial of solvent-accessible surface-area upon binding, contribute slightly favorably. Though the gas-phase electrostatic value ( $\Delta E_{\text{gas}}$ ) is in favor of the binding of all the noscapinoids, the overall electrostatic interaction energy ( $\Delta G_{\text{ele,PB(GB)}}$ ) is positive and unfavorable for the binding, perhaps due to large desolvation penalty of charged and polar groups that are not sufficiently compensated by complex formation. Comparing the net polar ( $\Delta G_{\text{PB(GB)}} + \Delta E_{\text{ele}}$ ) and nonpolar energies ( $\Delta G_{\text{sol-nonpolar}} + \Delta E_{\text{vdw}}$ ) contributions, we noticed that the binding of noscapinoids onto tubulin is mainly driven by nonpolar interaction.

Table 4.4. Change in binding free energy and its components (kcal/mol) for the noscapine derivatives **5a-5f** binding with tubulin.

Energy components (kcal/mol)	5a	5b	5c	5d	5e	5f
$\Delta E_{\text{ele}}$	-320.1	-318.6	-318.2	-314.7	-42.95	-340.7
$\Delta E_{\text{vdw}}$	-66.03	-69.19	-74.87	-68.41	-51.42	-72.01
$\Delta E_{\text{gas}}$	-386.2	-387.8	-393.0	-383.1	-94.36	-412.7
$\Delta G_{\text{sol-np}}$	-7.593	-7.906	-8.629	-7.070	-5.953	-7.857
$\Delta G_{\text{PB}}$	356.2	357.7	362.6	345.8	56.82	375.5
$\Delta G_{\text{solv,PB}}$	351.1	351.8	356.5	340.9	52.02	370.3
$\Delta G_{\text{ele,PB}}$	36.08	39.11	44.41	31.11	13.87	34.79
$\Delta G_{\text{bind, PB}}$	<b>-35.12</b>	<b>-35.94</b>	<b>-36.52</b>	<b>-42.22</b>	<b>-42.34</b>	<b>-42.25</b>
$\Delta G_{\text{GB}}$	350.9	349.7	352.0	342.1	52.04	370.2
$\Delta G_{\text{solv,GB}}$	343.3	341.8	343.4	335.1	46.09	362.3
$\Delta G_{\text{ele, GB}}$	30.77	31.08	33.84	27.43	9.091	29.44
$\Delta G_{\text{bind, GB}}$	<b>-42.85</b>	<b>-46.00</b>	<b>-49.64</b>	<b>-48.02</b>	<b>-48.27</b>	<b>-47.42</b>

#### 4.3.4 Predictive binding affinity of 5a-f with tubulin (LIE-SGB calculation)

The binding affinity ( $\Delta G_{\text{bind,pred}}$ ) of newly designed noscapinoids with tubulin was predicted based on computationally developed linear interaction energy model (LIE) utilizing the experimental activity of training set molecules. Since the molecular docking predicts accurate binding pose for the ligands onto the receptor, I have used the docking complexes of noscapinoids with tubulin and performed hybrid Monte Carlo simulation with generalized Born (SGB) continuum solvation model to develop a robust predictive model. Towards this end I have used the experimental binding energy of previously reported 12 noscapinoids as training set. The various interaction energy terms used in the model are included in Table 4.2 and are used to develop the LIE model. The values obtained for the three fitting parameters,  $\alpha$ ,  $\beta$  and  $\gamma$  are 0.076, - 0.010 and - 0.520, respectively. The largest contribution for the binding free energy comes from the van der Waals interactions. The predicted  $\Delta G_{\text{bind}}$  of the training set molecules based on LIE model is very close to the experimental  $\Delta G_{\text{bind}}$  (root mean square error was 0.288 kcal/mol). The quality of the fit can also be judged by the value of the squared correlation coefficient ( $R^2$ ) and analysis of variance (F-value).

$$\Delta G_{\text{bind}} = 0.0762\langle U_{\text{vdw}} \rangle - 0.00965\langle U_{\text{elec}} \rangle - 0.520\langle U_{\text{cav}} \rangle \quad (2)$$

$$(n = 12, R^2 = 0.776, s = 0.26, F = 1969.8, P = 0.001, \text{PRESS} = 1.243)$$

Because of high predictability, the LIE model was used to predict the  $\Delta G_{\text{bind}}$  of the newly designed noscapinoids. All the derivatives revealed improved predicted binding energy (ranging



from -5.568 to -5.965 kcal/mol) in comparison to the lead molecule (-5.214 kcal/mol). The derivative **5e** showed highest binding affinity ( $\Delta G_{\text{bind,pred}}$ ) of -5.965 kcal/mol in the series. The predicted binding free energy ( $\Delta G_{\text{bind}}$ ) of the noscapinoids, **5a-f** calculated based on MM-PBSA and MM-GBSA approaches as well as LIE-SGB, revealed strong interactions of newly designed noscapinoids onto tubulin. Inspired by our computational findings, we have made attempt to synthesize these compounds, **5a-f** to further evaluate their experimental activities.

#### 4.3.5 Chemical synthesis of **5a-f**

It is always be challenging in synthesizing the derivatives of noscapine because of its highly sensitive C-C bond between isoquinoline and isobenzofuranone ring components which is labile to strong acids and base. However, we have optimized the reaction conditions for the synthesis of these derivatives **5a-f** from 9-bromonoscapine **2c** as starting material without affecting the sensitive C-C bond. The reaction scheme is included in Figure 4.4. The 9-bromonoscapine was prepared from natural  $\alpha$ -noscapine using the synthetic scheme reported previously [18]. The complete chemical synthetic procedures for the preparation of noscapine derivatives, **5a-f** and their characterization using  $^1\text{H}$ ,  $^{13}\text{C}$  NMR and mass (ESI and HRMS), IR **spectral data** is described in the Appendix Section. Further single crystal x-ray analysis unambiguously confirmed the structure of **5b** (Figure 4.12). All the derivatives **5a-f** were purified over silica gel column chromatography and used for experimental studies.

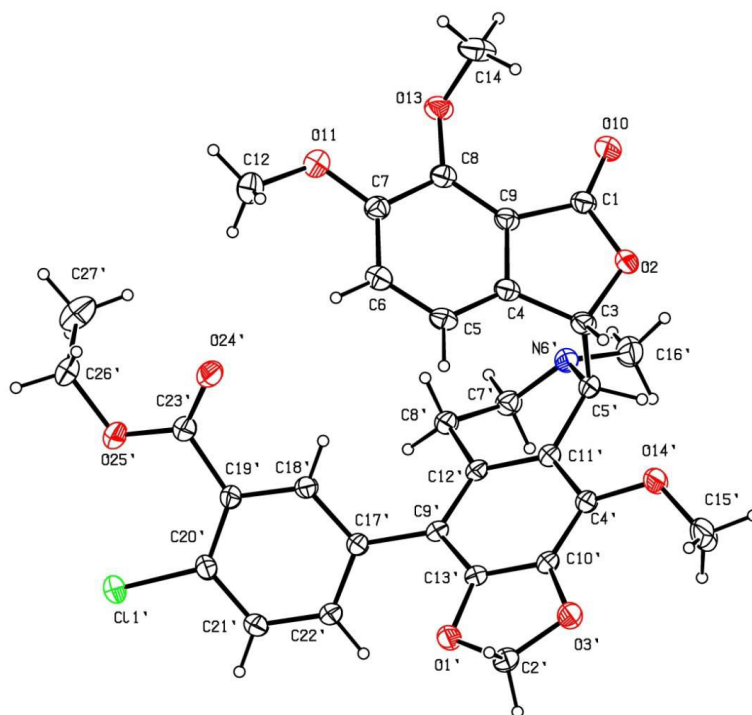
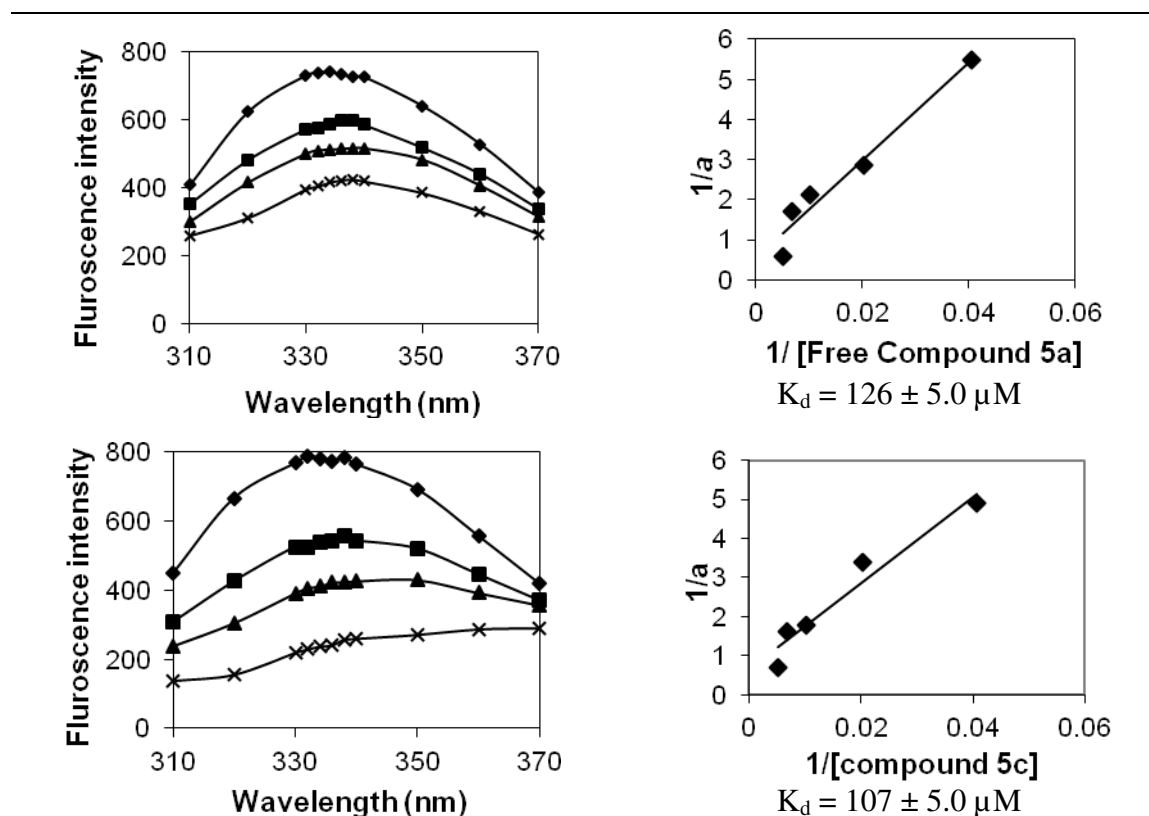


Figure 4.12. A view of **5b**, showing the atom-labelling scheme. Displacement ellipsoids are drawn at the 30% probability level and H atoms are represented by circles of arbitrary radii.

### 4.3.6. Noscapioids, **5a-5f** have higher tubulin binding activity than noscapine

We first determined if all of our noscapine analogs bind tubulin like the founding compound, noscapine. We found that the newly designed noscapioids **5a**, **5c-5e** reduced the intrinsic fluorescence of tubulin in a concentration-dependent manner (Figure 4.13a-d). The double reciprocal plots yielded a dissociation constant ( $K_d$ ) of  $126 \pm 5.0 \mu\text{M}$  for **5a**,  $107 \pm 5.0 \mu\text{M}$  for **5c**,  $71 \pm 4.0 \mu\text{M}$  for **5d**, and  $68 \pm 6.0 \mu\text{M}$  for **5e** binding to tubulin. We have previously reported the dissociation constant ( $K_d$ ) of  $152 \pm 1.0 \mu\text{M}$  for noscapine binding to tubulin [18]. The other two derivatives, **5b** and **5f** also showed potential binding to tubulin as indicated by the tryptophan quenching pattern, but we could not obtain reliable and reproducible  $K_d$  values due to a non-linear nature of the quenching pattern and higher absorbance of the compounds at the excitation and emission wavelengths (data not shown). These results thus indicate that the newly designed noscapine analogs bind to tubulin with a greater affinity than noscapine. Experimental  $\Delta G_{\text{bind}}$  of these compounds was calculated from the  $K_d$  value using the relationship:  $\Delta G_{\text{bind}} = RT \ln K_d$  where  $T = 298 \text{ K}$  and  $R = 0.00199 \text{ (kcal/mol.K)}$ . In fact, this experimentally determined value of  $\Delta G_{\text{bind}}$  (Table 4.2 and 4.3) are in the blueprint of predicted value of  $\Delta G_{\text{bind}}$  calculated based on LIE-SGB, MM-PBSA and MM-GBSA, suggesting that these methods are reasonably accurate in rational design of potent noscapioids.



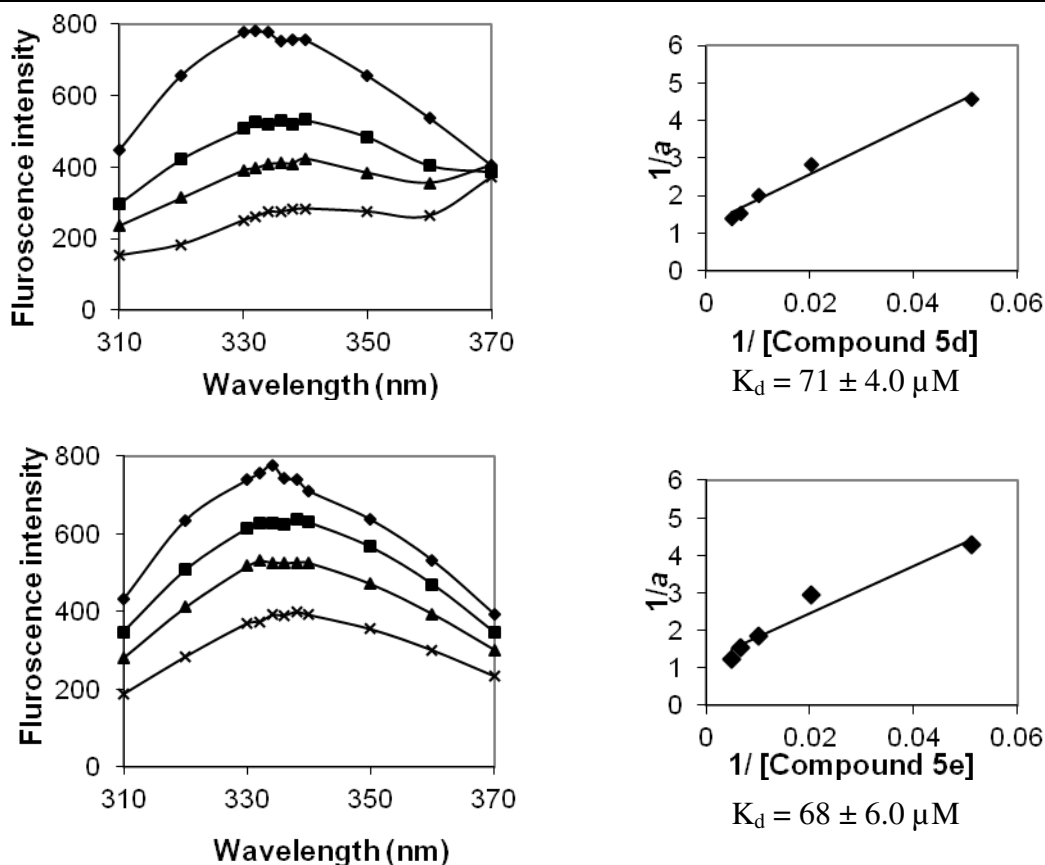


Figure 4.13. The tubulin fluorescence emission intensity is quenched by noscapinoids **5a**, **5c**, **5d** and **5e** in a concentration dependent manner. The change in fluorescence intensity is plotted as a function of concentration of drugs to calculate the  $K_d$  values.

#### 4.3.7 Effects of noscapine analogs on proliferation of cancer cells

After identifying tubulin as the target molecule, we extended our pharmacological study at the cellular level to determine if the compounds **5a-5f** affected cancer cell proliferation. As a preliminary screen, all compounds including the parent noscapine were evaluated for their anti-proliferative activity in three human cancer cell lines; human breast adenocarcinoma cells (MCF-7), human cervix cancer cells (HeLa) and human lung adenocarcinoma cells (A549). The  $IC_{50}$  values for the test compounds **5a-5f** for these three cell lines are collated in Table 4.5. All the compounds exhibited improved cytotoxic activities in comparison to the parent compound, noscapine. Especially three compounds **5b**, **5e** and **5f** possess potent cytotoxic activity. The  $IC_{50}$  value amounted to  $9.0 \pm 1.5 \mu M$ ,  $8.9 \pm 1.7 \mu M$  and  $9.2 \pm 1.4 \mu M$  with **5b**, **5e** and **5f** respectively for HeLa cells, which reflects a pronounced anti-proliferative activity. A similar low  $IC_{50}$  value of  $18.8 \pm 2.7 \mu M$ ,  $16.6 \pm 2.9 \mu M$  and  $17.8 \pm 2.5 \mu M$  was measured using **5b**, **5e** and **5f** respectively for the MCF-7 cells. In contrast, modest anti-proliferative activity for these compounds was noted against A549 cell line. Thus this preliminary screen with the three chosen cell lines revealed that **5b**, **5e** and **5f** as potent cytotoxic compounds as exemplified by their much lower  $IC_{50}$  values compared to

noscaphine. Besides the anti-proliferative effect, DAPI staining of the cells treated with noscapinoids showed condensed chromatin along with numerous fragmented nuclei (shown by white arrow heads), indicative of apoptotic cell death (Figure 4.14).

Table 4.5. IC<sub>50</sub> values (a drug concentration required to achieve a 50% inhibition of cellular proliferation) of noscapine derivatives **5a-5f** for various cancer cell types<sup>a</sup>.

Noscapine analogue	HeLa (μM)	A549 (μM)	MCF-7 (μM)
5a	22.8 ± 2.8	57.3 ± 3.9	41.3 ± 2.4
5b	9.0 ± 1.5	33.8 ± 3.5	18.8 ± 2.7
5c	21.2 ± 3.7	53.1 ± 3.7	40.7 ± 3.3
5d	20.3 ± 2.5	42.7 ± 2.9	34.3 ± 2.5
5e	8.9 ± 1.7	31.6 ± 2.6	16.6 ± 2.9
5f	9.2 ± 1.4	32.6 ± 2.5	17.8 ± 2.5
Noscapine	24.0 ± 2.9	62.9 ± 4.6	42.3 ± 2.7

<sup>a</sup> Cancer cells used in the assay namely, HeLa: human cervix cell line, A549: human lung adenocarcinoma epithelial cell line and MCF7: human breast epithelial cell line. Each value represents mean ± S.D. from three different experiments.

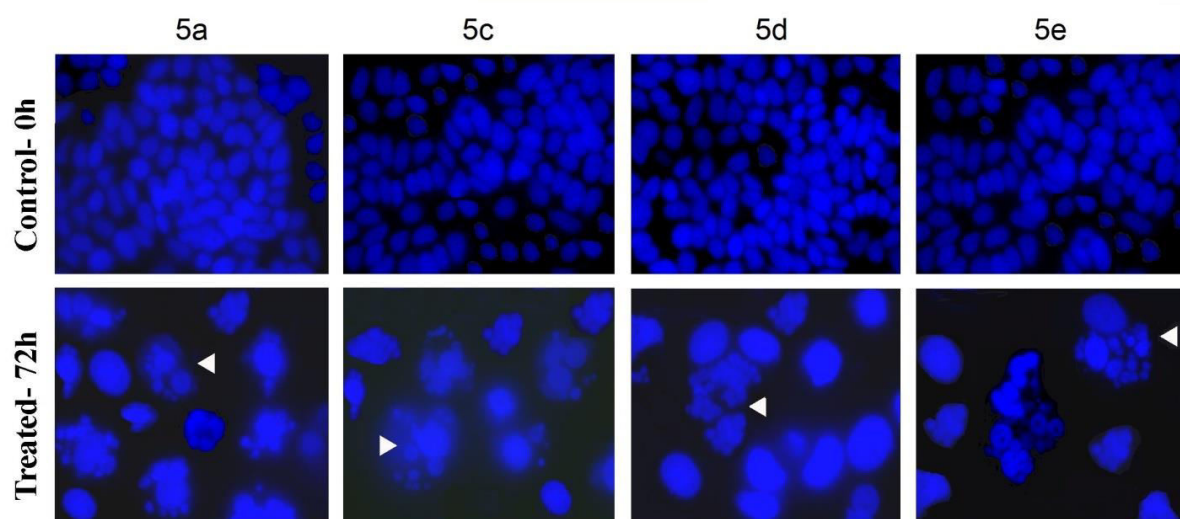


Figure 4.14. Morphologic indicators of apoptotic cell death include chromatin condensation along the nuclear envelope and plasma membrane blebbing followed by formation small apoptotic bodies. Panels show morphological evaluation of nuclei stained with DAPI in the absence and presence of the analogues (25 μM each). Several typical features of apoptotic cells such as condensed chromosomes, numerous fragmented micronuclei, and apoptotic bodies are evident (indicated by white head arrows) upon 72 hours of drug treatment. (Scale bar = 15 μm).

#### 4.3.8 Noscapinoids **5a-5f** alters the cell cycle profile and cause mitotic arrest at G2/M phase more actively than noscapine.

To ascertain the precise mechanisms of cell death, we next examined the effect of representative derivatives of noscapine **5c-f** on the cell cycle progression of MCF-7 cells using a fluorescence activated cell sorting (FACS) analysis. We determined the effect of these compounds at 25 μM for 0, 24, 48 and 72 hours of drug treatment. Figure 4.114a-d represents the cell cycle

profile in a three-dimensional disposition for these compounds.  $G_1$  phase of the cell cycle represent the unreplicated cells with  $2N$  DNA, while  $G_2$  and M phases represent the duplicated cells with  $4N$  DNA. Cells in the process of DNA duplication between  $2N$  and  $4N$  peaks represent S phase, when DNA is being synthesized. Less than  $2N$  DNA appears in populations of dying cells that degrade their DNA to different extents. MCF-7 cells treated with these compounds for 0, 24, 48 and 72 hours led to profound perturbations of the cell cycle profile at  $25\ \mu\text{M}$  (Figure 4.15a-d). Our result reveals that these derivatives of noscapine induce a massive accumulation of cells in the  $G_2/M$  phase at 24 hours. For example, the  $G_2/M$  cell population increases from 18.8 % in the control to ~ 58.7 % in MCF-7 cells treated with  $25\ \mu\text{M}$  of 5e for 24 hours. The distribution of cell populations over  $G_0/G_1$ , S,  $G_2/M$  and sub- $G_1$  phases of the cell cycle treated with  $25\ \mu\text{M}$  solution of noscapine derivatives is included in Table 4.6. Apropos to the  $G_2/M$  block, a characteristic hypodiploid DNA content (sub- $G_1$ ) was seen to be rising at 48 and 72 hours of drug treatment. The progressive increase of cells having hypodiploid DNA content (Table 4.6) reflects fragmented DNA, indicating dying cells.

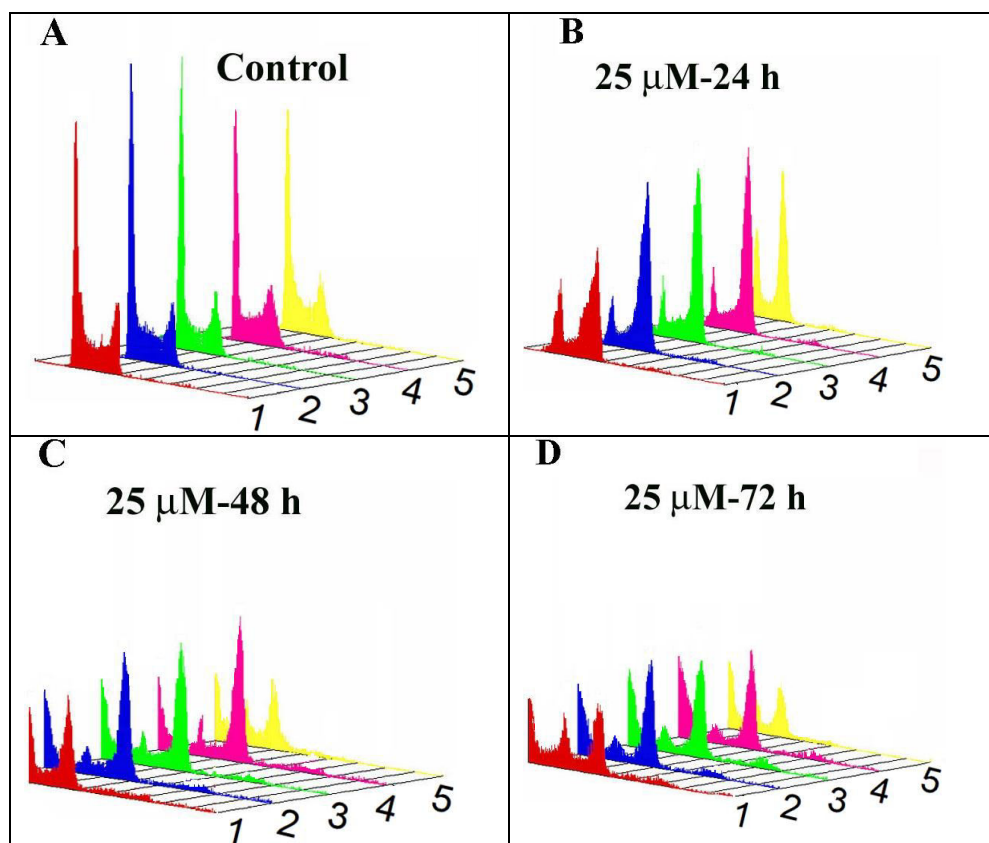


Figure 4.15. Noscapine analogs inhibit cell cycle progression at mitosis followed by the appearance of a characteristic hypodiploid (sub- $G_1$ ) DNA peak, indicative of apoptosis. Panel A-D depict analyses of cell cycle distribution in a three-dimensional disposition as determined by flow cytometry in MCF-7 cells treated with  $25\ \mu\text{M}$  concentration of noscapine analogs (1: 5c, 2: 5d, 3: 5e, 4: 5f and 5: 5a) for 0, 24, 48 and 72 hours respectively.

Table 4.6. Effect of noscapine derivatives on cell cycle progression of MCF-7 cells treated with 25  $\mu$ M solution for the indicated time (h) before being stained with propidium iodide for cell cycle analysis.

Cell cycle parameters (%)																
0 hour					24 hours				48 hours				72 hours			
	Sub-G <sub>1</sub>	G <sub>0</sub> /G <sub>1</sub>	S	G <sub>2</sub> /M	Sub-G <sub>1</sub>	G <sub>0</sub> /G <sub>1</sub>	S	G <sub>2</sub> /M	Sub-G <sub>1</sub>	G <sub>0</sub> /G <sub>1</sub>	S	G <sub>2</sub> /M	Sub-G <sub>1</sub>	G <sub>0</sub> /G <sub>1</sub>	S	G <sub>2</sub> /M
5a	0.32	64.3	15.7	24.5	8.42	16.28	4.26	42.5	27.4	16.3	3.24	24.6	29.3	18.5	5.16	19.6
5c	0.24	53.6	14.6	23.4	11.3	19.4	3.83	41.9	28.8	22.4	5.28	22.2	31.3	21.5	9.04	21.7
5d	0.18	68.4	12.3	19.3	7.43	14.3	3.77	65.2	36.5	6.47	3.29	44.6	47.5	7.25	4.08	35.6
5e	0.15	69.6	9.26	18.8	13.7	17.4	4.18	58.7	38.1	8.16	3.42	43.4	49.3	6.18	3.62	36.7
5f	0.17	55.3	14.6	21.4	9.37	12.5	3.58	56.2	35.8	7.15	3.08	49.8	50.2	4.39	2.63	32.4

#### 4.3.9 Toxicological evaluation

Toxicity in many tissues following chemotherapy is a major concern. Therefore, the search for a safe, well-tolerated regimen has been a major goal of clinical research. Antimitotic drugs that bind free or polymerized tubulin, such as *Vinca* alkaloids and taxanes, although effective treatment agents, are known to be cytotoxic to normal dividing cells. These drugs thus exhibit toxicities such as gastrointestinal (diarrhea, nausea, vomiting), myelosuppression (leucopenia), alopecia and peripheral neuropathies due to the blockage of axonal transport. To determine whether compound **5e** treatment results in toxicities to normal tissues, we did histopathologic analysis of vital organs such as liver, kidney, spleen, lung, heart, brain and duodenum of mice (Figure 4.16). Treatment with compound **5e** daily at a dose of 25 mg/kg body for 28 days failed to reveal any detectable pathological abnormalities in normal tissues as examined by H&E staining. Similarly, in a different experiment mice treated with a single dose of 50 mg/kg body weight also did not indicate any detectable pathologic abnormalities. Paraffin-embedded 5 micron-thick sections of the liver, kidney, spleen, lung, heart, duodenum and brain from animals of both treated and normal group were examined by H&E staining and included in Figure 4.16. There was a complete absence of any metastatic lesions in these organs in the treated animals. The liver showed normal hepatic lobular architecture. The kidneys revealed normal glomeruli, proximal and distal tubules, interstitium and blood vessels. The splenic follicles and vascular sinusoids were indistinguishable between the **5e**-treated and vehicle-treated control groups.



## CHAPTER 4

The lung tissue showed normal alveoli and the heart muscle showed normal morphology among the two groups. Microsections of the brain did not reveal any infarcted areas. The cerebral cortex, gray and white matter appeared normal. The gut showed normal mucosa, submucosa and muscularis mucosa.

Currently available anticancer drugs are known to depress bone marrow function, leading to decline of RBC, WBC and platelet counts during treatment regimens. Thus, we next examined if **5e** treatment had any effects on hematologic variables and organ-associated toxicities. Peripheral blood was examined for differences between **5e**-treated and vehicle-treated groups for complete blood count, WBC count, monocytes, eosinophils, RBC count, hemoglobin concentration, hematocrit, mean corpuscular volume, mean corpuscular hemoglobin, mean corpuscular haemoglobin concentration, and platelet count (Figure 4.17c & d). We next assessed organ-associated toxicity by measuring organ functions in **5e**-treated and vehicle-treated groups. Liver function tests (alanine transaminase, aspartate aminotransferase, alkaline phosphatase, bilirubin levels and albumin levels) and renal function tests (blood urea nitrogen and creatinine levels) were similar between treated and control groups (Figure 4.17a and b). Furthermore, **5e** does not alter the electrolyte balances. A standard electrolyte panel ( $\text{Na}^+$ ,  $\text{K}^+$ ,  $\text{Cl}^-$ ,  $\text{Ca}$ ) showed no abnormalities in electrolytes among the treated and control groups (Figure 4.16e). In addition, we were surprised to find no changes among the treated and vehicle-treated groups in total protein, albumin and glucose levels (Figure 4.17a and e). Also, during the dosage regimen, no abnormal behavior regarding food and water consumption and body weights was observed.

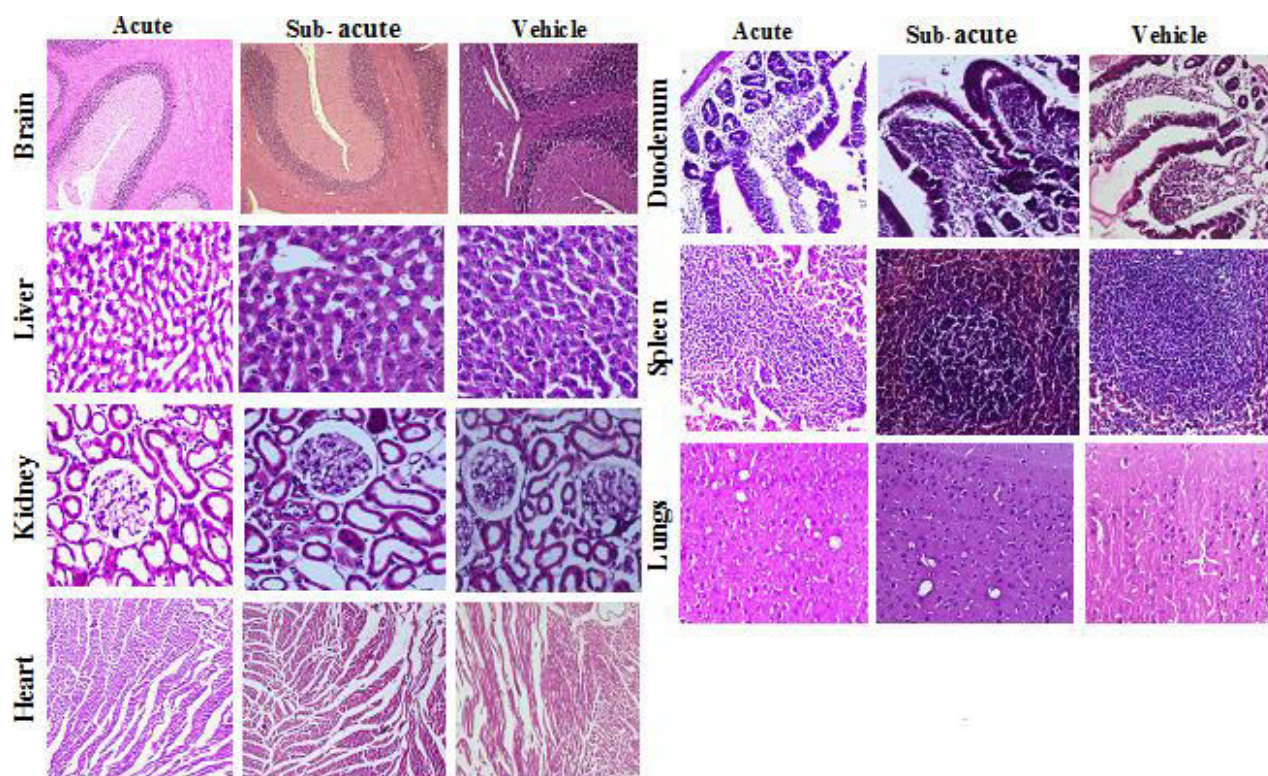
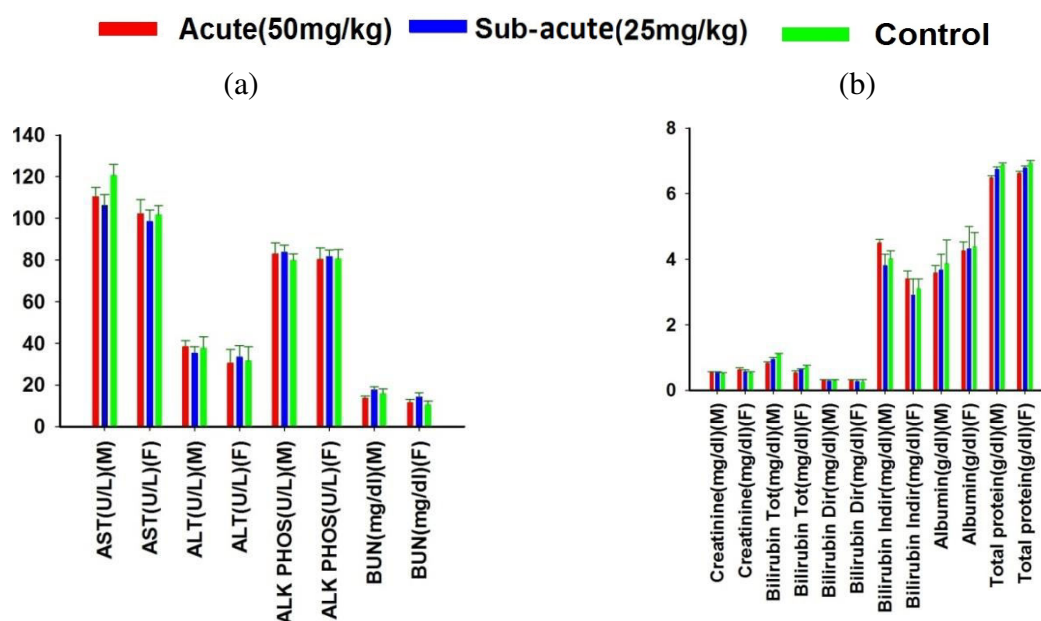


Figure 4.16. Treated animals (both male and female) with **5e** and vehicle fails to reveal any detectable pathologic abnormalities in normal tissues that are active in normal cell proliferation. Panels represent H&E staining of paraffin-embedded 5 micron-thick sections of the liver, kidney, spleen, lung, heart, duodenum and brain from **5e**-treated and untreated groups of mice under 200x magnifications. The liver showed normal hepatic lobular architecture. The kidneys revealed normal glomeruli, proximal and distal tubules, interstitium, and blood vessels. The splenic follicles and vascular sinusoids were indistinguishable between the **5e**-treated and vehicle-treated groups. The lung tissue showed normal alveoli and the heart muscle showed normal morphology among the two groups. Microsections of brain did not reveal any infarcted areas. The cerebral cortex, gray and white matters appeared normal. The gut showed normal mucosa, submucosa and muscularis mucosa.



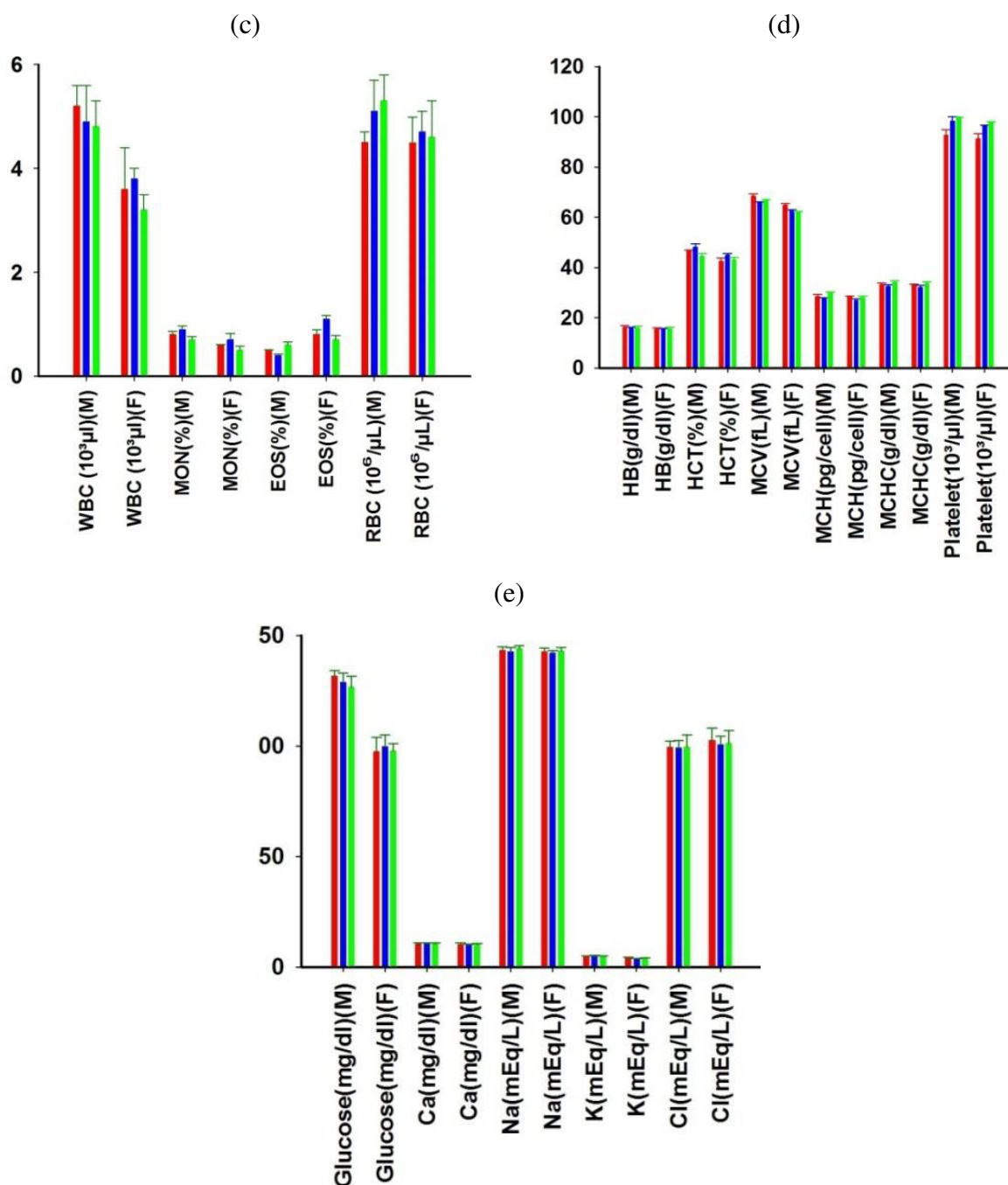


Figure 4.17. Treated animals (both male and female) with **5e** show no deviation in the toxicity profile when compared with vehicle-treated controls. Figure shows no toxicities related to hematological variables (a and b): liver function tests (alkaline transaminase (ALT), aspartate aminotransferase (AST), alkaline phosphatase (ALK phos), bilirubin levels and albumin levels), renal function tests (blood urea nitrogen (BUN) and creatinine levels); electrolyte panels (c and d): WBC count (WBC), monocytes (MON), eosinophils (EOS), RBC count (RBC), hemoglobin concentration (HB), Hematocrit (HCT), mean corpuscular volume (MCV), mean corpuscular hemoglobin (MCH), mean corpuscular hemoglobin concentration (MCHC) and platelet count; organ functions (e):  $\text{Na}^+$ ,  $\text{K}^+$ ,  $\text{Cl}^-$ , and  $\text{Ca}^{2+}$ . All show undistinguishable profiles among all variables examined for vehicle-treated and **5e**-treated groups.

#### 4.4 CONCLUSION

Inspired by the improved calculated binding affinity by computational methods for the designed derivatives, we have provided the simplest methods for the direct and regioselective synthetic strategies that provided a new series of products in high quantitative yields. Most importantly, our results show that biaryl substituted noscapine analogues have increased affinity to tubulin and the substitution impacted their therapeutic potential for a variety of cancer types. Furthermore, the mechanism of cell death caused by these analogues is preserved, such that, like noscapine, cell death is preceded by extensive mitotic arrest. *In vivo* toxicological evaluation of one of the compounds **5e** did not reveal any toxicity in the vital organs such as liver, kidney, spleen, lung, heart, brain and duodenum. In addition, there was no significant difference in hematological and blood biochemical parameters between the treated and untreated groups. Our data thus generate compelling evidence that these analogues indicate a great potential for further preclinical and clinical evaluation.

## REFERENCES

1. Mitchison, T.J. & Kirschner, M. *Dynamic instability of microtubule growth*. Nature, 312 pp 237-242. 1984.
2. Kirschner, M. & Mitchison, T.J. *Beyond self-assembly: From microtubules to morphogenesis*. Cell, 45 pp 329-342. 1986.
3. Van Tellingen, O., Sips, J.H., Beijnen, J.H., Bult, A. & Nooijen, W.J. *Pharmacology, bio-analysis and pharmacokinetics of the vinca alkaloids and semi-synthetic derivatives*. Anti-cancer Res, 12 pp 1699-1715. 1992.
4. Rowinsky, E.K. *The development and clinical utility of the taxane class of anti-microtubule chemotherapy agents*. Annu Rev Med, 48 pp 353-374. 1997.
5. Crown, J. & O'Leary, M. *The taxanes: an update*. Lancet, 355 pp1176-1178. 2000.
6. Goncalves, A., Braguer, D., Kamath, K., Martello, L., Briand, C., Horwitz, S., Wilson, L. & Jordan, M.A. *Resistance to taxol in lung cancer cells associated with increased microtubule dynamics*. Proc Natl Acad Sci USA, 98 pp 11737-41. 2001.
7. Ye, K., Ke, Y., Keshava, N., Shanks, J., Kapp, J.A., Tekmal, R.R., Petros, J. & Joshi, H.C. *Opium alkaloid noscapine is an anti-tumor agent that arrests metaphase and induces apoptosis in dividing cells*. Proc Natl Acad Sci USA, 95 pp 1601-1606. 1998.
8. Ye, K., Zhou, J., Landen, J.W., Bradbury, E.M. & Joshi, H.C. *Sustained Activation of p34(cdc2) is Required for Noscapine-Induced Apoptosis*. J Biol Chem, 276 pp 46697-46700. 2001.
9. Zhou, J., Panda, D., Landen, J.W., Wilson, L. & Joshi, H.C. *Minor alteration of microtubule dynamics causes loss of tension across kinetochore pairs and activates the spindle checkpoint*. J Biol Chem, 277 pp 17200–17208. 2002.
10. Zhou, J., Gupta, K., Yao, J., Ye, K., Panda, D., Giannakakou, P. & Joshi, H.C. *Paclitaxel-resistant human ovarian cancer cells undergo c-Jun NH<sub>2</sub>-terminal kinase-mediated apoptosis in response to noscapine*. J Biol Chem, 277 pp 39777-39785. 2002.
11. Ke, Y., Ye, K., Grossniklaus, H.E., Archer, D.R., Joshi, H.C. & Kapp, J.A. *Noscapine inhibits tumor growth with little toxicity to normal tissues or inhibition of immune Responses*. Cancer Immunol Immunother, 49 pp 217-225. 2000.
12. Landen, J.W., Lang, R., McMahon, S.J., Rusan, N.M., Yvon, A.M., Adams, A.W., Sorcinelli, M.D., Campbell, R., Bonaccorsi, P., Ansel, J.C., Archer, D.R., Wadsworth, P., Armstrong, C.A. & Joshi, H.C. *Noscapine alters microtubule dynamics in living cells and inhibits the progression of melanoma*. Cancer Res, 62 pp 4109-4114. 2002.

13. Landen, J.W., Hau, V., Wang, M.S., Davis, T., Ciliax, B., Wainer, B.H., Van Meir, E.G., Glass, J.D., Joshi, H.C. & Archer, D.R. *Noscapine Crosses the Blood-brain Barrier and Inhibits Glioblastoma Growth*. Clin Cancer Res, 10 pp 5187-5201. 2004.
14. Dahlstrom, B., Mellstrand, T., Lofdahl, C. & Johansson, M. *Pharmacokinetic properties of noscapine*. Eur J Clin Pharmacol, 22 pp 535-539. 1982.
15. Segal, M.S., Goldstein, M.M. & Attinger, E.O. *The Use of Noscapine (Narcotine) as an Anti-tussive Agent*. Dis Chest, 32 pp 305-309. 1957.
16. Loder, R.E. *Safe Reduction of the Cough Reflex with Noscapine: A Preliminary Communication on a New Use for an Old Drug*. Anaesthesia, 24 pp 355-358. 1969.
17. Santoshi, S., Naik, P.K. & Joshi, H.C. *Rational design of novel anti--microtubule agent (9-azido-Noscapine) from quanti-tative structure activity relationship (QSAR) evaluation of noscapinoids*. J. Biomol. Screening, 16 pp 1047-1058. 2011.
18. Naik, P.K., Chatterji, B.P., Vangapandu, S.N., Aneja, R., Chandra, R., Kanteveri, S. & Joshi, H.C. *Rational design, synthesis and biological evaluations of amino-Noscapine: A high affinity tubulin-binding noscapinoid*. J Comput Aided Drug Design, 25 pp 443-454. **2011**.
19. Naik, P.K., Lopus, M., Aneja, R. Vangapandu, S.N. & Joshi, H.C. *In silico inspired design and synthesis of a novel tubulin-binding anti--cancer drug: folate conjugated noscapine (Targetin)*. Journal of Computer aided molecular design, 26(2) pp 233-247. 2012.
20. Manchukonda, N.K., Naik, P.K., Santoshi, S., Lopus, M., Joseph, S., Sridhar, B. & Kanteveri, S. *Rational design, synthesis and biological evaluation of third generation  $\alpha$ -Noscapine analogues as potent tubulin binding anti--cancer agents*. Plos One, 8(10) e77970. 2013.
21. Jain, N., Yada, D., Shaik, T.B., Vasantha, G., Reddy, P.S., Kalivendi, S.V., Sreedhar, B. *Synthesis and antitumor evaluation of nitrovinyl biaryls: anticancer agents based on allocolchicines*. Chem Med Chem, 6(5) pp 859-868. 2011
22. Lee, C., Yang, W. & Parr, R.G. *Development of the Colle-Salvetti correlation-energy formula into a functional of the electron density*. Phys Rev B, 37 pp 785-789.1988
23. Becke, A.D. *A new mixing of Hartree-Fock and local density-functional theories*. J ChemPhys, 98 pp 1372-1377.1993.
24. Binkley, J.S., Pople, J.A. & Hehre, W.J. *Self-consistent molecular orbital methods. 21. Small split-valence basis sets for first-row elements*. J Am ChemSoc, 102 pp 939-947. 1980.
25. Gordon, M.S., Binkley, J.S., Pople, J.A., Pietro, W.J. & Hehre, W.J. *Self-consistent molecular-orbital methods. 22. Small split-valence basis sets for second-row elements*. J Am ChemSoc, 104 pp 2797-2803.1982.



26. Pietro, W.J., Francl, M.M., Hehre, W.J., Defrees, D.J., Pople, J.A. & Binkley, J.S. *Self-consistent molecular orbital methods. 24. Supplemented small split-valence basis sets for second-row elements.* J Am ChemSoc, 104 pp 5039-5048. 1982.
27. Berendsen, H.J.C, van der Spoel, D. & van Drunen, R. *GROMACS: A message passing parallel molecular dynamics implementation.* Computer Physics Communications 91 pp 43-56. 1995.
28. Daren, T., York, D. & Pedersen, L. *Particle mesh Ewald: An  $N\text{-log}(N)$  method for Ewald sums in large systems.* Journal of Chemical Physics, 98 pp 10089-10092.1993.
29. Hess, B., Bekker, H., Berendsen, H.J.C. & Fraaije, J.G.E.M. *LINCS: A linear constraint solver for molecular simulations.* J. Comput. Chem, 18 pp 1463-1472. 1997.
30. Laskowski, R.A., MacArthur, M.W., Moss, D.S. & Thornton, J.M. *PROCHECK: a program to check the stereochemical quality of protein structures.* J. App. Crystal, 26 pp 283-291. 1993.
31. Colovos, C. & Yeates, T.O. *Verification of protein structures: Patterns of non-bonded atomic interactions.* Protein Sci, 2 pp 1511-1519.1993.
32. Eisenberg, D., Luthy, R. & Bowie, J.U. *VERIFY3D: assessment 694 of protein models with three-dimensional profiles.* Methods Enzymol, 277 pp 396–404.1997.
33. Ramachandran, G.N., Ramakrishnan, C. & Sasisekharan, V. *Stereochemistry of polypeptide chain configurations.* J. Mol. Biol, 7 pp 95–99.1963.
34. Naik, P.K., Santoshi, S., Rai, A. & Joshi, H.C. *Molecular modelling and competition binding study of Br- Noscapine and colchicine provide insight into noscapinoid-tubulin binding site.* J. Mol. Graphics and Model, 29 pp 947-955. 2011.
35. Friesner, R.A., Banks, J.L., Murphy, R.B., Halgren, T.A., Klicic, J.J., Mainz, D.T., Repasky, M.P., Knoll, E.H., Shelley, M., Perry, J.K., Shaw, D.E., Francis, P. & Shenkin, P.S. *Glide: a new approach for rapid, accurate docking and scoring. 1. method and assessment of docking accuracy.* J. Med. Chem, 47 pp 1739–1749. 2004.
36. Halgren, T.A., Murphy, R.B., Friesner, R.A., Beard, H.S., Frye, L.L., Pollard, W.T., Banks, J.L. *Glide: a new approach for rapid, accurate docking and scoring. 2. Enrichment factors in database screening.* J. Med. Chem, 47 pp 1750-1759. 2004.
37. Case, D.A., Walker, R.C. et al. AMBER 11 (2010) University of California, San Francisco.
38. Cornell, W.D., Cieplak, P., Bayly, C.I., Gould, I.R., Merz, K.M. Jr, Ferguson, D.M., Spellmeyer, D.C., Fox, T., Caldwell, J.W. & Kollman, P.A. *A second generation force field for the simulation of proteins, nucleic acids, and organic molecules.* J Am Chem Soc 117 pp 5179–5197. 1995.

39. Ryckaert, J.P., Ciccotti, G. & Berendsen, H.J.C. *Numerical integration of the Cartesian equations of motion of a system with constraints: molecular dynamics of n-alkanes*. J Comput Phys, 23 pp 327–341. 1977.
40. Hornak, V., Abel, R., Okur, A., Strockbine, B. Roitberg, A. & Simmerling, C., *Comparison of multiple Amber force fields and development of improved protein backbone parameters*. Protein, 65 pp 712-25. 2006.
41. Berendsen, H. J. C., Postma, J. P. M., van Gunsteren, W. F., DiNola, A. & Haak, J. R. *Molecular dynamics with coupling to an external bath*. J. Chem. Phys, 81 pp 3684- 3691. 1984.
42. Srinivasan, J., Cheatham, T.E., Cieplak, P., Kollman, P. A. & Case, D. A. *Continuum Solvent Studies of the Stability of DNA, RNA, and Phosphoramidate–DNA Helices*. J. Am. Chem. Soc, 120 pp 9401–9409. 1998.
43. Kollman, P.A., Massova, I., Reyes, C., Kuhn, B., Huo, S., Chong, L., Lee, M., Lee, T., Duan, Y., Wang, W., Donini, O., Cieplak, P., Srinivasan, J., Case, D.A., Cheatham, T.E. *Calculating structures and free energies of complex molecules: combining molecular mechanics and continuum models*. Acc Chem Res, 33 pp 889-97. 2000.
44. Xiu-Long Shen & Midori Takimoto-Kamimura & Jing Wei & Qing-Zhi Gao. *Computer-aided de novo ligand design and docking/molecular dynamics study of Vitamin D receptor agonists*. J Mol Model, 18 pp 203–212. 2012.
45. Xiaodi Niu, Xiaohan Gao, Hongsu Wan, Xin Wang & Song Wang. *Insight into the dynamic interaction between different flavonoids and bovine serum albumin using molecular dynamics simulations and free energy calculations*. J Mol Model, 19 pp 1039–1047. 2013.
46. Jingjing Guo, Xiaoting Wang, Huijun Sun, Huanxiang Liu & Xiaojun Yao. *The molecular basis of IGF-II/IGF2R recognition: a combined molecular dynamics simulation, free-energy calculation and computational alanine scanning study*. J Mol Model, 18 pp 1421-1430. 2012.
47. Zhou, R., Frienser, R.A., Ghosh, A., Rizzo, R.C., Jorgensen, W.L. & Levy, R.M. *New linear interaction method for binding affinity calculations using a continuum solvent model*. J PhysChem B, 105 pp 10388–10397. 2001.
48. Aneja, R., Vangapandu, S.N., Lopus, M., Viswesarappa, V.G., Dhiman, N., Verma, A., Chandra, R., Panda, D. & Joshi, H.C. *Synthesis of microtubule-interfering halogenated Noscapine analogues that perturb mitosis in cancer cells followed by cell death*. Biochem. Pharmacol, 72 pp 415-426. 2006.

## CHAPTER 4

49. Aneja, R., Vangapandu, S.N., Lopus, M., Chandra, R., Panda, D. & Joshi, H.C. *Development of a novel nitro-derivative of Noscapine for the potential treatment of drug-resistant ovarian cancer and Tcell lymphoma*. Mol Pharmacol, 69 pp 1801–1809. 2006.
50. Bruker SAINT (Version 6.28a) & SMART (Version 5.625). Bruker AXS Inc., Madison, Wisconsin, USA. 2001
51. Sheldrick, G.M. *A short history of SHELX*. Acta Crystallogr, A64 pp 112-122. 2008
52. Flack, H.D., Bernardinelli, G. *Reporting and evaluating absolute-structure and absolute-configuration determinations*. J. Appl. Cryst, 33 pp 1143-1148. 2000
53. Hamel, E. & Lin, C.M. *Glutamate-induced polymerization of tubulin: characteristics of the reaction and application to the large-scale purification of tubulin*. Arch. Biochem. Biophys, 209 pp 29-40. 1981.
54. Panda, D., Chakrabarti, G., Hudson, J., Pigg, K., Miller, H.P., Wilson, L. & Himes, R.H. *Suppression of microtubule dynamic instability and treadmilling by deuterium oxide*. Biochemistry, 39 pp 5075-5081. 2000.
55. Bradford, M. M. *A rapid and sensitive method for the quantitation of microgram quantities of protein utilizing the principle of protein/ dye binding*. Anal. Biochem, 72 pp 248–254. 1976.
56. Joshi, H.C. & Zhou, J. *Gamma tubulin and microtubule nucleation in mammalian cells*. Methods Cell Biol, 67 pp 179-193. 2001.
57. Zhou, J., Gupta, K., Aggarwal, S., Aneja, R., Chandra, R., Panda, D. & Joshi, H.C. *Brominated derivatives of noscapine are potent microtubule-interfering agents that perturb mitosis and inhibit cell proliferation*. Mol Pharmacol, 63 pp 799–807. 2003.
58. Hota, S.K., Barhwal, K., Ray, K., Singh, S.B., Ilavazhagan, G. *Ceftriaxone rescues hippocampal neurons from excitotoxicity and enhances memory retrieval in chronic hypobaric hypoxia*. Neurobiology of Learning and Memory. 89 pp 522-32. 2008.
59. Hota, S.K., Hota, K.B., Prasad, D., Ilavazhagan, G., Singh, S.B. *Oxidative-stress-induced alterations in Sp factors mediate transcriptional regulation of the NR1 subunit in hippocampus during hypoxia*. Free Radical Biology & Medicine. 49 pp 178-91. 2010.
60. Aneja R, Dhiman N, Idnani J, Awasthi A, Arora SK, Chandra R, Joshi HC (2007) *Preclinical pharmacokinetics and bioavailability of noscapine, a tubulin-binding anticancer agent*. Cancer Chemother Pharmacol 60:831-839
61. Idanpaan-Heikkila JE (1968) *Studies o the fate of 3H-noscapine in mice and rats*. Ann Med Exp Biol Finn 46:201

# **CONCLUSION AND FUTURE DIRECTION**



## CONCLUSION AND FUTURE DIRECTION

Microtubules have long been considered an ideal target for anticancer drugs because of the essential role they play in mitosis, forming the dynamic spindle apparatus. As such, there is a wide variety of compounds currently in clinical use and in development that act as antimetabolic agents by altering microtubule dynamics. Despite the initial impressive response by these MT binding drugs such as taxanes and vinca alkaloids, their potential is somewhat restricted by the development of multi drug resistance, toxicity, hypersensitivity and limited bioavailability. Therefore, there is a continual need to develop novel drugs that are efficacious, well-tolerated, non-toxic, orally available, can overcome resistance to other chemotherapeutic and display better pharmacologic profiles. Noscapine (an opium alkaloid) has recently shown great potential as a microtubule binding anti-cancer agent. Noscapine alters tubulin dynamics and leads to programmed cell death and its relatively non toxic profile, oral availability and efficiency against various drug resistant cell lines indicates its potential as a chemotherapeutic agent for the treatment of human cancers to treat various malignancies in the clinic. Furthermore, it was found to be effective against a wide variety of cancer cells (according to the NC 60 cell line screen) but the effective concentration was found to be in high micromolar ranges. Therefore, attempts were required to be made to design a new generation of noscapine derivatives for better therapeutic outcome. The initial efforts in this have already been encouraging as indicated by the development of few more potent derivatives, but complete elimination of the disease could not be achieved. Thus, the paramount goal is to develop a more potent derivative of noscapine by structural modifications.

Availability of structure activity data of many derivatives of noscapine led to develop a reasonable QSAR prediction model and thus guided in rational design of more potent derivatives of noscapine. We have designed novel derivatives of noscapine based on quantitative structure activity relationship of known noscapine derivatives. To achieve this we have first determined the bioactive conformation of noscapine derivatives using quantum mechanics optimization in reference to experimentally determined noscapine structure. The  $IC_{50}$  value of already existing noscapine derivatives with CEM cancer cell line was determined and used for developing the QSAR model. To obtain quantitatively the effects of various structural parameters of the noscapine derivatives on their biological activity, QSAR analysis with different types of molecular descriptors was operated. We used genetic function approximation algorithm of variable selection and generated robust QSAR models with high predictability for the external data set. The QSAR model guided us towards designing two new derivatives, 9-azido-noscapine and reduced 9-azido-noscapine. The activity of these new compounds was predicted using the developed QSAR model, which motivated



us further towards synthesis of these compounds. Validation of the model was achieved by experimentally determining value of  $pIC_{50}$  for both the compounds (5.585 M) which turned out to be very close to predicted  $pIC_{50}$  (5.731 and 5.710 M). Thus, this model was established to be a good rapid screening tool which could be used in future to uncover new and more potent anti-tumor drugs based on noscapine derivatizations.

Noscapine binds to tubulin composed of  $\alpha$ - and  $\beta$ -tubulin, which exist as various isotypes. Although, noscapinoids bind at the interphase between  $\alpha$ - and  $\beta$ -tubulin; their interaction is more biased towards  $\beta$ -tubulin. The distribution of the isotypes of  $\beta$ -tubulin is different among cells of different tissue of origin. Furthermore, their drug-binding properties are significantly different. Also the existence of different isotypes of tubulin and their differential expression in cancer cells has been related to resistance towards the currently used chemotherapeutic agents. Effectiveness of noscapine in a wide range of cancers and various drug resistant cancer cell lines generated an interest to computationally investigate the details of interaction of noscapinoids towards different isotypes of  $\beta$ -tubulin. We found that the binding score of a specific noscapinoid with each type of tubulin isotype is different. Specifically, amino-noscapine has the highest binding score with  $\alpha\beta_I$ ,  $\alpha\beta_{II}$ ,  $\alpha\beta_{III}$  and  $\alpha\beta_{IV}$  isotypes. More importantly, both amino-noscapine and bromo-noscapine have the highest binding affinity with  $\alpha\beta_{III}$  (overexpression of  $\alpha\beta_{III}$  has been associated with resistance to a wide range of chemotherapeutic drugs for several human malignancies) in the pattern of amino-noscapine (-34.70 and -46.23 kcal/mol), bromo-noscapine (-32.05 and -38.09 kcal/mol) and noscapine (-28.02 and -38.86 kcal/mol) based on both MM-PBSA and MM-GBSA calculations. The interaction analysis revealed that amino acids, Ser 239, Leu253, Ile 368, consistently contribute to the binding energy for all the three ligands, indicating their importance in interaction with the ligands targeted towards  $\alpha\beta_{III}$ -tubulin isotype. The information gained in this study could pave a way for more efficient design of novel noscapinoid, which could be specifically targeted towards cancer cells. Knowledge of the isotype specificity of noscapinoid may allow for development of novel therapeutic agents based on this drug.

In pursuit of developing novel noscaponoids, we have rationally designed six new biaryl substituted noscapine analogues which possess increased tubulin-binding and anti-proliferative activity using structure based design approach. Initially a library of noscapine derivatives was screened out using molecular docking, molecular dynamics simulation, and binding free energy calculation. The predictive binding affinity indicated that the newly designed noscapinoids bind to tubulin with a greater affinity. Six new derivatives with improved predicted binding affinity than the lead molecule were selected for further analysis. MM-PBSA and MM-GBSA methods have

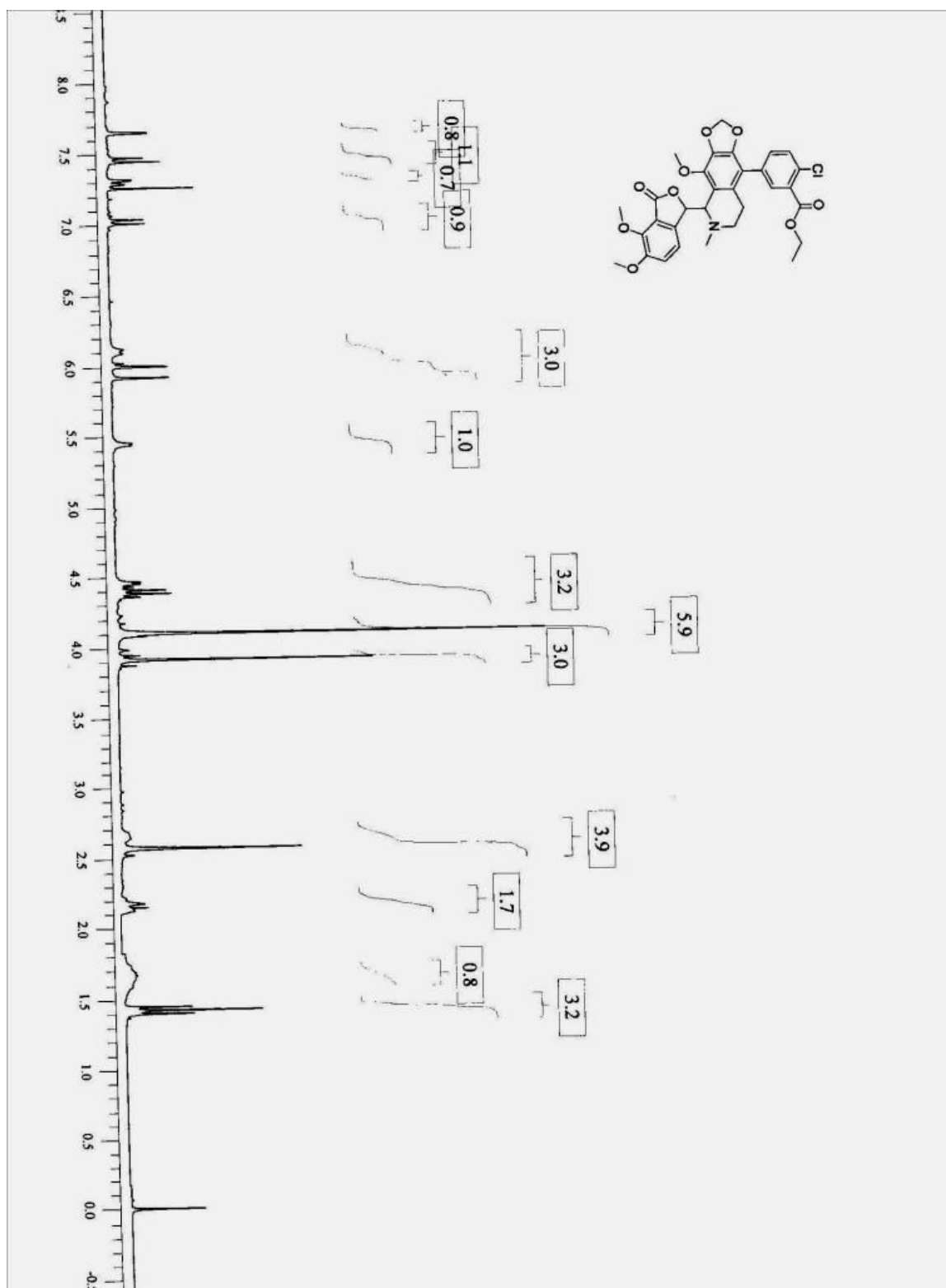
been used to further investigate the mechanistic details of the interaction of these new derivatives with tubulin. The analysis suggests that newly designed noscapinoids bind to tubulin with a greater affinity than the parent compound in the following order of magnitude: 5e > 5f > 5d > 5c > 5b > 5a. Analysis of the binding energy contribution of amino acids in the binding site also reveals that Leu253 is consistently important, contributing to the binding energy among all the noscapinoids.

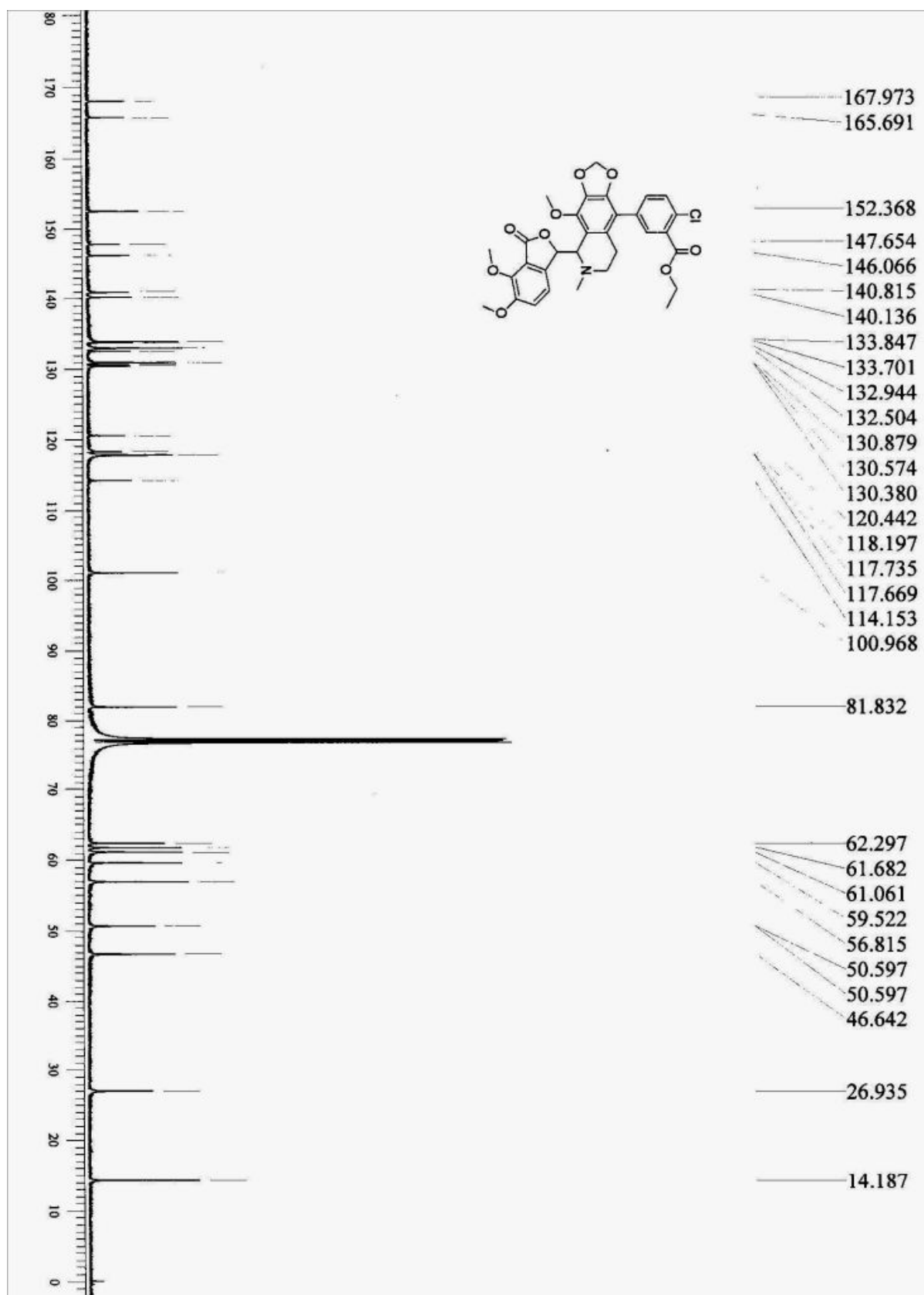
Guided by the computational findings, these new biaryl type  $\alpha$ -noscapine congeners were synthesized from 9-bromonoscapine using optimized Suzuki reaction conditions for further experimental evaluation. Most importantly, our results show that biaryl substituted noscapine analogues have increased affinity to tubulin and the substitution impacted their therapeutic potential for a variety of cancer types. It was also demonstrated that this series of noscapinoids are able to arrest mitosis and inhibit cell proliferation with significantly higher efficiency than noscapine in various human cancer cell lines. These compounds perturbed DNA synthesis, delayed the cell cycle progression at S phase and G2M phase as well as induced apoptosis in cancer cells. *In vivo* toxicological evaluation of one of the compounds **5e** did not reveal any toxicity in the vital organs such as liver, kidney, spleen, lung, heart, brain and duodenum. In addition, there was no significant difference in hematological and blood biochemical parameters between the treated and untreated groups. Hence the newly designed noscapinoid, 5e is a safe and effective anticancer drug with a potential for the oral treatment of cancer and holds great promise for further clinical studies.

Our data thus generate compelling evidence that these analogs indicate a great potential for further preclinical and clinical evaluation. Also the analysis of interaction of noscapinoids with different isotypes can be further exploited for better and more efficient design of noscapinoids. Knowledge of the isotype specificity of noscapinoids may lead to the improvement of both efficacy and specificity of cancer treatments in different tissues. Thus future holds promises both in the form of further clinical evaluation of already designed noscapinoids in this study and more efficient and specific targeting of cancers of different tissue origin by exploiting the interaction mechanism of noscapinoids towards different tubulin isotypes.



# **APPENDIX**

**$^1\text{H}$  NMR,  $^{13}\text{C}$  NMR and ESI/HRMS spectra of Noscapinoids** **$^1\text{H}$  NMR spectra of 5b**

$^{13}\text{C}$  NMR spectra of 5b

## HRMS spectra of 5b

Acq. File: n/a

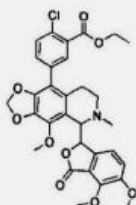
Sample ID: n/a

Acq. Date: n/a

Sample Comment: n/a

Acq. Time: n/a

## Elemental composition calculator



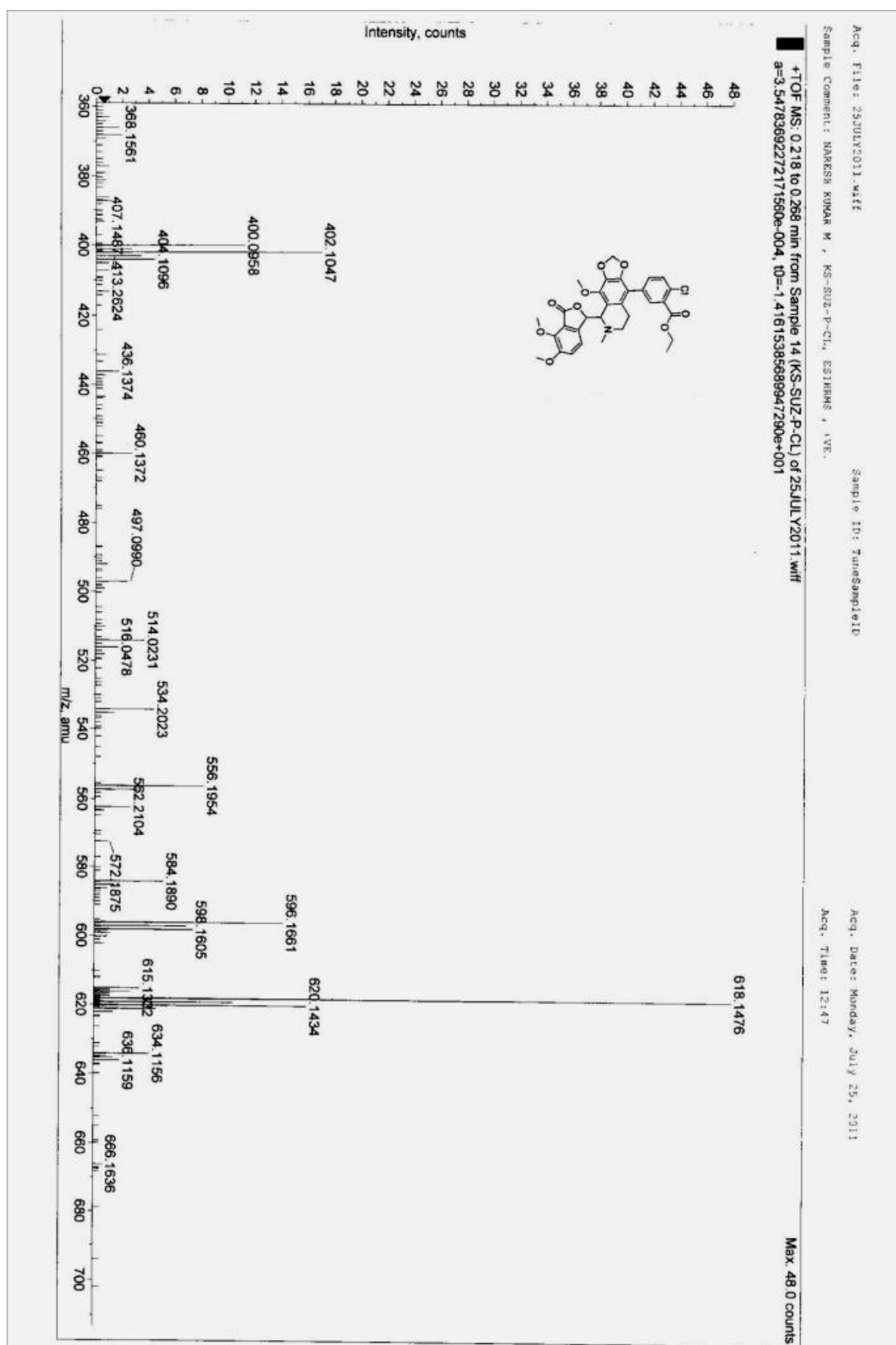
Target m/z: +618.1476 amu  
 Tolerance: +5.0000 ppm  
 Result type: Elemental  
 Max num of results: 100  
 Min DBE: -0.5000 Max DBE: +50.0000  
 Electron state: OddAndEven  
 Num of charges: 0  
 Add water: N/A  
 Add proton: N/A  
 File Name: 25JULY2011.wiff

	Elements	Min Number	Max Number
1	Cl	0	1
2	C	0	31
3	H	0	32
4	N	0	2
5	Na	0	1
6	O	0	9

	Formula	Calculated m/z (amu)	mDa Error	PPM Error	DBE
1	C31 H30 N O9 Na Cl	618.1506	-3.0793	-4.9816	16.5



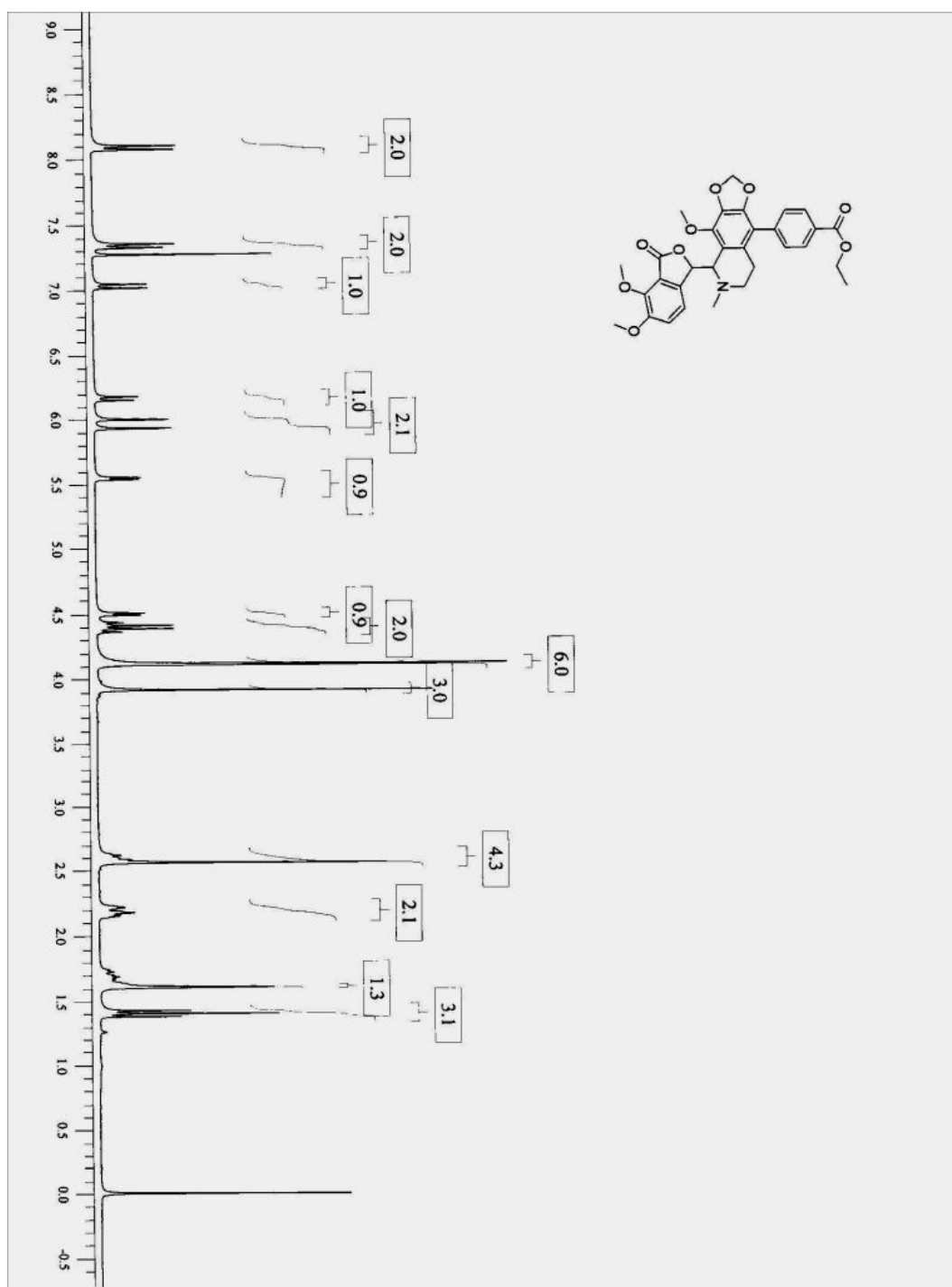
## ESI spectra of 5b

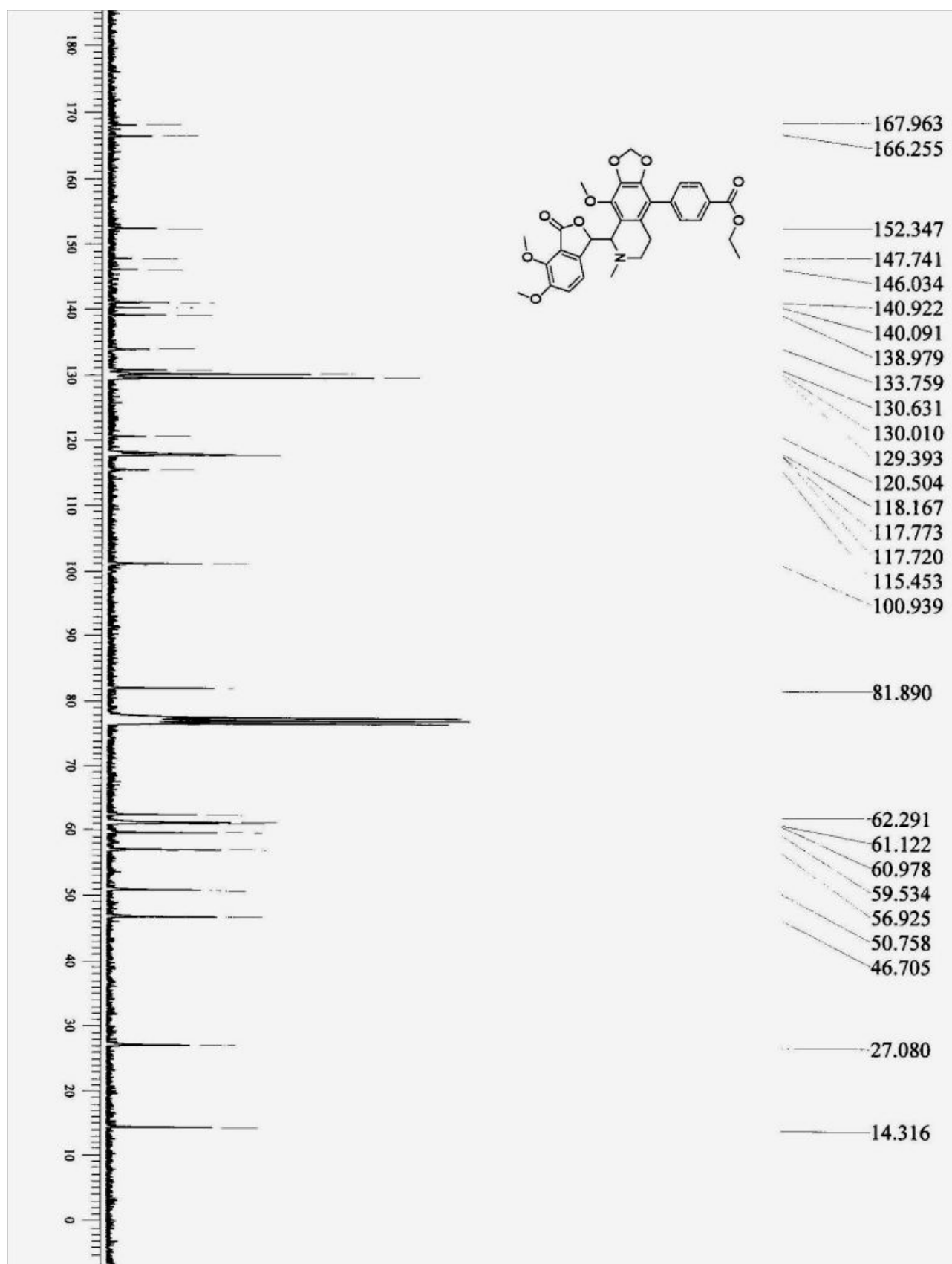


---

<sup>1</sup>H NMR spectra of 5c

---



$^{13}\text{C}$  NMR spectra of 5c

## HRMS spectra of 5c

Acq. File: n/a

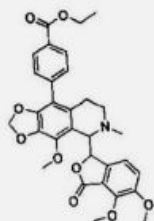
Sample ID: n/a

Acq. Date: n/a

Sample Comment: n/a

Acq. Time: n/a

## Elemental composition calculator

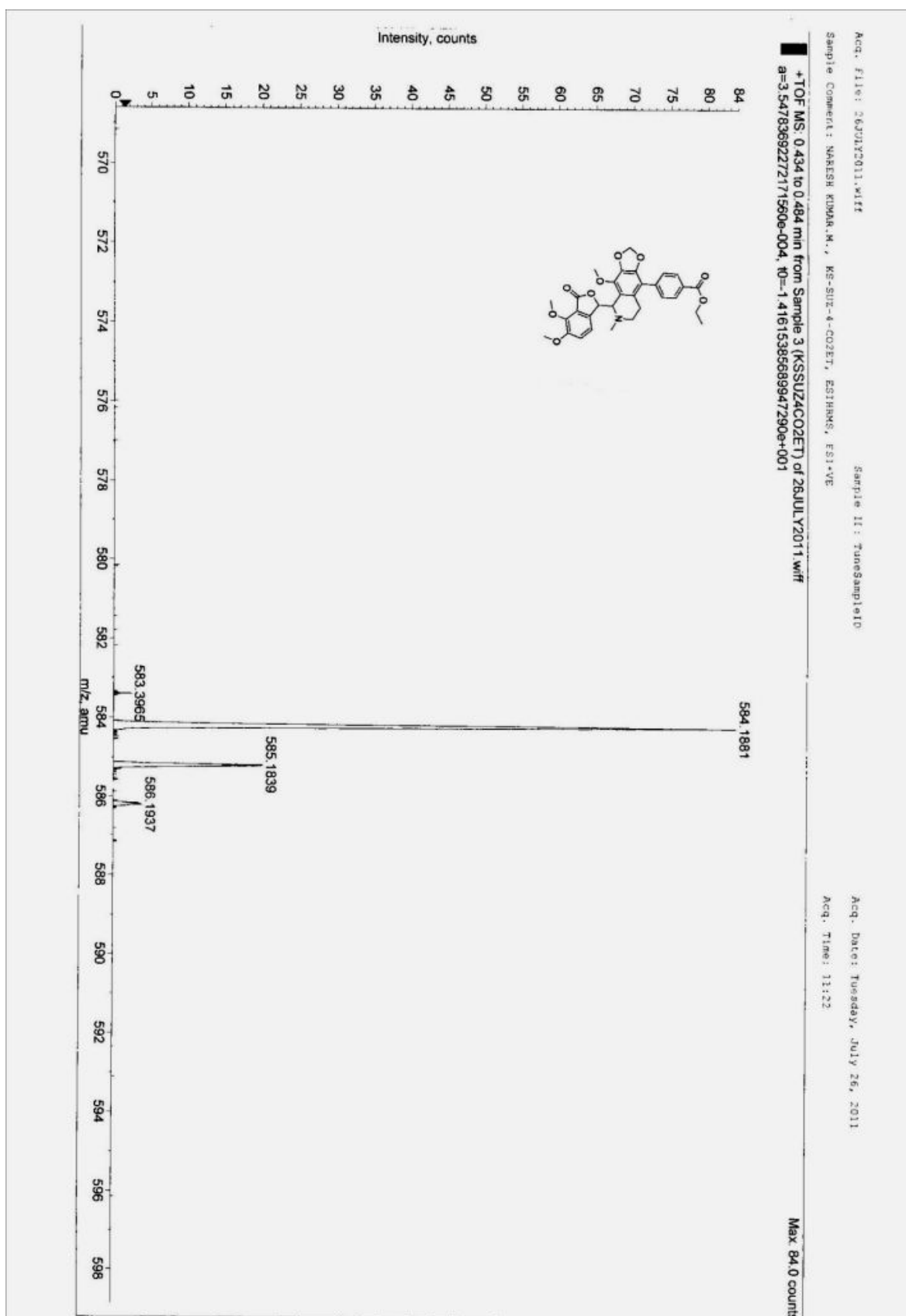


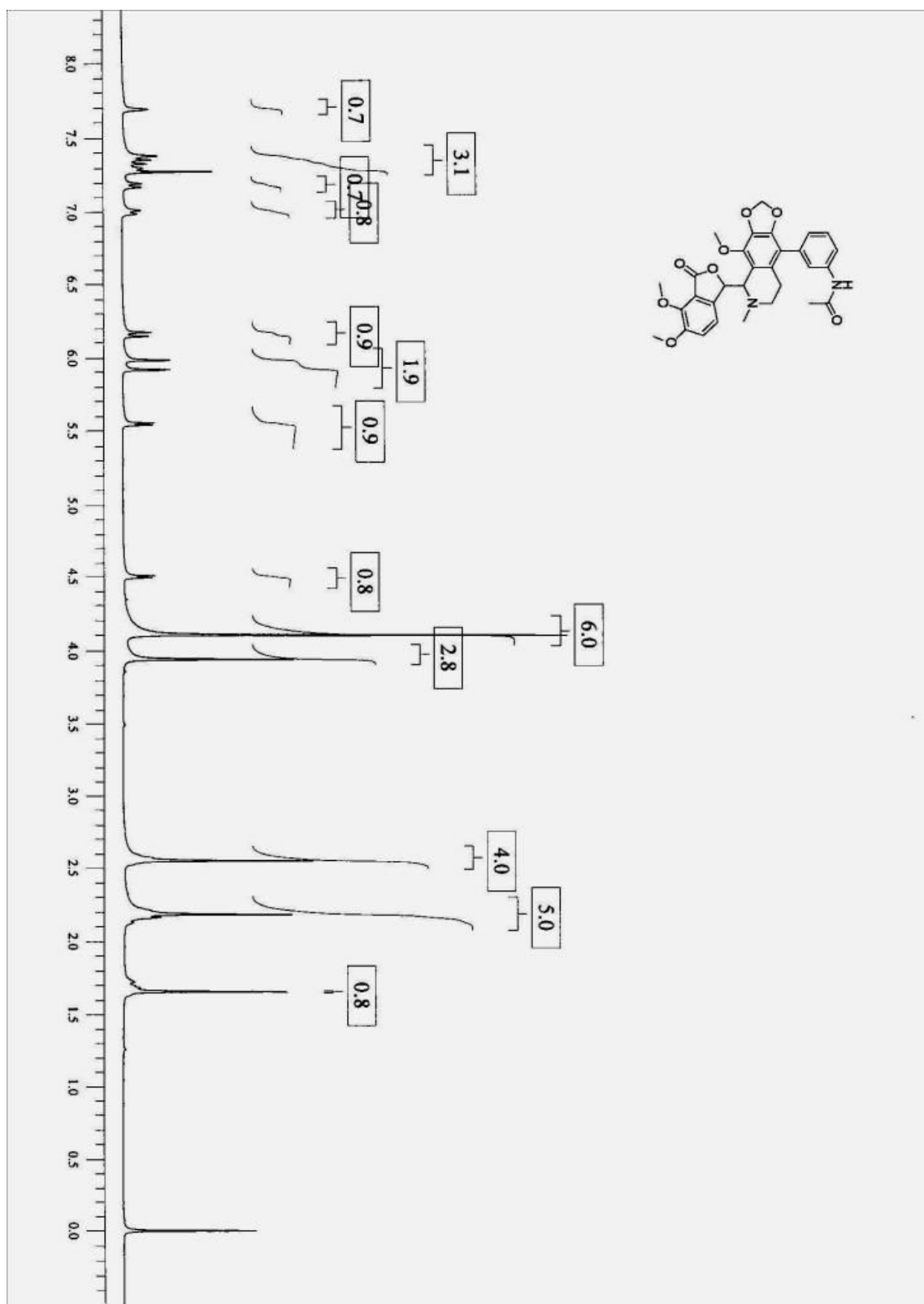
Target m/z: +584.1881 amu  
 Tolerance: +5.0000 ppm  
 Result type: Elemental  
 Max num of results: 100  
 Min DBE: -0.5000 Max DBE: +50.0000  
 Electron state: OddAndEven  
 Num of charges: 0  
 Add water: N/A  
 Add proton: N/A  
 File Name: 26JULY2011.wiff

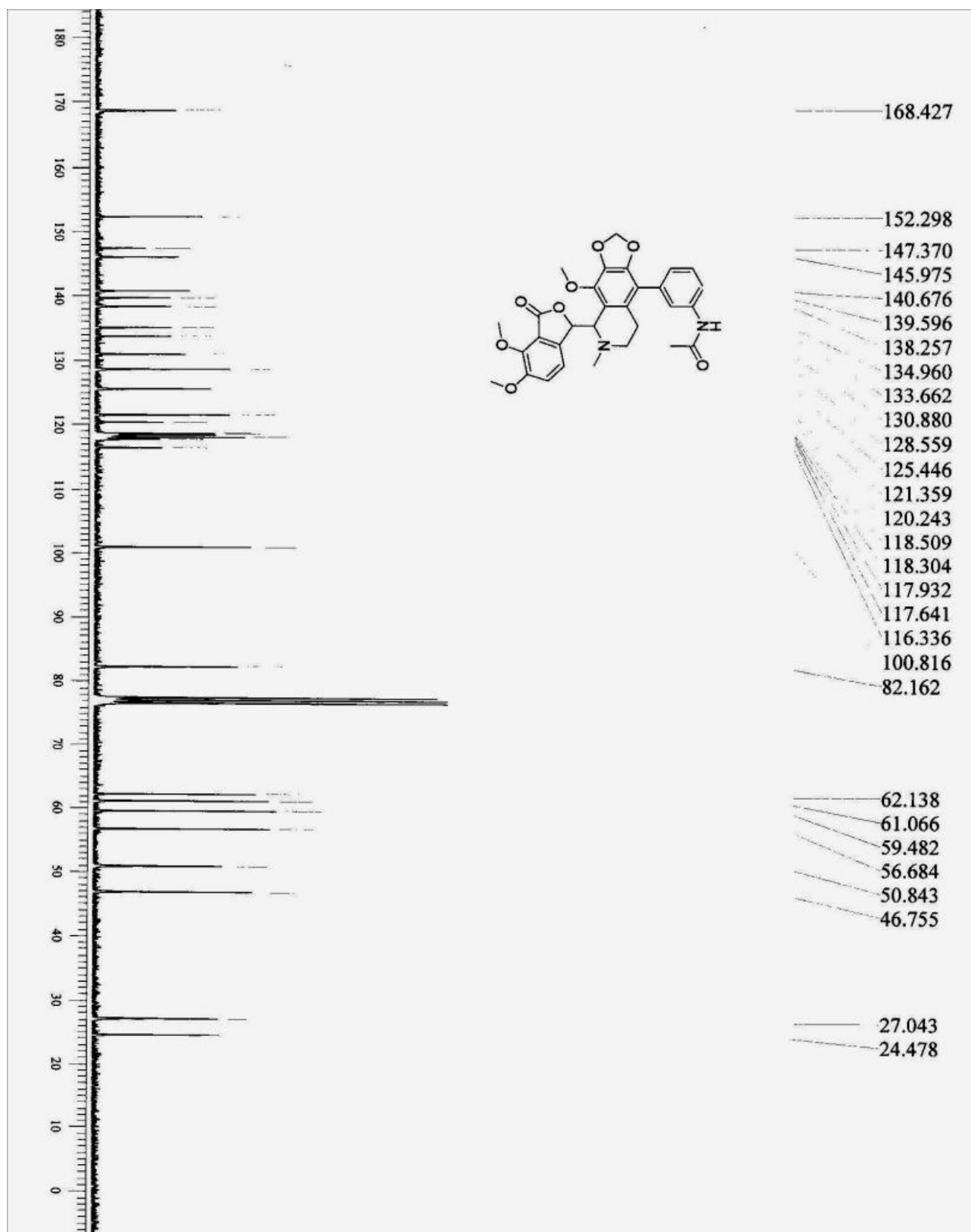
	Elements	Min Number	Max Number
1	C	0	31
2	H	0	32
3	N	0	2
4	Na	0	1
5	O	0	9

	Formula	Calculated m/z (amu)	mDa Error	PPM Error	DBE
1	C31 H31 N O9 Na	584.1896	-1.5517	-2.6561	16.5

## ESI spectra of 5c



$^1\text{H}$  NMR spectra of 5f

$^{13}\text{C}$  NMR spectra of 5f



## HRMS spectra of 5f

Acq. File: n/a

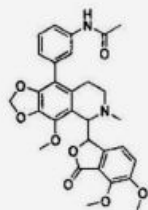
Sample ID: n/a

Acq. Date: n/a

Sample Comment: n/a

Acq. Time: n/a

## Elemental composition calculator

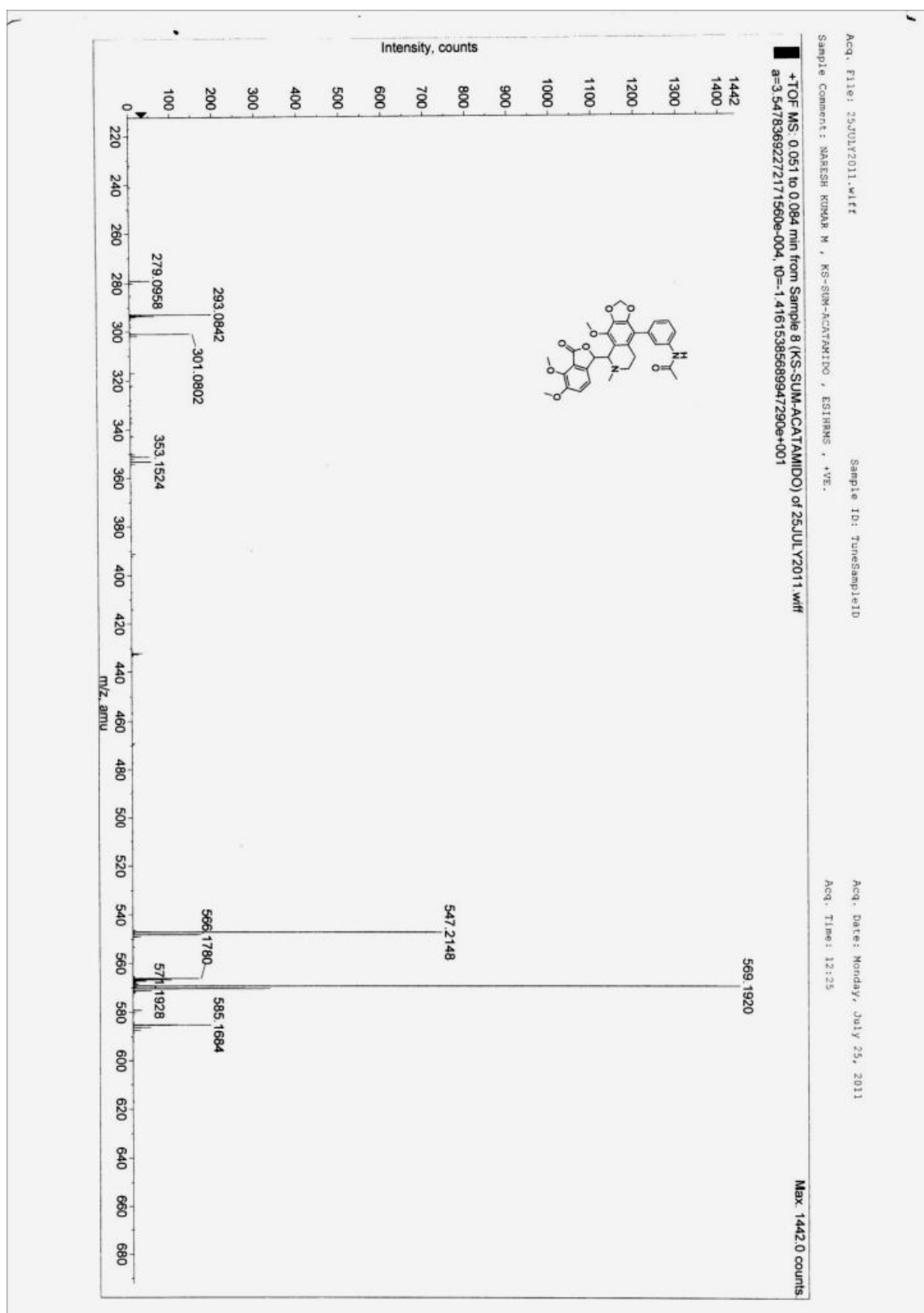


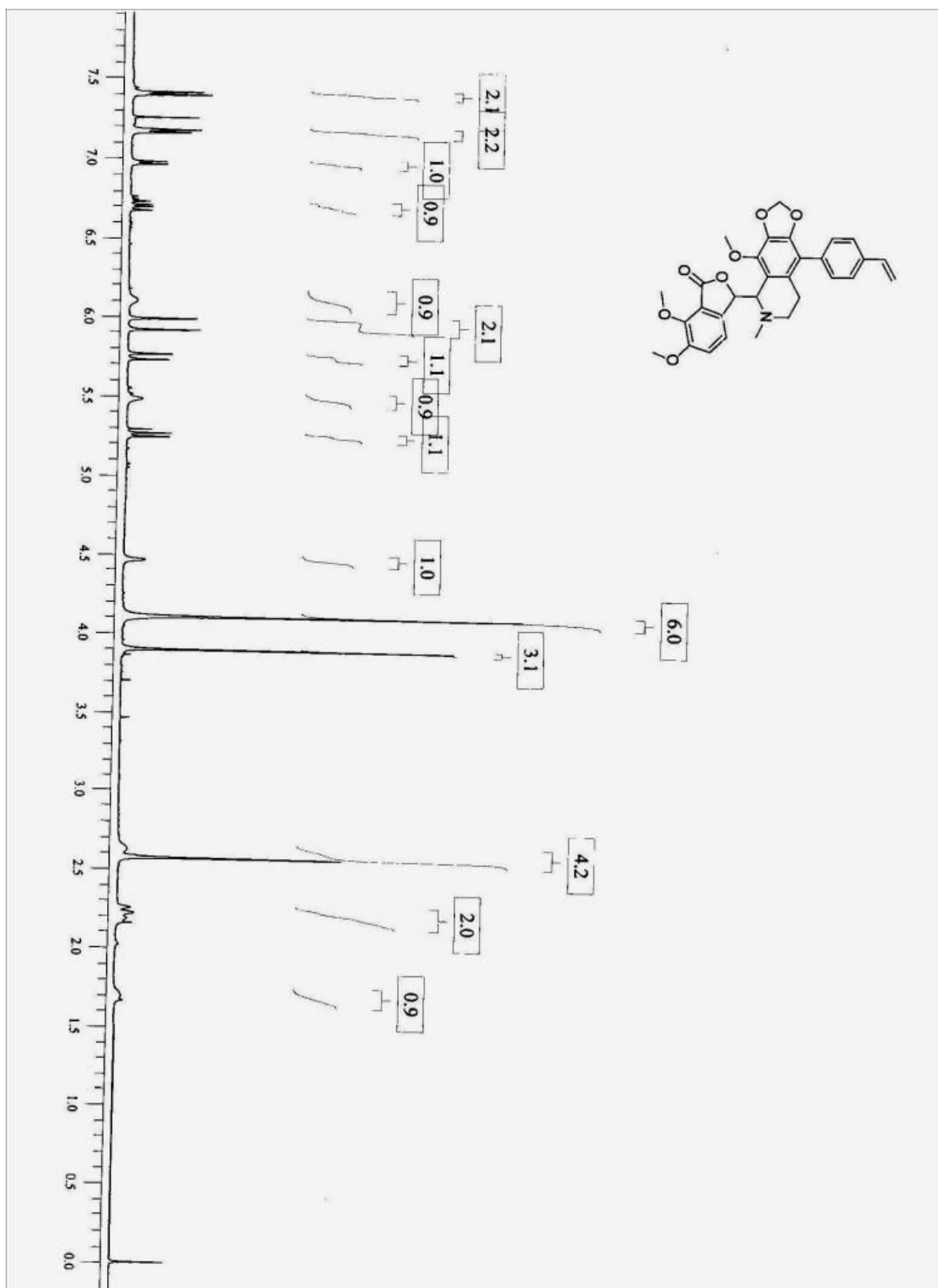
Target m/z: +569.1920 amu  
 Tolerance: +5.0000 ppm  
 Result type: Elemental  
 Max num of results: 100  
 Min DBE: -0.5000 Max DBE: +50.0000  
 Electron state: OddAndEven  
 Num of charges: 0  
 Add water: N/A  
 Add proton: N/A  
 File Name: 25JULY2011.wiff

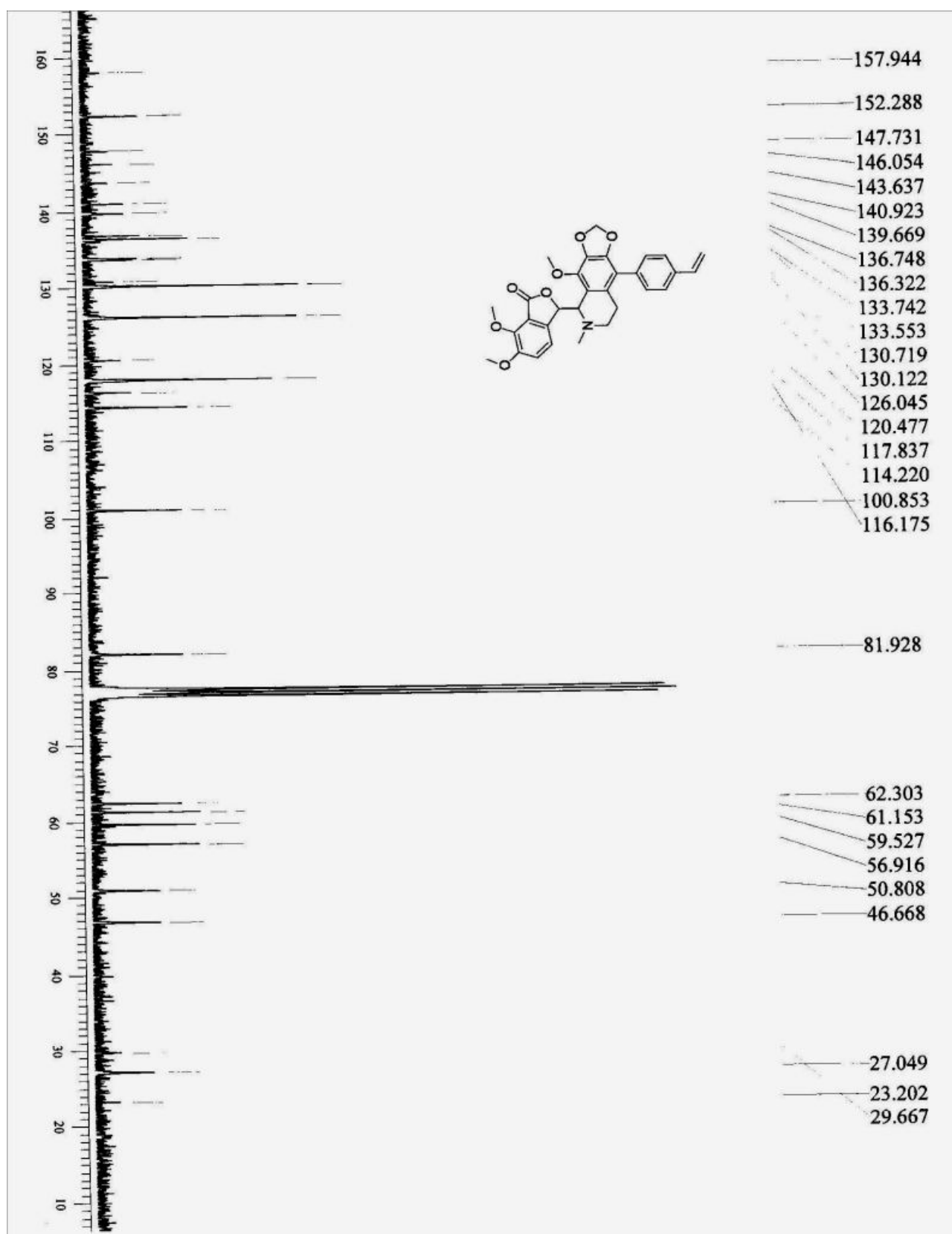
	Elements	Min Number	Max Number
1	Br	0	1
2	C	0	30
3	H	0	31
4	N	0	2
5	Na	0	1
6	O	0	8

	Formula	Calculated m/z (amu)	mDa Error	PPM Error	DBE
1	C30 H30 N2 O8 Na	569.1899	2.0139	3.5382	16.5

## ESI spectra of 5f



$^1\text{H}$  NMR spectra of 5d

$^{13}\text{C}$  NMR spectra of 5d

## HRMS spectra of 5d

Acq. File: n/a

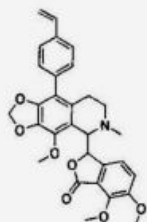
Sample ID: n/a

Acq. Date: n/a

Sample Comment: n/a

Acq. Time: n/a

## Elemental composition calculator

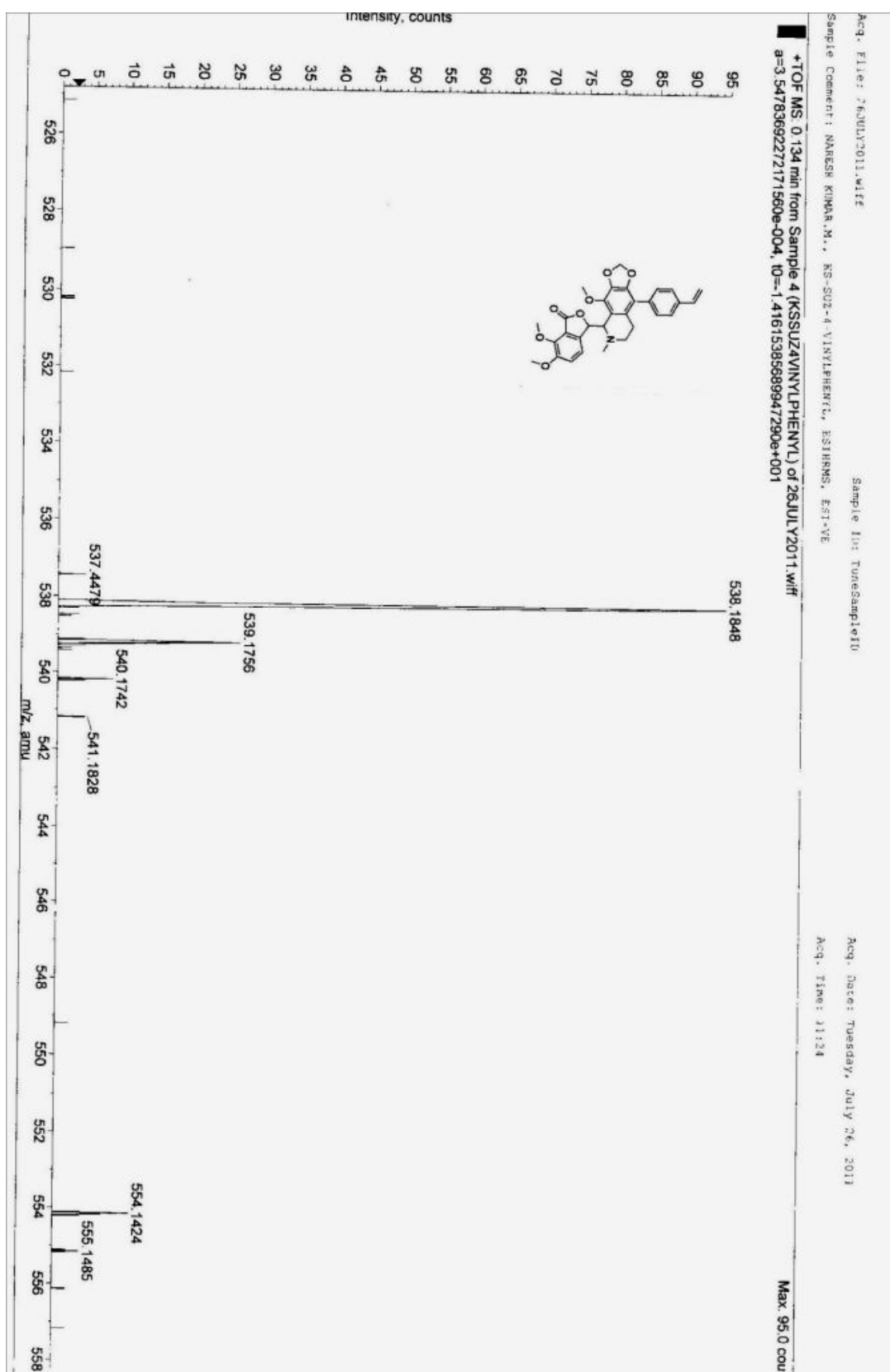


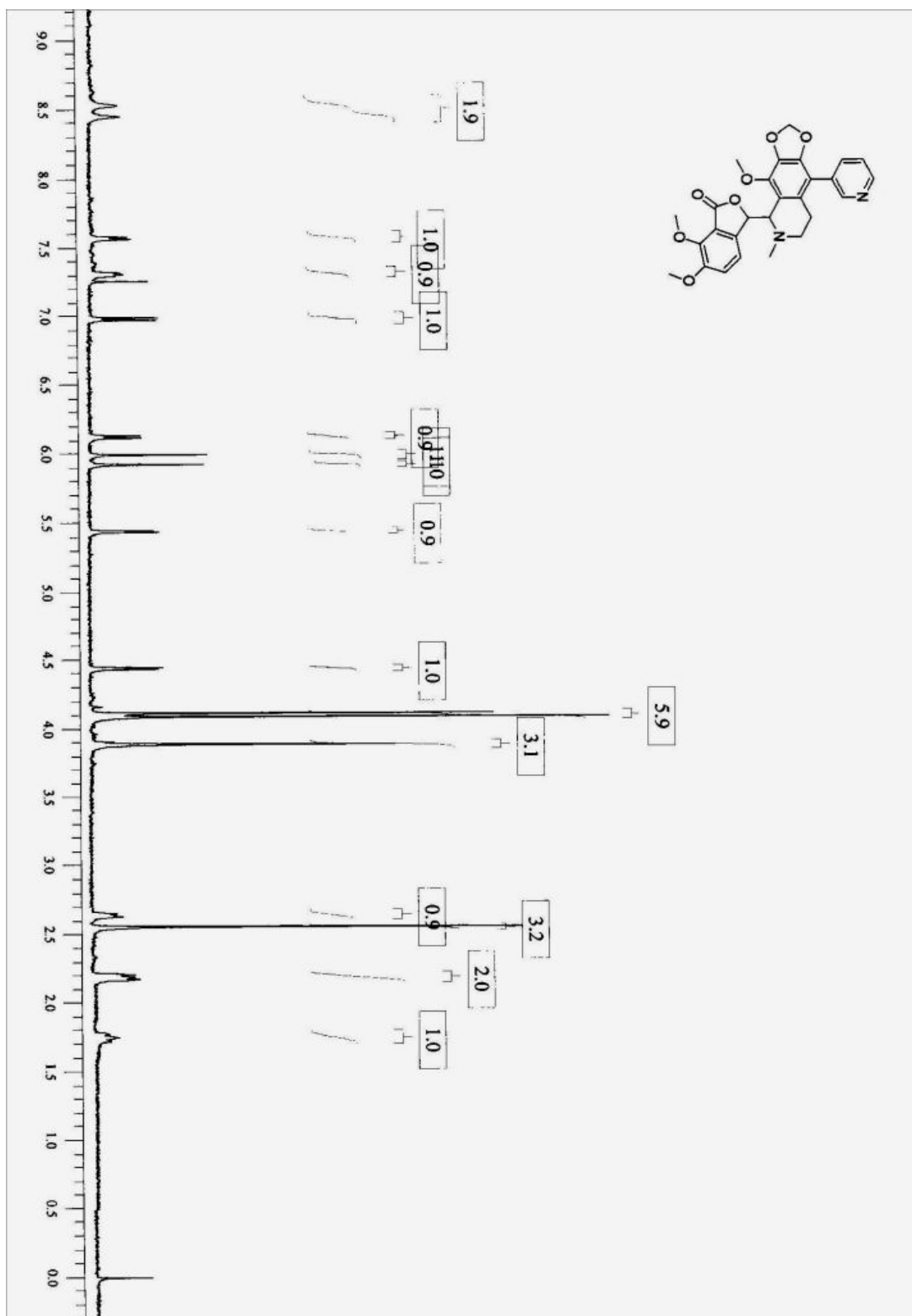
Target m/z: +538.1848 amu  
 Tolerance: +5.0000 ppm  
 Result type: Elemental  
 Max num of results: 100  
 Min DBE: -0.5000 Max DBE: +50.0000  
 Electron state: OddAndEven  
 Num of charges: 0  
 Add water: N/A  
 Add proton: N/A  
 File Name: 26JULY2011.wiff

	Elements	Min Number	Max Number
1	C	0	31
2	H	0	32
3	N	0	2
4	Na	0	1
5	O	0	9

	Formula	Calculated m/z (amu)	mDa Error	PPM Error	DBE
1	C30 H29 N O7 Na	538.1841	0.6276	1.1662	16.5

## ESI spectra of 5d



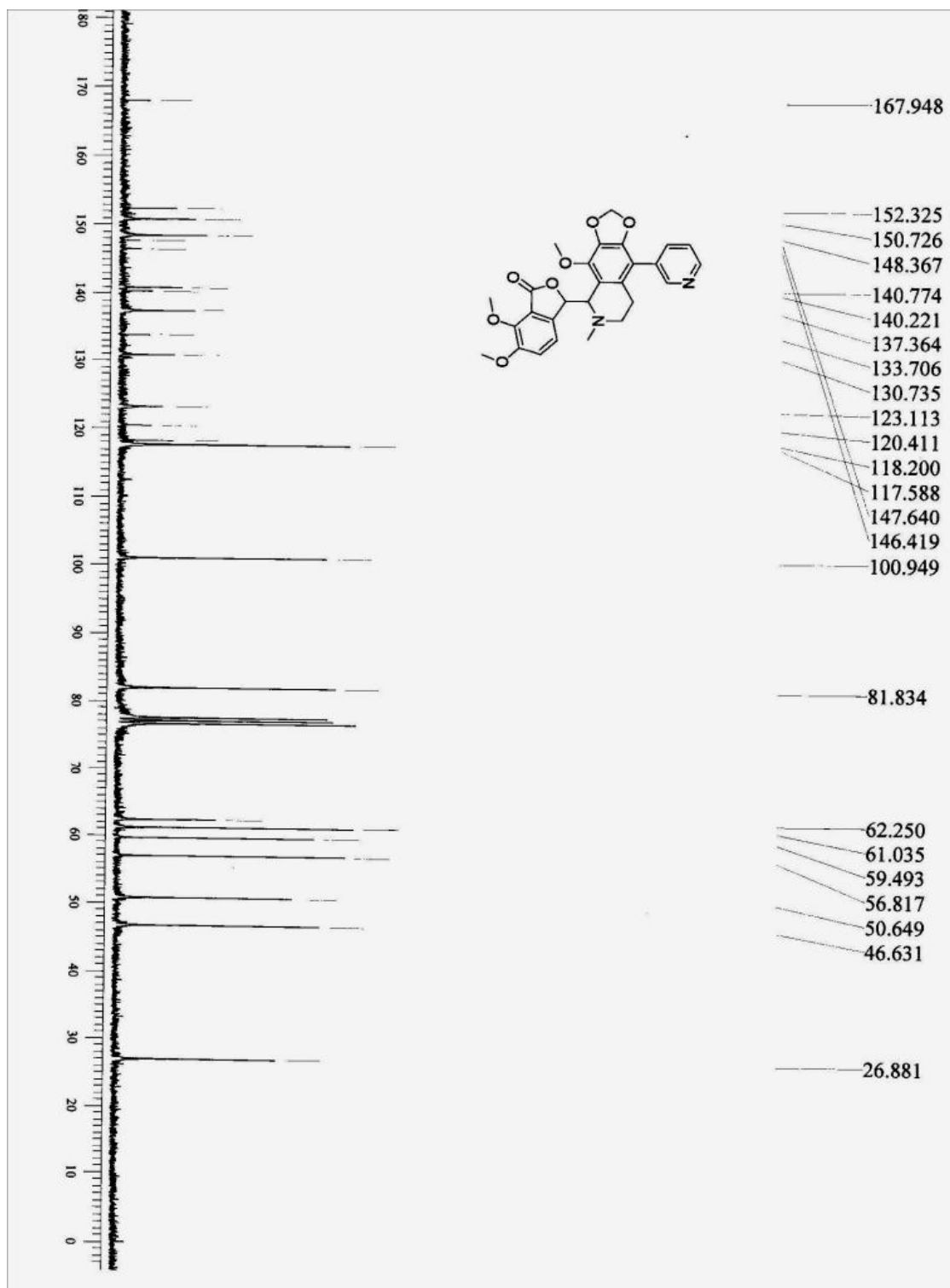
$^1\text{H}$  NMR spectra of 5e



---

<sup>13</sup>C NMR spectra of 5e

---



## HRMS spectra of 5e

Acq. File: n/a

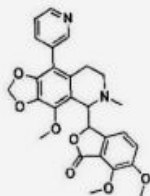
Sample ID: n/a

Acq. Date: n/a

Sample Comment: n/a

Acq. Time: n/a

## Elemental composition calculator

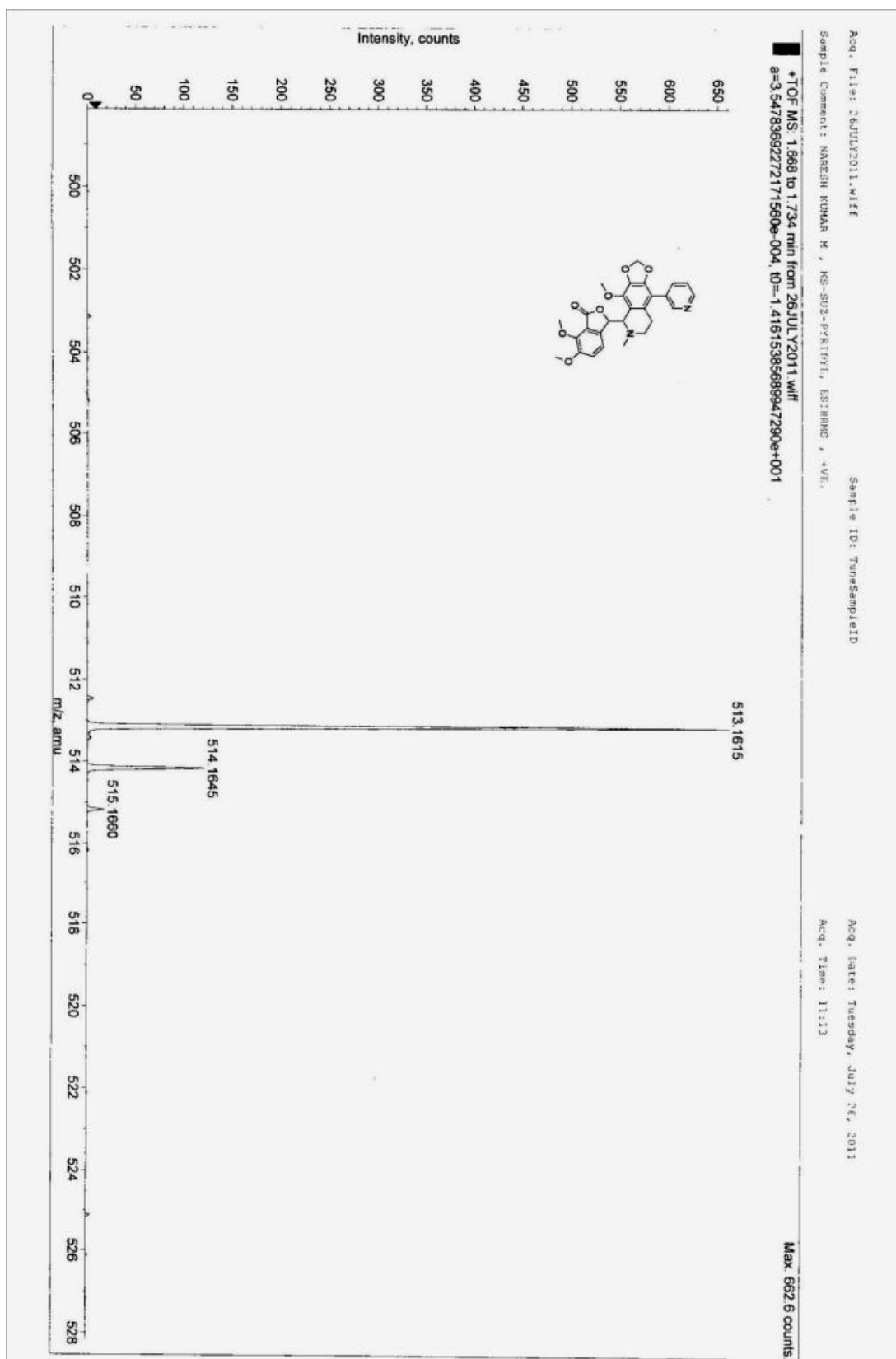


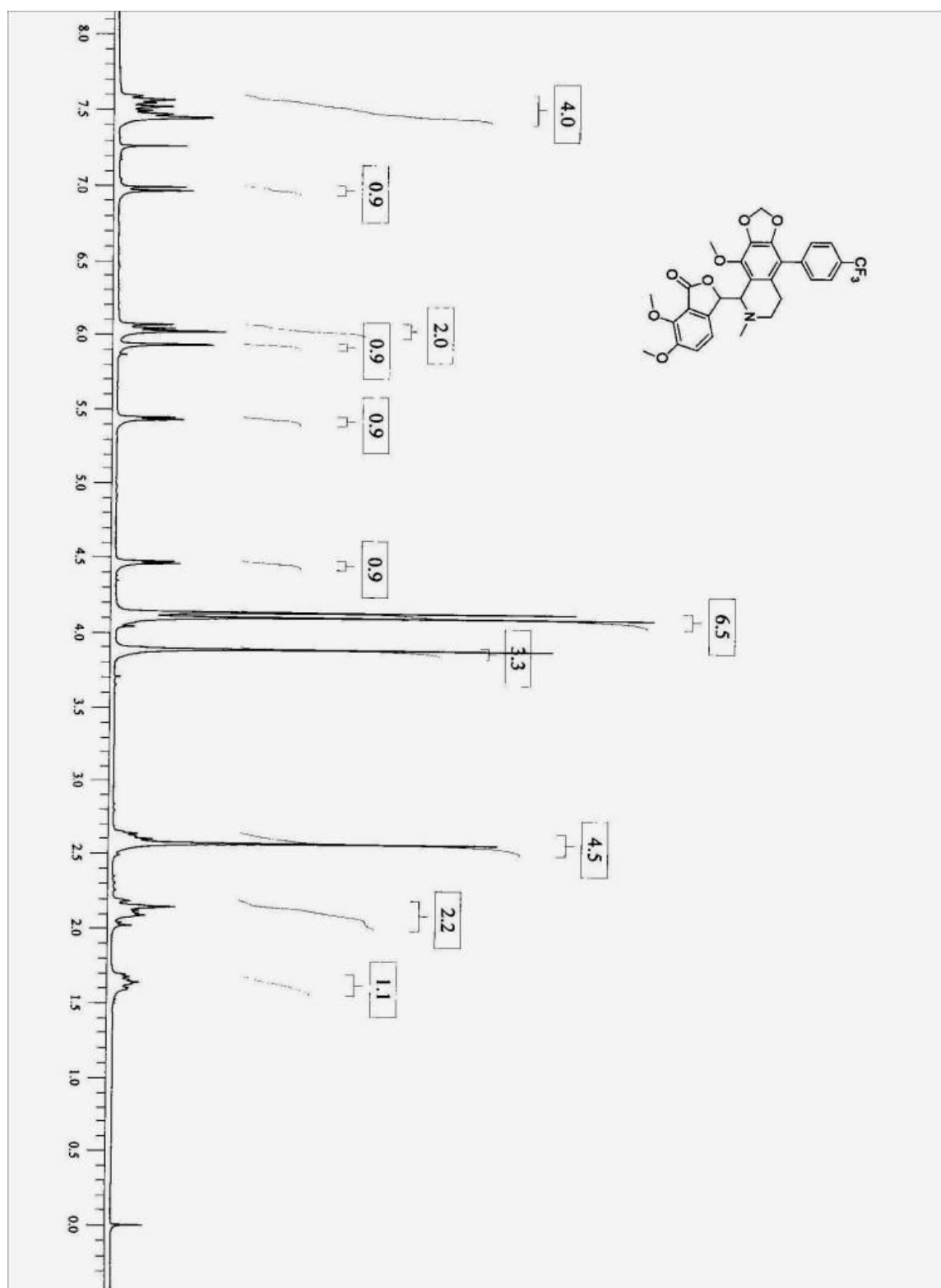
Target m/z: +513.1615 amu  
 Tolerance: +5.0000 ppm  
 Result type: Elemental  
 Max num of results: 100  
 Min DBE: -0.5000 Max DBE: +50.0000  
 Electron state: OddAndEven  
 Num of charges: 0  
 Add water: N/A  
 Add proton: N/A  
 File Name: 26JULY2011.wiff

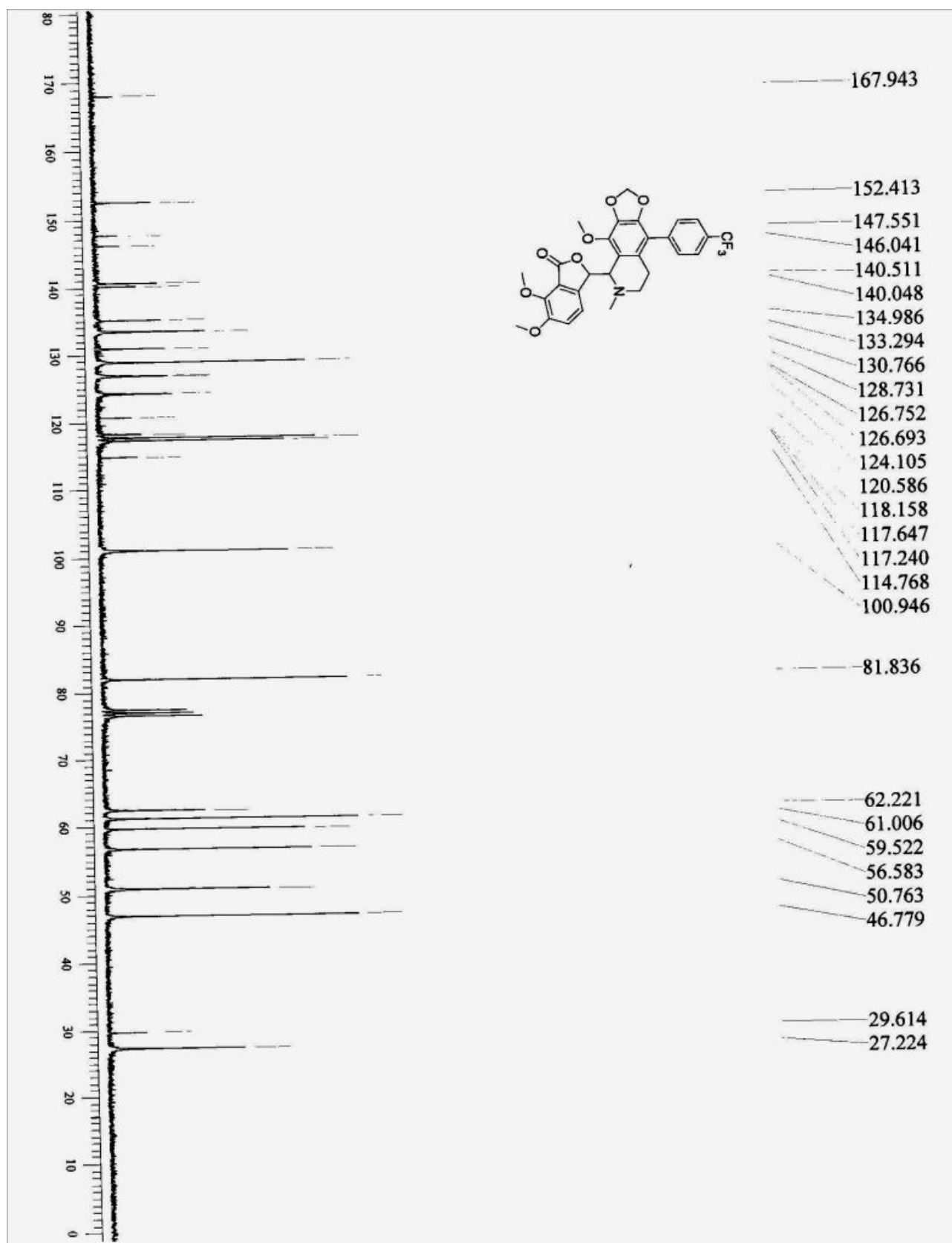
	Elements	Min Number	Max Number
1	C	0	29
2	H	0	30
3	N	0	2
4	Na	0	1
5	O	0	9

	Formula	Calculated m/z (amu)	mDa Error	PPM Error	DBE
1	C <sub>27</sub> H <sub>26</sub> N <sub>2</sub> O <sub>7</sub> Na	513.1637	-2.2712	-4.4259	15.5

## ESI spectra of 5e



$^1\text{H}$  NMR spectra of 5a

$^{13}\text{C}$  NMR spectra of 5a

## HRMS spectra of 5a

Acq. File: n/a

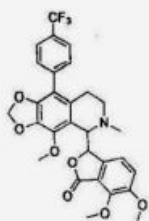
Sample ID: n/a

Acq. Date: n/a

Sample Comment: n/a

Acq. Time: n/a

## Elemental composition calculator

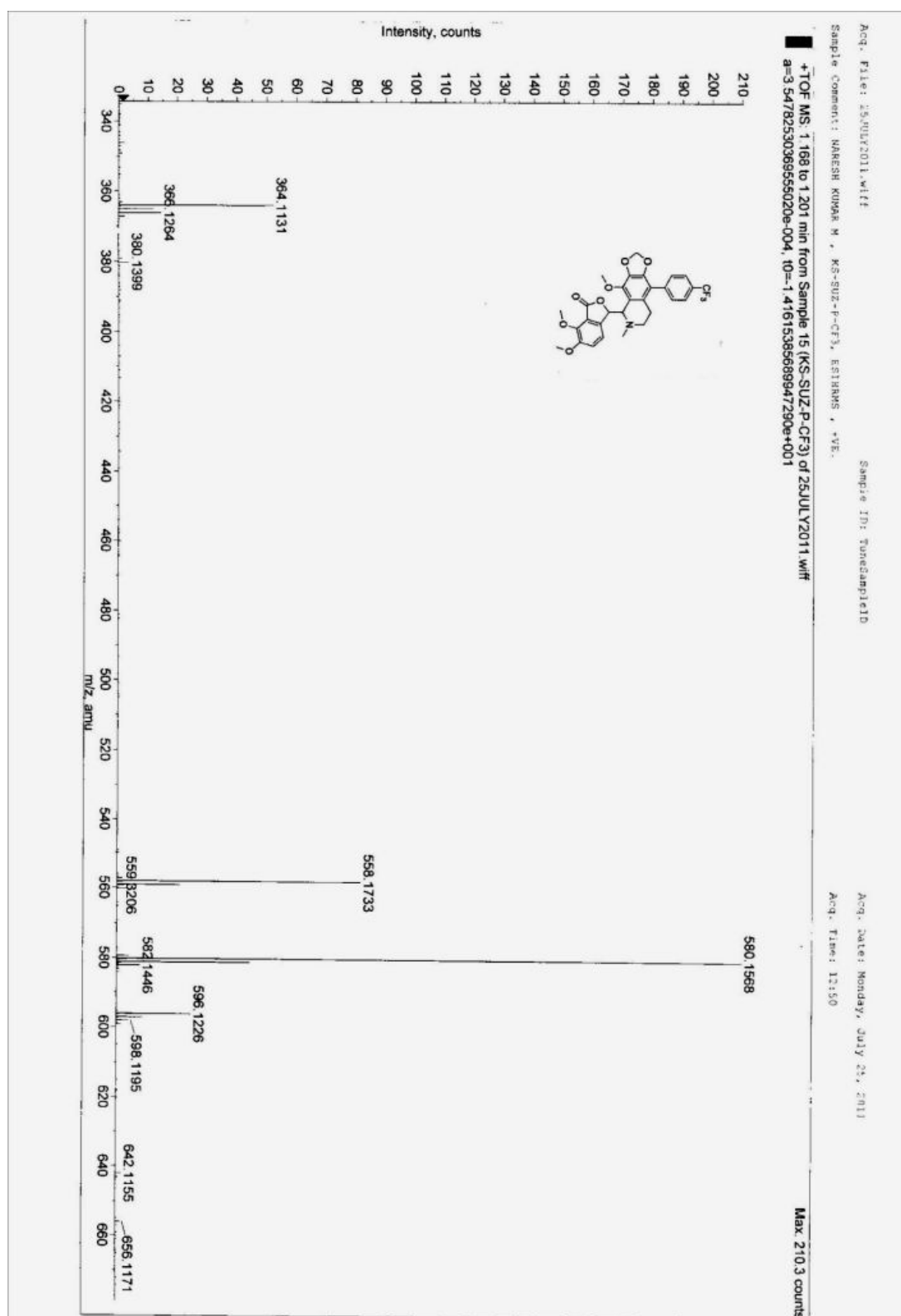


Target m/z: +580.1568 amu  
 Tolerance: +5.0000 ppm  
 Result type: Elemental  
 Max num of results: 100  
 Min DBE: -0.5000 Max DBE: +50.0000  
 Electron state: OddAndEven  
 Num of charges: 0  
 Add water: N/A  
 Add proton: N/A  
 File Name: 25JULY2011.wiff

	Elements	Min Number	Max Number
1	C	0	29
2	F	0	3
3	H	0	27
4	N	0	2
5	Na	0	1
6	O	0	9

	Formula	Calculated m/z (amu)	mDa Error	PPM Error	DBE
1	C29 H26 N O7 F3 Na	580.1559	0.8930	1.5392	15.5

## ESI spectra of 5a







## **LIST OF PUBLICATIONS**

## LIST OF PUBLICATIONS

## PUBLICATIONS

1. **Seneha Santoshi**, Pradeep K. Naik and Harish C. Joshi (2011). Rational design of novel anti-microtubule agent (9-azido-noscapine) from quantitative structure activity relationship (QSAR) evaluation of noscapinoids. *Journal of Biomolecular Screening*. 16(9):1047-1058. [ISSN: 1087-0571, **IF: 2.207**]
2. **Seneha Santoshi** and Pradeep K. Naik (April 2014). Molecular insight of isotypes specific  $\beta$ -tubulin interaction of tubulin heterodimer with noscapinoids. *Journal of computer aided Molecular design*. 28:751-763. [ISSN: 0920-654X, **IF: 3.368**]
3. **Seneha Santoshi** and Pradeep K. Naik (2012). Evaluation of structure activity relationship of Noscapinoids utilizing field based 3D QSAR modeling. *International Journal of Fundamental and Applied Sciences*. 1: 481-87. [ISSN: 2278-1404]
4. **Seneha Santoshi**, Naresh Kumar Manchukonda, Manu Lopus, Silja Joseph, Charu Suri, Sunil K Hota, Saroj K Das, Srinivas Kantevari and Pradeep Kumar Naik (2014). Rational design of biaryl pharmacophore substituted noscapine derivatives as potent tubulin binding anticancer agents (communicated to *Journal of computer aided Molecular design* [ISSN: 0920-654X, **IF: 3.368**]

## CONFERENCE PRESENTATIONS

1. **Seneha Santoshi** and Pradeep K. Naik. A three dimensional QSAR model building utilizing structural determinants of noscapine derivatives for tubulin binding affinity prediction. **Poster presented** in International conference on “biotechnology advances :omics approaches and way forward (ICBA-2012)” organized by centre of biotechnology (supported by DST-FIST, govt. of India) Siksha ‘o’ Anusandhan University, Bhubaneswar 20 -22 December, 2012.)